Investigating the antimicrobial potential of metallic based nanoparticles and their integration within biocompatible polymers

Etelka Chung

Submitted to the University of Hertfordshire in partial fulfilment of the requirements of the degree of Doctor of Philosophy

School of Physics, Engineering and Computer Science, University of Hertfordshire, Hatfield, Hertfordshire, AL10 9AB

December 2022

Abstract

Antimicrobial resistance of pathogenic infections is a rising global issue resulting in less effective antibiotic treatments against infections, thus leading to prolonged hospitalisation, higher mortality rates and increased healthcare costs. Therefore, the aim of this research is to extend the exploration of nanomaterials with antimicrobial activity and utilise them for the development of biomedical devices. In this endeavour, nanoparticles have been found to provide one possible alternative solution to tackle the challenges of antibiotic resistance. Metal nanoparticles, in particularly silver and copper, have shown promising antimicrobial potential for bioengineering and biomedical material applications. However, only a limited number of nanoparticles and their effects on common bacteria from hospital acquired infections (HAI) have been studied. This investigation extends knowledge of the antimicrobial activity of relevant nanoparticles.

In this research, a variety of nanoparticles, including mono-metallic, bimetallic and graphene-based materials, were screened against common fungi, Gram-negative and Gram-positive bacteria that were listed by World Health Organisation (WHO) as a priority for the development of new antibiotics due to their multiple antibiotic resistances. Results demonstrated that these metallic based nanoparticles exhibited antimicrobial activity against a wide range of microbes, with elemental silver (Ag), bimetallic silver copper (AgCu) and elemental copper (Cu10) suspension nanoparticles displaying the broadest range of efficacies, with minimal inhibitory concentrations as low as 7.81 μg/ml. Upon the selection of antimicrobial nanoparticles, extended investigations on the antimicrobial activity were performed against *E. coli, S. aureus* and *C. albicans.*

Based on the antimicrobial range and efficacy results, bimetallic AgCu nanoparticles were selected for further investigation. The properties of AgCu were explored and compared to Cu10 and Ag to help understand the link between the physio-chemical properties and the antimicrobial efficacy. It was found that hydrodynamic size and release of ions contributed the most to the antimicrobial effect of the nanoparticles. With this in mind, the mechanisms of action of the AgCu nanoparticles were investigated. Through observational techniques such as TEM and SEM, it was found

that AgCu nanoparticles caused morphological changes to the microbes, including cell membrane damage, shrinkage in cell size by 10-35% and leakage of internal material. Furthermore, physical contact with *C. albicans* and *S. aureus* was observed. In bacterial cells, an increase of up 318% in oxidative stress and decrease in deoxyribonucleic acid (DNA) production to less than 13% was measured after incubation with AgCu nanoparticles.

The selected nanoparticle, AgCu, was then fabricated into polymers with potential biomedical applications. Firstly, AgCu nanoparticles were incorporated into polydimethylsiloxane (PDMS) films. Films were produced with nanoparticles well dispersed throughout the film as observed via scanning electron microscopy (SEM); however no antimicrobial activity was exhibited. As a result, the films were surface treated with UV lamp, which resulted in an increase of AgCu nanoparticle exposure and ion release, leading to a 9.8% to 71.8% reduction in microbial growth ($P = 0.05$), depending on the microbial strain.

A second application involved incorporating AgCu nanoparticle into polycaprolactone/polyethylene oxide (PCL/PEO) polymers. Through the disk diffusion method, it was found that the AgCu incorporated PCL/PEO films exhibited antimicrobial activity towards *E. coli, S. aureus* and *C. albicans.* The films had hydrophilic properties and partly dissolved upon contact with water. This resulted in the exposure and release of AgCu nanoparticles and ions thus leading to antimicrobial activity with zone of inhibition diameters between 1.04 cm to 4.20 cm, depending on microbial strain and AgCu nanoparticle concentration. Additionally, pores were found on the surface of the PCL/PEO polymers which has been suggested to provide benefits as wound dressing applications. However, the toxicity and biocompatibility of these AgCu nanoparticle incorporated PCL/PEO polymers requires investigation and validations with mammalian cells.

These experiments have proven that certain nanoparticles provide antimicrobial activity against a wide spectrum of pathogenic species and can be incorporated in to polymers to fabricate antimicrobial films. However, further studies are required to fully elucidate the mechanism of action, the factors that can influence their antimicrobial effectiveness and toxicity as biomedical applications.

Acknowledgements

Over the course of my doctorate, I had the most wonderful support and help from people that made this PhD and thesis possible through their contributions whether big or small.

Firstly, I would like to thank my mum, dad and sister for their love and support throughout my whole life and especially during the PhD adventure and Covid era. Thank you for taking care of me with a warming home and delicious meals.

I would also like to give a special thanks to my supervisors Dr Guogang Ren, Dr Yuen Ki Cheong and Dr Ian Johnston at the School of Physics, Engineering and Computer Science, University of Hertfordshire, for the continuous support and opportunity to conduct this exciting research. From the same school, I am appreciative for SEM training and help provided by Mr Kenneth Henman, TEM help provided by Dr Sufyan Akram and Tensiometer training provided by future Dr Aaqib Ayub. Additionally, I am also very grateful for Mr Mansukhlal Vadalia, Dr Andrew Timms and Mr James Stanley at the School of Life and Medical Sciences, University of Hertfordshire, for their advice and ideas in microbiology and chemical analysis. I would like to thank the PhD students in both departments for their friendship, support and memorable times.

It was such an honour to have the opportunities to meet and collaborate with the inspiring individuals from different universities. In particular, a special thanks to Dr Jie Huang and Hessah Alotaibi from University College London (UCL) department of mechanical engineering for the research collaboration and ideas, and Professor Mohan Edirisinghe and team from the same department for the review paper collaborations.

Lastly, I would like to give my thanks to School of Physics, Engineering and Computer Science, University of Hertfordshire, for financially supporting this PhD. I am grateful for all the equipment and scientific instruments available at this institute to aid my research.

Table of contents

Contents

List of Figures

List of Tables

List of Equations

List of Acronyms

Abbreviation	Full form
General	
±	Plus or minus
abs	Absorbance
a.u.	Arbitrary unit
β	Beta
µg/ml	Micrograms per millilitre
µl	Microlitres
µm	Micrometres
µM	Micromolar

λ_{max}	Lambda max
CDC	Centers for Disease Control and Prevention
CFU	Colony Forming Units
cm	Centimetre
EUCAST	The European Committee on Antimicrobial Susceptibility Testing
HAIs	Health-care associated infections
M	Molar
mg	Milligrams
MIC	Minimal inhibitory concentration
ml	Millilitre
mm	Millimetre
mM	Millimolar
mV	Millivolt
NHS	National Health Service
nm	Nanometres
rpm	Revolutions per minute
SPR	Surface Plasmon Resonance
US EPA	United States Environmental Protection Agency
UV	Ultraviolet
WHO	World Health Organisation
w/w%	Weight per weight percentage
wt/v%	Weight per volume percentage
ζ-potential	Zeta potential

Nanoparticle

Ag	Silver
AgCu	Silver copper
AVNP	Antiviral nanoparticle
CeO_2	Cerium (IV) oxide
Cu	Copper
Cu10	Copper nanoparticles between 10-30 nm
Cu60	Copper nanoparticles between 60-100 nm

CuO	Copper oxide
CuZn	Copper zinc
EGO	Expanded graphene oxide
EU graphene	European Commission graphene
GO30	Graphene oxide averaging 30nm
GO ENG	Engineered graphene oxide
GOP	Graphene oxide platelets
MNP	Metallic Nanoparticle formulation
QNA Ag	Tesima™ thermal plasma produced silver
QNA Cu	Tesima™ thermal plasma produced copper
RG GO-NH carboimidazole	Reduced Graphene oxide amine
RG NH	Reduced Graphene amine
RG NH_2	Reduced Graphene azanide
RG O Fe_3O_4	Reduced Graphene iron oxide
RG Pd(O)	Reduced Graphene Palladium (II) oxide
RG TEPA	Reduced Graphene tetraethylenepentamine
WC	Tungsten carbide
ZnO	Zinc oxide

Microorganisms

A. baumannii	*Acinetobacter baumannii*
B. sublitis	*Bacillus subtilis*
C. albicans	*Candida albicans*
C. tropicalis	*Candida tropicalis*
E.coli	*Escherichia coli*
E. faecalis	*Enterococcus faecalis*
K. pneumonia	*Klebsiella pneumonia*
MRSA	Methicillin-resistant *Staphylococcus aureus*
P. aeruginosa	*Pseudomonas aeruginosa*
S. aureus	*Staphylococcus aureus*
S. pyogenes	*Streptococcus pyogenes*
S. typhimurium	*Salmonella typhimurium*

Biology

ATP	Adenosine triphosphate
DNA	Deoxyribonucleic acid
NADH	Nicotinamide adenine dinucleotide
ROS	Reactive oxygen species

Equipment

EDAX	Energy dispersive spectroscopy
ICP-OES	Inductively coupled plasma optical emission spectrometry
NTA	Nanoparticle tracking analysis
SEM	Scanning Electron Microscope
TEM	Transmission Electron Microscopy
UV-Vis	Ultraviolet-visible spectroscopy

Materials and Reagents

DAPI	4', 6'-diamidino-2-phenylindole
DCM	Dichloromethane
DMSO	Dimethyl sulfoxide
H_2-DCFDA	2', 7'-dichlorodihydrofluorescein diacetate
IMS	Industrial methylated spirit
LDPE	Low density polyethylene
MH	Mueller Hinton
NH_4OH	Ammonium hydroxide
PBS	Phosphate-buffered saline
PCL	Poly(ε-caprolactone)
PDMS	Polydimethylsiloxane
PEO	Poly(ethylene oxide)
PET	Poly(ethylene terephthalate)
PLA	Polylactic acid
PMMA	Poly(methyl methacrylate)
PVDF	Polyvinyldiene fluoride
YPD	Yeast Peptone Dextrose

General introduction

Introduction to nanoparticles

Nanoparticles are a broad class of materials with dimension sizes within the nanoscale of typically less than 100nm [6]. Although nanoparticles exist in nature, the journey of nanotechnology began in 1959 when Nobel-Prize winner, Richard Phillips Feynman introduced the idea during his talk “There’s Plenty of Room at the Bottom” at the American Physical Society meeting. Feynman theorised that the manipulation of matter at nanoscopic levels can create novel materials with enhanced desired properties [7, 8]. Since then, years of research have explored the unique chemical and physical properties of nanoparticles to enhance applications in the modern world. For example, engineered nanoparticles can be commonly found in stain-repellent fabric and transparent sunscreen [9]. Bae *et al.* (2009) found that silica nanoparticle treatment were able to produce water-repellent cotton fabrics that were also repellent to stains [10]. In contrast, titanium dioxide and zinc oxide nanoparticles are used in sunscreen for their effective ability to protect the user from UVB and UVA sun radiation. As the nanoparticles are at the nanoscale, they are practically transparent to the naked eye and are desired in preference to microsized particles which produce an opaque white case on the skin [11]. Such nanoscopic dimensions can be hard to picture, therefore the schematic diagram in Figure 0.1 illustrates the scale of matters ranging from micro- to nano- sizes to put things into perspective.

As a result of their high surface area to volume ratio, nanoparticles have different or enhanced properties in comparison to their bulk materials due to an increase in reactivity at a molecular level [12]. Such properties may provide potential advantages in various bioengineering applications and are being exploited in medical applications including drug delivery and cancer treatment [13, 14]. Furthermore, certain nanoparticles have shown promising results to combat pathogens, including those with antimicrobial resistance and ability to produce biofilms [15].

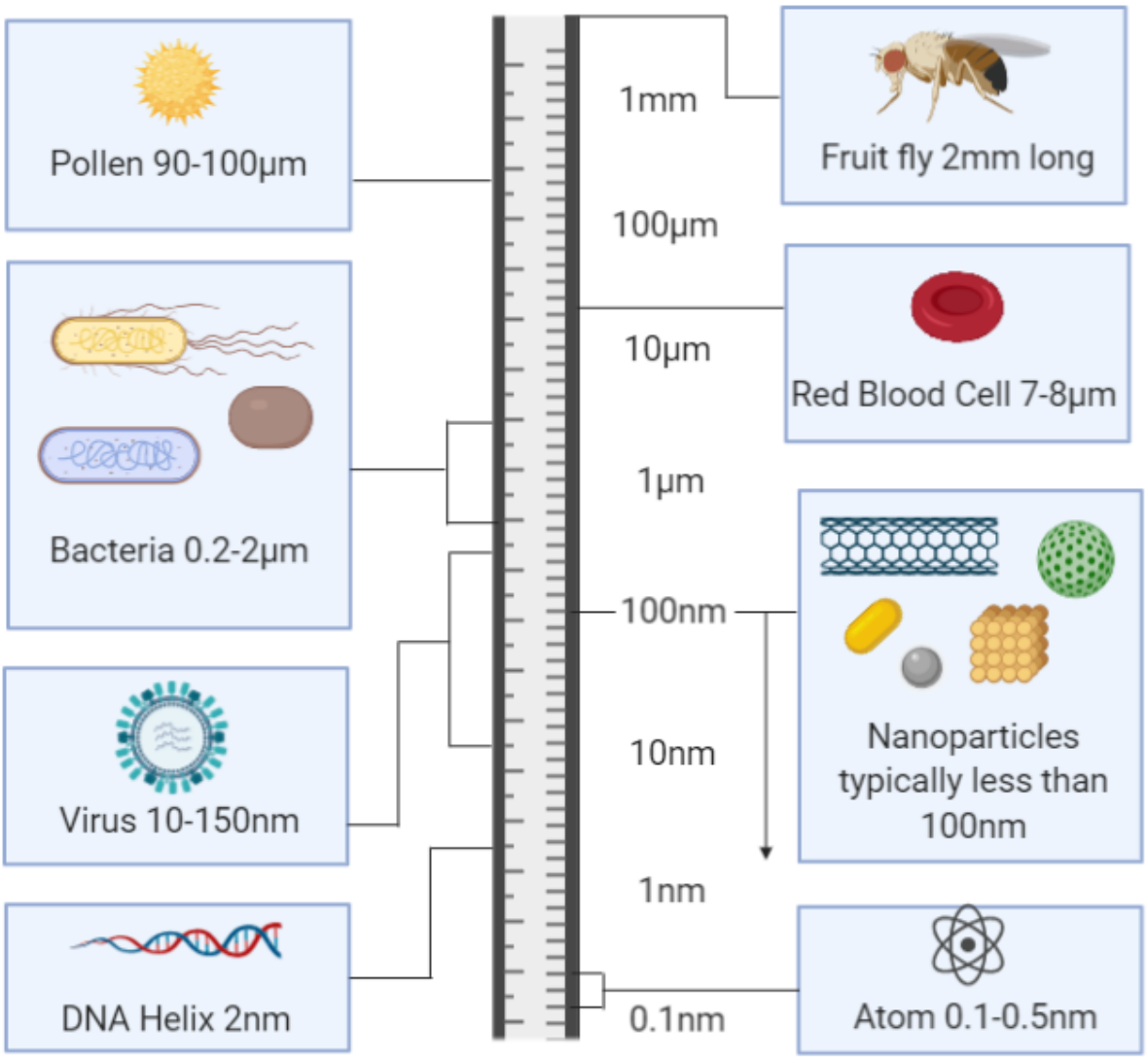

Figure 0.1: Schematic comparison of micro- and nano-components. Nanoparticles are found within the nanoscale with sizes that are typically less than 100nm. Schematic figure created with BioRender.com.

Problem statement

Despite the current medical technology and treatment, pathogenic infections are a huge health threat to humans across the world. Every year, antibiotic resistant infections are responsible for at least 700,000 cases of death globally [16]. Since the availability of prescribed antibiotics in the 1940s, antibiotics are the standard choice of treatment for bacterial infections, due to their effective results and low costs. However, it has been found that the use of antibiotics, particularly their overuse and unnecessary treatments, has led to the evolution of antibiotic-resistant strains of pathogens, which are linked to high morbidity and mortality rates [17, 18]. Although government, researchers and pharmaceutical companies are developing and discovering new antimicrobial agents, the UK government commissioned a review that estimated that every year around 10 million people will lose their lives as a result of infections caused by microbes with antibiotic resistance [19]. As a result, nanoparticles have sparked interest for their unique antimicrobial mechanisms of action against a wide range of infectious pathogens and may provide alternative pathway to combat antimicrobial resistance [20].

The importance of nanoparticles is seen through their unique properties that can be utilised for potential applications in different fields. For example, silver nanoparticles have been largely investigated as a result of their recognised antimicrobial properties. However, a wide number of nanoparticles have been less explored for their antimicrobial activity [21]. Whilst the use of nanoparticles for their antimicrobial properties can now be found in applications such as wound dressing and dental materials, their mechanisms of action against microbes remain unclear and hypothesised [22]. Studies on the characteristics of antimicrobial nanoparticles and their interaction with microorganisms will aid and facilitate their use in biomedical applications.

Aims and objectives

The aim of this doctorate research is to address the problems described in the previous section by investigating the antimicrobial properties of nanoparticles and fabricating the chosen antimicrobial nanoparticle into biocompatible polymers. To address the problems of pathogenic infection and antimicrobial resistance, the first aim was to identify nanoparticles with antimicrobial activity and select the highest performing antimicrobial nanoparticle for further investigations. The second aim was to investigate the potential mechanisms of the selected nanoparticle to understand the physiochemical properties and behaviour towards microbes. Lastly, the third aim was to successfully fabricate the selected antimicrobial nanoparticle into biocompatible polymer and to investigate their antimicrobial activity for potential biomedical applications. This research was divided into five objectives:

1) Screening and selecting of nanoparticles - high throughput screening process involving wide range of nanoparticles and different species of microbes using different screening methods.
2) Investigation of the selected nanoparticles on microbes by determining the minimal inhibitory concentration, growth rate over time and rate of inhibition through cell viability.
3) Characterisation of the selected nanoparticles to understand and compare their dry state and changes to their behaviour in hydrodynamic states.
4) Investigation of the mechanisms of action of the selected nanoparticle against Gram-negative, Gram-positive and fungi by performing quantitative biological assays and qualitative techniques.
5) Fabrication of the selected antimicrobial nanoparticle into biocompatible polymers

The plan of this research project is illustrated in Figure 0.2 as a flow chart.

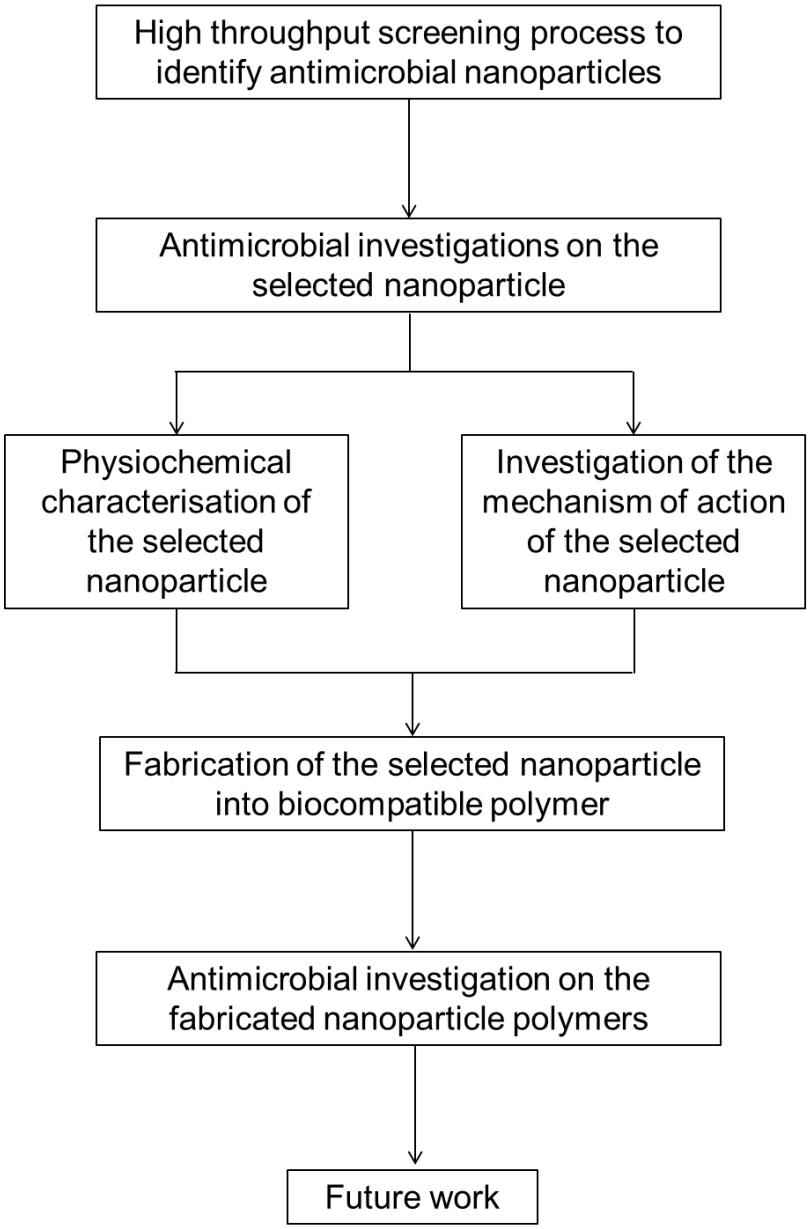

Figure 0.2: Flow chart of research project plan

Outline of thesis

This PhD thesis is divided into seven chapters followed by references compiled together at the end and an appendix with supporting information and publications. Firstly, Chapter 1 reviews the literature surrounding nanoparticles, antimicrobial properties and their potential applications in the biomedical field.

Chapter 2 provides the general materials and methods used throughout the experimental investigations of this PhD, whilst Chapters 3 to 7 report more focused experimental investigations.

In Chapter 3, a wide variety of nanoparticles were examined for antimicrobial properties against common nosocomial pathogens, using biological assays to screen and determine ones with the highest efficacy.

In Chapter 4, the selected nanoparticle with high antimicrobial activity, bimetallic silver copper (AgCu), was characterised, alongside elemental silver (Ag) and elemental copper (Cu) for comparison, to further understand their physical and chemical properties.

Qualitative observational techniques and assays were used in Chapter 5 to investigate the mechanisms of action of AgCu nanoparticles against bacteria and fungi.

Chapter 6 focuses on the incorporation of the selected nanoparticle (AgCu) into polydimethylsiloxane (PDMS) polymers and its antimicrobial properties for potential biomedical applications.

Similarly, Chapter 7 investigates the antimicrobial activity of AgCu incorporated poly(ε-caprolactone)/poly(ethylene oxide) (PCL/PEO) polymers.

Lastly, Chapter 8 draws together the summary of findings and concludes the thesis with proposed future work that could be conducted for further scientific findings to supplement the outcomes obtained from this PhD.

Chapter 1 Literature Review

1.1 Nanoparticle synthesis and processing

Currently, two main approaches are used to synthesise nanoparticles: a bottom up approach and a top down approach. Like natural biological systems, the bottom up approach refers to when materials are built from atoms or molecules and are assembled into conformation. Generally, the products of this approach are smaller in size and more cost effective. The top down approach refers to the production of nanoparticles by breaking down bulk materials into the particles that are within the nanoscale size [23, 24]. Figure 1.1 schematically shows the two approaches for nanoparticle synthesis.

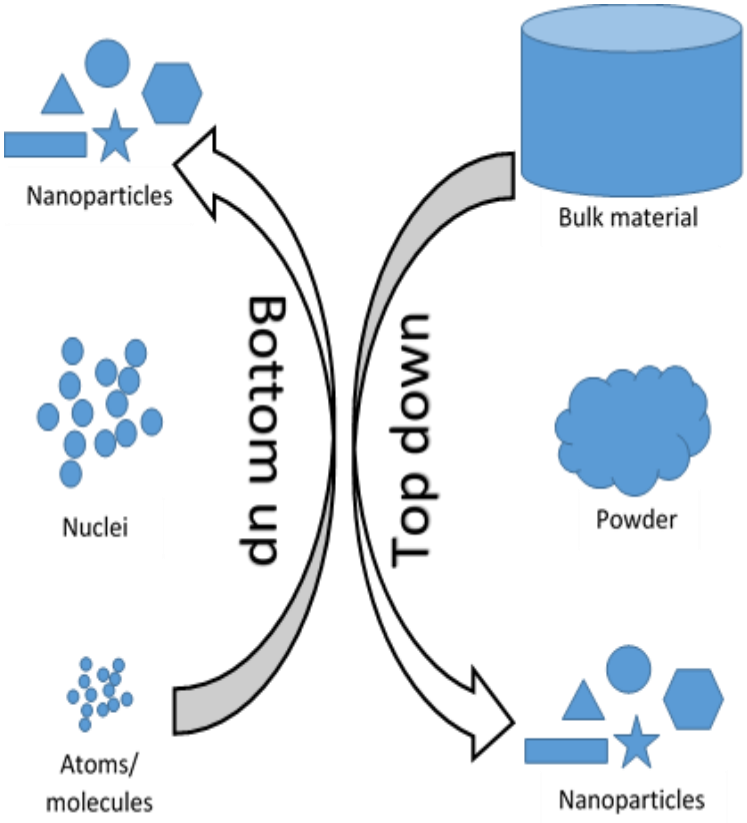

Figure 1.1: Bottom up and top down approaches for nanoparticle synthesis. On the left hand side, bottom up synthesis of nanoparticles is shown schematically from the build-up of atoms/molecules to produced nanoparticles. Similarly, the right hand side schematically illustrates top down nanoparticle synthesis, which involves the breakdown of bulk material to nanoparticles.

The top down approach involves mechanical and physical methods such as ball milling and grinding. For example, Salah, et al. (2011) used a ball milling method to reduce the size of ZnO particles from 600 nm to nanoparticles of roughly 30 nm [25]. Alternatively, thermal plasma synthesis can be used to break down solid materials into vapour and cooled to form nanoparticles [26]. Ren, et al. (2009) investigated CuO generated from the Tesima™ plasma process - Figure 1.2 shows a schematic diagram of the process [27]. Although these techniques are well established, the processes are energy consuming and material produced has an increased possibility of agglomeration and contamination [24, 28].

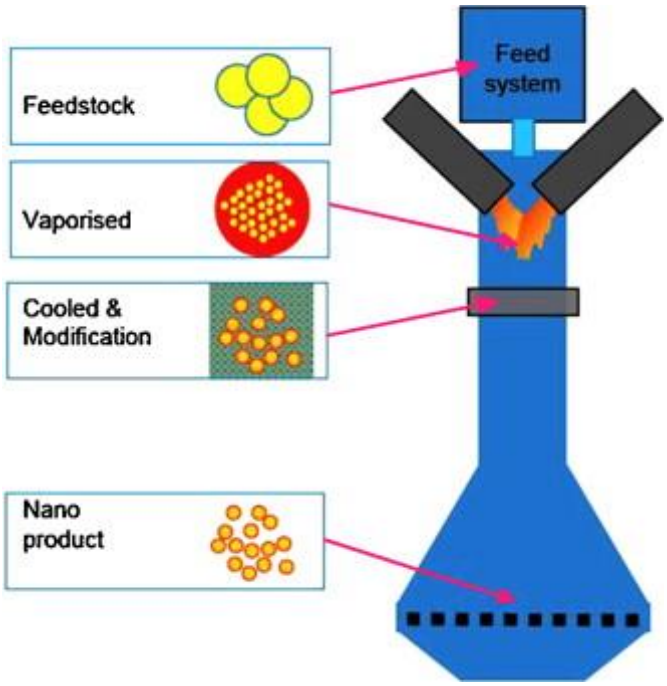

Figure 1.2: Schematic diagram of Tesima™ plasma taken from Ren *et al.* (2009). This top down approach utilises heat to break down bulk materials to form particles within the nanoscale.

Within the bottom up approach, the synthesis of nanoparticles may be classified into two categories:

1. Gas-phase synthesis: nanoparticles are generated through the interaction of gaseous precursor components over a catalyst or prepared surface. Carbon nanotubes are commonly synthesised this way as the method is highly economical

[29]. In a published article, Mattei *et al.* (2019) used a gas-phase process to synthesise Au-Pt-Pd trimetallic nanoparticles [30].

2. Liquid-phase synthesis: within this type of synthesis, techniques include precipitation and sol-gel process. These methods are preferred in comparison to gas-phase synthesis, as a lower temperature is required and nanoparticles are produced at a higher rate. The precipitation process produces nanoparticles from salts in solvents with the use of precipitation agents, which are then filtered and thermally treated [29]. Rashid *et al.* (2020) have reported the production of 9-15 nm iron oxide nanoparticles (Fe_3O_4) using a precipitation method. Sol-gel synthesis is a similar process, which produces a gel from powder materials [31]. This method is considered to be one of the most well-established types of liquid phase synthesis. Dörner *et al.* (2019) used the sol-gel method to synthesise CuO nanoparticles with sizes ranging from 20-40 nm [32]. A schematic diagram of liquid-phase synthesis is shown in Figure 1.3.

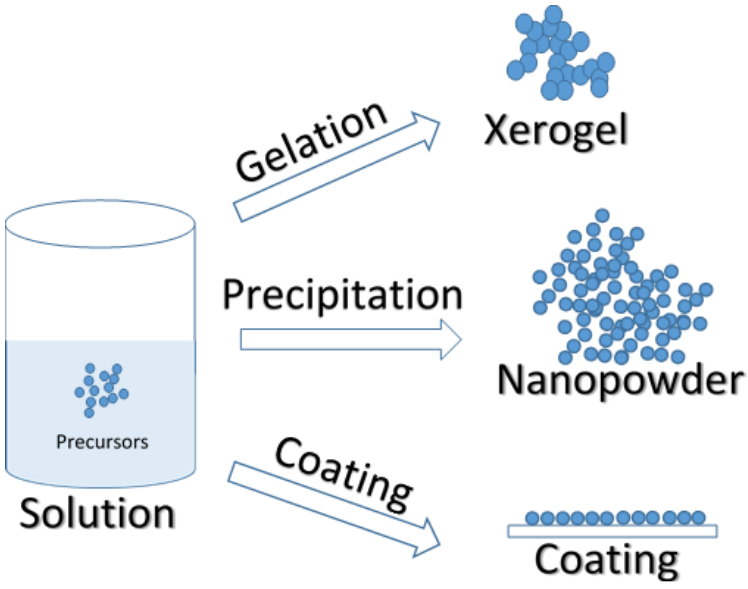

Figure 1.3: Examples of liquid-phase synthesis. As part of the bottom up approach to synthesis nanoparticles, salt precursors in solvent solution can be used to produce nanoparticles. The gelation of the solution can produce nanoparticles in xerogel form. With the aid of precipitation agents and thermal treatment, nanopowder can be formed. Lastly, materials can be dipped into the solution to create a coating of nanoparticles onto the material.

1.2 Antimicrobial properties of nanoparticles

Whilst nanoparticles possess many beneficial properties, including optical and electrical properties, the main focus of this thesis is on their antimicrobial properties. It has been found that the physiochemical properties of nanoparticles contribute largely to their toxicity towards pathogens; in particular, their size, shape, composition and surface properties [22]. Furthermore, antimicrobial activity of nanoparticles can be enhanced through alterations of their properties [33].

1.2.1 Size

As previously mentioned, nanoparticles range between 1-100nm and smaller sized particles have shown an increase in antimicrobial activity. As the overall size of nanoparticles decreases, the surface area to volume ratio increases, which enables more interaction between particles and pathogens [22]. Moreover, Butler *et al.* (2015) reported that smaller silver nanoparticles induced higher genotoxic response, whilst nanoparticles that were larger than 10 nm were unable to enter bacterial cells and cause internal damage [34]. The size of nanoparticles can have an effect on their antimicrobial activity and there are ways to alter the size. One example of this would be using physical method of ball milling to reduce particle size. Karthik *et al.* (2017) synthesised nanoparticles from plant leaves and ball milled them for 15 hours, which reduced the nanoparticle size from 114 nm to 45 nm, but increase the antimicrobial activity [35]. Other methods of reducing particle sizes include pH and temperature alteration during synthesis [36, 37]. Conversely, smaller sized particles have shown an increase in toxicity towards mammalian cells; thus concentration and leaching of nanoparticles from products will need to be researched prior to this application [38, 39]. Although single nanoparticles can be of small dimensions, agglomeration of particles will increase the overall size and may reduce antimicrobial effectiveness [40].

1.2.2 Surface

Agglomerations are a gathering of particles caused by attractions from their particle surface charge. Strong charges will cause repulsion between particles resulting in dispersed nanoparticles, whereas weak or neutral charges can lead to agglomerations [41]. Figure 1.4 visually shows the difference between dispersed nanoparticles and agglomerations. The surface charge of nanoparticles can also lead to attraction or repulsion to microbial cells. The negatively charge components

in bacterial and fungi cell wall lead to an overall negative microbial surface charge; thus nanoparticles with positive surface charge are more likely to interact through opposite charge attraction. It has been reported that the ability of nanoparticles to form physical contact with microbial cells contributes to their antimicrobial activity. Badawy *et al.* (2011) found that positively charged nanoparticles were more toxic towards bacterial cells than negatively charged nanoparticles due to their ability to interact with bacterial cells, which can induce cell membrane damage, pitting and ability to enter the cell [42]. The zeta potential (ζ-potential) can be modified to improve their properties, including increased stability of suspension or enhanced antimicrobial activity. For example, decreasing the pH will result in an increase in ζ-potential from the increased concentration of positive hydrogen ions in acid. As reported by Guo *et al.* (2018), at pH 12 the ζ-potential of ash nanoparticles was -45.4 mV; however when decreased to pH 4, the ζ-potential increased to 9.4 mV [43].

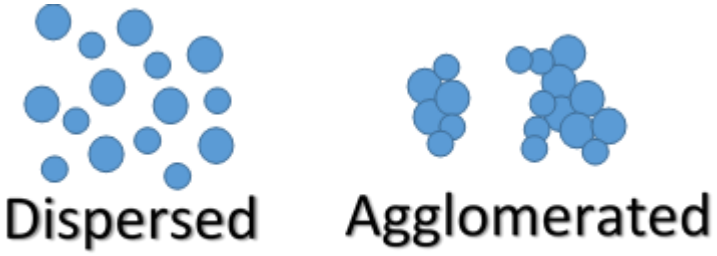

Figure 1.4: Physical schematic appearance of dispersed nanoparticles (nanoparticles existing as single particles) compared to agglomeration of nanoparticles (nanoparticles clustered together that increases the overall size of nanoparticles)

1.2.3 Shape

Observations of nanoparticles at high magnifications have proven that they exist naturally in a variety of shapes. They can be sorted into two categories as represented; high aspect ratio particles have longer lengths than widths; in comparison to low aspect ratio particles with similar lengths to widths [44, 45]. Microscopy, e.g. scanning electron microscope (SEM) or transmission electron microscope (TEM), can be used to observe nanoparticles at high magnifications to identify nanoparticle shapes, for example in Figure 1.5, TEM was used to observe different nanoparticle morphology [46]. Although it is not fully understood, certain nanoparticle shapes can provide a more efficient antimicrobial activity. It is hypothesised that the shape of the nanoparticle contributes to surface area and ion release which can both influence the antimicrobial activity [47, 48]. As well as surface properties and size, the morphology of nanoparticles can be controlled. During synthesis, the chemical, temperature and time duration largely contributes to their final shape [49]

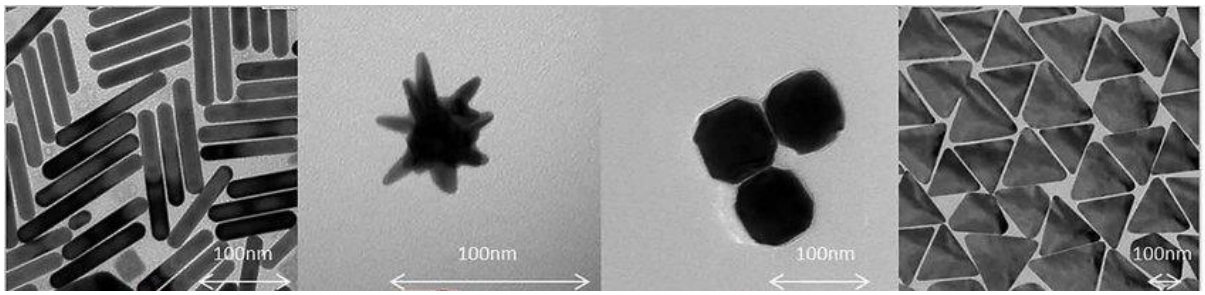

Figure 1.5: TEM images of nanoparticles varying in shapes including rod, star, spherical and triangular. Image adapted from Bouloudenine and Bououdina (2016).

1.2.4 Composition

Nanoparticles can consist of a range of materials. Firstly, nanoparticles can be made from a single element (e.g. elemental silver nanoparticle). Alternatively, they can consist of a mixture of two or more elements (e.g. metal oxides, the combination of a metal element and oxygen). Or lastly, intermetallic alloys are compounds composed of a combination of two or more metals or another element bonded together to form a defined stoichiometric structure [50, 51]. Metallic oxide nanoparticles, for example Zinc Oxide (ZnO), have engendered a growing interest in research for their ability to form an oxidation-reduction reaction, which is a supported theory of nanoparticle mechanism of action [52]. Currently, the nanoparticle mechanism of action is still hypothetical and the number of nanoparticles that have been tested for antimicrobial activity is limited. Table 1.1 summarises some monometallic, bi-/inter-metallic and metal oxide nanoparticles that have been studied for antimicrobial effects. Furthermore, studies have reported synergistic effects of antimicrobial nanoparticles; Garza-Cervantes *et al.* (2017) found the antimicrobial activity of silver increased when it was combined with certain transition metals including zinc, but only a limited variation of combinations were investigated [53].

Recently, graphene and other carbon-based nanoparticles have been increasingly researched as they may have a wider application due to less toxicity in comparison to metals, but still exhibit antimicrobial properties [54]. As an example, carbon nanoparticles extracted from kitchen soot were found to employ antimicrobial activity against bacteria [55]. However, another study found that the concentration of graphene and graphene oxide nanoparticles to exhibit antibacterial activity were higher than the critical biosafety concentration [56].

Table 1.1: Summary of nanoparticles that have been tested for antimicrobial activity. Examples of monometallic, bi-/intermetallic and metal oxides nanoparticles that have been investigated against certain strains of pathogens.

Monometallic nanoparticles	**Size (nm)**	**Pathogen tested**	**Reference**
Ag	19-58	*Staphylococcus aureus* *Klebsiella pneumoniae*	[57]
	52	*P. aeruginosa* *S. aureus*	[58]
Cu	82	*P. aeruginosa* *S. aureus*	[58]
	12-15	*E. coli*	[59]
	50-60	*Bacillus subtilis* *S. aureus* *E. coli*	[60]
Au	19-48	*S. aureus* *K. pneumoniae*	[57]
Bi-/inter-metallic nanoparticles			
AgCu	83.3-419.2	*Bacillus subtilis* *Salmonella typhimurium*	[61]
Ag/Co	16	*E. coli*	[62]
Au-Ag	20-24	*S. aureus* *K. pneumoniae*	[57]
Fe/Ag	110	*P. aeruginosa* *S. aureus*	[58]
Fe/Cu	100		
Al/Cu	112	*E. coli* *S. aureus*	[63]
Metal oxide nanoparticles			
CuO	5-10	*S. aureus* *E. coli*	[64]
	20-95	*E. coli* MRSA	[27]
ZnO	100-800	*E. coli* *S. aureus*	[65]
TiO_2	10	*S. aureus*	[66]
FeOOH	2-5	*E. coli* MRSA	[67]

1.3 Characterisation of nanoparticles

Certain properties can influence the antimicrobial activity of nanoparticles and in order to investigate and understand their properties, nanoparticles are required to be characterised. The study of nanoparticle characterisation is made possible through instrumentation techniques to explore their chemical and physiochemical properties [68]. A summary of instrumental techniques used in relation to the properties investigated is displayed in Table 1.2**.**

Table 1.2: Instruments used to investigate and characterise the properties of nanoparticles

Property characterised	**Instrumental technique**
Size	SEM, DLS, NTA, TEM
Size distribution	DLS, NTA
Shape	SEM, TEM
Surface charge	ζ-potential
Agglomeration state	ζ-potential, DLS, NTA, TEM, SEM
Optical properties	UV-Vis
pH	pH meter
Chemical structure	XRD, Raman spectrometry
Ion dissociation	ICP - OES

1.3.1 Chemical composition

The analysis of the chemical composition can enhance the understanding of the physical properties and consistency of materials to detect presence of any impurities. Raman spectroscopy is an analytic technique that uses principles of vibrational spectroscopy to study vibrational and rotational states when certain wavelengths of light interact with the sample [69, 70]. A laser light is applied onto the sample and the emitted radiation is collected, filtered and detected by a charged coupled device (CCD detector). The data can then be used to produce a Raman spectrum where intensity of radiation is plotted against a shift in wave-number (cm^{-1}). From the spectrum, composition, crystallinity, quantity and quality of the sample can be determined. Width and intensity of peaks can identify the quality and quantity,

respectively, whereas the characteristics of Raman frequencies and polarisation of peaks can identify the composition and crystallinity, respectively [70].

Alternatively, x-ray diffraction (XRD) can also be used to identify the chemical composition and crystallographic order of a sample. This analytical technique utilises x-rays to radiate a sample at an incident angle and then detects the intensity of diffraction from lattice points in the sample to form a spectrum. The software and database within the instrument can identify the crystal arrangement from the spectrum to determine the composition and crystallography [71, 72]. The relationship between the diffraction peaks and crystal structure of the sample can be determined from Bragg's equation (Equation 1); where *n* represents the order of diffraction, λ is the wavelength of the x-ray, d is the space between the crystal lattice planes and θ is the diffraction angle of incidence [72, 73]. Additionally, the diffraction Bragg's law is schematically shown in Figure 1.6.

$$n\lambda = 2dsin\theta$$

Equation 1: Bragg's equation

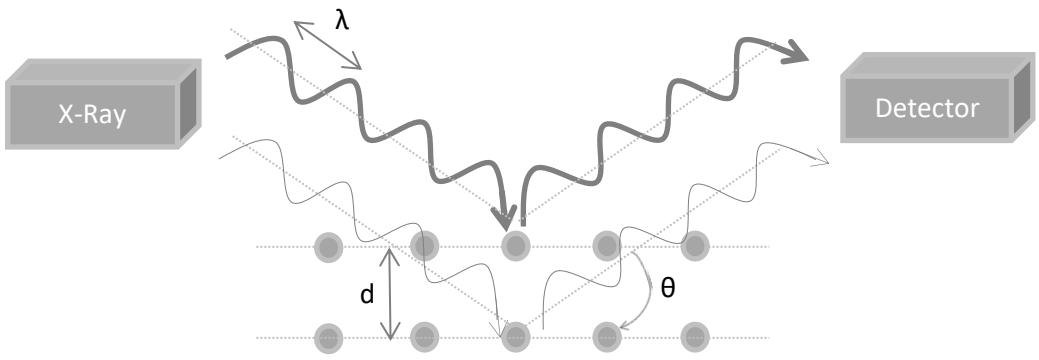

Figure 1.6: Schematic diagram of x-ray diffraction from a lattice in relation to Bragg's equation where λ is the x-ray wavelength, d is the distance between the crystal lattice planes of the sample and θ is x-ray diffraction angle of incidence. The sample is irradiated by a source of x-ray and the detector collects the intensity diffraction from lattice points (grey dots) in the sample. Bragg's equation is then used to determine the relationship between the distributions of intensity peaks.

1.3.2 pH and ion dissolution

pH measurements are used to identify the acidity or alkalinity of aqueous substances as a result of hydrogen ions. Substances range on a pH scale of 0 to 14. Pure water is considered to be neutral with a general pH of 7 at 25^{o}C; pH less than 7 are characterised as acidic and those greater than 7 as alkaline [74]. To measure the pH, ion-selective electrodes that are protected by pH-sensitive glass are used to detect a voltage created by hydrogen ions in the aqueous sample. Greater concentrations of hydrogen ions will result in a lower pH value, thus a more acidic sample [75]. In a suspension, nanoparticles can undergo oxidative dissolution to form ions. The formation of positive ions will reduce positive hydrogen ions and therefore increase the pH and lower the acidity. A larger concentration of positive ions released will result in a greater pH of the suspension [76, 77]. According to literature, smaller sized nanoparticles release more ions in comparison to larger sized particles, and additionally sheet shaped nanoparticles release more ions than block shaped nanoparticles. This is due to larger surface areas for nanoparticle dissolution [78, 79].

Ions can be measured using various instruments, including inductively coupled plasma optical emission spectrometry (ICP-OES). In brief, liquid samples are pumped into the machine and turned into an aerosol with argon gas; it is then heated by a plasma torch to excite electrons which results in the emission of photons. These photons are detected and are can be used to characterise the elements in the material and quantify their concentrations [80].

1.3.3 Surface charge and agglomeration

Nanoparticles have an electrostatic surface charge, which is determined as the zeta potential (ζ-potential) [81]. The ζ- potential of nanoparticles and their high surface area can lead to interactions between particles, resulting in agglomeration – particles that are loosely gathered together which can be separated by mechanical stress [41]. Agglomerates can be visually observed by scanning electron microscope (SEM) and transmission electron microscope (TEM), whilst nanoparticle tracking analysis (NTA) and dynamic light scattering (DLS) can detect them via an increase in size of particles. Alternatively, ζ- potential can be measured using instruments such as a

ZetaSizer to analyse the surface charge of nanoparticles to predict the stability of nanoparticles and formation of agglomerates in a suspension. To measure the ζ-potential, a voltage is applied to the electrodes in contact with the suspension; nanoparticles will be attracted to the opposite charge and travel through the suspension to that electrode. Like DLS, scattered laser lights are used to detect the movement of particles at multiple voltages; ζ- potential can be calculated through the velocity of the particle at different voltages [81, 82].

Overall, the ζ- potential value ranges from +100 to -100 mV. Nanoparticles with ζ-potential at the extreme ends of the range will have strong repulsion force against each other and result in minimal agglomeration. On the other hand, values that are closer to neutral are considered to be unstable; the weak charges allow particles to interact with each other, which can result in the formation of agglomerates within the suspension. Typically the instability range is between ±30 mV; however some regard the instability range of colloidal solutions as ±20 mV [83, 84].

In addition to predicting the stability of a suspension, the interaction between nanoparticles and other particles such as microbial cells can be predicted through their ζ- potential. Both bacterial and fungal cells commonly have a negative surface charge due to negatively charged components in the cell wall. Therefore, nanoparticles with positive charge are more likely to interact with microbial cells through the attraction between opposite charges. In contrast, strongly negative nanoparticles are unlikely to interact with microbial cells due to electrostatic repulsion preventing close contact [41]. The surface charge of microbial cells can be measured using the same instrumental technique as described for nanoparticles [81]. Likewise, agglomeration of microbial cells can occur, which can also be observed through SEM and TEM [85].

1.3.4 Size and shape

The characterisation of nanoparticle morphology can be determined through observations at high magnifications; commonly SEM and TEM are used.

SEM is able to provide close up surface observations of organic and inorganic materials. This characterisation technique utilises electron beams to interact with a sample and emitted electrons, x-rays and visible light are measured by detectors to produce a three dimensional image [86]. TEM works by a similar principle where

electron beams are focused by a condenser lens onto and through a sample. Transmission of electrons is detected to produce an image in relation to density where dark areas represent lower levels of electron transmission detected while light areas represent higher levels of electron transmission [87]. Whilst both techniques have a higher resolution and magnification rate than traditional microscopes, longer sample preparation, including conductive coating may be required, and images obtained are in black and white. Typically, SEM can be used for overall observation and topography of samples, whereas TEM, with a higher magnification range, is used to study individual particles and internal details of biological samples [88].

In addition to shape, the size of nanoparticles has been found to relate to their antimicrobial activity. SEM and TEM can be used to measure the size of nanoparticles through scale comparison in their dry state, whilst the characterisation of nanoparticle hydrodynamic size (the diameter size of nanoparticles in aqueous suspension) and its distribution can be more accurately measured using other instrumental techniques [89].

In a suspension, dispersed particles are constantly moving in a random motion due to bombardment from surrounding particles. This movement is described as Brownian motion. The size of the particle will contribute to the Brownian motion; larger particles move slower in comparison to smaller particles with fast motion [90, 91]. The Brownian motion of particles that can be detected by light and the velocity is identified as the diffusion coefficient (D). By applying the Stokes-Einstein's equation (Equation 2), the hydrodynamic radius (R_h) of nanoparticles can be calculated, where K_B is Boltzmann's constant, T is temperature, and η is viscosity of suspension.

$$D = \frac{K_B T}{6\pi\eta R_h}$$

Equation 2: Stokes-Einstein's equation

Both DLS and NTA utilise light produced by lasers to measure the Brownian motion of particles to determine particle size. DLS measures changes in intensity of light over a period of time, whereas NTA analyses single particles. Although DLS is able

to detect particles that are affected by gravity and larger particles than NTA, it can underestimate the concentration of small particles and detect agglomerations as larger particles [92].

1.3.5 Optical properties

Ultraviolet Visible spectroscopy (UV-Vis) can characterise the optical properties of a material via absorption of ultraviolet and visible light wavelengths within the electromagnetic spectrum. Specifically, the ultraviolet region is from 10 to 400nm and visible light region is from 400 to 800nm [93].

To measure the absorbance, a beam of electromagnetic light is projected through a sample. Absorption of light at certain wavelengths results in the molecule absorption of photons which can promote electron excitation to a greater energy state. The difference in energy states is described as the band gap which is unique for different molecules due to differences in their chemical structure. The absorption spectra of a material are displayed as a graph with absorbance against wavelength; an example of an absorption spectrum is shown in Figure 1.7 [94]. The maximum peak of the data is known as the lambda max (λ_{max}), which can be used to compare different materials [95].

In regards to nanoparticles, light from the UV-vis range can excite and cause the oscillation of electrons on the surface of nanoparticles; this is called Surface Plasmon Resonance (SPR). The size and shape of a nanoparticle can influence its SPR which can shift the λ_{max}. Larger sized particles, generally more than 20nm, can red shift the λ_{max} and result in a longer wavelength. On the other hand, smaller sized particles generally less than 20nm can be blue shifted and produce a shorter wavelength. Agglomerations result in an overall larger particle size and can red shift the λ_{max} [96-98]. In terms of nanoparticle shape, Mie's theory explains that spherical nanoparticles produce a single SPR band, in contrast to anisotropic nanoparticles where two or more SPR bands can be produced on the absorption spectra depending on the shape [96, 99]. For example rod shaped nanoparticles can be detected with two bands of SPR; a stronger band corresponding to the electrons on the long axis of the particle, whilst a weaker band corresponds to the electrons on the short axis [98].

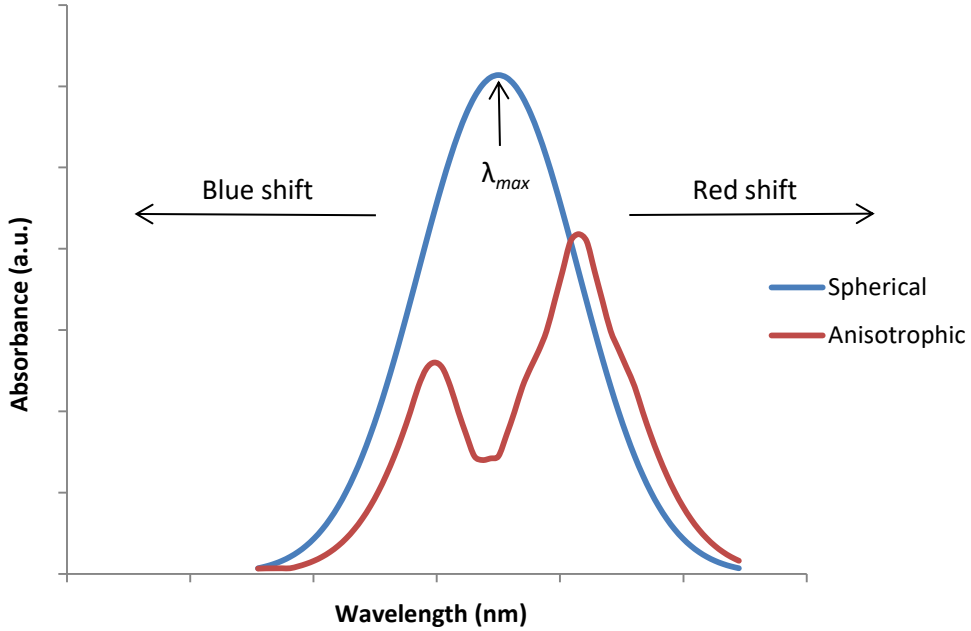

Figure 1.7: Example of nanoparticle UV-Vis spectra. Blue line represents spherical nanoparticles where one λ_{max} is obtained and red line represents anisotrophic nanoparticles where two or more absorbance peaks can be obtained. Blue shift (lower wavelength) is normally seen in smaller nanoparticles and red shift (increased wavelength) is seen in larger nanoparticles or agglomerations.

1.4 Pathogenic infection

Pathogens are defined as organisms that can cause disease in their host; they are taxonomically divided into viruses, bacteria and fungi. Although in the developed world, pathogenic infections are not the leading cause of mortality, they can prolong hospitalisation periods and outbreaks of pathogens, such as coronavirus (COVID-19), can cause many deaths and international health threats [100, 101]

Nosocomial and health-care associated infections (HAIs) are a type of bacterial or fungal infection that is contracted during treatment in hospital. In the UK, approximately 10% of patients acquire a HAI during their stay in hospital, which costs the National Health Service (NHS) roughly £1 billion per year. One of the major issues of HAIs is resistance against antibiotics causing delay in providing the

effective antibiotic or antibiotic cocktail, thus leading to longer hospitalisation and greater chances of mortality [102-104]. Although both types of bacteria are common in HAIs, Gram-negative bacteria are found to have a higher resistance against antibiotics [105, 106]. Overall, bacterial sizes vary from 0.5 µm to 5 µm in diameter [107]. Figure 1.8 shows a schematic diagram and TEM images highlighting the differences between Gram-negative and Gram-positive bacterial cell walls with scale bars for size reference [108].

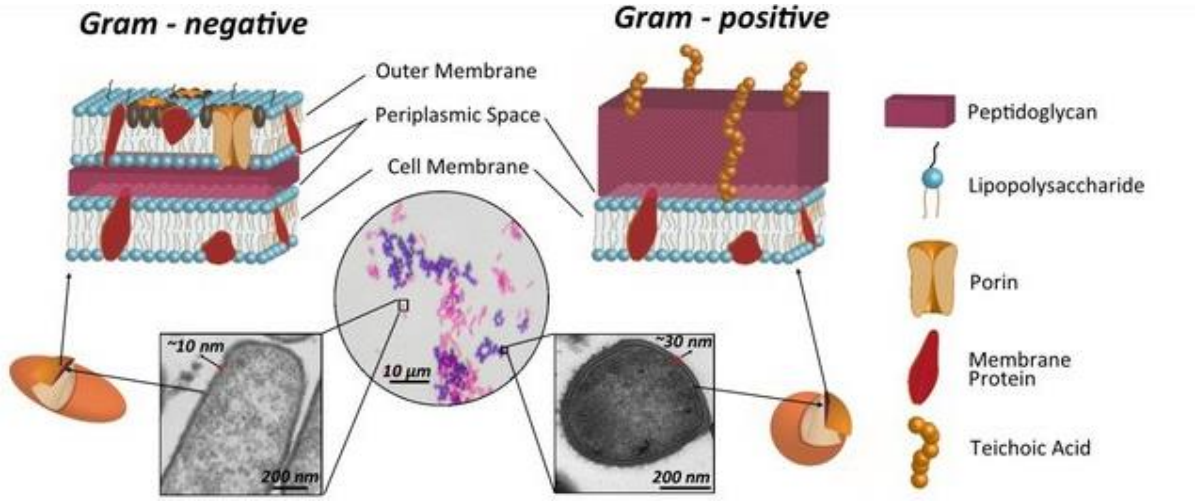

Figure 1.8: Schematic diagram and TEM images to compare Gram-negative and Gram-positive bacterial cell wall. Gram-positive cells have a thicker peptidoglycan which can retain crystal violet stain, resulting in purple colour. In contrast, Gram-negative have a thinner peptidoglycan, presence of outer membrane and forms a pink colour when Gram stained. Images are taken from Elbourne *et al.* (2019).

1.4.1 Gram-negative bacteria

The most common Gram-negative bacteria that cause HAIs are *E. coli*, *K. pneumoniae, Enterobacter* spp., *P. aeruginosa* and *Acinetobacter* spp. [109, 110]. Due to the outer bacterial membrane, Gram-negative bacteria are more likely to develop antibiotic resistance as antibiotics have to penetrate through the protective barrier [111]. The cell wall of a typical Gram-negative bacterium consists of three major layers: cytoplasmic membrane, peptidoglycan layer and a bilayer membrane consisting of lipopolysaccharides and phospholipids. When the Gram-staining

method is done, the cells produce a pink colour as a result from the bacteria's inability to retain crystal violet due to a thin peptidoglycan layer [112].

1.4.2 Gram-positive bacteria

In contrast, Gram-positive bacteria produce a purple colour after undergoing Gram-staining. The major layers of the cell walls of Gram-positive bacteria are slightly different to those of Gram-negative. A thicker layer of peptidoglycan, which contains teichoic acids, is able to retain crystal violet which results in the purple colour after treatment [112, 113]. In hospitals, Gram-positive bacteria commonly cause blood stream infections; the most frequent Gram-positive bacteria to cause HAIs are *Staphylococcus* spp., *Streptococcus* spp., and *Enterococcus.* Although compared to Gram-negative bacteria, the resistance levels to antibiotics are less, the UK's first resistant bacteria was Gram-positive [114, 115].

1.4.3 Fungi

The kingdom fungi are a separate branch of microorganisms and are harder to treat in comparison to bacteria, as fungi are eukaryotic cells, as are humans [116]. *Candida* infections are the most frequent type of fungal HAIs and are responsible for a large percentage of central venous catheter infections [117]. In comparison to bacteria and viruses, fungi on average have larger cells, with some length of yeast cells typically between 3-5 µm in diameter, but they can reach up to 100 µm in diameter during some stages of colonisation [118]. Figure 1.9 compares an SEM image of *C. albicans* cells to those of *E. coli* and *S. aureus* [119]. Although fungal infections can be treated with antifungal agents, a rise in resistance is seen, thus increasing mortality rate due to the delay in suitable treatment [120].

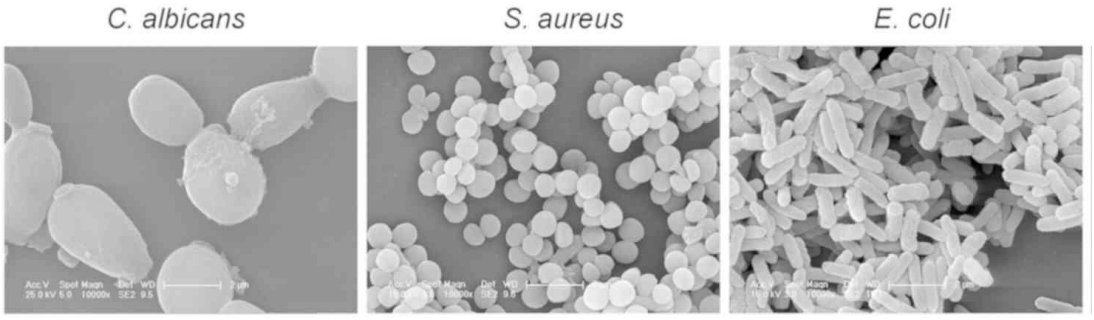

Figure 1.9: SEM images of fungi *C. albicans* and two bacteria, *S. aureus* and *E. coli*, for size comparison. Images adapted from Kong *et al.* (2019).

1.4.4 Virus

Lastly, viruses are one of the smallest types of pathogens, varying from 100 to 800 nm in size; comparison of *Salmonella senftenberg* bacteria and Ebola virus can be seen in Figure 1.10 for size differences [121]. Unlike the previous pathogens, viruses are protein capsids that depend on a host to replicate their genetic information. Due to this dependency, antibiotics cannot target or inhibit viruses; instead antiviral treatment can be prescribed [121, 122].

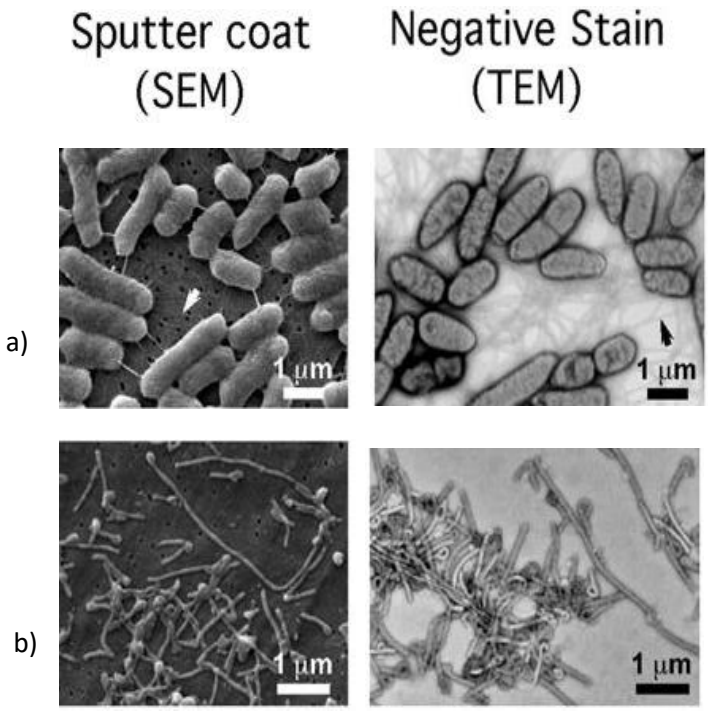

Figure 1.10: SEM and TEM comparisons of microbes. a) bacteria (Salmonella senftenberg) and b) viruses (Ebola). Images adapted from Golding *et al.* (2016)

1.5 Antimicrobial resistance

Antibiotics are a type of drug that inhibits the growth or destroys microorganisms; they are prescribed to treat and suppress bacterial infections but are not effective against viruses. The long-term or inappropriate use of antibiotics can lead to disruption of gut microflora, which causes diarrhoea for the user from the imbalance of microbes, and the development of antibiotic resistance in microorganisms. Penicillin was discovered in 1928 and further developed so that it could be prescribed in the 1940s; the extensive and sometimes unnecessary exposure to antibiotics resulted in the evolution of one of the first antibiotic resistant bacteria in 1962 in the UK [18, 115, 123]. It is estimated that antibiotic resistant pathogens cause an additional $20 billion cost in healthcare in the US and are responsible for an alarming annual death rate of 23,000. In 2017, the World Health Organisation (WHO) produced a priority list of pathogens that are in urgent need of new effective antibiotics due to the alarming rate of increase in antibiotic resistance. This list includes 12 species of bacteria, as shown in Table 1.3, and, unfortunately, most of them commonly cause infections in hospitals [18].

As a mechanism of action against microorganisms, antibiotics target certain pathways, such as cell wall synthesis [124]. However, microorganisms can prevent the accumulation of antibiotics to reduce and resist the antimicrobial effects. There are currently three main mechanisms of resistance: (1) mutations in the microorganism's outer membrane to allow a decrease of antibiotic uptake or increase in efflux of antibiotic from the cells; (2) change in the target site where the antibiotic attaches to the microorganism (commonly due to spontaneous mutation) thus reducing the sensitivity to the antibiotic and (3) the production of inactivating enzymes [124-127].

Table 1.3: WHO priority list of pathogens that urgently require new antibiotics. As a result of multiple-antibiotic resistance, the 12 listed bacteria are in priority for the discovery of new antibiotics as they pose threat to human health with current limited treatments [18].

	Bacteria	**Antibiotic resistance**
Critical	*Acinetobacter baumanii*	Carbapenem-resistant
	Pseudomonas aeruginosa	Carbapenem-resistant
	Enterobacteriaceae	Carbapenem-resistant
High	*Enterococcus faecium*	Vancomycin-resistant
	Staphylococcus aureus	Methicillin-resistant, vancomycin-intermediate and resistant
	Helicobacter pylori	Clarithromycin-resistant
	Campylobacter spp.	Fluoroquinolone-resistant
	Salmonellae	Fluoroquinolone-resistant
	Neisseria gonorrhoeae	Cephalosporin-resistant, fluoroquinolone-resistant
Medium	*Streptococcus pneumoniae*	Penicillin-non-susceptible
	Haemophilus influenza	Ampicillin-resistant
	Shigella spp.	Fluoroquinolone-resistant

Similarly to antibiotics, antifungal drugs are used to treat fungal infections. Although fungal infections are not as common as bacterial infections in humans, antifungal drug resistance has also been seen in fungal species. Due to the low occurrence of these infections, less research and development has been done on new antifungal drugs; however existing available treatments are limited. The similarity between fungal cells and human cells (as they are both eukaryotic) causes limitations for novel antifungal targets.

Currently, the most common antifungal drug mechanism of action targets RNA synthesis and the cell wall. Other mechanisms of action include targeting the membrane lipid ergosterol, for example azole antifungal drugs can inhibit ergosterol biosynthesis. Antifungal resistance of fungi is mainly due to: (1) changes in fungal target enzymes, membrane lipid composition or cell wall composition leading to reduced uptake of the antifungal drug or affinity between antifungal drug and fungi; (2) activation of an efflux pump to reduce accumulation of the antifungal drug and (3) production of biofilms [128].

1.6 Routes to transmission

Due to the increasing population density and the common use of touch technology, it has been found that microbes, including opportunistic pathogens and antibiotic resistant strains, are easily transmitted across surfaces [129, 130]. Commonly touched objects like computer mice, shopping cart handles, mobile phones and elevator buttons, are highly contaminated with bacteria and disinfectants can only partially clean the devices [130, 131]. Moreover, Reynolds *et al.* (2005) showed that spread of 86% of pathogens was linked to contact with hands [132].

The presence of bacteria and fungi is particularly problematic in environments such as hospitals because it can lead to infections, especially for those who are immunocompromised [106]. Microbial contamination can be transmitted through physical contact, airborne and droplet transmission [133]. Whilst some routes may be harder to control, certain procedures are set in place to reduce the microbial growth. For example, catheters are commonly used in hospital for the insertion into or release of fluids from the body. Prior to insertion of venous catheters, the skin of

the patient must be sterilised with antiseptics and catheter tubes are recommended to be replaced at least every 72 to 96 hours to minimise microbial colonisation [134, 135]. Some catheters, depending on the location and clinical indication, can be used for longer. For example, urinary catheters can be used for up to 8 days before replacement; however, it has been reported that the reduction of catheter duration decreases the length of hospitalisation and risk of infection [136]. Even with these precautions in place, it has been reported that central line catheters are responsible for 87% of primary bloodstream infections and catheters are associated with 95% of urinary tract infections in the United States [137]. Hence the investigations of antimicrobial materials are required to reduce and prevent microbial infections that can lead to morbidity and burden the health economy.

1.7 Metallic nanoparticle mechanism of action against microbes

Certain metals, especially silver and copper, have been known to exhibit antimicrobial activity against bacteria for thousands of years. The nanoscaled versions of these metals have shown enhanced antimicrobial properties and have been utilised in various applications, however their exact mechanism of action is not fully understood. It is believed that there are several possible mechanisms of action; these theorised mechanisms of action include: 1) increased production of reactive oxygen species (ROS), 2) cell membrane interaction, 3) release of ions and 4) enzyme inhibition. Some mechanisms may overlap between the categories and in addition, multiple mechanisms can occur simultaneously which reduces the development of resistance against nanoparticles [138-140]. Figure 1.11 summarises the potential mechanism of action of nanoparticles against bacterial cells. Unlike mammalian cells, bacterial cells contain a cell wall; Gram-positive bacteria cell walls consist of a thick peptidoglycan layer and Gram-negative bacteria cell walls comprise of a thin peptidoglycan layer surrounded by an additional lipopolysaccharide outer membrane. Within the wall, other components may be present such proteins, which include the electron transport chain. Due to the presence of negatively charged groups embedded within the walls, such as phosphate, carboxylate, and sulphate, the bacterial cell wall has an overall negative surface charge which can lead to the attraction of nanoparticles, and interactions which can lead to cell death [105, 138].

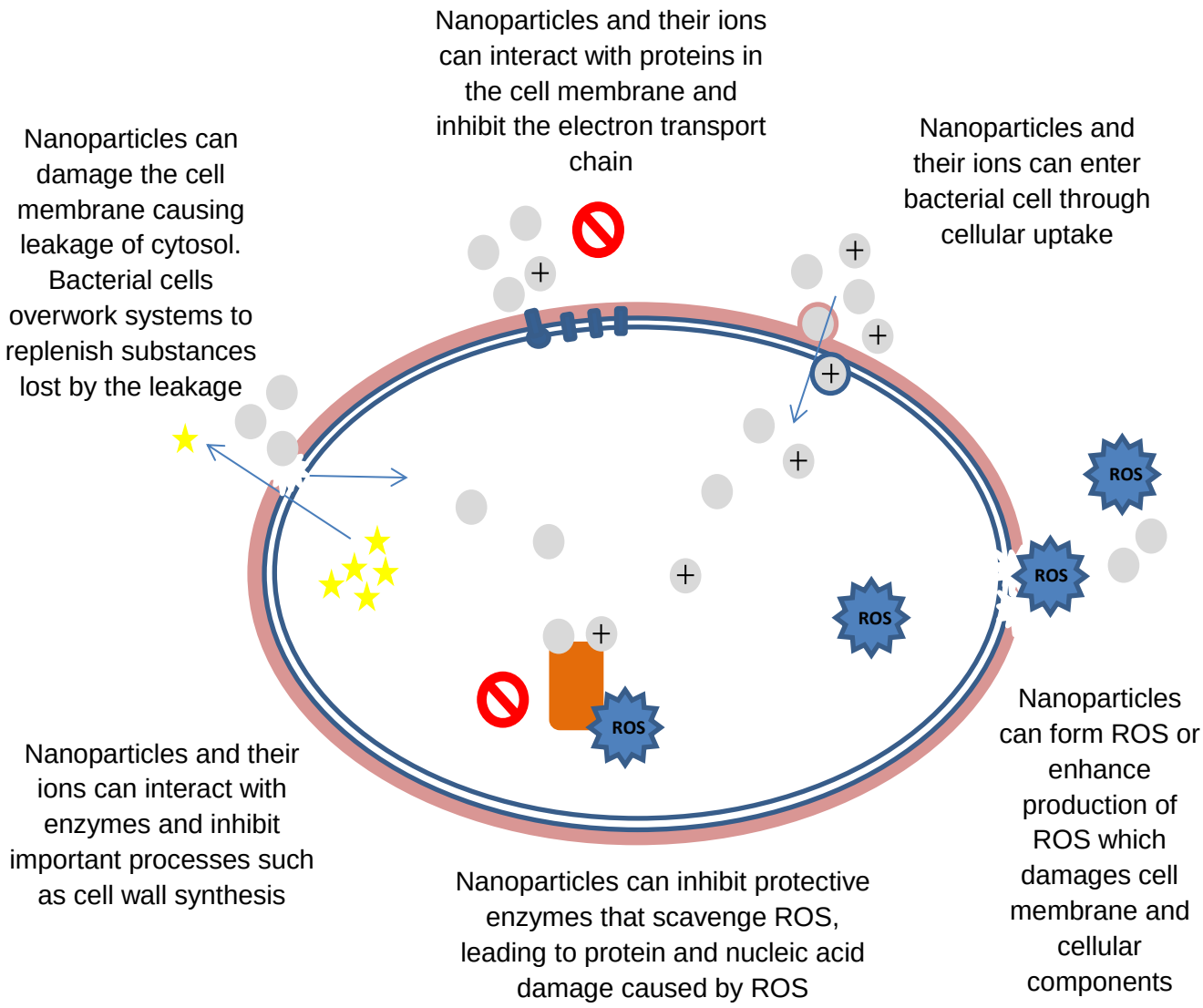

Figure 1.11: Schematic diagram of possible nanoparticle mechanism of action against bacteria. Grey spheres are used to represent nanoparticles; those with plus sign are used to represent nanoparticle ions - however nanoparticles can vary in shapes. Yellow stars are used to represent bacterial cytosol and nutrients contained within.

1.7.1 Cell membrane interaction

The interaction between nanoparticles and bacterial cell wall can result in membrane damage through alteration of cell membrane charge and formation of ROS (this will be explained further in later section). The cell wall functions as a barrier to protect and contain all the components inside the cell. In addition, various metabolic pathways, such as the electron transport chain, are located inside the cell wall. Damage to the cell membrane caused by nanoparticles can lead to uncontrolled leakage of the cytosol and reduction in adenosine triphosphate (ATP) production. Cells may increase the metabolic activity and ions to compensate for the loss caused by the leakage; however the high demands can lead to severe damage to these systems [138, 141]. This type of mechanism has been seen in silver nanoparticles with the interactions observed scanning electron microscope (SEM) and transmission electron microscope (TEM) [142, 143].

Upon interaction with the cell membrane, it has been observed that nanoparticles, in particularly those below 100nm, are able to enter the bacterial cell through cellular uptake. Once internalised, the nanoparticles can cause more damage by interacting with cell components leading to inhibition of essential pathways such as protein synthesis [138].

As a whole, nanoparticle interactions with bacterial cell membrane results in cell wall damage, ion and ATP depletion, cellular uptake, essential pathway disruption and ultimately cell death [138, 141].

1.7.2 Release of ions

Similar to cell membrane interaction mechanism, nanoparticles can produce ions which can interact with the cell membrane and internal cellular components. Damage to the cell membrane can occur through positive ions inducing a difference in surface charge and through the interaction and inhibition of membrane proteins such as the electron transport chain [138, 144]. Ions can enter the cell through transport protein, whilst certain ions, such as Ga^{3+}, have been found to be mistaken for nutrient (due to its chemical similarity to Fe^{3+}) and enter the cell via active uptake [145, 146]. Once inside, ions can cause damage through the interaction with proteins and nucleic acid functional groups, which can lead to structural changes, deoxyribonucleic acid (DNA) damage, ROS generation and disrupt enzyme activity [138, 144].

1.7.3 Enzyme interaction

As stated previously, nanoparticles and their ions can interact with internal cellular components of bacterial cells. Some of these components are enzymes and the inhibition can cause disruption to essential processes within the cell [144]. For example, Li *et al.* (2010) found evidence that silver nanoparticles deactivated respiratory chain dehydrogenase and therefore inhibited cellular respiration [147]. Other examples include inhibition of phosphatemannose isomerase (cell wall synthesis enzyme), interaction with nicotinamide adenine dinucleotide (NADH) dehydrogenase (respiratory chain reaction enzyme) and superoxide dismutase (superoxide-radical scavenging enzyme); the interactions between nanoparticles and these enzymes could lead to inhibition of cell wall synthesis, inhibition of respiration and increased generation of ROS, respectively [139, 148-151].

1.7.4 Reactive oxygen species (ROS)

Like enzyme interaction, ROS is linked to other mechanisms of action as other interactions can lead to the excess ROS generation. ROS is a group of reactive species that contain oxygen; these include radicals (superoxide anion and hydroxyl radicals), single oxygen and hydrogen peroxide [138]. Bacterial cells have mechanisms to protect cells and repair damaged cells against low concentrations of ROS. However, bacteria cannot cope with high concentrations, thus leading to oxidative stress caused by ROS. Oxidative stress can result in cell membrane damage, protein and nucleic acid degradation, and eventually cell death [138, 152, 153]. Nanoparticles can produce ROS through reduction of oxygen and oxidation of water to damage bacterial cells or through enhanced expression of inflammatory cells and oxidation promoting metabolic enzymes. Additionally, nanoparticles can inhibit protective enzymes that scavenge for ROS thus preventing bacterial protective mechanism [151, 154, 155].

1.8 Current applications of antimicrobial nanomaterials

With the range of useful properties that nanoparticles exhibit, there are currently products and applications with incorporated nanoparticles. Although some are still at prototype stages, a few are already commercialised. However, they are not commonly used for several reasons such as cost or low antimicrobial efficiency; hence updated antimicrobial nanotechnology is required.

1.8.1 Surface films and coating

One of the most well-known applications of antimicrobial nanomaterials is the coating of silver nanoparticles on the surfaces of objects such as laptops and keyboards [156]. Recently, Corning® has produced an antimicrobial glass for electronic mobile devices. Corning® Gorilla® Glass 3 is a scratch-resistant glass with incorporated silver to produce antimicrobial effects. Muzslay *et al.* (2014) reported that the glass was effective at reducing MRSA and *K. pneumonia* contamination [157].

In 2016, diarrhoeal disease was the ninth highest cause of death globally. The primary cause of diarrhoea is through the consumption of food or water that is contaminated with bacteria including pathogenic strains of *E. coli* [158]. To control contamination and to extend the life of fresh vegetables, fruit juice and meat, antimicrobial nanoparticles are incorporated into prototype food packaging but studies are still required to understand leaching and effects of nanoparticle consumption. Ahmed *et al.* (2018) used a compression moulding technique to produce plasticized polylactide composite films containing bimetallic silver-copper nanoparticles and cinnamon essential oils. The film was found to have antibacterial activity against common pathogens found on chicken meat [159]. Similarly, to produce antimicrobial low density polyethylene (LDPE) films, Emamifar *et al.* (2010) mixed Ag and ZnO nanoparticle powders with LDPE resin pellets in an extruder machine and a blowing machine to produce a 50 µm thick nanocomposite film. Antimicrobial activity tests against *L. plantarum* were done and showed that nanosilver films were more effective than nanozinc oxide films [160]. Lastly, An *et al.* (2008) generated a silver nanoparticle polymer-based coating for vegetables by adding silver nitrate to polyvinylpyrrodlidone followed by glycerol. Asparagus spears were immersed in the coating and it was found to prolong their life when evaluating the firmness, weight loss and colour [161].

1.8.2 Fabrics and fibres

Textile fibres have been incorporated with nanoparticles to produce clothing and shoe pads with special properties [162]. The addition of antimicrobial nanoparticles is primarily used to exploit their antimicrobial properties to decrease odour producing bacteria and fungi, but recent studies are investigating the applications to reduce

bacterial contamination that may cause disease [163-166]. Studies have shown a variety of ways to produce nanoparticle incorporated fibres, with silver as the common antimicrobial nanoparticle. Gerber *et al.* (2011) prepared silver-tricalcium phosphate nanoparticles using flame spray synthesis and generated polyamide fibres with incorporated nanoparticles through the process of extrusion and melt-spinning fibres. The polymer fibres were able to effectively destroy 99.99% of *E. coli* and 99.6% of *S. sanguinis* within 24 hours [167]. Alternatively, Zhang *et al.* (2012) immersed cotton fabrics with chitosan and $AgNO_3$ nanoparticle solutions to produce cotton fabrics with silver nanoparticles. The fabrics were able to inhibit *E. coli* and had less fabric colour change after 81 washes [168]. Lastly, pressurised gyration was used by Illangakoon *et al.* (2017) to produce nanoparticle embedded polymer fibres, with the application of antimicrobial filters that were successful at reducing *P. aeruginosa* [169]. Figure 1.12 schematically illustrates a modified gyration apparatus used for this production.

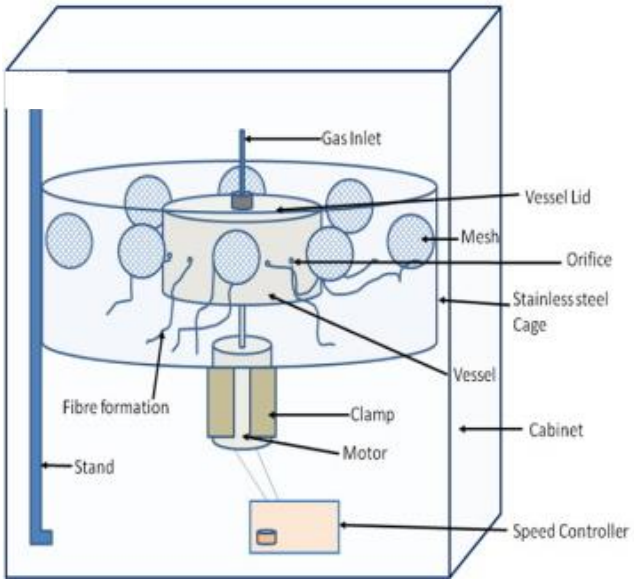

Figure 1.12: Schematic diagram of modified pressurised gyration rig used to collect nanoparticle incorporated fibre discs. Polymer solution is spun under pressure to form fibres on the inside surface of the stainless steel cage. Image was taken from Illangkoon *et al.* (2017),

1.8.3 Healthcare applications

Contaminated surfaces are one of the leading causes of hospital infection transmission; some bacteria and fungi can survive for up to four months on inanimate surfaces [170, 171]. To reduce pathogens on contaminated surfaces, paints have been treated with nanoparticles to produce an antimicrobial coating finish that protects and prevents surfaces from supporting bacterial or fungal growth. Oil-based antimicrobial paints are increasingly used in hospitals to provide a reduced pathogenic environment on wooden, glass and polystyrene surfaces [172]. Equally, antimicrobial polymer coating has been developed to protect devices made from stainless steel, glass or polyvinyl fluoride. However, studies have shown that antimicrobial nanoparticle containing paints and coating are effective against only limited types of bacteria [173].

Furthermore, some medical implant devices have antimicrobial nanoparticle coating to reduce infections and/or surgical complications – for example titanium oxide nanoparticle coating on heart valve implants is used to inhibit *Streptococcus* species and *E. coli* [174, 175]. Other types of implants made with nanoparticles include silver incorporated polymer catheters [176, 177].

Lastly, wound dressings infused with nanoparticles have been shown to be particularly useful in decreasing the risk of infections in wounds and aiding the healing process. The current commercial dressing, Biatain® AG non-adhesive foam dressing, contains a silver complex that is effective at inhibiting *S. aureus* and other bacteria [178, 179].

1.9 Potential antimicrobial biomedical nanopolymers

The general term biocompatibility describes the compatibility between the material and living tissues; these include no causation of toxicity or immune response when the material is exposed or interacts with the body or body fluids [180]. Biocompatibility properties of materials are essential and are required when used in contact with live animals and humans to avoid adverse effects such as rejection, foreign body reaction, fibrosis or death of the patient [180-182]. Materials that meet biocompatibility requirements can be used as biomedical devices with applications that include temporary or permanent contact with the body [182, 183]. Temporary applications include catheters and surgical sutures, and permanent applications

include orthopaedic implants and dental implants [135, 184, 185]. Biocompatible materials are also used in tissue engineering to synthesise tissue or organs outside the body for replacement and in cosmetic applications, such as soft tissue augmentation (e.g. implants of silicone gel or saline filled silicone shells for breast augmentation) [183, 186].

Although biocompatibility is one of the most important properties for implants, there are also other important properties. As the body is continuously in motion, and exercise and emotions can cause sudden movements, the material must have mechanical strength properties to withstand shock [182]. Furthermore, the healthy human body is constantly at a temperature of 37^{o}C (±0.5); the temperature may increase during illness and hyperpyrexia, and decrease during hypothermia [187]. Therefore, the materials must function within those temperature ranges and without changes in their properties. Certain implants are more complicated as they are devices that require electricity, for example a pacemaker. A surface coating that insulates electricity is required to prevent leakage of electricity from the device that can potentially cause health risks to the patient, and also to prevent electrical impulses from the patient causing interference with the device [182].

As the human body includes various components, different polymers will be suitable for different regions of the body. Dependent on the application required, the choice of polymer can vary in the biomedical industry; there are some biocompatible polymers for biomedical applications and potential nanoparticle incorporation for antimicrobial polymers [182].

1.9.1 Polydimethlysiloxane (PDMS)

Since the successful synthesis of silicone in 1950, polydimethylsiloxane (PDMS) has been widely used for biomedical applications and electronic chip components. This synthetic silicone-based polymer is cheap to manufacture and mainly consists of repeated silicone, oxygen bonds and methyl groups. By substituting the PDMS methyl group with another one (e.g. phenyl), the properties of the PDMS can be altered for various applications. General properties of PDMS include flexibility, elasticity, optical transparency and low manufacturing costs. In terms of biomedical applications, further properties of PDMS allow versatile applications [188]. Firstly, PDMS is highly permeable. The ability to allow the diffusion of gas through the

material enables PDMS to be used for a contact lens, to grow artificial skin and for cell culture testing [188, 189]. Furthermore, biocompatibility of PDMS supports the material to be used in contact with biological tissue. It has been found that PDMS is non-toxic and triggers a minimal inflammatory response. Therefore, PDMS have been used to make or coat medical implants such as catheters and micro valves [188].

Although there are many beneficial properties of PDMS, the hydrophobicity of the material can lead to adhesion of microbes to the surface and promote microbial infections [190]. A possible solution to reduce infection would be the incorporation of antimicrobial agents into the PDMS. There are several ways reported to incorporate antimicrobial agents into polymers; for example the antimicrobial subtilisin enzymes can be immobilised into a polymer [191]. Similarly, using electrostatic adsorption, polymers can be coated with silver nanoparticles that exhibited antibacterial properties [192]. Alternatively, air plasma treatment can be used to embed silver nanoparticle seeds onto the surface of PDMS films and further chemical treatments can result in a coating of silver ions [190]. Moreover, synthesis of nanoparticles on PDMS film have been produced through a reduction in metal salts [193]. Although these methods have been tested to provide antibacterial activity, some processes require high energy and take a long time.

1.9.2 Polyvinyldiene Fluoride (PVDF)

PVDF is a strong biocompatible polymer that is cost-effective to produce via a polymerization process. Whilst PVDF is a chemically inert polymer, its piezoelectric effect can encourage wounds to heal making it advantageous for surgical sutures and potentially a ‘Nanogenerator’ [182, 194]. However, it has been found that PVDF produces films with rough surfaces and low thermal stability. Additionally, it has poor adhesion to other materials, thus PVDF is hardly used to coat implant devices. Despite its poor material adhesion, Guo *et al.* (2012) developed scaffolds of polyurethane (PU) and PVDF by electrospinning. This produced biocompatible material, which was able to enhance the activity of fibroblast, with piezoelectric properties (from PVDF) and mechanical properties (from PU) [195]. Furthermore, gold nanoparticles were successfully incorporated to PVDF to produce a film [196]. Although antimicrobial tests were not performed, the addition of antimicrobial

nanoparticles could potentially produce an antimicrobial material; thus it could be considered for wound healing biomedical applications.

1.9.3 Poly(methyl methacrylate) (PMMA)

One of the most commonly used materials for oral dentures is PMMA. This acrylic material has many advantageous properties such as biocompatibility, lack of taste, odour or toxicity, ease of fabrication and moulding, and it can adhere to teeth well. Whilst its properties result in frequent use in dentistry, the applications are not limited and there are other biomedical applications including intraocular lens, rhinoplasty and as bone cement [182, 197].

Unfortunately, bacterial adherence on PMMA is a microbial implication especially when it is used as oral dentures and intraocular lenses [198, 199]. Firstly, intraocular lenses are implanted after cataract operations. Although it is rare, endophthalmitis can develop as a result of bacterial colonisation and it has been found that bacteria are 20 times more likely to adhere to intraocular lenses made of PMMA than those made from hydrogel [199]. Similarly, PMMA oral dentures can promote bacterial adhesion and formation of biofilms; this can lead to infections such as gingival inflammation and other problems including bad breathe [198]. As a result, investigations have suggested the incorporation of nanoparticles can reduce bacterial adhesion. For example, the addition of 3 wt % of titanium dioxide into PMMA reduced 92% of *P. aeruginosa* surface attachment [200].

1.9.4 Poly(ethylene terephthalate) (PET)

Belonging to the polyester family, PET polymers are usually made from an ester exchange reaction. Due to its biocompatibility, mechanical properties and abrasion resistance, PET is frequently used in polymers for biomedical applications. This material can be found in a range of healthcare products including heart valves, catheters and sutures [201, 202]. In addition to biocompatibility, it has been found that PET implants can recruit endothelial cells and promote healing. A surface coating can be combined to enhance their application, for example a coating of collagen or albumin can be found on PET vascular devices which reduce blood loss and rate of infection [203].

However, bacteria can easily adhere onto PET surfaces, thus resulting in unwanted contaminations and possible infections [201, 202]. In comparison to PMMA, PET

surfaces had more bacterial attachment and denser biofilm colonisation [198]. Surface modification of PET has been investigated to reduce contamination, such as insertion of alkyl and hydroxyl groups [201].

1.9.5 Polycaprolactone (PCL)

PCL is a FDA-approved polymer that has been utilised as biomaterials due to their useful properties. In addition to being a biodegradable and biocompatible polymer, PCL has strong mechanical properties and provide suitable environment for cell and tissue regeneration [204, 205]. Commonly, PCL has been used within bone tissue engineering to provide scaffolds implants; with melting points of 55-60°C, PCL scaffolds can be 3D printed into required size and shape [206].

Despite their useful applications, biomedical implants are often associated with bacterial infections as microbes can adhere to the surface of implants [207]. Fortunately PCL can be used as antimicrobial carriers to deliver antibiotics. For example, PCL coating with vancomycin antibiotic was able to produce a sustainable release of vancomycin, which is commonly used to treat MRSA [208]. Furthermore, electro-spun PCL with the addition of CuO nanoparticles have been reported to exhibit antimicrobial properties against several microbes including *S. aureus, E. coli* and *P. aeruginosa,* and has been suggested to be useful in wound dressing applications [209].

1.9.6 Polyethylene oxide (PEO)

PEO, also known as polyethylene glycol (PEG), are polymers of ethylene oxide. Typically, PEO has a higher molecular weight (above 20,000 g/mol) in comparison to PEG with a molecular weight of less than 20, 000 g/mol [210]. As a FDA-approved polymer, PEO has many useful properties including low toxicity, biocompatibility and water solubility. As a result, PEO has been utilised in biomedical devices such as tissue scaffolding, drug delivery and surface coating [211, 212].

The surface of PEO has resistance to the adhesion of biomolecules; therefore PEO can be used as a surface coating to prevent protein and cell adhesion [213]. Similarly, it has been found that the microbial adhesion towards PEO is more weak in comparison to glass surfaces [214]. PEO polymers can also act as a carrier polymer for drug release [215, 216]. Consequently, the addition of antimicrobial agents to materialise antimicrobial polymer blends involving PEO has been

investigated. For example, PEO carrying antibiotics doxycycline has been incorporated into PMMA polymer and electrospun to produce fibres with antimicrobial properties against *S. mutans* [216].

1.10 Surface treatment of nanomaterials

While the incorporation of antimicrobial nanoparticles into polymers seems promising, polymers can be biologically inert and/or cover the nanoparticles leaving the surface unexposed and unable to produce antimicrobial activity. Surface treatment may be required to activate the material by altering the surface morphology (e.g. roughness) or chemical properties (e.g. hydrophobicity); this can be done through different ways, although not all are considered to be effective at enhancing antimicrobial activity of nanoparticle incorporated polymers [217, 218].

1.10.1 Physical treatment

The surface of polymers can be treated physically to alter the roughness at the micro or nanoscale. This results in changes to the wettability to a more hydrophobic state. In comparison to other surface treatments, this method is cheap and simple [218]. For example, Xu *et al.* (2011) demonstrated physical treatment of polyethylene film, by laminating the film against a wire mesh template and removal of cooled set film. This method resulted in super-hydrophobicity and abrasion resistance [219]. Although super-hydrophobic materials can reduce bacterial adhesion to the surface, antimicrobial agents (if present) may have reduced efficacy from the limited contact between microbes and surface [220].

1.10.2 Chemical treatment

Generally, chemical surface treatment involves dipping or spraying a polymer with liquid chemicals to alter the surface properties. Although this method can treat large scale polymers at low costs and remove presence of debris and microbes, post washing and drying of the sample may be required; thus production of hazardous waste will need to be considered when selecting the chemicals [218]. The surface treatment of polymer films to enhance the wettability through chemical treatment has been demonstrated by Fávaro *et al.* (2007). The use of potassium permanganate in hydrochloric acid solution resulted in oxidation and hydrolysis of polymer surface which increased the hydrophilicity [221]. Alternatively, amine groups can be chemically coupled onto resin to increase the adhesion of metals [222]. Chemical

surface treatment can potentially activate the antimicrobial activity of nanoparticles incorporated in polymers.

1.10.3 Plasma treatment

Plasma treatment can modify the surface of polymers by exposing them to inert gases containing particles; for example gases such oxygen, nitrogen and hydrogen, and particles including ions, radicals and free electrons [218]. Generally, the treated surface results in an increase of hydrophilicity and adhesion, although other changes have been observed. Masruroh and Santjojo (2018) investigated plasma treatment using nitrogen gas on polystyrene film and decreased surface roughness and contact angle; thus the film became more hydrophilic. This was due to the nitrogen radicals inducing a reactive surface on the polystyrene leading to breakage of hydrogen bonds and production of new functional groups [223]. On the other hand, Chen *et al.* (2012) used O_2 plasma to activate a polydimethylsiloxane (PDMS) surface. The treatment resulted in increased hydrophilicity and the formation of silanols [224].

1.10.4 Ultraviolet radiation treatment

Originally, UV radiation treatment was used to harden materials through polymerization. However, due to its effective and economical ability to alter the surface properties, UV radiation can be used to treat certain polymers, usually to enhance hydrophilicity and adhesion. When a polymer is UV treated, free radicals are produced through oxidation of the polymer surface. Oxygen or ozone can react with these radicals leading to the formation of carbonyl and carboxyl groups [218]. Toworfe *et al.* (2003) explored UV treatment on PDMS films. It was found that the hydrophilicity increased with treatment time; however the thickness of the film decreased with treatment time [225]. Furthermore, Formosa *et al.* (2008) investigated the application of UV radiation on PET. IT was found that the treatment increased the hydrophilicity and accelerated endothelialisation of cells [226]. The increase in hydrophilicity could potentially increase the contact between microbes and antimicrobial nanoparticle incorporated polymer materials.

1.10.5 Thermal annealing treatment

The strength of a polymer can be enhanced by thermal annealing. This process involves an increase of temperature during fabrication and slowly cooling down of

the polymer to set it. The heat during production induces changes to the polymer's properties and morphology. As a whole, polymers tend to cross link and produce high crystallinity, leading to increased strength and elasticity [218]. Thermal annealing of polylactic acid (PLA) was studied by Vadas *et al.* (2020). At an annealing temperature of 85°C, it was found that the procedure increased crystallinity which resulted in heat resistance and increased polymer strength by 120-200% [227]. Whilst thermal annealing can transform polymers with beneficial properties, it has been found that higher temperatures can induce cracks on the polymer surface [228]. Depending on the scale of the induced cracks, this method can potentially expose antimicrobial nanoparticles incorporated into polymer materials.

Chapter 2 General materials and methods

2.1 Nanoparticle suspension

In general, nanoparticles used in this study were either engineered using patent Tesima^{TM} plasma process, gifted by European Commission or purchased from manufacturers. For information about individual nanoparticles, please refer to section 3.2. All nanoparticle powders were stored at room temperature in the dark and used as received or otherwise descriptions can be found in section 3.2, 4.2, 5.2, 6.2 or 7.2. Nanoparticle suspensions were prepared as a 0.5 wt/v% (5000µg/ml) water based stock suspension. Desired mass of nanoparticles was measured into sterile Eppendorf tubes on analytical scales (Fisher Scientific, UK) and poured into sterile Falcon tubes. Corresponding volumes of sterile pure water (Acros, UK) were added using a sterile syringe or pipette, and mixed with vortex (Fisherbrand, UK) for a few seconds. The suspension was sonicated for 2 minutes (pulse sequence applied for 20 seconds followed by 5 second rest) at 40% using a high frequency liquid processor (FisherBrand120, Fisher Scientific, UK) or Vibra-cell750 (Sonics & Materials®, USA) and cooled with cold tap water immediately after. The suspensions were stored at room temperature until required. Further dilutions were made by dispersing stock in a Fisher Brand Ultrasonic bath (Fisher Scientific, UK) for 1 minute and diluting with sterile pure water. An addition of ammonium hydroxide (NH_4OH, 4%) at 2% of the suspension was added for samples containing silver.

2.2 Microbial cultures

A. baumannii was purchased from Public Health England and the remaining microbes were kindly provided by the University of Hertfordshire microorganism collection.

2.2.1 Cultures on solid media

Bacteria and fungi were sub-cultured onto nutrient agar and yeast peptone dextrose (YPD) agar, respectively (see Appendix for agar preparation protocol), using a sterile loop. These agar plates were incubated for 24 hours at an optimal temperature of 37°C for growth, and then stored at 4°C until required. The stored agar plates were regrown every month to ensure viability of microbes.

2.2.2 Cultures in aqueous media

Bacteria and fungi were sub-cultured into broth media (see Appendix for broth preparation protocol). Using a sterile loop, bacteria or fungi was transferred from an agar plates into universal tube with nutrient broth or YPD broth, respectively. These tubes were incubated for 24 hours in a MaxQ8000 incubated shaker set at 37^{o}C and 180 rpm. Cultures were used immediately and discarded after use.

2.3 Software

Unless stated, all schematic diagrams were created using Microsoft PowerPoint 2010, except for Figure 0.1 which was made using Biorender.com (free basic version) and for Figure 3.6 which was made using ChemDraw 21.0. All quantitative data analysis was performed on Microsoft Excel 2010, except for built in software analysis on certain equipment such as ZetaSizer and Tensiometer. All qualitative data analysis was performed on ImageJ (1.52a free version).

Chapter 3 Effects of nanoparticles on common nosocomial pathogens

3.1 Introduction

Nosocomial infections are defined as infections contracted during hospitalisation which were absent before admission. Up to 10% of hospital patients are affected by nosocomial infections, with higher risks for patients that are in the intensive care unit, burn unit, neonatal care, are immunocompromised or undergoing organ transplant surgery [13, 104, 229]. Annually, almost 99,000 deaths in the United States and 90,000 deaths in Europe are due to nosocomial infections [230, 231]. Although antibiotics and antifungal treatments can be prescribed to treat these infections, the high mortality rates are linked to the antibiotic resistance of pathogens causing nosocomial infections, which limits the availability and effectiveness of treatments for these infections [232]. As a result, these infections can lead to longer hospitalisation periods, increased mortality rates and higher costs [13, 104, 233].

In 2017, WHO provided a list of 12 antibiotic resistant pathogens that urgently require the development of new antibiotics to combat the threat of resistance. Unfortunately, a large proportion of microbes on the list are common nosocomial pathogens, such as *Acinterbacter baumannii, Pseudomonas aeruginosa* and *Staphylococcus aureus* [13, 234]. Furthermore, in the last 20 years, only 6 new classes of antibiotics have been approved; however, they have been effective only towards Gram-positive bacteria [235].

Certain nanoparticles have shown antimicrobial activity and are potentially an alternative in combating microbes and their antibiotic resistance. With dimensions typically less than 100 nm, nanoparticles have gained in interest and have been employed in biomedical applications. Studies have reported promising results with nanoparticles, in particular metallic nanoparticles, with effective antimicrobial activity against both fungi and bacteria including those that cause nosocomial infections [6, 22]. While certain compositions of nanoparticles may present toxicity to humans, especially at high concentrations, graphene-based nanoparticles have shown antimicrobial activity with less toxicity towards mammalian cells [54].

Although certain nanoparticles have shown potential in antimicrobial applications, only a limited number of nanoparticles and pathogens have been tested [6, 22, 236]. Therefore, the investigation of nanoparticles for antimicrobial activity against nosocomial pathogens is essential.

Outline of the research work:

This chapter investigates the antimicrobial activity of 26 different nanoparticles with aim to select those with the highest efficacy for further study. A range of nanoparticle compositions including metallic, oxides, carbon-based and formulations are tested against a broad variety of Gram-negative bacteria, Gram-positive bacteria and fungi. These microbes were selected due to their common occurrence to cause nosocomial infections and are listed as a critical priority for new antibiotics by WHO. An initial antimicrobial screening was performed on all nanoparticles by using the agar well diffusion method and the broth inhibition assay (Section 3.2.1 and 3.2.2). Nanoparticle samples that showed antimicrobial activity were then tested further for their efficacy by investigating the minimal inhibitory concentration (section 3.2.2). Based on the results, the selected nanoparticle was then further studied to investigate the microbial reduction and viability over a time period (section 3.2.3 and 3.2.4).

3.2 Materials and methods

Initially, 26 nanoparticles were investigated for antimicrobial activity against 10 microbes to identify ones with antimicrobial activity. Based on results, nanoparticles with good antimicrobial activity were selected for further efficacy tests. Table 3.1 summarises the microorganisms used in this study. Cultures were prepared using protocols in Chapter 2, section 2.2. Table 3.2 summarises the manufacturer details for all the nanoparticle powders used in this study. In particular, all the QNA products were engineered using the patented Tesima^{TM} plasma process by Ren *et al.* (2013). Nanoparticle stock suspension was made then further diluted to stated concentrations following the protocol in Chapter 2, section 2.1.

Table 3.1: Microorganisms used in this study

	Microorganism	**ATCC**	**Biosafety level**
Gram-negative	*Acinetobacter baumannii*	19606	2
	Pseudomonas aeruginosa	25668	2
	Klebsiella pneumonia	15380	2
	Escherichia coli	*	1
	Salmonella typhimurium	*	1
Gram-positive	*Enterococcus faecalis*	29212	2
	Staphylococcus aureus	*	1
	Streptococcus pyogenes	*	1
Fungi	*Candida albicans*	2091	1
	Candida tropicalis	20336	1
*Lab strain of microorganisms without an ATCC identification			

Table 3.2: Summary of nanoparticles used in this study. Nanoparticles were separated into four categories based on their composition. Where available, manufacturer notes on particle size range (nm) are included, * indicates no manufacturer information on particle size.

	Nanoparticle	Composition	Particle size range (nm)	Manufacturer
Single element	Cu10	Copper	10-30	Canfuo Nano Technology® (Suzhou, China)
	Ag	Silver	20-40	Alfa Aesar (UK)
	QNA Ag	Silver	100	QinetiQ Nanomaterials (Farnborough, UK)
	QNA Cu	Copper	100	QinetiQ Nanomaterials (Farnborough, UK)
	Cu60	Copper	60-100	Canfuo Nano Technology® (Suzhou, China)
Alloy	AgCu	Silver, Copper	80-100	Sigma-Aldrich (Dorset, UK)
	CuZn	Copper, Zinc	90-110	Sigma-Aldrich (Dorset, UK)
Oxides	ZnO	Zinc oxide	*	Alfa Aesar (UK)
	QNA CuO Sphere	Copper oxide	10-15	Intrinsiq Materials® (formally QinetiQ Nanomaterials)
	CuO Rod	Copper oxide	40-60	Canfuo Nano Technology® (Suzhou, China)
Formulations	MNP3	Graphene oxide and copper	*	Intrinsiq Materials® (formally Qinetiq Nanomaterials)
	MNP4	Graphene oxide, silver and copper	*	Intrinsiq Materials® (formally Qinetiq Nanomaterials)
	AVNP2	Carbon, oxide, tungsten, silver, Copper	*	Intrinsiq Materials® (formally Qinetiq Nanomaterials)
Carbon based	GOP	Graphene oxide	*	NanoInnova Technologies SL. (Madrid, Spain)
	GO ENG	Graphene oxide	*	NanoInnova Technologies SL. (Madrid, Spain)
	GO30	Graphene oxide	*	NanoInnova Technologies SL. (Madrid, Spain)
	EGO	Expanded Graphene oxide	*	NanoInnova Technologies SL. (Madrid, Spain)
	RG NH_2	Carbon, hydrogen, nitrogen, sulphur	*	NanoInnova Technologies SL. (Madrid, Spain)
	RG O Fe_3O_4	Iron, carbon, hydrogen, nitrogen, sulphur	*	NanoInnova Technologies SL. (Madrid, Spain)
	RG NH	Carbon, hydrogen, nitrogen, sulphur	*	NanoInnova Technologies SL. (Madrid, Spain)
	RG Pd(O)	Palladium, carbon, hydrogen, nitrogen, sulphur,	*	NanoInnova Technologies SL. (Madrid, Spain)
	RG TEPA	Carbon, hydrogen, nitrogen, sulphur	*	NanoInnova Technologies SL. (Madrid, Spain)
	RG GO-NH carboimidazole	Carbon, hydrogen, nitrogen, sulphur	*	NanoInnova Technologies SL. (Madrid, Spain)
	CeO_2	Cerium oxide	*	European Commission
	EU graphene	Graphene	*	European Commission
	WC	Tungsten carbide	150-200	Sigma-Aldrich (US)

3.2.1 Initial tests (the agar well diffusion method and the broth inhibition assay)

For the agar well diffusion method, bacterial and fungal samples (grown following the protocol in Chapter 2, section 2.2) were diluted to ~1-3 x 10^7 colony forming units (CFU) per ml. A spectrometer (Cecil instrumentation CE 1021, UK) was used to measure absorbance of cell optical density, where 1.0 abs at 600 nm is equivalent to ~1-3 x 10^7 CFU/ml *Candida* [238] and 0.1 abs at 600 nm is equivalent to 3x10^7 CFU/ml bacteria [239]. Prepared Mueller Hinton (MH) agar plates (see Appendix for preparation protocol) were labelled with numbers corresponding to nanoparticle solutions. Inside a sterilised flow cabinet, sterile cotton swabs were dipped inside the broth culture and spread onto prepared MH agar plates, as shown in Figure 3.1. 4 mm holes were made using a sterile metal hole punch. Holes were filled with 30 µl of nanoparticle suspension at 0.1 wt/v% (1000 µg/ml) which was freshly dispersed in a Fisher Brand Ultra sonic bath (Fisher Scientific, UK) for 1 minute duration. For negative controls, 30 µl of antibiotic/antifungal (15 µg/ml) was pipetted into the well holes. Plates were then incubated at 37°C for 24 hours. Clear rings were identified as zones of inhibition and measured in cm.

For the broth inhibition assay, bacterial and fungal samples were diluted to ~1-3 x 10^4 CFU/ml in nutrient and YPD broth, respectively (see Appendix for broth preparation protocol). Final volumes of freshly dispersed 0.1 wt/v% (1000 µg/ml) nanoparticles and microbial broth were added in duplicate to wells of 96-well Nuclon Delta surface plates (Thermofisher, UK) in a sterile flow cabinet. Pipette tips were changed between wells to prevent cross contamination of nanoparticles and microbes. Plates were incubated at 37°C temperatures for 24 hours. Indicator assay resazurin (0.02%) (Sigma-Aldrich, UK) was the added to each well and further incubated for 24 hours prior to examination. Colour change from purple to pink was recorded.

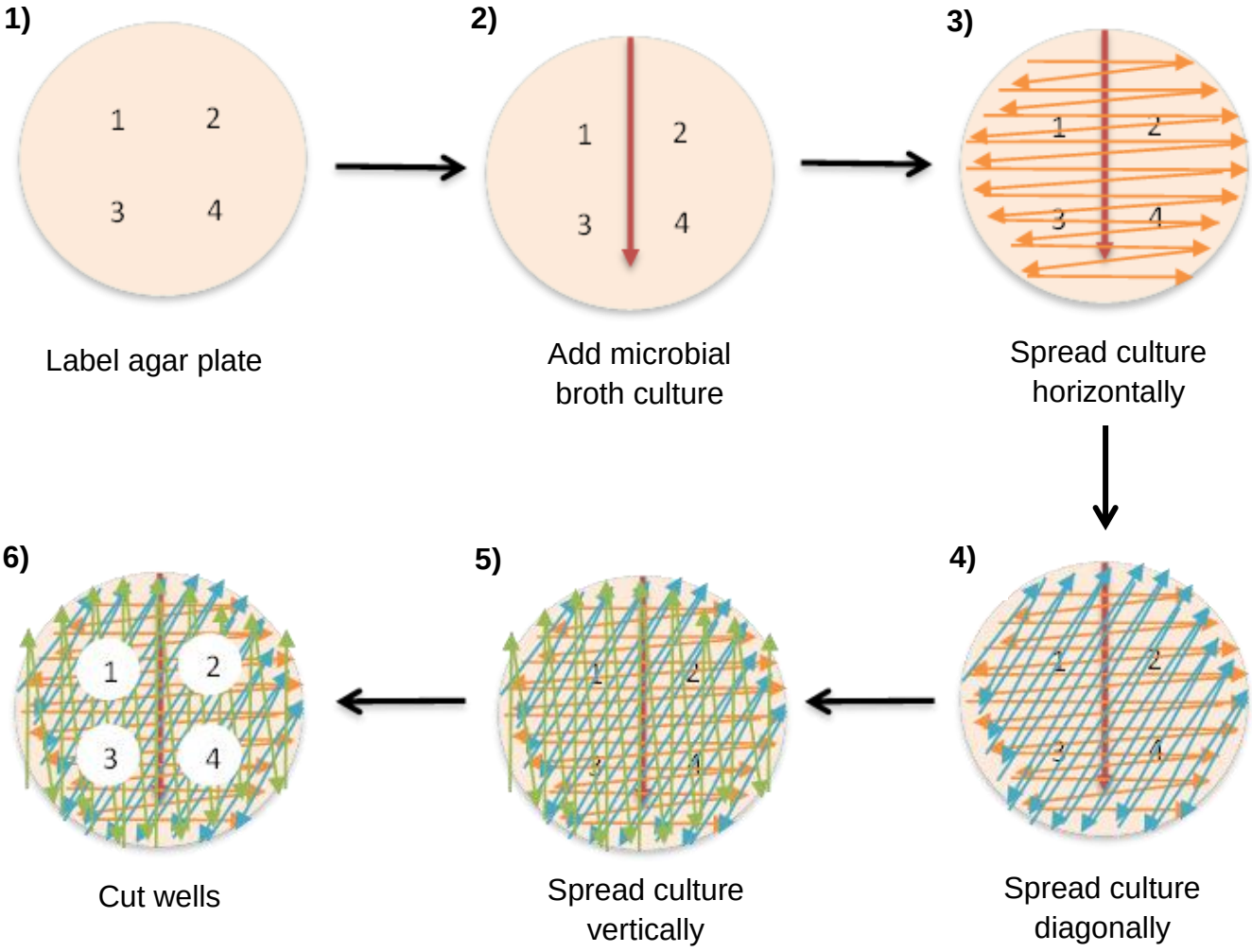

Figure 3.1: Schematic diagram of agar inoculation for the agar well diffusion method. 1) Agar plate was labelled, 2) Microbial broth culture was spread onto the middle of the agar using a cotton swab, 3) Microbes were spread horizontally across the agar using same cotton swab, 4-5) Microbes were spread diagonally and vertically, respectively, to ensure plate was fully and evenly inoculated with microbes, 6) Sterile metal hole punch was used to cut 4 mm well to hold nanoparticle suspensions.

3.2.2 Minimal inhibitory concentration (MIC)

Based on the results obtained from the agar well diffusion method and broth assays (section 3.2.1) five nanoparticles (Cu10, Cu60, AgCu, CuO rod and Ag) were selected for further investigation against six microbes (*A. baumannii, P. aeruginosa, K. pneumonia, S. aureus, C. albicans* and *C. tropicalis*).

In a 96 well plate, 200 µl of each nanoparticle suspension at concentrations of 0.05 wt/v% (500 µg/ml) were added to the top row, in quadruplicate. Remaining wells (minus controls) contained 100 µl of MH broth. Using a multichannel pipette, 100 µl of nanoparticle suspension from the row A was transferred and mixed into the following row (B) to form a 2-fold dilution. This was repeated until row G to form a dilution concentration gradient from 500 µg/ml to 7.81 µg/ml, which were reduced by half after addition of microbes. Microbial cultures were diluted to ~1-3 x10^4 CFU/ml with MH broth and 100 µl added to three of the four nanoparticle quadruplicates. The remaining nanoparticle dilution without the addition of microbes was used as a negative control to check for microbial contamination in the nanoparticle suspension and to test for nanoparticle reaction with the resazurin dye. Positive control (broth and microbes), negative control (broth) and antibiotic treatment (dilution concentration gradient from 32 to 1 µg/ml) was added in row G (see Appendix for antibiotic preparation protocol). The template of the 96 well plate is displayed in Figure 3.2. Plates were incubated at 37°C for 24 hours. Resazurin (0.02%) was added to all wells and incubated for a further 24 hours before assessing a colour change (see Appendix for resazurin preparation protocol). The well with the lowest concentration of nanoparticle that remained blue was taken as the MIC. To avoid contamination, one microbial sample was used per plate.

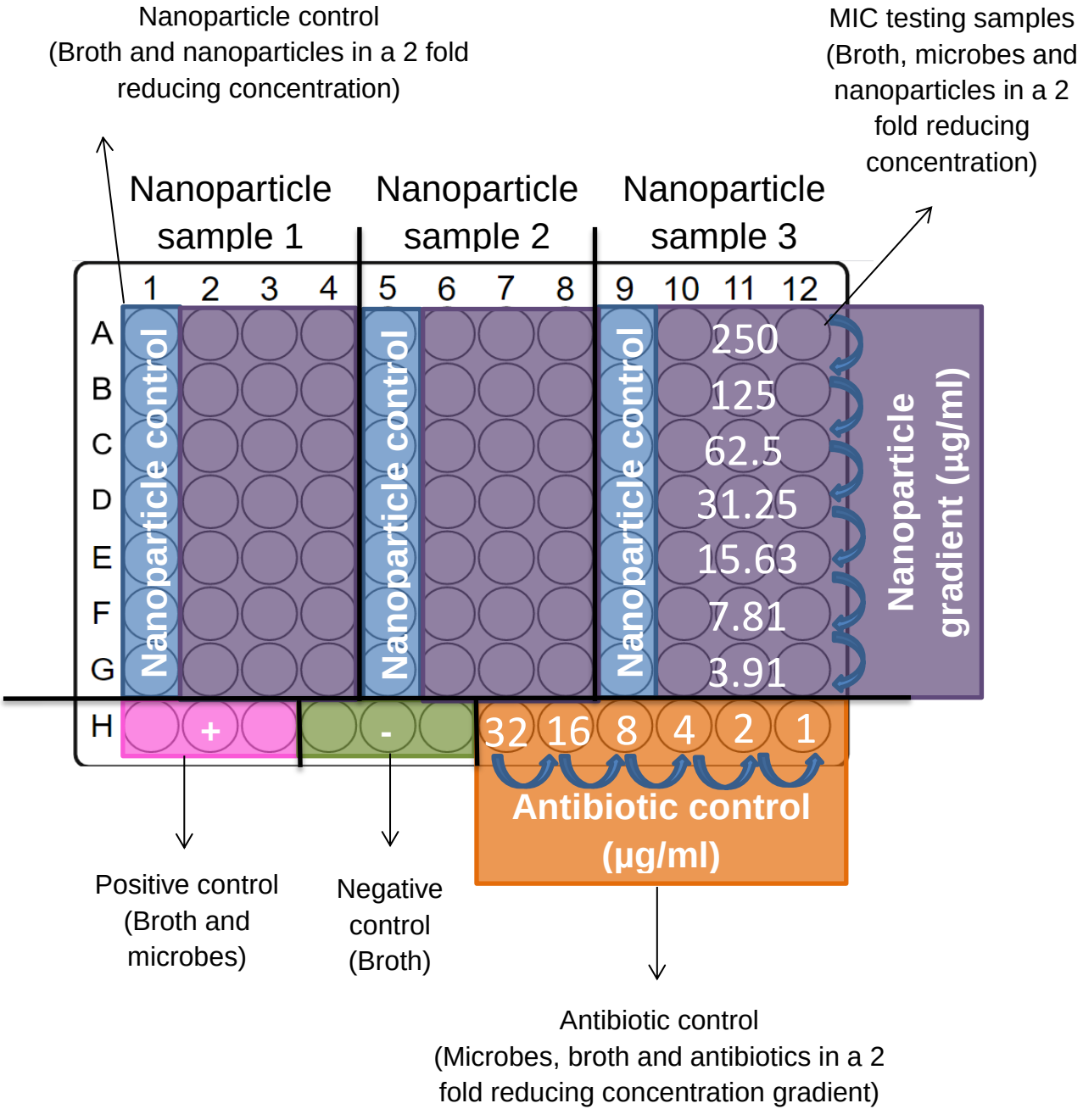

Figure 3.2: 96 well plate template for MIC investigations. Areas highlighted in blue are nanoparticle controls which will consist of nanoparticles in a 2 fold reducing concentration and broth. Areas highlighted in purple contain the same concentration dilution of nanoparticles with the addition of microbial broth. Positive controls (highlighted in pink) consist of microbial broth. Pure broth was used for negative control (highlighted in green). Orange highlights the antibiotic control, which consists of microbial broth and antibiotics in a 2 fold reducing concentration.

3.2.3 Kinetic growth rates

Based on the antimicrobial assays conducted, AgCu nanoparticles were selected for further investigations. AgCu nanoparticle suspensions were added to the top row of a 96 well plate and 2 fold diluted down to make up a final concentration of 64 μg/ml to 0.49 μg/ml. Microbes were adjusted to ~1-3 x 10^4 CFU/ml and added to the wells. Spectrometer (CLARIOstar, BMG Germany) was used to monitor the microbial growth by measuring the absorbance every hour with a 100 rpm orbital shake for 5 seconds prior every measurement and continuous incubation at 37°C. Initial absorbance was used as a blank. The absorbance of AgCu nanoparticles at different concentrations has been considered during data analysis (data can be found in Appendix). Polynomial regression line of the data was calculated and presented.

3.2.4 Cell viability

Microbes were adjusted to ~1-3 x 10^7 CFU/ml and incubated with AgCu nanoparticle suspensions at concentrations 100 μg/ml and corresponding MIC. At every hour, 90 μl of the sample was taken and treated on ice with 5 μl of propidium iodide (400 μM) and SYTO9 (33.4 μM) dye (Thermo Fisher Scientific, USA) for 15 minutes on shaker (100 rpm) in the dark. Then, 10 μl of treated samples were transferred onto a glass slide and viewed on a fluorescent confocal microscope with corresponding filters (Nikon, USA). Number of live (fluorescent green) and dead (fluorescent red) cells were counted using ImageJ. Results were presented as percentage of live cells in relation to live control cells without AgCu nanoparticle treatment.

3.3 Results

3.3.1 Screening and selection of nanoparticle

By using the agar well diffusion method, the antimicrobial activity of nanoparticle suspensions was able to be identified through the zone of inhibition. A clear ring of agar shows antimicrobial activity, as the microbes were unable to grow due to the presence of nanoparticles, and the diameter of the ring shows the extent of the antimicrobial efficacy. Out of the 26 nanoparticles tested, 12 showed antimicrobial activity against at least one of the microbes. As presented in Table 3.3, the zone of inhibition diameters varied from 0 to 2.7 cm, with AgCu nanoparticles most effective and with antimicrobial activity against all microbes tested. In contrast, all graphene-based nanoparticles showed no antimicrobial activity. Nanoparticles were most effective at inhibiting Gram-negative bacteria (30.77%) and least effective against fungi (7.69%).

Further inhibition experiments were conducted to analyse the nanoparticle antimicrobial activity. Resazurin dye was used to determine viable cells through colour change of blue to pink via a reduction reaction when viable cells were present [240]. In Table 3.4, the results show that metallic nanoparticles had antimicrobial activity, with Cu10 and AgCu effective towards 100% of the microbes tested. Again, graphene-based nanoparticles were the least effective and showed no antimicrobial activity. The nanoparticle inhibition of Gram-negative and Gram-positive bacteria seemed to be similar (40.7% and 44.4%, respectively), but inhibition was less effective towards fungi (29.3%).

The MIC was investigated to analyse the antimicrobial efficacy of five of the nanoparticles that showed the most antimicrobial activity based on the agar well diffusion method and the broth inhibition assay results (section 3.3.1). As displayed in Table 3.5, Ag and AgCu nanoparticles showed the highest efficacy as the lower concentrations were able to inhibit the growth of the microbes. Cu10, Cu60 and CuO Rod showed the weakest efficacy with the same MIC results when tested against the same microbes. Antibiotic control was used to test the susceptibility of the microbe and found none of the microbes had antibiotic resistance. Considering all the screening results, AgCu nanoparticles were selected for further investigations.

Table 3.3: Results of the agar well diffusion experiment. Zone of inhibition diameters are measured in cm; 0 represents no inhibition zone. Nanoparticles MNP3, WC, GOP, GO ENG, GO30, EGO, RG NH2, RG Oxide Fe3O4, RG NH, RG Pd(o), RG TEPA, RG GO-NH carboimidazole, CeO2 and EU graphene were tested but not included in this table as all showed no inhibition.

		Single elements					Oxides			Alloys		Formulations	
		Ag	QNA Ag	QNA Cu	Cu10	Cu60	CuO Rod	ZnO	CuO sphere	AgCu	CuZn	AVNP2	MNP4
Gram-negative	*Acinetobacter baumanii*	0.9	0	0	0	0	0	0	0	1.85	0	0.7	0
	Pseudomonas aeruginosa	0	0	2.7	2.35	2.35	1.95	0	2.15	1.2	0	0	0
	Klebsiella pneumonia	0.6	0	0	0	0	0	0	0	1.4	0	0	0
	Escherichia coli	0.55	0	0	0	0	0	0	0	0.8	0	0	0
	Salmonella typhimurium	0.6	0	0	0	0	0	0	0	1.4	0	0.6	0
	Nanoparticle inhibition % (2.d.p) = 30.77												
Gram-positive	*Enterococcus faecium*	0	0	0	0	0	0	0	0	1.4	0	0	0
	Staphylococcus aureus	0	0	0	0	0	0	0	0	1.7	0	0.85	0
	Streptococcus pyogenes	0.8	0	0	0	0	0	1.4	0	1.9	1.4	0.75	0.6
	Nanoparticle inhibition % (2d.p) = 23.08												
Fungi	*Candida albicans*	0	0.85	0	0	0	0	0	0	1	0	0	0
	Candida tropicalis	0	0.65	0	0	0	0	0	0	0.7	0	0	0
	Nanoparticle inhibition % (2.d.p) = 7.69												

Table 3.4: Broth inhibition assay results. – represents antimicrobial inhibition (no microbial growth), + represents no antimicrobial activity (microbial growth). Nanoparticles MNP3, MNP4, WC, GOP, GO ENG, EGO, RG NH2, RG Oxide Fe3O4, RG NH, RG Pd(o), RG TEPA, RG GO-NH carboimidazole, CeO2 and EU graphene were tested but not included in this table as there was no microbial inhibition.

		Single elements					Oxides			Alloys		Formulations
		Ag	QNA Ag	QNA Cu	Cu10	Cu60	CuO Rod	ZnO	CuO sphere	CuZn	AgCu	AVNP2
Gram-negative	*Acinetobacter baumannii*	-	-	-	-	-	-	+	+	-	-	-
	Pseudomonas aeruginosa	-	-	-	-	-	-	+	+	-	-	-
	Klebsiella pneumonia	-	-	-	-	-	-	-	+	-	-	-
	Escherichia coli	-	-	-	-	-	-	-	+	-	-	-
	Salmonella typhimurium	-	-	-	-	-	-	+	+	-	-	-
	Nanoparticle inhibition % (2d.p) = 40.74											
Gram-positive	*Enterococcus faecium*	-	+	-	-	-	+	+	-	+	-	-
	Staphylococcus aureus	-	-	-	-	-	-	+	+	-	-	-
	Streptococcus pyogenes	-	-	-	-	-	+	-	-	-	-	-
	Nanoparticle inhibition % (2d.p) = 44.44											
Fungi	*Candida albicans*	-	-	-	-	-	+	+	-	+	-	+
	Candida tropicalis	-	-	+	-	+	+	+	-	+	-	+
	Nanoparticle inhibition % (2d.p) = 25.93											
	% of microbes susceptible	**100**	**90**	**90**	**100**	**90**	**60**	**30**	**40**	**70**	**100**	**80**

Table 3.5: MIC results of nanoparticles. The MIC of nanoparticles against six microbial species was determined through colour change of resazurin dye from blue to pink in the presence of viable cells. The MIC value was identified as the lowest concentration that remained blue after 24 hours of incubation with microbes.

Microbe	Nanoparticle MIC (μg/ml)				
	Cu10	Cu60	CuO Rod	AgCu	Ag
A. baumannii	31.25	31.25	31.25	31.25	15.63
P. aeruginosa	250	250	250	7.81	7.81
K. pneumonia	250	250	250	15.63	15.63
E. coli	125	125	>250	7.81	250
S. aureus	125	125	125	31.25	15.63
C. albicans	250	250	250	62.50	31.25
C. tropicalis	125	125	125	31.25	31.25

3.3.2 Further antimicrobial investigations on selected nanoparticle (AgCu)

The growth rates of microbes after treatment of AgCu nanoparticles at various concentrations were observed over 24 hours. As shown in Figure 3.3, the addition of AgCu nanoparticles showed the same trend line as the control microbes, however at higher concentrations of AgCu nanoparticle (31.2 µg/ml or higher), inhibit of microbes growth in all species. Lower concentrations of AgCu nanoparticles were able to reduce and delay the growth of microbes and still followed the control growth trend line.

E. coli was the most susceptible to AgCu nanoparticles, out of the tested microbes, as concentrations of 7.8 µg/ml or higher were able to inhibit the bacteria. In contrast, *S. aureus* had the least susceptibility to AgCu nanoparticles with inhibition requiring concentrations of 31.3 µg/ml or more.

As cell viability is not considered when measuring the optical density, fluorescent cell viability test was also performed to investigate the cell viability of microbes after AgCu nanoparticle suspension treatment over time. Bacterial cells were killed faster than fungal cells as shown in Figure 3.4. Immediately after AgCu nanoparticle treatment at 100 µg/ml (0 hours), the cell viability of *E. coli* and *S. aureus* reduced to 4.1% and 83.5%, respectively. In contrast, at the same concentration, the cell viability of *C. albicans* was at 94.8%. After 5 hours of AgCu nanoparticle treatment at 100 µg/ml, less than 99% of the *S. aureus* cells were viable, no viable cells were observed for *E. coli,* whilst *C. albicans* had 9.8% cell viability. When treated with AgCu nanoparticles at MIC concentrations, a similar trend was shown but killing rate was slower. After 5 hours of AgCu nanoparticle treatment at MIC value, *S. aureus, E. coli* and *C. albicans* had a cell viability of 4.9%, 0.1% and 17.4%, respectively.

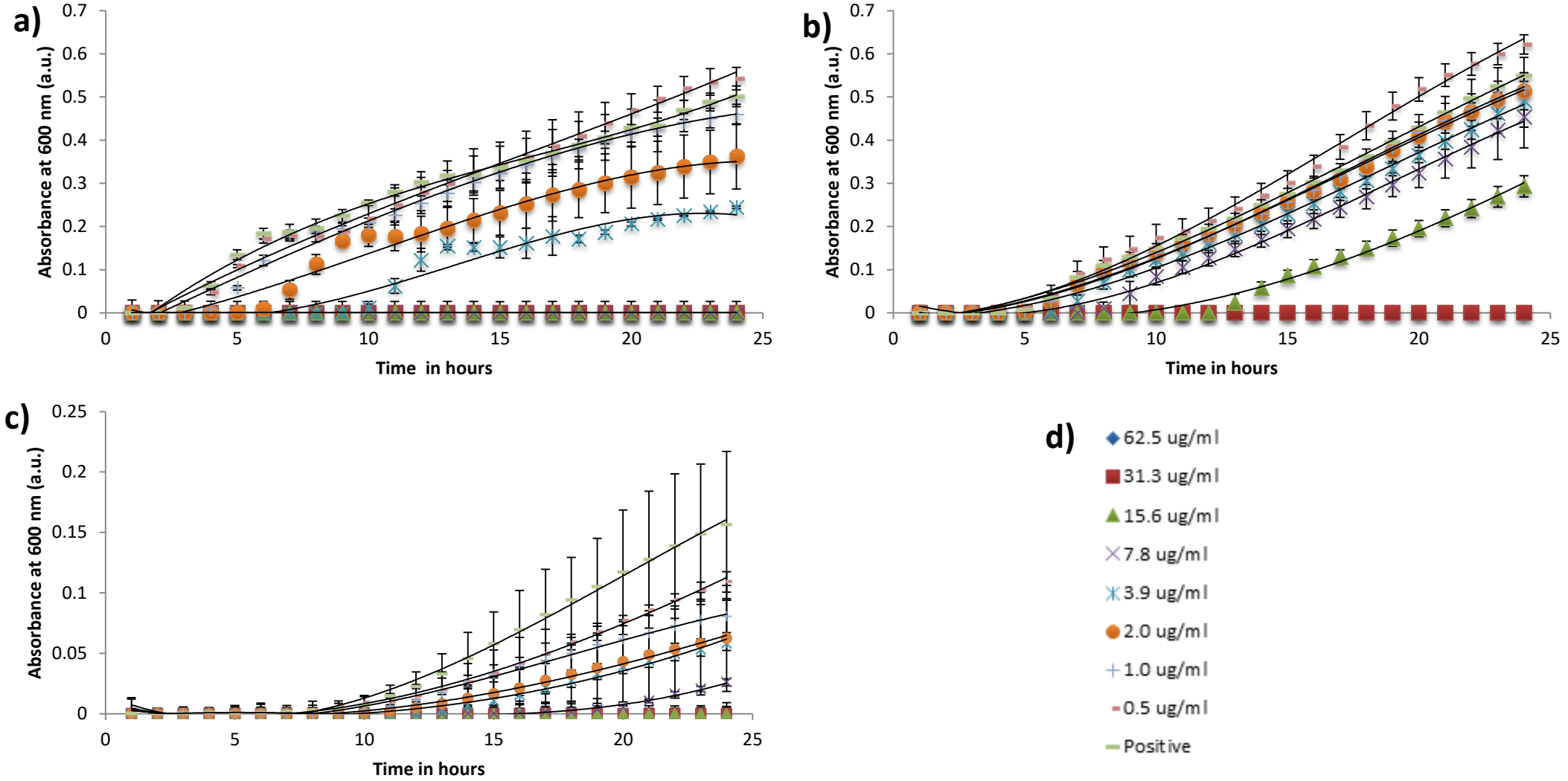

Figure 3.3: Growth rates of microbes after AgCu nanoparticle treatment. a) *E. coli*, b) *S. aureus* and c) *C. albicans*, over a 24 hour period with eight concentrations of AgCu nanoparticles, as shown in d, and positive control of microbial growth without treatment. Error bars denote the standard deviation of three replicates. Polynomial regression line (order 3) is used to present the line of best fit.

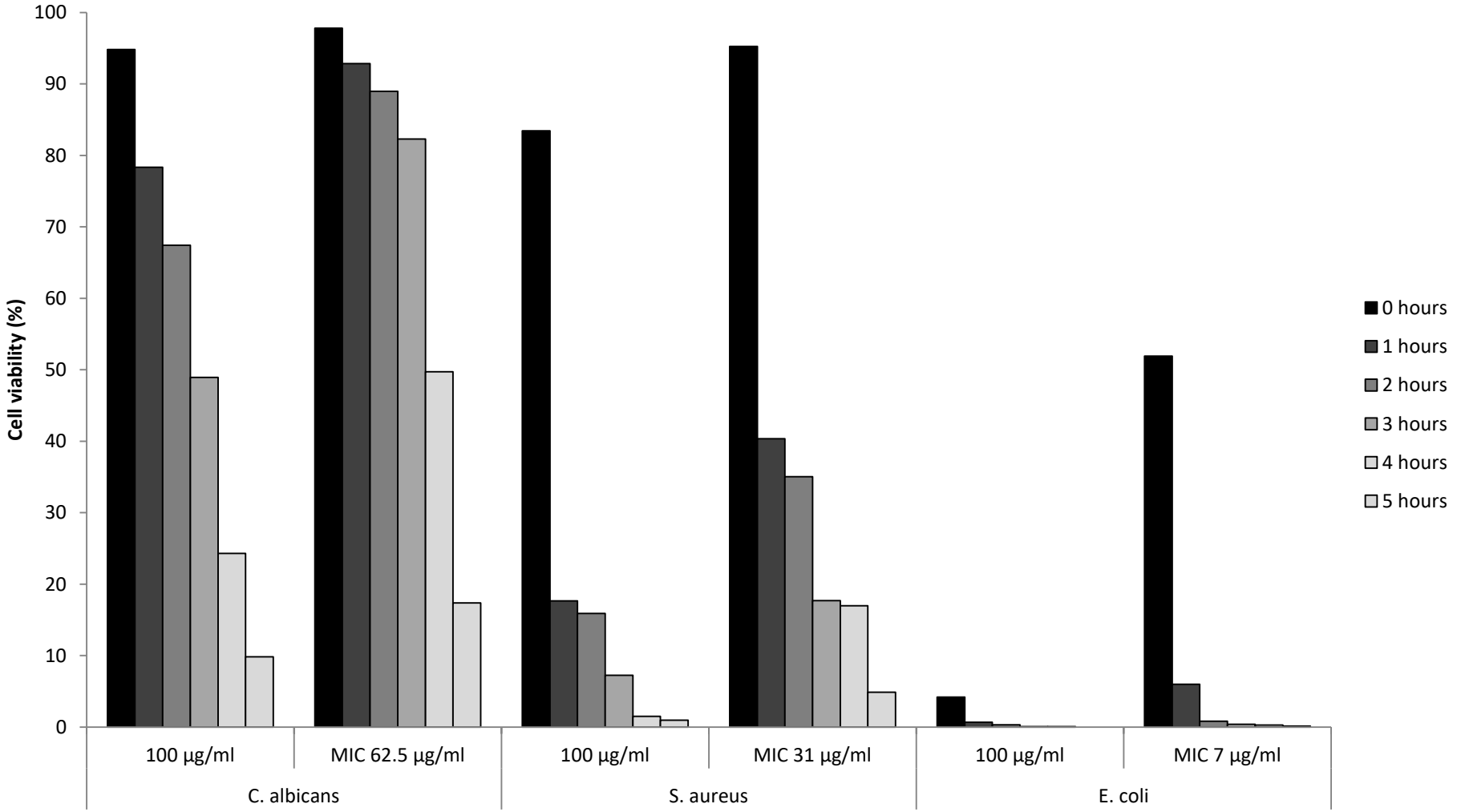

Figure 3.4: Propidium iodide and SYTO9 cell viability of microbes after AgCu nanoparticle treatment. The cell viability of microbes *C. albicans*, *S. aureus* and *E. coli* were observed hourly over a 5 hours period after AgCu nanoparticle treatment at 100µg/ml and at corresponding MIC value. Viability is presented as a percentage in relation to positive control without treatment.

3.4 Discussion

Several experiments were conducted to investigate the antimicrobial potential of 26 nanoparticles to select and explore one with the highest antimicrobial activity. To select the highest performing nanoparticles, experiments were conducted in three stages; firstly nanoparticles were screened to see if they possessed antimicrobial activity at 1000 μg/ml concentration through the agar well diffusion and the broth inhibition assay. Secondly, nanoparticles with antimicrobial activity were tested for their MIC. Using the first and second stage, AgCu nanoparticle was selected based on the broadness of antimicrobial activity against nosocomial pathogens and lower concentrations required to inhibit the microbes. Lastly, further tests were performed on AgCu nanoparticles for more information on their antimicrobial activity.

3.4.1 The agar well diffusion method

The agar well diffusion method is commonly used to assess the antimicrobial activity of a sample through visible inhibitory zones [241]. An example is shown in Figure 3.5. Although others have reported antimicrobial activity of similar nanoparticles using this method, a large proportion of the tested sample did not show antimicrobial activity as a zone of inhibition was not present. This may be due to the limited physical contact between nanoparticles and microbes, and the differences in nanoparticle diffusion rate, which can be influenced by their physical characteristics including size and shape [241-243]. Additionally, like some antibiotics, certain nanoparticles may get trapped during diffusion from aggregations or interactions with solid components in the agar [244]. Thus the results may not be as comparable between different nanoparticles due to their difference in physical characteristics. For example, Aunkor *et al.* (2020) reported that their synthesised graphene oxide had antimicrobial activity against a broad range of microbes, with 27-41 mm zone of inhibition. In contrast, all of the graphene-based nanoparticles tested in this experiment had no antimicrobial activity and did not produce a zone of inhibition. Whilst the shape and size of these graphene-based nanoparticles were not provided by the manufacturer, antimicrobial activity were reported in spherical and sheet shaped graphene and graphene-based nanoparticles with diameter sizes varying from 0.479 to 5.25 μm [245-247].

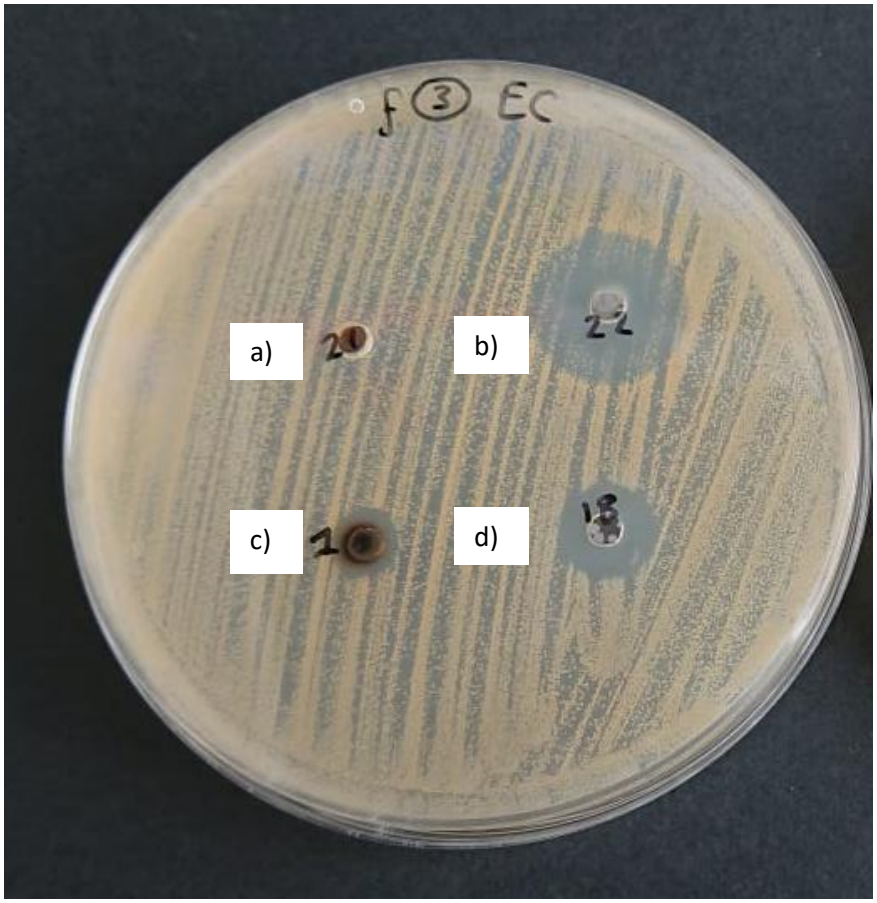

Figure 3.5: Zone of inhibition of S. aureus on MH agar plate. a) No zone of inhibition seen from CuZn nanoparticle treatment, b), c) and d) bactericidal zone of inhibition from AgCu nanoparticles, AVNP2 nanoparticles and antibiotic gentamicin, respectively. Nanoparticle suspensions were at 1000 µg/ml concentration; whilst antibiotic concentration corresponded to the breakpoint provided by EUCAST for antibiotic susceptibility testing.

Metals based nanoparticles showed antimicrobial activity towards at least one type of tested microbe, with AgCu nanoparticles having antimicrobial activity towards all tested microbes. This is supported by a published study, where AgCu was found to have a higher antimicrobial activity in comparison to the single elements of Ag and Cu. It was suggested that AgCu can work synergistically together against bacterium hence more antimicrobial activity and a larger zone of inhibition than single element was measured for most microbes tested [61]. As expected, Ag also showed antimicrobial effect towards more than half of the bacteria tested. However, published studies show that Ag was more effective than the results obtained for this experiment. For example, Ag nanoparticles synthesised by Joshi & Davi (2014) produced a 14 ± 1.0 mm and 14 ± 0.5 mm zone of inhibition against *S. aureus* and *E. faecalis,* respectively, however no zone of inhibition was found in this report for Ag nanoparticles against those two bacteria. This could be due to the larger size of nanoparticles in this study (20-40 nm and 100 nm) compared to the reported synthesised nanoparticles that were 5.5 ± 3.1 nm [248]. Smaller nanoparticles are able to diffuse through agar at a faster rate and have a larger surface area which is more prone to ion release. It has been reported that physical contact between the nanoparticle and microbe and release of ions is one of the antimicrobial mechanisms of Ag [241, 249].

Moreover, in this experiment, all Cu and CuO nanoparticles had no effect on *E. coli* and *S. aureus,* whereas Ren *et al.* (2009) found antibacterial activity against both bacteria. Similarly, Ag nanoparticles tested in this experiment had no effect on *P. aeruginosa,* however both Salomoni *et al.* (2017) and Lozhkomoev *et al.* (2018) found antibacterial activity against the bacteria. A reason for this difference may be linked to the mechanism of action of nanoparticles; the published studies tested the antimicrobial activity of the nanoparticles by incubating the nanoparticles with the bacteria in broth [27, 58, 250]. In contrast, microbes in this experiment were grown on agar and nanoparticle suspensions were then added into cut wells in the agar. Nanoparticles and microbes were able to make full contact in the published studies, whereas the agar zone inhibition experiment only allowed nanoparticles that diffused through the agar to contact the bacteria. Although the agar well diffusion method is commonly used to evaluate microbial susceptibility and one study found little difference between the agar well diffusion method and broth assay methods, others

theorised that samples may diffuse from the cut wells more slowly and may bind to agar matrix before they reach the microbe thus showing less antimicrobial activity [241, 251, 252]. The permeability of agar allows smaller particles to travel faster thus the size of metal nanoparticle and free ion availability will contribute to the contact between microbe and nanoparticles. This is a limiting factor of this experiment, consequently an alternative broth inhibition assay was performed to compare results and to screen for antimicrobial nanoparticles.

3.4.2 The broth inhibition assay

The broth inhibition assay was performed to investigate the antimicrobial activity of nanoparticles where they were able to make physical contact with microbes in a broth suspension. The addition of resazurin indicator dye after 24 hours of incubation can identify the presence of metabolically live cells through the reduction of resazurin to resorufin (Figure 3.6) resulting in a colour change from purple blue to fluorescent pink [1, 2, 253].

In comparison to the agar well diffusion method, the broth inhibition assay reported more antimicrobial activity, which is likely due to the direct contact between microbes and nanoparticles in a free broth suspension. Results displayed in Table 3.2.1 showed that metallic nanoparticles exhibited the best antimicrobial activity, with nanoparticles containing Ag and pure Cu most efficient whilst graphene-based nanoparticles showed no antimicrobial activity. An example of resazurin colour change is seen in Figure 3.7, where viable cells are identified through the colour change from blue to pink. It is not surprising that Ag and pure Cu were most efficient as heavy metals have been known to be toxic to some bacteria and fungi for several reasons; for example, metals can become ions in aqueous solutions and increase the acidity. Additionally, both fungi and bacteria are known to uptake essential trace metals such as Cu, but at high uncontrolled levels, these free trace metal ions can produce toxic cellular effect [254, 255]. Therefore, further investigations are required to select which Ag and Cu containing nanoparticles with the highest efficacy.

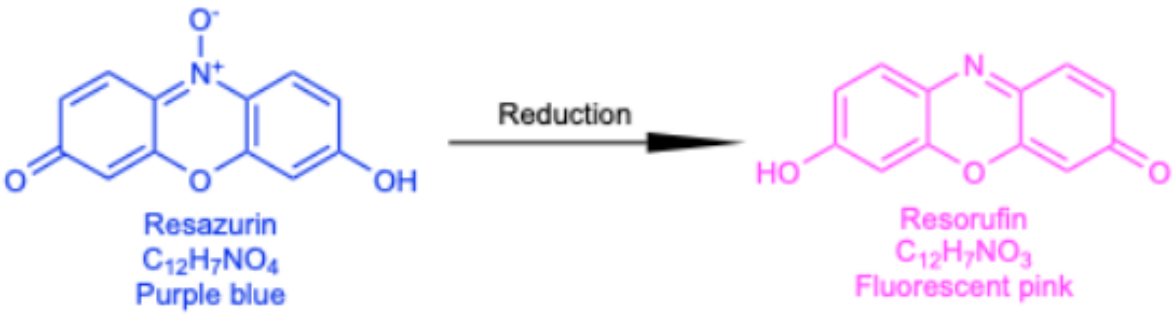

Figure 3.6: Chemical conversion of resazurin reduced to resorufin in the presence of metabolically active cells. Resazurin, which is a blue colour, can be irreversibly reduced by enzymes present in metabolically active cells to resorufin, which is fluorescent pink [1, 2]. Chemical structure was drawn using ChemDraw 21.0.

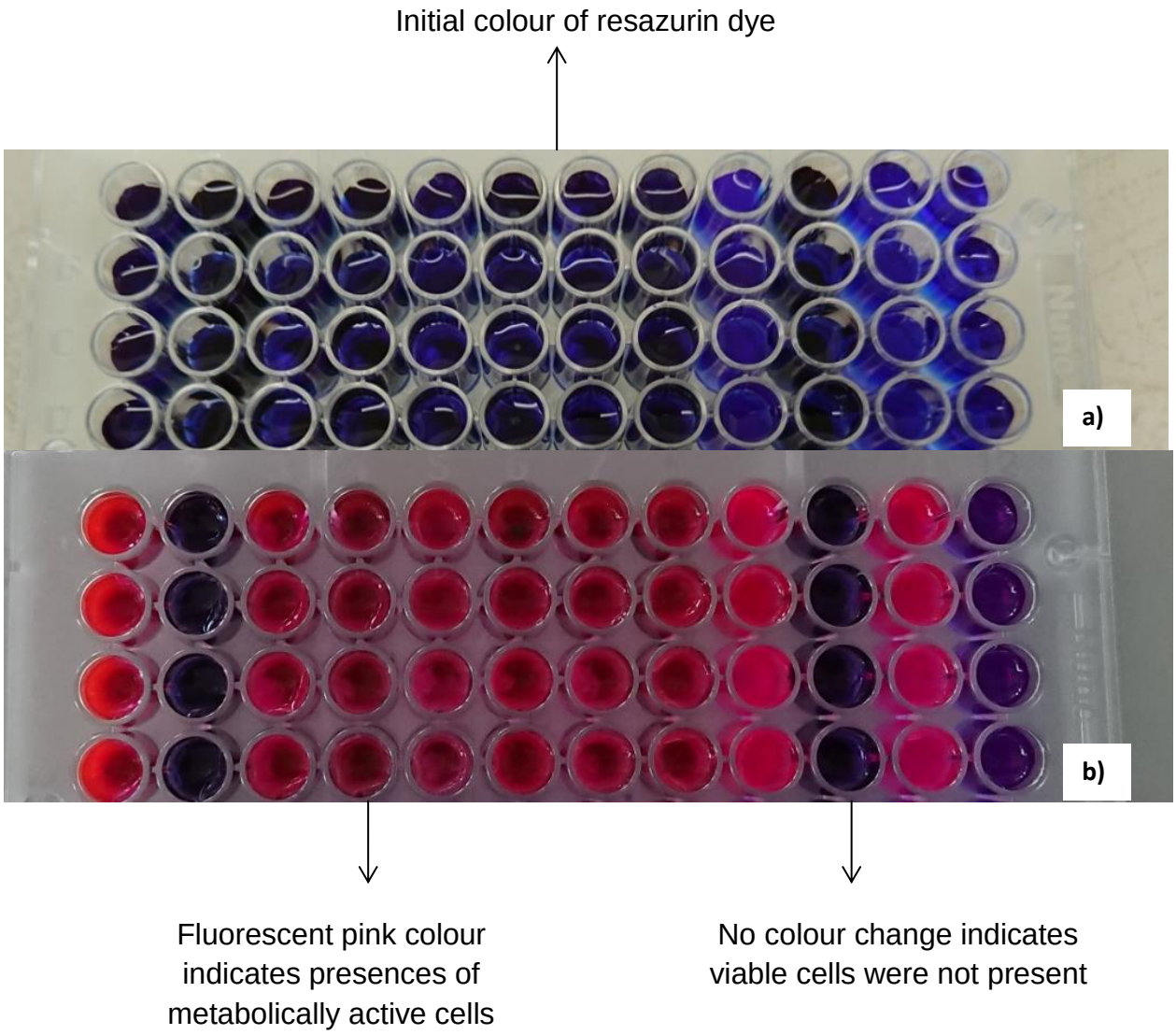

Figure 3.7: Broth inhbition assay. a) Treated samples immediately after adding resazurin (0.02%) and b) after 24 hour incubation with resazurin. Pink indicates live viable microbes, thus nanoparticles did not have antimicrobial activity. Purple indicates non-viable microbes, hence nanoparticles added were antimicrobial.

In both experiments, all of the graphene and graphene oxide-based nanoparticles had no antimicrobial effect. Wu *et al.* (2018) reported that graphene oxide stimulated both Gram-negative and Gram-positive bacterial growth by acting like a protective biofilm when incubated with nutrients; however, when surrounding the surface of bacteria, it can suppress essential nutrients and induce cell death via production of oxidative stress. Both Wu *et al.* (2018) and Liu *et al.* (2011) found graphene and graphene oxide nanoparticles to have antimicrobial effect but only when incubated in saline solution. Ergo, since the inhibition assay was performed with broth, graphene oxide may have stimulated microbial growth instead of producing antimicrobial activity [245, 256]. As both the agar well diffusion and the broth inhibition assay showed no antimicrobial activity for graphene-based nanoparticles, no further investigations on them will be conducted.

Despite the fact that ZnO has been reported for having antimicrobial activity, only 30% of the microbes tested in this experiment were susceptible. Antimicrobial activity has found to be correlated to particle size and concentration. Thus reports showing antimicrobial activity may have used smaller particles that were able to exhibit a broader range of antimicrobial activity [257]. On the other hand, zinc is a common nutrient for humans and microorganisms; about 10% of human protein is incorporated with zinc serving metabolic and regulatory functions, and zinc ABS transporters are present in both Gram-negative and Gram-positive bacteria to allow replication and virulence [258]. In conjunction, it has been found that some bacteria have regulatory mechanisms to maintain zinc ion concentrations within the bacteria – excess ions can be removed via efflux, thus preventing damage to bacteria [259]. Therefore, it is not unusual for ZnO to have antimicrobial activity against only a few microbes. However, since the broadness of antimicrobial activity against microbes is low, ZnO was not selected for further investigations.

Both the agar well diffusion method and the broth inhibition assay clearly display that some nanoparticles have better antimicrobial efficacy than others. By comparing the results, the nanoparticles with the strongest and broadest antimicrobial activity against the three categories of microbes were selected for further investigation. Based on the zone of inhibition diameter and percentage of microbes inhibited, 5 nanoparticles were selected, Cu10, Cu60, CuO Rod, Ag and AgCu, to investigate the MIC against microbes.

3.4.3 MIC

The MIC measures the potency of an antimicrobial agent by determining the minimal concentration required to inhibit the growth of a specific strain of microbe under controlled *in vitro* conditions [260, 261]. In this thesis, the MIC was investigated by using resazurin to analyse the cell viability after nanoparticle treatment in a decreasing concentration gradient. The lowest tested concentration with no viable cells, as indicated by no colour change of resazurin, was determined as the MIC, as shown in Figure 3.8. The MIC is one of the important parameters in determining the outcome of an antimicrobial agent. An insufficient dose will lead to survival of pathogens and may result in antimicrobial resistance. Antimicrobial agents with a low MIC are preferred as they have high efficacy with lower risk of toxicity [261]. Furthermore, higher concentrations of materials will result in higher costs.

As shown previously in Table 3.5, overall Ag nanoparticle had the lowest MICs against most of the pathogens. The MIC of AgCu nanoparticles was the same or slightly higher than Ag for some microbes, however it was more effective towards *E. coli* than Ag. All three copper type nanoparticles were equal with the highest MICs ranging from 31 to 250 μg/ml, except for CuO rod nanoparticles against *E. coli* which exceeded 250 μg/ml. This is not surprising as silver nanoparticles are well known to have strong antimicrobial activity and previous publications have shown that Ag nanoparticles were more effective than copper nanoparticles [262, 263]. Ruparelia, *et al.* (2008) reported that Ag nanoparticles had a MIC of 120 μg/ml against *S. aureus* in comparison to Cu nanoparticles with a slightly higher MIC of 140 μg/ml. Whilst the MIC of Cu nanoparticles were similar to the results obtained in this study (125 μg/ml), the Ag nanoparticles in this study (15.6 μg/ml) was significantly lower.

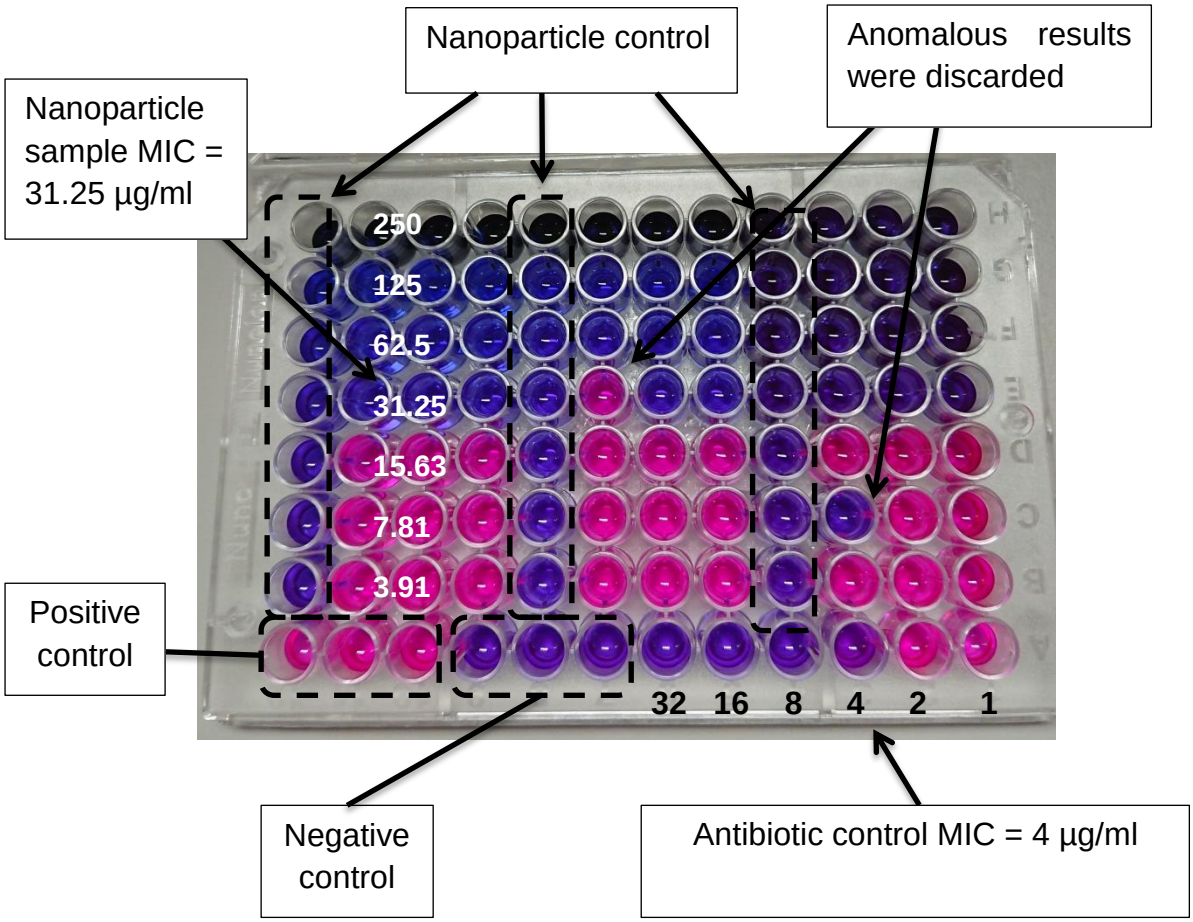

Figure 3.8: 96 well plate showing colour change of resazurin used for determining the MIC. Resazurin dye was used to identify the MIC value of nanoparticles which was determined as the lowest concentration without colour change. Pink colour indicates viable cells, whereas blue colour indicates no viable cells thus microbial inhibition. This example well plate shows nanoparticle sample had a MIC of 31.25 µg/ml and was not contaminated as the controls were showing the correct colour indication.

On the other hand, Valodkar *et al.* (2011) reported that copper nanoparticles had higher antimicrobial efficacy than silver nanoparticles, against *S. aureus*. Copper nanoparticles were found to have a MIC of 0.29 µg/ml compared to silver nanoparticles with 0.34 µg/ml [264]. Not only is there a difference in efficacy, the MIC of the nanoparticles is significantly lower than the MIC obtained in this study. The difference in efficacy might be due to various parameters. For example, Valodkar *et al.* (2011) used starch solution as a stabilising agent and microwave energy to synthesise the nanoparticles, in comparison to Ruparelia *et al.* (2008) who produced nanoparticles through wet chemical synthesis using nitrate salt precursors and sodium borohydride. These parameters may have produced nanoparticles with different sizes and surface charges in comparison to the nanoparticles used in this study and therefore led to a difference in antimicrobial efficacy.

Kalińska *et al.* (2019) reported that the antimicrobial efficacy of AgCu nanoparticle was greater than that of copper but lower than that of silver. In this study, some of the data supports this, for example against *S. aureus* copper nanoparticles had the highest MIC (125 µg/ml), Ag nanoparticles with the lowest (15 µg/ml) and AgCu nanoparticles were in the middle (31.5 µg/ml). However, this trend did not apply to all tested microbes; in particular, AgCu nanoparticles had the lowest MIC against *E. coli* at 7.5 µg/ml, whereas the other nanoparticles were at 250 µg/ml or above. This agrees with Zain *et al.* (2014) who reported that silver copper bimetallic nanoparticles have higher antimicrobial activity than silver and copper against *E. coli*. Again, the difference in MIC values might be linked to the physiochemical properties of the nanoparticles. Therefore to investigate the attribution of physiochemical properties towards the antimicrobial efficacy is characterised in Chapter 4. Based on the antimicrobial efficacy of the nanoparticles and broadness of antimicrobial activity, as tested by MIC, the broth inhibition assay and the agar well diffusion method, AgCu nanoparticles was selected as it is the nanoparticle with the highest antimicrobial activity and was further investigated.

3.4.4 Kinetic growth rates

The linear relationship between microbial cells and measured optical density is based on the Lambert-Beer law, and can be used to estimate cell count [265, 266].

The growth of microbes after treatments with AgCu nanoparticles at various concentrations was monitored for 24 hours through the optical density measured by spectrometry at 600 nm. As cells multiply, the cell density increases which can be detected by the increase in turbidity of the sample. The detection of the turbidity of the sample at several time points allows the evaluation of the growth rate and can be used to compare to other AgCu nanoparticle treatment concentrations, as shown previously in Figure 3.3.

The results supported the MIC results; all AgCu nanoparticle concentrations at the microbe corresponding MIC value or higher did not show microbial growth. However, at lower concentrations, growth was shown but at a decreased rate. Using *E. coli* as an example, all samples with AgCu nanoparticles at the MIC value (7.8 μg/ml) or higher had no detected growth. Meanwhile, concentrations that were lower than the MIC value showed growth, with higher growth rates when the concentration was lower. Furthermore, despite showing growth, lower concentrations of AgCu nanoparticles have the ability to increase the lag phase and delay the microbial growth. For example, at 3.9 μg/ml AgCu nanoparticle treatment concentration, growth of *E. coli* was detected after 11 hours, in comparison to concentration of 2.0 μg/ml, where growth was detected after 7 hours of treatment. This demonstrates that the antimicrobial activity of AgCu nanoparticles is concentration dependent. Several reports of similar results have also been reported where the antimicrobial activity of Ag and Cu nanoparticles are concentration dependant against microbes, including *E. coli* and *S. aureus* [248, 267-270].

However, for *C. albicans* the growth curve showed no growth for both treatments of 31.3 μg/ml and 15.6 μg/ml despite the MIC value of 62.5 μg/ml. A reason for this is that fungal yeast cells grow at a slower rate than bacterial cells [271]. As mentioned, AgCu nanoparticles have the ability to increase the lag phase and delay microbial growth. The measurement of no change in optical density may have been the extended lag phase due to the presence of AgCu nanoparticles and growth of *C. albicans* may have been seen after a longer period of time. Furthermore, only optical density is measured in this method and the viability of cells is not accounted for. Thus the AgCu nanoparticles may have inhibited the microbial growth, so cells did

not multiple and no change in optical density was observed; however, the cells are still viable which was shown by the resazurin colour change in the MIC experiment.

Interestingly, in the bacterial samples, the treatment at 0.5 μg/ml had a higher absorbance than the positive control, which suggests that the treatment encouraged bacterial cell growth. However, this might be an overestimation due to interferences with the detected optical density. It is known that debris of dead cells, filamentous growth and fluorescent proteins may affect the absorbance and the estimation of sample cell density [272, 273]. In this experiment, the higher optical density in relation to the control could be an overestimation as a result of cell debris caused by the AgCu nanoparticle treatment. A common theory of metallic nanoparticle mechanism of action is that the physical contact between nanoparticles and the microbe can cause damage to the cell wall [139]. The cell wall damage may lead to leakage of internal cellular organelles and cell wall debris, and therefore increase the turbidity of the sample. The mechanism of action of AgCu nanoparticles, including cell wall damage, will be investigated in Chapter 5.

This experiment has shown that the antimicrobial ability of AgCu nanoparticles is concentration dependent. Concentrations below the MIC values are able to delay the growth of microbes and in some cases might be able to inhibit the growth, but the inhibited cells are still viable after 24 hours of treatment.

3.4.5 Cell viability

Fluorescent dyes were used to observe the cell viability over 5 hours to investigate the effects of antimicrobial AgCu nanoparticle. Propidium iodide is a nucleic acid stain which produces a red fluorescence when bound to DNA. It is used to identify dead cells as the dye can only penetrate cells with disrupted membrane. In contrary, Syto9 is a nucleic acid stain which produces a green fluorescence. Although Syto9 can penetrate both live and dead microbial cells, propidium iodide has a stronger affinity for nucleic acid and can displace Syto9. Therefore, when used together, propidium iodide identifies the dead cells whilst Syto9 identifies the live cells [274]. The visual observations of the fluorescent cells can be seen in Figure 3.9 to Figure 3.11. In contrast to the spectrometry growth rate method, this experiment can identify the cell viability of the microbes from the fluorescence.

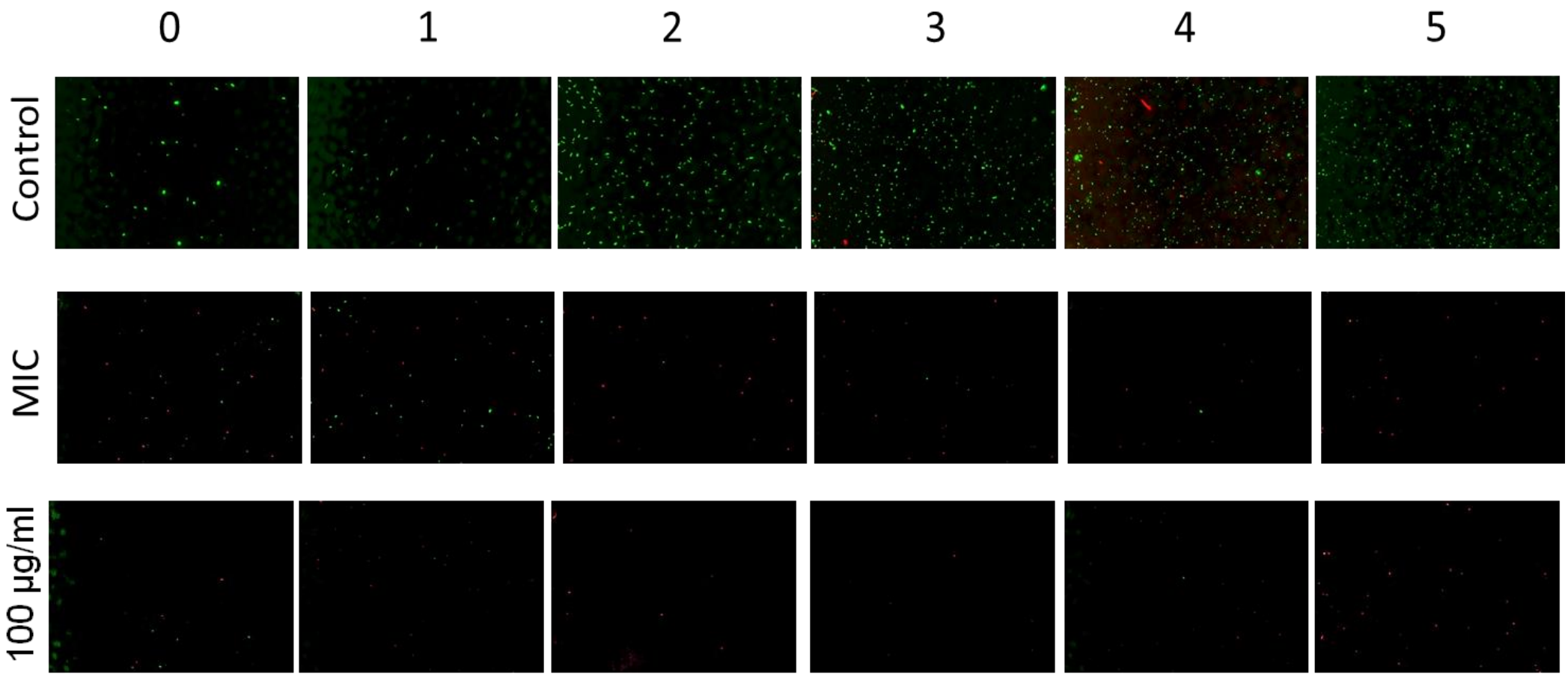

Figure 3.9: Propidium iodide and SYTO9 fluorescent microscope image of *E. coli* during AgCu nanoparticle treatment. Fluorescent green cells indicate live cells and fluorescent red indicates dead cells. Numbers indicate the hours after treatment. Control cells are grown without presence of AgCu nanoparticles, MIC samples were incubated with 7.5 µg/ml of AgCu nanoparticles and final sample was incubated with 100 µg/ml of AgCu nanoparticles.

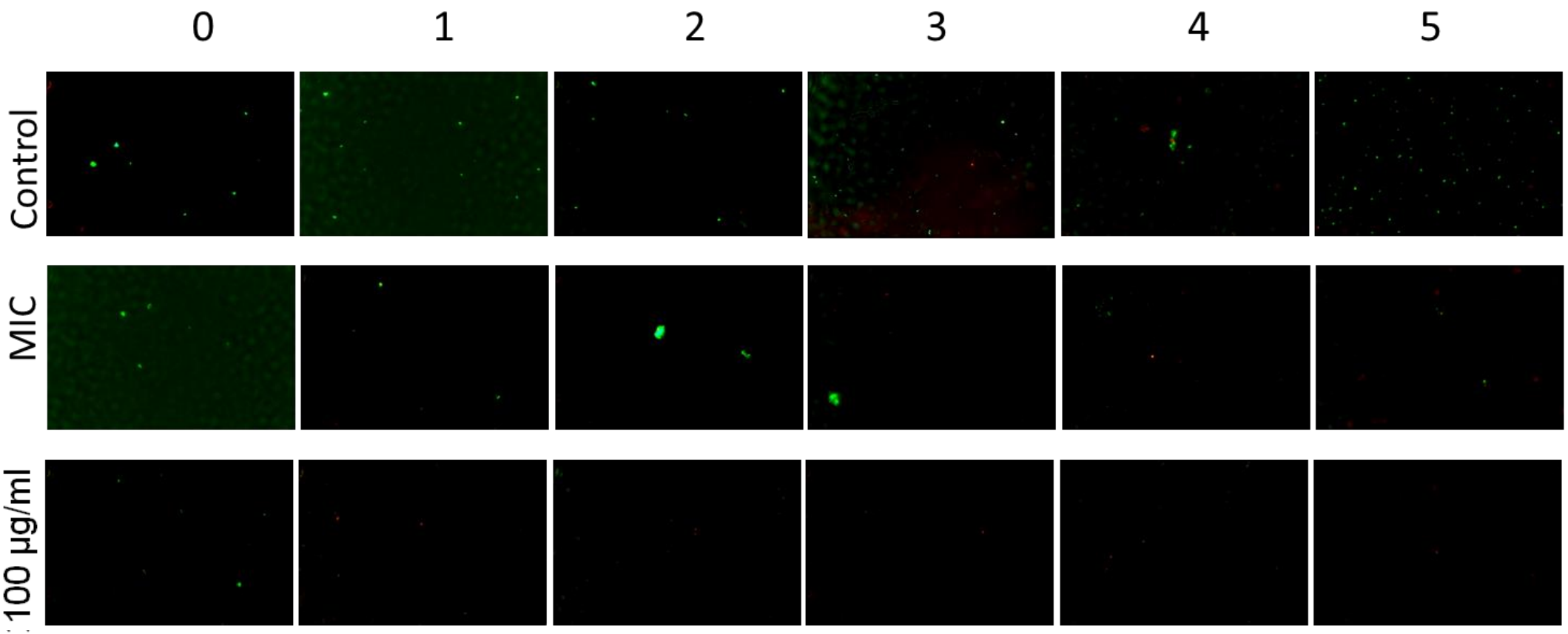

Figure 3.10: Propidium iodide and SYTO9 fluorescent microscope images of *S. aureus* during AgCu nanoparticle treatment. Fluorescent green cells indicate live cells and fluorescent red indicates dead cells. Numbers indicate the hours after treatment. Control cells are grown without presence of AgCu nanoparticles, MIC samples were incubated with 31.25 µg/ml of AgCu nanoparticles and final sample was incubated with 100 µg/ml of AgCu nanoparticles.

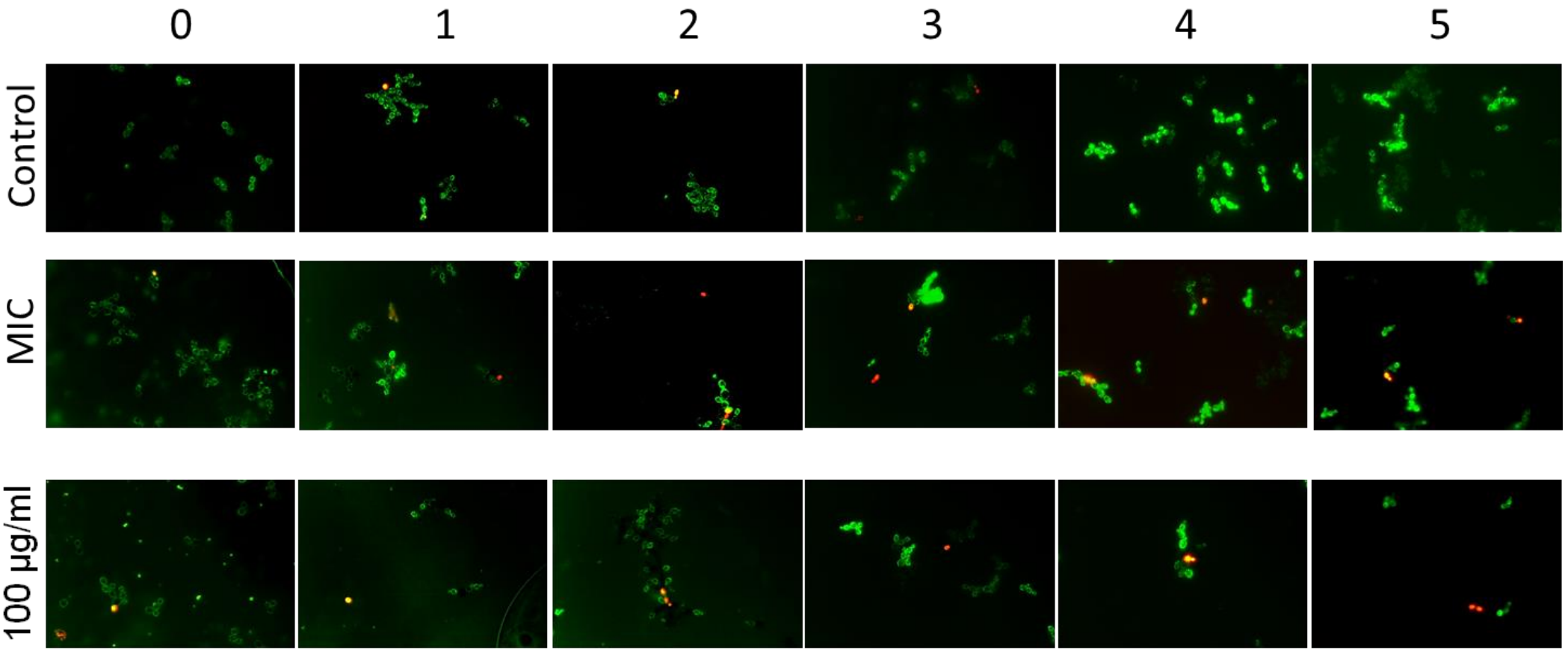

Figure 3.11: Propidium iodide and SYTO9 fluorescent microscope images of *C. albicans* during AgCu nanoparticle treatment. Fluorescent green cells indicate live cells and fluorescent red indicates dead cells. Numbers indicate the hours after treatment. Control cells are grown without presence of AgCu nanoparticles, MIC samples were incubated with 62.5 µg/ml of AgCu nanoparticles and final sample was incubated with 100 µg/ml of AgCu nanoparticles.

Supporting the previous results, it was found that bacteria were more susceptible to AgCu nanoparticles than *C. albicans.* The AgCu nanoparticles were able to kill a higher percentage of bacteria and at a faster rate than against *C. albicans.* For example, after 5 hours of AgCu nanoparticle treatment at the MIC concentration, only 0.1% of *E. coli* was viable, in comparison to just over 17.4% of *C. albicans.* Furthermore, AgCu nanoparticles were able to produce antimicrobial activity immediately upon contact. At 100 μg/ml, an immediate reduction of 95.8% and 16.6% in cell viability was observed in *E. coli* and *S. aureus,* respectively. However, less effect was seen in *C. albicans,* with a 5.2% reduction immediately upon contact. Furthermore, intermediate colours of yellow and orange cells were observed in *C. albicans* samples but were not seen in *E. coli* and *S. aureus* samples. These intermediate colours are in relation to the level of cell membrane damage. Damage to the cell membrane allows the permeation of propidium iodide into the cell which displaces the Syto9 and results in red fluorescent. However, the quantity of permeated propidium iodide reduces with less membrane damage thus resulting in less displacement of Syto9 and leads to intermediate colours [275, 276]. This indicates that some of the *C. albicans* cell membrane was less damaged than bacterial cells. Moreover, longer contact between AgCu nanoparticles and fungi cells is required to damage the cell membrane. Both Paszkiewicz *et al.* (2016) and Reyes *et al.* (2020) found that AgCu nanoparticles were more effective towards bacteria (*E. coli* and *S. aureus*) than fungi (*C. albicans*).

Whilst the mechanism of action of metallic nanoparticles is still unclear, it is hypothesised that nanoparticles interact with and penetrate the cell wall to produce antimicrobial activity. Bacterial cell wall consists of lipopolysaccharides and peptidoglycan, in contrast, fungal yeast cell wall consists of an outer cell wall (mannan and cell wall proteins) and an inner wall (chitin, β-1-6 glucan and β-1-3 glucan). The difference in cell wall composition and structure could be responsible for the difference in susceptibility between the microorganisms; hence AgCu nanoparticles were more antimicrobial effective towards bacterial cells than fungal cells [139, 277, 278]. The mechanism of action of AgCu nanoparticles will be explored in Chapter 5.

3.4.6 Summary

To summarise, two methods were used to screen 26 different types of nanoparticles for antimicrobial activity and found 11 nanoparticles with activity against at least one of the 10 tested pathogens. Five of the most effective nanoparticles were further investigated for their MIC and it was found that Ag and AgCu had the highest antimicrobial efficacy. Although Ag had the lowest MIC ranges for some of the microbes, AgCu was selected as the optimal antimicrobial nanoparticle due to its broad range of antimicrobial activity against bacteria and fungal pathogens and low MIC value in comparison to other nanoparticles tested. Further antimicrobial investigations on AgCu nanoparticles were performed and found that the nanoparticles had immediate antibacterial activity, however it took a bit longer for antifungal effects to be detected. This may have been due to the slower growth rate of fungal yeast cells in comparison to bacterial cells. Moreover, the antimicrobial activity is concentration dependant; lower concentrations can inhibit and delay the growth of microbes, but concentrations levels at the MIC value or higher is required for cell death. Therefore, with the strong antimicrobial efficacy, AgCu nanoparticles have a potential for antimicrobial applications and will be further investigated to understand how their physiochemical properties contribute towards antimicrobial activity.

Chapter 4 Characterisation of antimicrobial nanoparticles (Ag, Cu10 and AgCu) and their properties and performance on antimicrobial activity

4.1 Introduction

For thousands of years, metals have been used for various applications due to their advantageous properties, such as strength, good electrical conductivity and high fracture toughness [279]. With the discovery of nanotechnology, metallic nanoparticles have sparked wide interest in their enhanced properties in comparison to their bulk material. In particular, metallic nanoparticles have been shown to exhibit antimicrobial properties, which confer their suitability for biomedical applications including drug delivery and medical devices [21].

Amongst metals, Ag nanoparticles have received the most attention for their antimicrobial properties, including efficacy towards microbes with antibiotic resistance [280, 281]. This has resulted in their wider exploitation as an antimicrobial agent in applications including fabrics, detergents and steriliser sprays [21, 281]. Cu has been studied less in comparison to silver; nevertheless, it has been recognised by the United States Environmental Protection Agency (US EPA) as an antimicrobial metal and has been used in applications such as antimicrobial coating [282]. Lastly, AgCu alloy has also displayed antimicrobial activity. However, its properties have not been explored until recently. Zain *et al.* (2014) compared Ag, Cu and AgCu alloy nanoparticles and found AgCu alloy had the greatest antimicrobial effect against *B. subtilis* and *E. coli* [283]. On the other hand, Kalińska *et al.* (2019) reported that Ag nanoparticles were more antimicrobial towards *E. coli, S. aureus* and *C. albicans,* in comparison to Cu and AgCu nanoparticles [263]. The contrast in results may be due to differences in synthesis and precursor materials as well as the physiochemical properties of the nanoparticles in each experiment. Whilst the elements themselves contribute to the antimicrobial activity, the physiochemical properties of nanoparticles, such as size, also contribute largely to their antimicrobial activity [22, 236].

The size of nanoparticles is regarded as one of the main factors that promote antimicrobial properties, as smaller sizes particles in general result in greater levels of interaction/penetration to microbial cells. As the size of nanoparticles decreases, the surface area to volume ratio increases. Therefore, nanoparticles with larger surface area, which equate to more elemental atomic level exposure, have greater interaction with microbes [236, 284]. Other factors include the shape and surface charge of nanoparticles, which have been reported to influence the antimicrobial efficacy through the surface area of the shape, ionic particle release rate, attraction towards microbial cells due to surface charge and their suspension stability of the nanoparticles [41, 42, 47, 48].

Previous research suggests that Ag, Cu and AgCu alloy nanoparticles possess many beneficial properties, including antimicrobial activity. The characterisation of their properties enables a further understanding of their antimicrobial activity against a broad range of bacteria and fungi. Moreover, the understanding of nanoparticle properties is needed prior to antimicrobial and biomedical applications. With this in mind, it is imperative to study the physical and chemical properties of the nanoparticles.

Outline of the research work:

This chapter investigates and characterises the properties of Ag, Cu and AgCu nanoparticles, which were selected based on their effective antimicrobial screening activities from Chapter 3. The physical morphology of these nanoparticles was observed using SEM and TEM. ZetaSizer was used to measure the ζ- potential and their hydrodynamic size in suspension states. Furthermore, NTA was used to measure the hydrodynamic size distributions and particle concentrations. Lastly, optical properties were measured using UV-Vis and the pH of suspension supernatants from Ag, Cu and AgCu were also investigated.

4.2 Materials and methods

In this study, the properties of elemental silver (Ag), elemental copper (Cu10) and bimetallic Silver Copper (AgCu) nanoparticles were investigated. The preparation of nanoparticle stock suspensions and manufacturer details can be found in Chapter 2, section 2.1 and Chapter 3, section 3.2, respectively. Further dilutions of nanoparticle suspensions were made by diluting stock suspension with pure water to produce desired concentrations. Prior to experiments, all samples were dispersed by vortex and in a sonic bath for 1 minute.

4.2.1 SEM

Freshly dispersed nanoparticle suspensions in ethanol at 1000 μg/ml were pipetted onto a carbon tape and vacuumed for 1 hour or until dried. Additionally, nanoparticle powder placed onto carbon tape using small spatula. Both powder and dispersed suspension samples were gold sputtered (Agar Scientific, UK) for 45 seconds and then their surface morphologies were imaged using an SEM from JCM5700 (JEOL, UK) set at 20V with x6000 magnification.

4.2.2 TEM

AgCu and Cu10 nanoparticles were freshly dispersed in ethanol and the supernatant was pipetted onto a carbon-supported TEM mesh grid and left to dry under vacuum. The grids were then imaged on TEM JEOL-1400 (JEOL, UK). For Ag nanoparticles, image was taken from Li *et al.* (2013).

4.2.3 UV-Vis spectroscopy

Freshly dispersed nanoparticle samples were measured using a Quartz glass cuvette inside a UV-Vis Spectrophotometer (Agilent Technologies, USA). Initial concentration of 31.25 μg/ml was measured and then concentration increased until peak absorbance was between 1-2. Parameters were set to double Beam Mode 200V with scan rate at 600 nm/min starting at wavelength 800 nm and ending at 200 nm. All samples were measured with sterile distilled water as a blank control. The cuvette was cleaned using acetone and dried with compressed air between each sample.

4.2.4 pH

Freshly dispersed nanoparticle suspensions were diluted to concentrations from 1000 to 10 μg/ml. The pH of the supernatant was measure carefully without disturbing nanoparticle sediments immediately and after 14 days, using a hand held pH meter (Jenway, UK). The pH probe was cleaned using acetone and pure water between each sample. The experiment was carried out in triplicate. The mean average of the triplicates were calculated and presented as a scatter graph with the error bars to denote standard deviation of the means.

4.2.5 ZetaSizer and NTA

The surface charge of Ag, Cu10 and AgCu nanoparticles were investigated. Additionally, Cu10 with the addition of NH_4OH (same concentration and preparation as Ag and AgCu nanoparticle suspension) was also investigated. The ζ- potential of freshly dispersed nanoparticles at 100 μg/ml, 250 μg/ml and MIC values (found in Chapter 3, Table 3.5) was measured. All experiments were measured with a Zetasizer (Malvern Instruments, UK) using SOP V2 DTS1060. The capillary cell was rinsed with industrial methylated spirit and distilled water between each sample. All ζ- potentials were measured in triplicate, with 100 measurements per replicate. Data are presented as a scatter graph of the mean measurement with standard deviations denoted by the error bars.

The hydrodynamic sizes of freshly dispersed nanoparticles at 100 μg/ml, 250 μg/ml and MIC values (found in Chapter 3, Table 3.5) were measured using the DLS function of a Zetasizer (Malvern Panalytical, UK). All measurements were performed in triplicate, with 100 measurements per replicate. Data are presented as a scatter graph of the mean hydrodynamic diameter with standard deviations denoted by the error bars.

Using a NTA Nanosight NS300 (Malvern Panalytical, UK) with Blue405 laser type, the hydrodynamic size distribution of the freshly dispersed nanoparticle samples at 10 μg/ml concentration was measured. Programme was set to continuous mode (5 replicates of 30 seconds at 20 μl/min) and samples were dispersed via vortexting and 1 minute sonic bath prior to measurement. Built in software analysis was used to find the size distribution and the data are presented as a histogram using the average mean of the 5 replicates.

4.3 Results

4.3.1 Morphologies of nanoparticles and their sizes

To observe the physical morphology of the nanoparticles, SEM was used to image powdered and dispersed nanoparticles at x6000 magnification. As shown in Figure 4.1, dispersed nanoparticles were less agglomerated than the powered version; however, agglomerations were still present. In regards to the dispersed samples, Cu10 nanoparticles were more agglomerated than Ag and AgCu nanoparticles. All three nanoparticles were observed to be spherical in shape. Closer magnification of the nanoparticles was observed using the TEM. AgCu, Ag and Cu10 nanoparticles were observed to be between 86 to 36 nm, 22 to 13 nm and 28 to 43 nm, respectively. As shown in Figure 4.2, all the nanoparticles were spherical; however, some of the Cu10 nanoparticles were cubical.

The hydrodynamic particle size of the nanoparticles was investigated using DLS on a Zetasizer (Malvern Panalytics, UK). As shown in Figure 4.3, the particle size decreased as the concentration of nanoparticles increased; especially in the Cu10 sample where the lowest measured concentration (31.25 µg/ml) had a mean diameter size of 894.6 nm, in contrast, the highest measured concentration (250 µg/ml) had a mean diameter of 716.0 nm. Both Ag and AgCu had similar particle size at 250 µg/ml concentration, a mean diameter of 176.7 nm and 170.6 nm, respectively, and a slightly higher diameter at 31.25 µg/ml (198.4 nm and 181 nm, respectively). Cu10 nanoparticle suspension with addition of NH_4OH resulted in a slight increase in hydrodynamic size, with diameters of up to 915 nm.

The size distribution of Ag, AgCu and Cu nanoparticles was also investigated using NTA Nanosight300 (Malvern Panalytics, UK). As shown in Figure 4.4, the overall size distribution of nanoparticles ranged from 32 to 594 nm; however the majority of nanoparticles were between 51-400 nm. The most frequently detected particle diameter size was between 101-150 nm. Ag and AgCu nanoparticles had a more distinctive peak (at 101-150 nm) whilst Cu nanoparticles were quite broadly ranged between 101-350 nm. The captured images of the particles show that Cu10 had larger sized particles, in contrast, Ag and AgCu nanoparticles were observed to look quite similar.

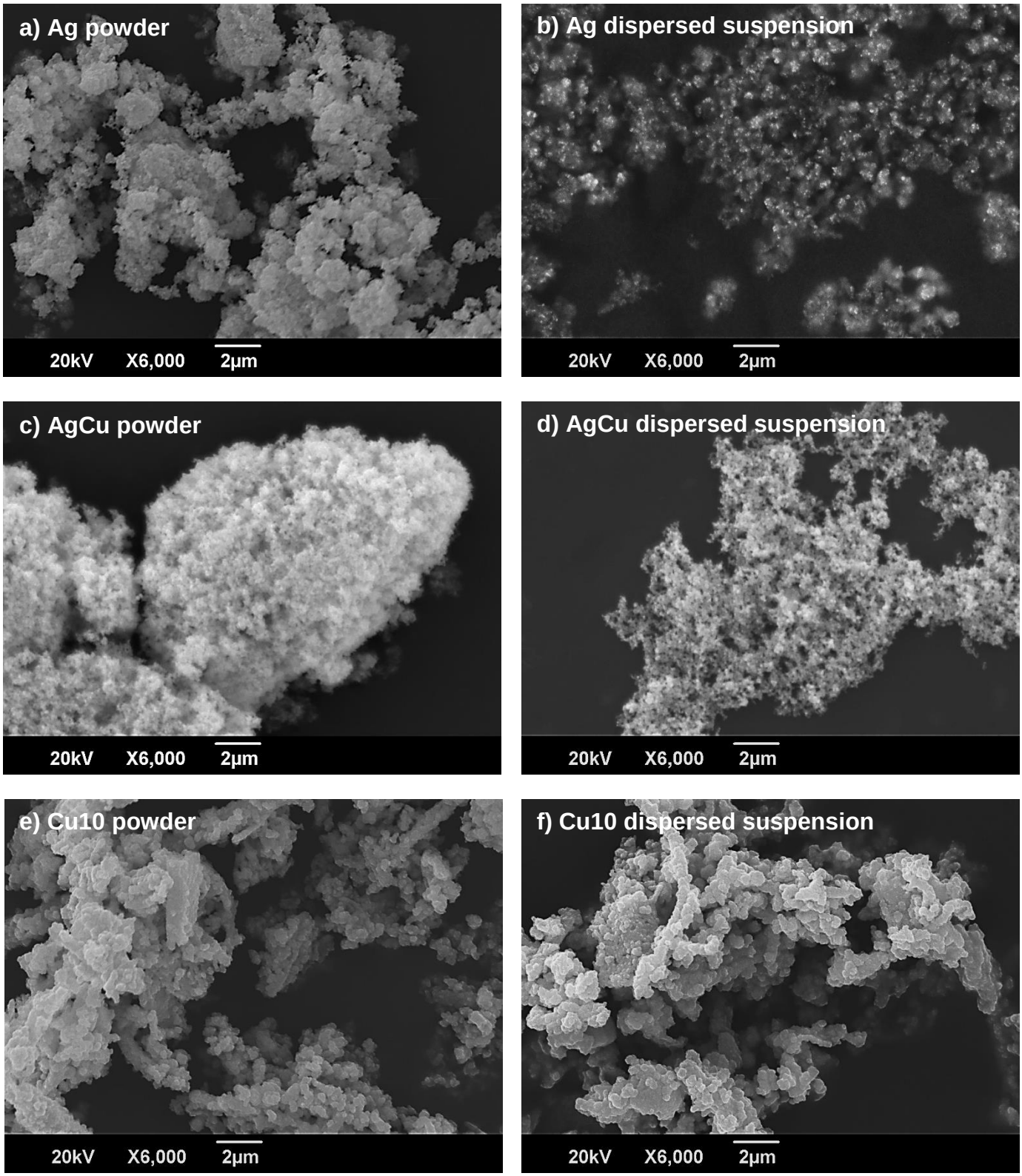

Figure 4.1: SEM images of antimicrobial metallic nanoparticles. SEM images of nanoparticle samples at magnification of x6000. a) Ag powder, b) Ag dispersed suspension, c) AgCu powder, d) AgCu dispersed suspension, e) Cu10 powder and f) Cu10 dispersed suspension

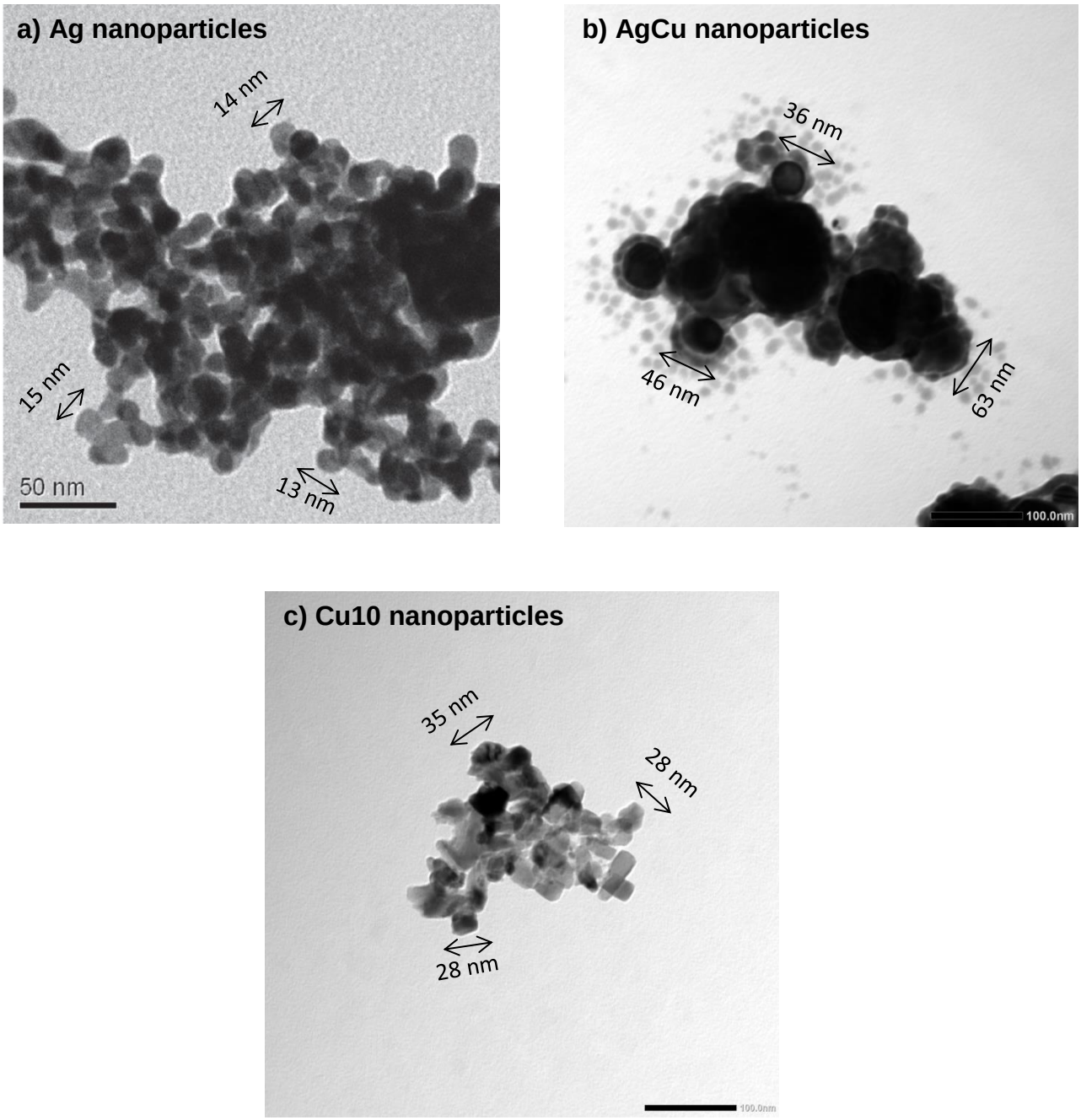

Figure 4.2: TEM images of antimicrobial metallic nanoparticles. TEM images of dispersed nanoparticles. a) Ag (taken from Li et al. (2013), b) AgCu and c) Cu10. The sizes of the particles were measured using ImageJ and annotated onto the images.

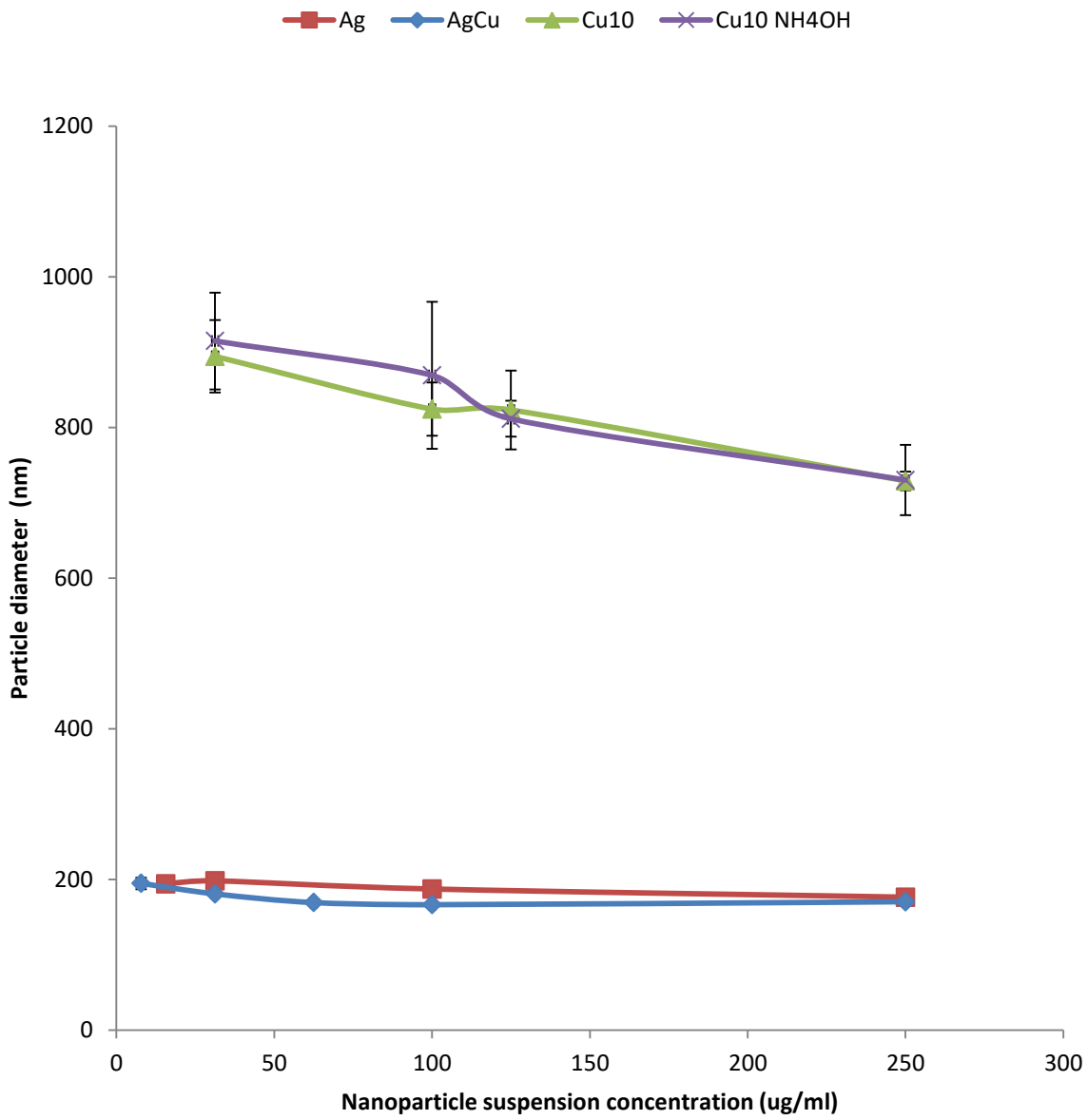

Figure 4.3: Hydrodynamic size of metallic nanoparticles. The influence of concentration on the hydrodynamic size of nanoparticles was measured using a dynamic light scattering technique. The mean results of particle diameter in nm are presented as Ag (red), AgCu (blue), Cu10 (green) and NH_4OH treated Cu10 (purple). Error bars denote the standard deviation.

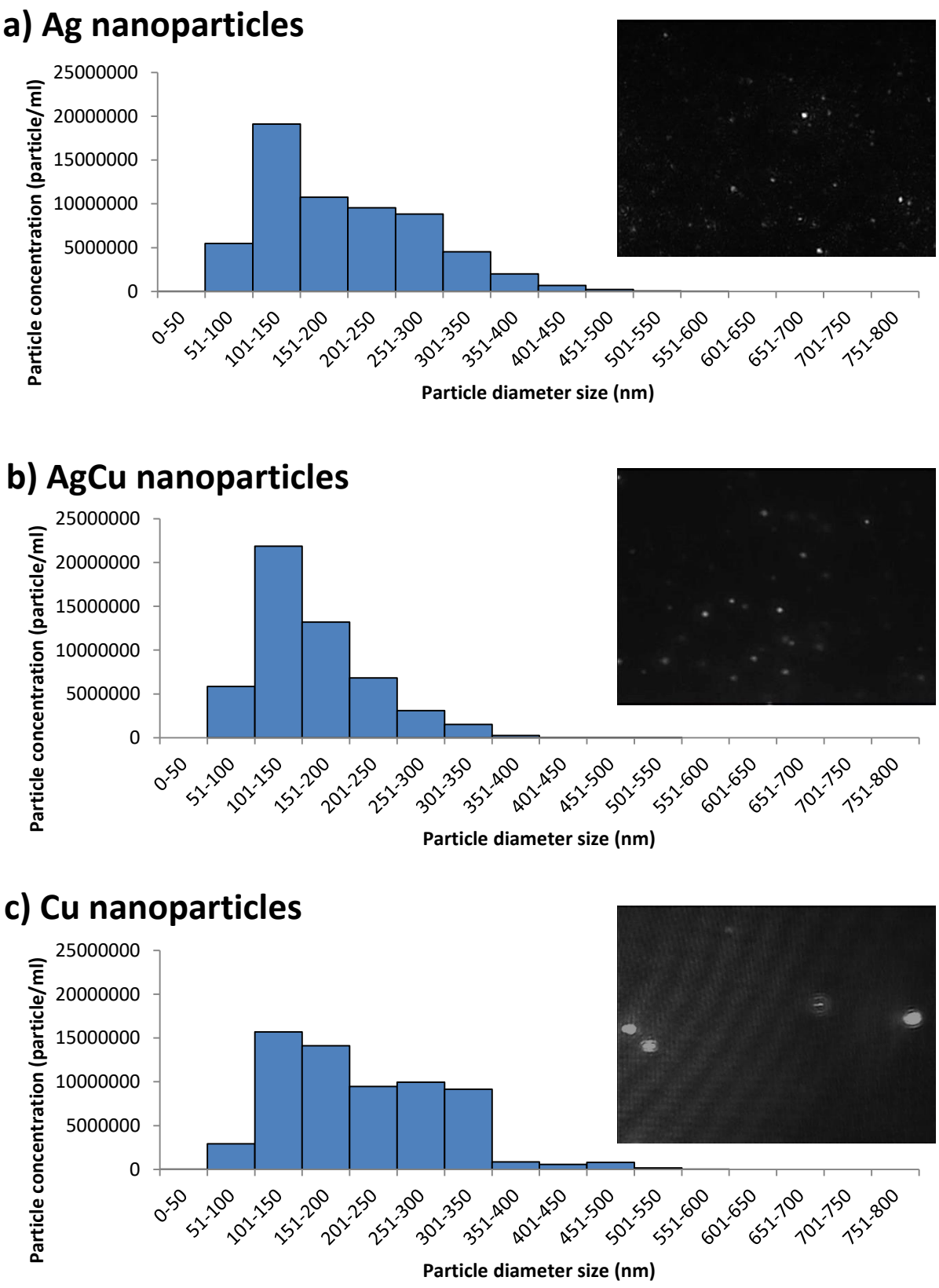

Figure 4.4: Nanoparticle hydrodynamic size distribution. The hydrodynamic diameter size distribution in nm of nanoparticle suspensions at 10 µg/ml was measured by the NTA, with an example of recorded observed particles; a) Ag nanoparticles, b) AgCu nanoparticles and c) Cu nanoparticles.

4.3.2 Optical and chemical properties

UV-Vis spectrometry was used to analyse the optical properties of Ag, Cu10 and AgCu with Figure 4.5 displaying the UV-Vis absorption spectra of the three nanoparticles at 250 µg/ml concentration. The λ_{max} values of Ag and AgCu were 402 nm and 410 nm, respectively, whereas no λ_{max} peaks were detected for Cu10. Both Ag and AgCu showed a single absorbance peak, with AgCu showing a sharper and higher absorbance. Whilst other concentrations were measured, the concentration at 250 µg/ml produced optimal absorbance (between 0-2 abs); data from other concentrations can be found in the Appendix (with the λ_{max} AgCu nanoparticles between 410 to 417 nm with lower concentrations showing longer wavelength).

The Zetasizer (Malvern panalytics, UK) was used to analyse the ζ- potential of Ag, AgCu, Cu10 and NH_4OH treated nanoparticles as shown in Figure 4.6. ζ- potential values outside the ±20 mV range are regarded as stable. In all three samples, the increase in concentration resulted in greater stability. In all concentrations measured, Ag and AgCu suspensions were stable; however, for Cu10, concentrations below 250 µg/ml were unstable. The addition of NH_4OH improved the stability of Cu10 slightly at 31.25 µg/ml, however the ζ- potential was similar to the untreated sample for the rest of the tested concentrations. AgCu and Ag nanoparticle suspensions have a negative surface charge, whilst Cu10 had a positive surface charge.

Furthermore, the pH of nanoparticle suspensions was measured using a glass pH probe. Without nanoparticles, the water control was found to be an average pH 6.73 which is slightly acidic, but in the average range for water pH. For Ag and AgCu nanoparticles, there was a positive correlation between the increase in pH and the increase in nanoparticle concentration. As shown in Figure 4.7, Ag reached the greatest pH followed by AgCu with an alkaline measurement of pH 9.02 and pH 7.98 at 800 µg/ml, respectively. On the other hand, Cu10 was more acidic than water and maintained pH 6.69-6.70 with no correlation to the increase in concentration. The NH_4OH control shows minimal influence on the alkalinity of Ag and AgCu and had roughly the same pH as water (except at 200 µg/ml). After 14 days, an increase in pH was seen for both Ag and AgCu, as displayed in Figure 4.7. However, no change was seen in Cu10 samples.

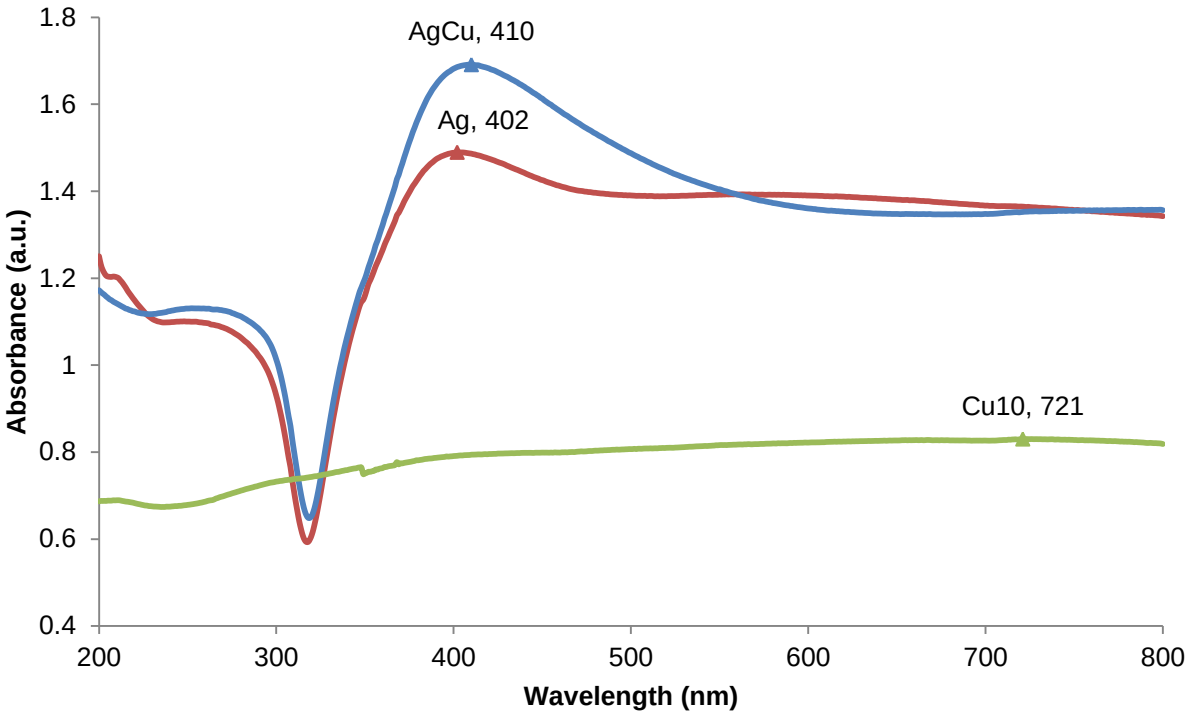

Figure 4.5: Absorption spectra of UV-Vis results. Using a UV-Vis spectrometer, the adsorption spectrum of nanoparticle suspensions were measured and presented as AgCu (blue line), Ag (red line) and Cu10 (green line), with the λ_{max} value of each sample displayed at the peak value of each line. All samples were at 250 µg/ml concentration

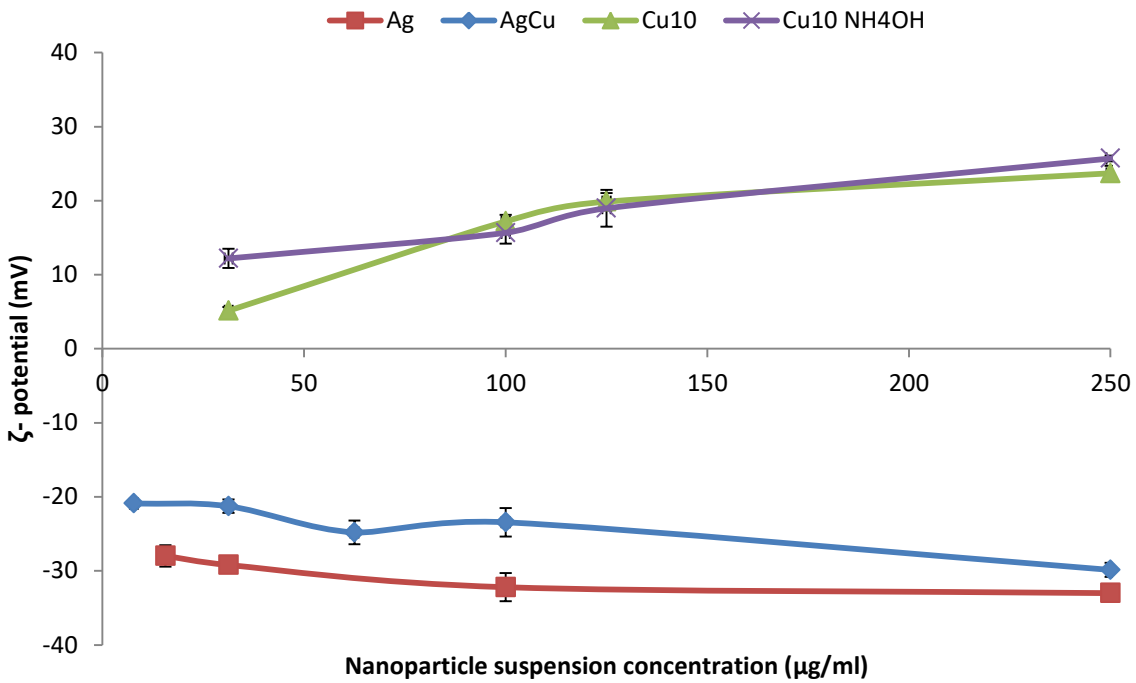

Figure 4.6: ζ- potential of nanoparticles. The influence of concentration on the ζ- potential of nanoparticles was measured using a ZetaSizer (Malvern, Panalytics, UK). The mean average results of 100 replicates is presented in mV as Ag (red), AgCu (blue), Cu10 (green) and NH_4OH treated Cu10 (purple). Error bars denote the standard deviation. Stable ζ-potential are regarded as values outside the ±20 mV region.

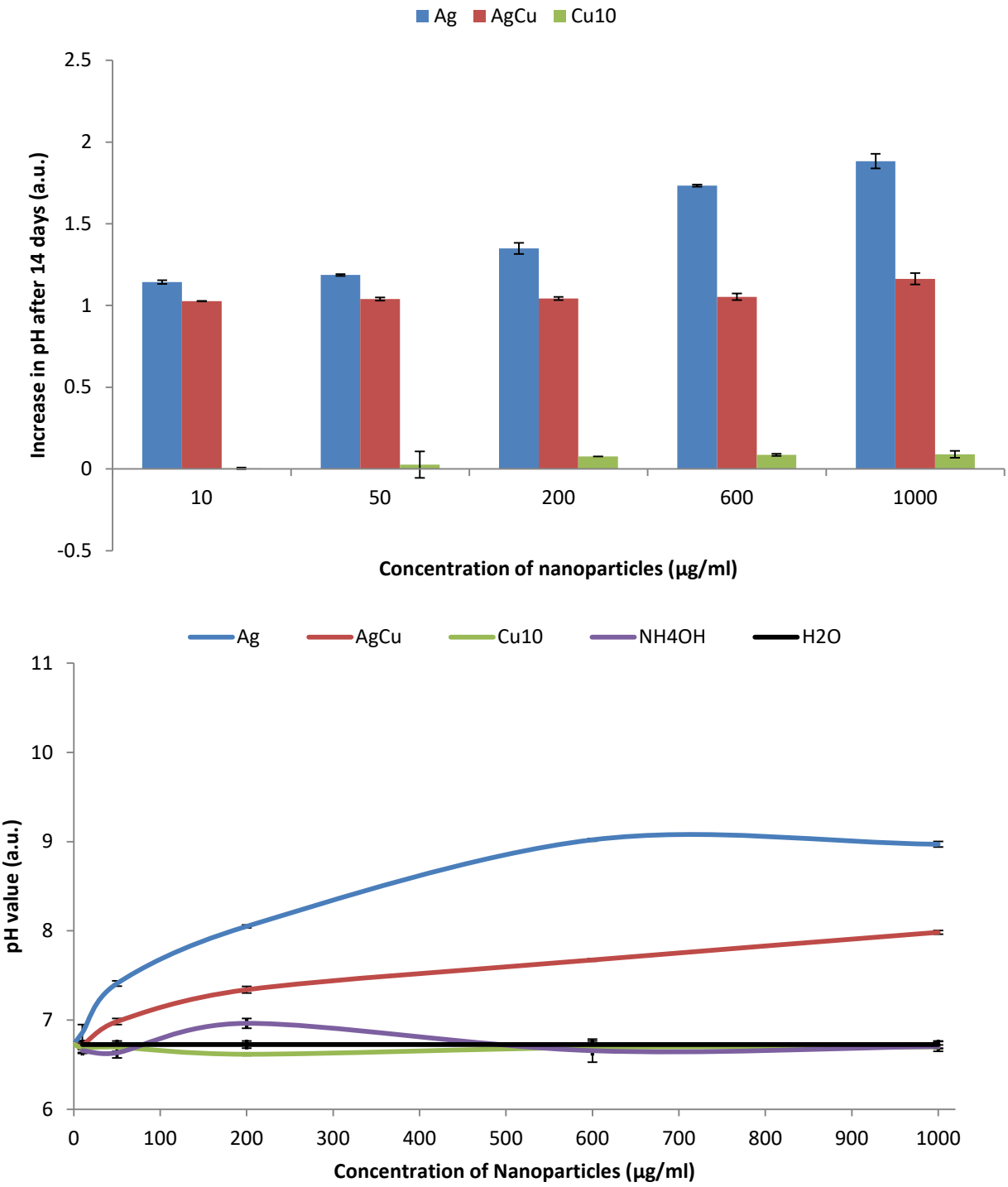

Figure 4.7: Comparison of nanoparticle supernatant pH influenced by the change in nanoparticle concentration and time. a) The pH increase between freshly dispersed nanoparticle suspensions and those left undisturbed for 14 days. b) The pH value of nanoparticle suspension after 14 days. The experiments were performed in triplicates and the mean average results are presented as AgCu (blue), Ag (red) and Cu10 (green). Controls of ammonium hydroxide (NH_4OH) and pure water were also measured and presented as purple and black respectively. Error bars are denoted as standard deviation of results.

4.4 Discussion

The properties of nanoparticles are known to have a key contribution to their useful applications. The characterisation of nanoparticles can be used to understand their behaviour in a suspension and to identify properties that contribute to their antimicrobial activity.

4.4.1 Surface charge, stability and size

ζ- potential is frequently measured to analyse nanoparticles to understand their stability in a suspension and electrostatic charge of the surface. Typically, a stable suspension will have a ζ- potential of ±30 mV; values outside of that range are more likely to result in agglomeration of particles [83, 285, 286]. However, some reports have accepted ζ- potential of ±20 mV of colloidal solutions as stable and with minimal aggregation [84]. Additionally, it has been reported that the ζ- potential is also directly linked to the antimicrobial efficacy of metal nanoparticles, with more positively charged nanoparticles exhibiting greater antimicrobial activity due to the attraction to negatively charged microbial cells [42, 287].

The ζ- potential of the tested nanoparticles became more stable as the concentration increased. At 100 μg/ml concentration, the ζ- potential of Ag and AgCu were -32.2 mV and -23.4 mV, respectively, which is regarded as stable as they are outside the instability range of ±20mV. Similar results were obtained previously; for example, Erdogan *et al.* (2019) and Saeb *et al.* (2014) reported that the ζ- potential of their Ag nanoparticles was -32.3 mV and -30 mV, respectively. AgCu nanoparticles have been reported with -27.9 mV ζ- potential, however, the value changed with the Ag to Cu ratio [288]. It has also been found that the ζ- potential of Ag, AgCu and Cu reached +27.8 to +33.9 mV [283]. In contrast, at the same concentration, the ζ- potential value of Cu10 (+17.2 mV) indicates that the suspension is unstable, as it is between -20 and +20 mV. This suggests that the suspension is likely to have formed agglomerates which concur with the UV-vis results, physical observations and the hydrodynamic size measurements. Kalińska *et al.* (2019) also found that Cu nanoparticles were unstable with a ζ- potential of -9.25 mV. Although Ag and AgCu nanoparticle suspensions were treated with NH_4OH to aid dispersion, NH_4OH treatment on Cu10 nanoparticle treatment did not improve the ζ- potential and stability of Cu10. Ammonium hydroxide can contribute to the dissolution of Cu [289].

However, since a small concentration of ammonium hydroxide was added to the nanoparticle suspension, low rates of Cu dissolution may have occurred, thus an improvement in stability was undetected. The differences in ζ- potential could be due to synthesis, substrates and environment of the suspension.

The surface charge of a particle acts like an energy barrier of electrostatic repulsion; ζ- potential values closer to 0 have the least energy, whilst the further away from 0, the larger the energy. Particles with ζ- potential values that are outside the unstable range have enough electrostatic energy to repel and prevent agglomeration; on the other hand, particles with ζ- potential values within the unstable range have less electrostatic energy to repel and therefore can agglomerate [43]. Figure 4.8 gives a visual example to represent the repulsion energy contributed by the ζ- potential.

Agglomerations can increase the overall size of nanoparticles and reduce the surface area to volume ratio. The antimicrobial activity of nanoparticles has been linked to their small size and large surface areas, which can release ions that are toxic to microbes [22, 249]. The ζ- potential suggests that the instability of Cu10 nanoparticles might have resulted in agglomerations, which increases the overall size, thus leading to reduced antimicrobial activity. With the addition of NH_4OH, the ζ- potential of Cu10 nanoparticle suspension at 31.25 μg/ml slightly increased, however the values were still within the unstable range, whilst the remaining concentrations the ζ- potential was similar to that of Cu10 without NH_4OH treatment. This suggests that the NH_4OH did not have significant effect on the stability of Cu10 nanoparticle suspension. In contrast, Ag and AgCu nanoparticles are more stable and therefore contributed to higher antimicrobial efficacy thus a lower MIC value in comparison to Cu10. However, it is invalid to compare the nanoparticles as they have many other different properties.

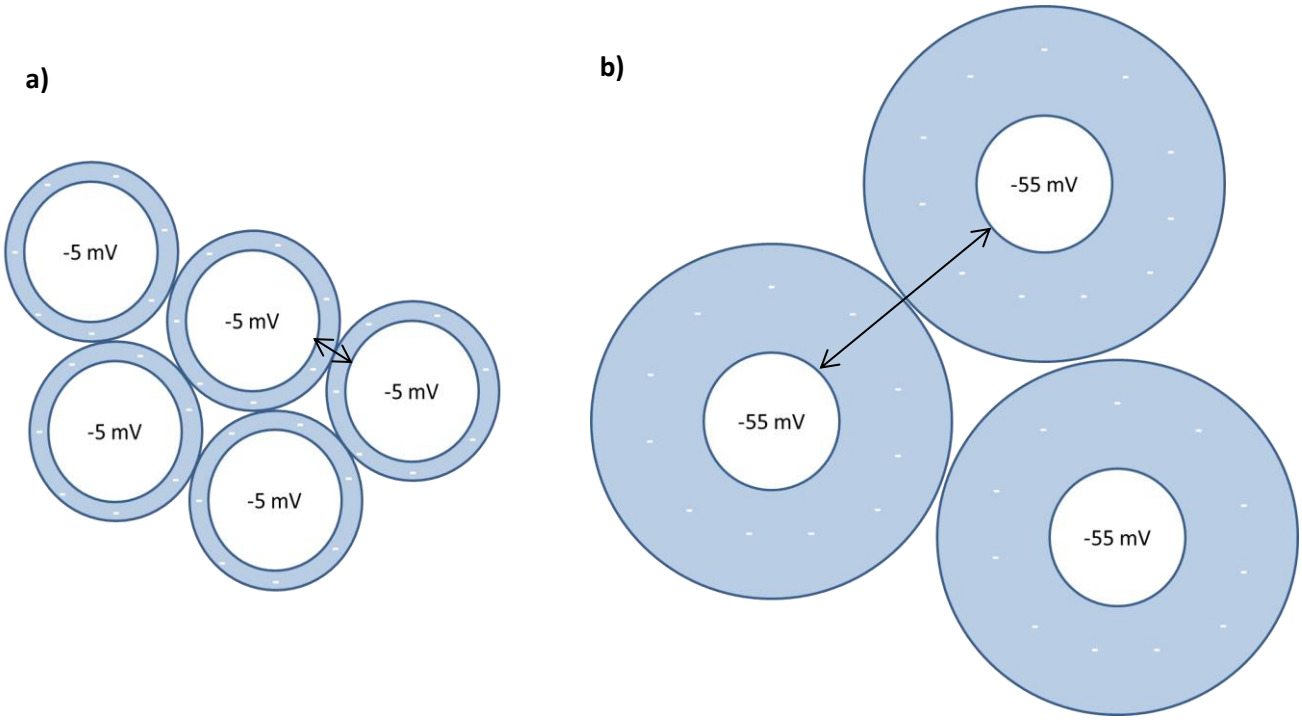

Figure 4.8: Example of surface charge contribution to repulsion energy between particle cells. a) Particles with ζ- potential values within the unstable range have low electrostatic energy to repel surrounding particles. Therefore particles can come close into contact and result in agglomerations. b) Particles with ζ- potential value outside the unstable range have higher electrostatic energy and can repel surrounding particles. This results in more dispersed particles in a suspension. White circle represents a particles and blue area surrounding the particle represents the electrostatic energy barrier produced by the surface charge of the particle. The distance between particles is highlighted by the double ended arrow.

As observed with the TEM and measured using ImageJ, the nanoparticles varied in diameter in the dry state. AgCu nanoparticles were the largest with diameter size between 86 to 36 nm, Cu10 nanoparticles were smaller with diameters of 43 to 28 nm and Ag nanoparticles were the smallest at 22 to 13 nm. However, in solution, the particles can behave differently to their dry state; the particle surface can be influenced by the solution environment, thus this can result in functionalisation or agglomeration of nanoparticles [89]. The hydrodynamic diameter is the diameter of a dynamic particle in solution. Techniques, such as NTA and DLS, can utilise laser lights to characterise the hydrodynamic particles sizes through Brownian motion of nanoparticles in solution [89, 92].

The hydrodynamic size of the tested nanoparticles at different concentrations correlated with their ζ- potential. As the ζ- potential value became more stable, the smaller the hydrodynamic size of the nanoparticles. The most significant difference was seen in Cu10 sample; at 31.25 μg/ml the ζ- potential was unstable (5.13 mV) and the hydrodynamic size was 894.6 nm. However, at 250 μg/ml, the ζ- potential was 23.7 mV and the hydrodynamic size decreased to 716.0 nm. This suggests that the increase in nanoparticle cell density resulted in greater surface charge, which enabled the nanoparticles to repel each other and therefore, reduced agglomerations. Furthermore, as mentioned earlier, throughout all tested concentrations Ag and AgCu nanoparticles had stable ζ- potential and the hydrodynamic size were smaller than Cu10, with diameters ranging from 176.7-198.4 nm and 166.7-194.95 nm, respectively. Hence, nanoparticles with stable ζ-potential had more surface charge to repel each other with reduced chances of agglomerations. However, Ag and AgCu nanoparticle suspensions had an addition of NH_4OH to aid dispersion. The hydrodynamic size of NH_4OH treated Cu10 was also tested and found that it had no significant effect, which suggests that the NH_4OH treatment did not affect their hydrodynamic size.

The DLS showed that lower concentrations of nanoparticles have larger sized particles. However, a slight difference in hydrodynamic sizes was measured between the DLS and NTA. At 10 μg/ml, the NTA did not pick up many Cu10 particles above 600 nm. In contrast, the average hydrodynamic size of Cu10 at 31.25 μg/ml, as measured by DLS, was 874.2 nm. A reason for this is that the NTA is unable to

measure particles larger than 1000 nm, whereas DLS can detect particles up to 10 μm [89, 290]. Furthermore, DLS takes the average size; hence larger agglomerations can skew the results and lead to a larger average size measurement [89]. Although the ζ- potential of AgCu was stable and less likely to form agglomerations, the hydrodynamic size distribution measured by NTA showed that the sizes ranged from 51 nm to 517 nm, thus there were some agglomerations which resulted in larger sizes. Overall, the results show that the majority of the nanoparticles were between 100-150 nm which shows that most of AgCu nanoparticles in the suspension were relatively small with few agglomerations as indicated by the larger sized particles. Ag nanoparticles also showed similar results with stable ζ- potential and diameter size range between 32 - 594 nm. This shows that both Ag and AgCu nanoparticles had consistent particles sizes. On the other hand, the size distribution of Cu10 nanoparticles was more spread with a less distinctive frequency at a particular size. This agrees with the surface charge; as the Cu10 nanoparticles had an unstable ζ- potential, agglomerations are likely to form and hence larger particle sizes were measured.

The images obtained from the NTA and SEM also correlate with the ζ- potential and hydrodynamic size. The NTA utilises a camera to detect the scattering of laser light in order to visualize the nanoparticles. As particles increase in size, they scatter more light which results in a brighter light intensity [291]. The NTA images visually show that Cu10 nanoparticles were larger in comparison to the Ag and AgCu nanoparticles, which were similar in size. In addition, Cu10 nanoparticles had brighter light intensity compared to the other nanoparticles. From the SEM images, it was observed that sonication dispersed the Ag and AgCu nanoparticles in suspension as the particles looked less agglomerated. However, the powder samples and sonicated samples did not have a significant difference in the Cu10 samples, where both samples look agglomerated. As can be seen in Figure 4.9 - prior to sonication, settled nanoparticles and agglomerates can be seen in suspensions; after one minute of sonication, the samples were dispersed however some agglomerates were still present at the bottom of the Cu10 sample. This agrees with the instability of Cu10 suspension which led to agglomerations and resulted in larger sized hydrodynamic particles.

a) **b)**

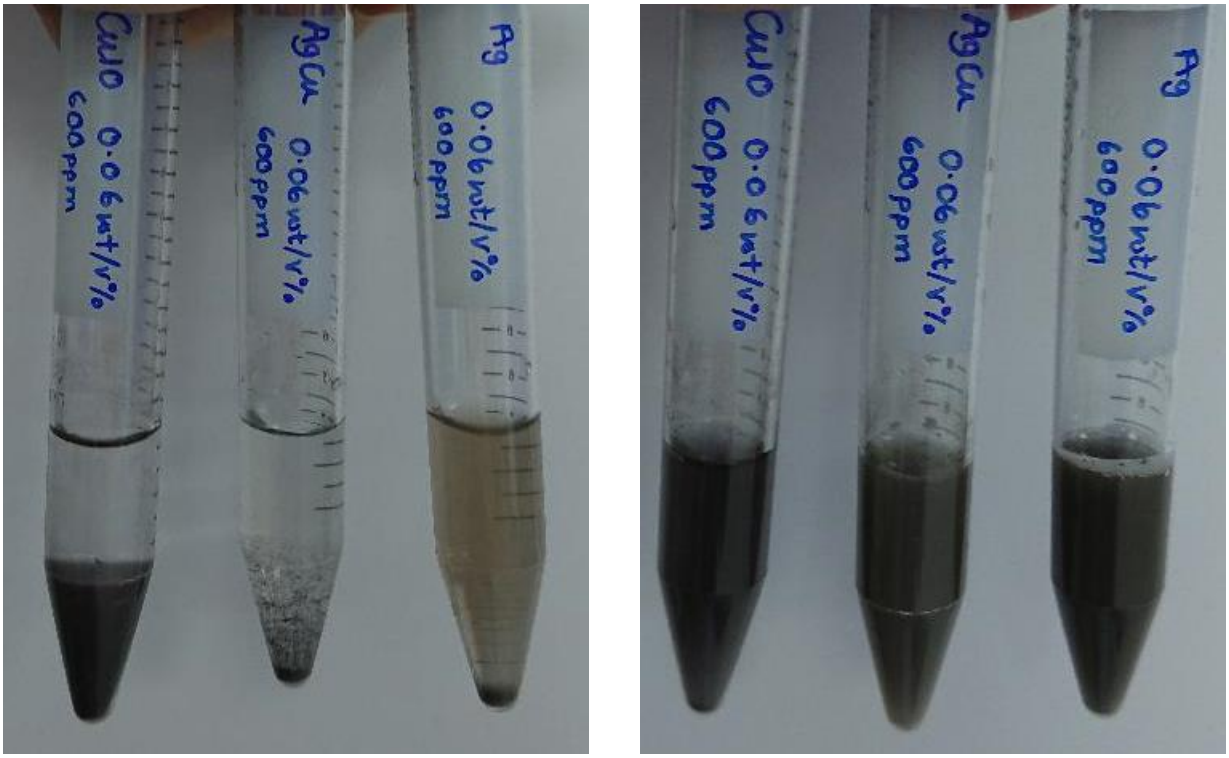

Figure 4.9: Visual observation of nanoparticle suspensions before and after sonication. a) Nanoparticle suspensions 2 weeks after liquid sonication treatment; nanoparticles and possible agglomerates can be observed at the bottom of the conical tube. b) Dispersed nanoparticle suspension after one minute sonic bath treatment.

It has been reported that the antimicrobial activity of nanoparticles is size dependent, with smaller nanoparticles producing higher toxicity [22, 39]. In Chapter 3, it was found that both Ag and AgCu had similar MIC values. In contrast, Cu10 had a higher MIC values; the MIC results from Chapter 3 are displayed in Figure 4.10. In relation to the hydrodynamic size, a correlation is seen between the antimicrobial efficacy (as measured by MIC) and the hydrodynamic size, with smaller hydrodynamic size producing better antimicrobial activity. For example, the hydrodynamic sizes of Ag and AgCu were similar with a mean of 176.7 nm and 170.6 nm, respectively, at 250 µg/ml and their MIC values were 62.5 µg/ml or less, except for Ag nanoparticles against *E. coli.* On the other hand, Cu10 had a larger hydrodynamic size of 716 nm at the same concentration and the MIC values were between 125 to 250 µg/ml, except against *A. baumannii*. This suggests that the size of nanoparticles contributed to the antimicrobial efficacy.

Similar results were reported by Jeong *et al.* (2014) and found that smaller Ag nanoparticles (10 nm) had more antimicrobial activity than larger Ag nanoparticles (100 nm) at the same mass per volume concentration. It was suggested that smaller nanoparticles had higher antimicrobial activity due to their higher surface area to volume ratio, which results in higher chances of physical contact with microbes and increased release of ions. Although the mechanisms of action of nanoparticles are unclear, it has been hypothesised that physical contact and ions can react with and damage biological molecules, thus leading to cell death [139]. This suggests that hydrodynamic size of nanoparticles is an important factor that contributes to their antimicrobial activity.

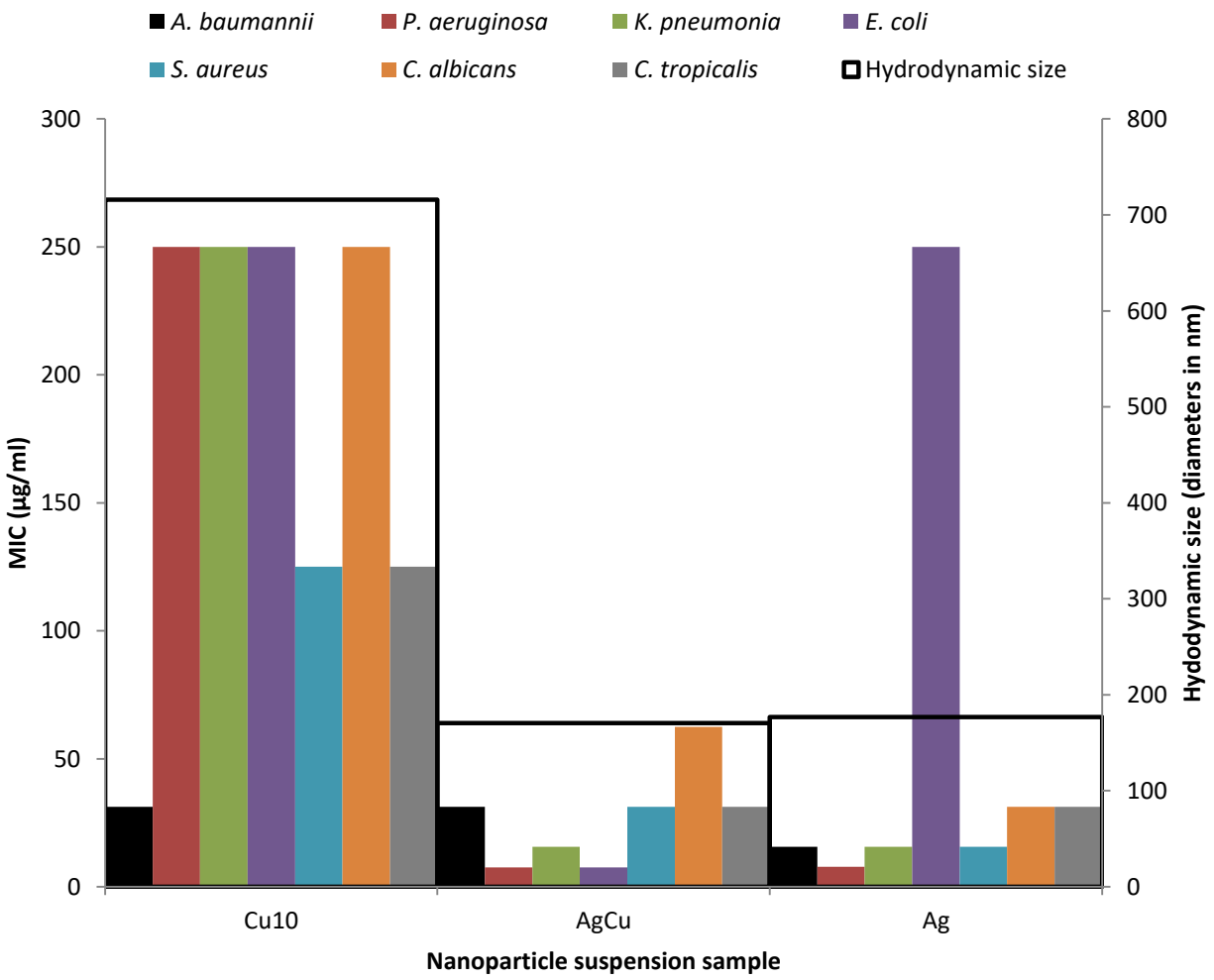

Figure 4.10: MIC results from Chapter 3 compared to hydrodynamic size of nanoparticles. Bar graph displaying the MIC results (obtained from the broth inhibition assay in Chapter 3) of AgCu nanoparticles, Ag nanoparticles and Cu10 nanoparticles against Gram-negative bacteria (*A. baumannii, P. aeruginosa, K. pneumonia, E. coli*), Gram-positive bacteria (*S. aureus*) and fungi (*C. albicans and C. tropicalis*) and the hydrodynamic sizes of the nanoparticles.

Other than stability, the ζ- potential can be used to investigate the surface attraction between nanoparticles and microorganisms. Although different types of microbes have differences in their cell wall, most have a negative net surface charge. The negative charge is a result of the presence of phosphate groups in fungi, and carboxyl, phosphate and amino groups in bacteria [292, 293]. As mentioned, the surface charge of nanoparticles is linked to their antimicrobial efficacy [42, 287]. Badawy *et al.* (2011) investigated the antimicrobial activity of charged Ag nanoparticles and found positive particles had greater activity than negative particles against *Bacillus* species. The positive Ag nanoparticles and the bacteria were attracted to each other, thus could easily interact leading to bacterial cell wall damage and cell death. The negatively charged particles were found to have less antimicrobial activity due to reduced interaction, except for highly negatively charged particles where electrostatic repulsion restrained microbe to particle contact [42].

In this study, Cu10 was the only sample to have a positive surface charge out of the tested nanoparticles. This suggests that the nanoparticles and the microbes are likely to be attracted to each other and contributes to the physical contact interaction, which has been suggested to be one of the mechanisms of action of nanoparticles. However, Cu10 had less antimicrobial efficacy in comparison to those of Ag and AgCu, as a higher MIC value was required to kill the microbes. In regards to this, it suggests that the surface charge alone is not the main cause of antimicrobial activity and other properties of nanoparticles can overcome the attraction and interaction between nanoparticle and microbe; however, again it is invalid to compare between different materials due to differences in other parameters.

4.4.2 Optical properties and morphology

The optical properties of metal nanoparticles are determined by their SPR which can shift depending on their particle size and shape. The SPR is the oscillation of electrons on the surface of material. By using light to excite the electrons, UV-Vis spectroscopy can measure the intensity of light after passing through the suspension to produce an absorption spectrum, with a maximum peak denoted as the λ_{max}. It has been found that smaller nanoparticles (<20 nm) have a shorter wavelength, whilst larger particles (>20 nm) have a longer wavelength. Hence, agglomeration of particles can be detected by observation of longer wavelengths than predicted [98, 294].

The λ_{max} absorption of Ag nanoparticles, 402 nm, agrees with reports from previous studies [295, 296]. Typically, the λ_{max} absorption range of Ag is reported to be between 400-500 nm [297]. The low wavelength suggests that the particles are of small size as it is blue shifted in wavelength. For example, the Ag nanoparticles synthesised by Singh, Bharti and Meena (2015) were observed to be 40-100 nm in size through the TEM and had a λ_{max} of 427 nm. In contrast, the Ag nanoparticles in this study was smaller (13-22 nm as observed and measured by ImageJ, respectively) and had a shorter λ_{max} of 402 nm.

Likewise, the λ_{max} value of AgCu nanoparticles at 410nm is consistent with Paszkiewicz *et al.* (2016). In contrast, Rivera-Rangel *et al.* (2020) investigated AgCu nanoparticles with an average size of 23.9 ± 4.1 nm and found their nanoparticles had a longer wavelength (472 nm). Although the nanoparticles had a smaller diameter size to the AgCu nanoparticles in this study (86-36 nm), it consisted of a higher Cu concentration. The AgCu nanoparticles investigated by Rivera-Rangel *et al.* (2020) consisted of a 1:1 Ag:Cu ratio, whereas the AgCu nanoparticles in this study consisted of 39:1 Ag:Cu ratio (as stated by the manufacturer). Since Cu generally have a longer wavelength, the red shift in wavelength was likely to be caused by Cu components in the alloy [296, 298]. Hence the higher Ag content in the AgCu nanoparticles in this study resulted in a short wavelength despite being larger in diameter.

Lastly, no peaks were detected in the measured absorbance spectra of Cu10. Generally, Cu nanoparticles are reported to have an absorption range of 550-600 nm [296, 298]. The anomaly in this result may have been caused by large agglomerations in the suspension. The UV absorption spectrum of Ag, AgCu and Cu are visually compared to literature spectrums in Figure 4.11.

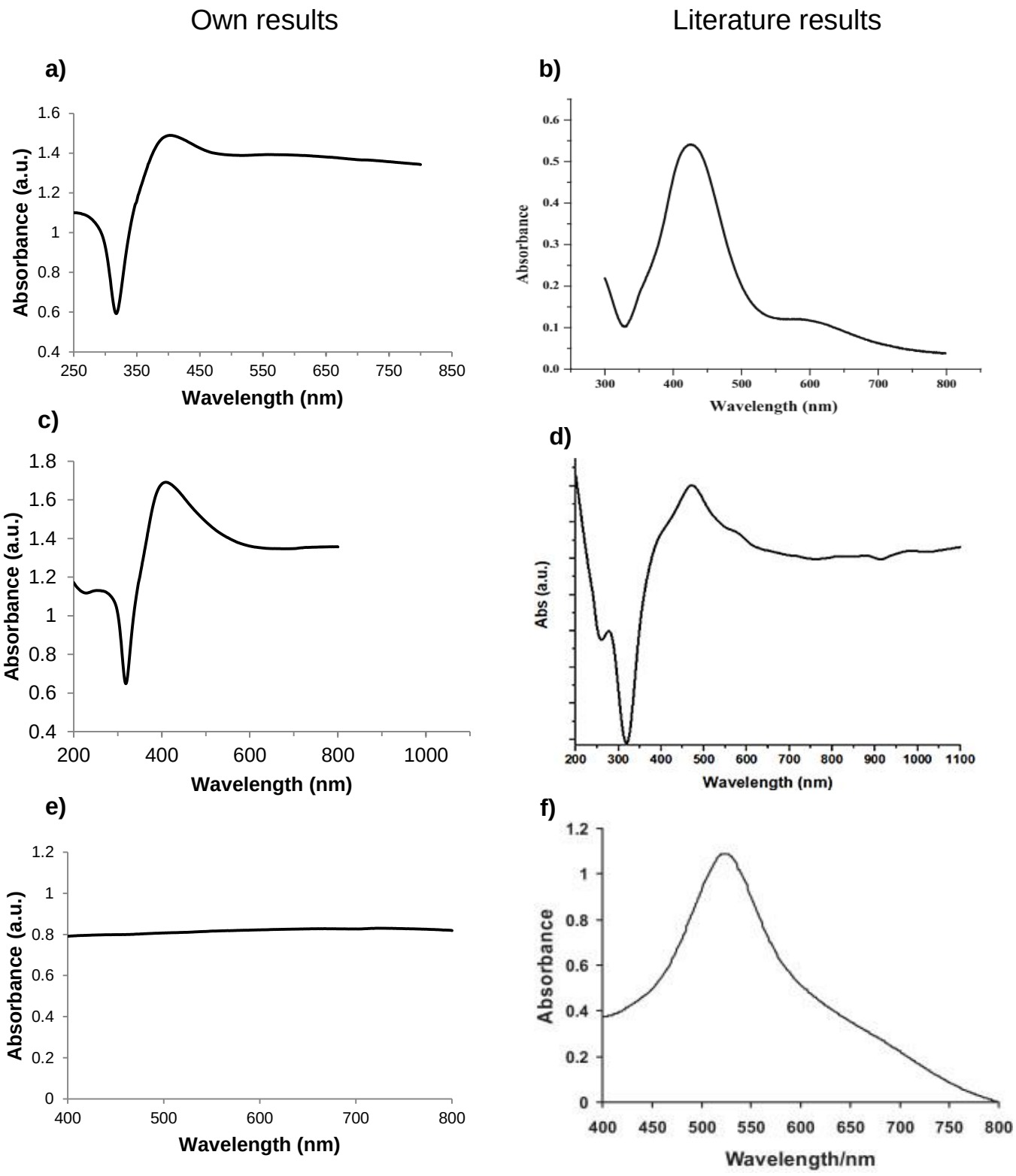

Figure 4.11: Visual comparison of obtained Ag, AgCu and Cu10 UV-Vis spectrum against literature UV-Vis spectrum. a) Obtained Ag nanoparticle UV-Vis spectrum, b) Ag nanoparticle UV-Vis spectrum from [3], c) obtained AgCu nanoparticle UV-Vis spectrum, d) AgCu nanoparticle UV-Vis spectrum from [4], e) obtained Cu10 nanoparticle UV-Vis spectrum, f) Cu nanoparticle UV-Vis spectrum from [5].

The shape of nanoparticles can influence the number of peaks in an absorption spectrum; in Mie's theory, spherical nanoparticles produce a single peak from one SPR band, while anisotropic nanoparticles can produce more peaks, depending on the shape and SPR bands produced [99]. The single peak in both Ag and AgCu indicates that the nanoparticles were without anisotropic features and AgCu did not have contamination of single elements of Ag and Cu.

The morphology of the nanoparticles was further clarified by observations through the TEM where all three nanoparticles were observed as spherical shaped; however, Cu10 contained some particles that looked cubical. As mentioned before, the shape of nanoparticles were found to be linked to their antimicrobial activity. Cha *et al.* (2015) reported that the antimicrobial activity of ZnO nanoparticles was related to their shape due to their better compatibility with the enzyme surface to allow enzyme inhibition. It was found that triangular shaped ZnO nanoparticles had the highest inhibitory effect on enzyme β- galactosidase which was suggested to have been a result of the triangle corner forming better compatibility with the active site [299]. However, it could also be argued that nanoparticles at smaller sizes would be able to interact with the active site.

Helmlinger *et al.* (2016) found that platelet shaped Ag nanoparticles had the highest efficacy towards *E. coli*, followed by spherical shaped Ag nanoparticles, whilst cubical shaped Ag nanoparticles had the least antimicrobial efficacy. In contrast, Hong *et al.* (2016) reported that cubic Ag nanoparticles had the highest antimicrobial activity towards *S. aureus* in comparison to spherical and wire shaped Ag nanoparticles. Due to the slight differences in observed shape, Ag and AgCu may have had better antimicrobial activity than Cu10 as a result of the shape of the nanoparticle. However, in the previously mentioned reports, the size of the nanoparticles differed for the shapes and the smallest tested nanoparticle in both reports exhibiting the most antimicrobial activity. It was suggested that the smaller nanoparticles had higher dissolution rate and a larger surface area to volume ratio that contributed to the enhanced antimicrobial activity [300, 301]. Hence, the size of the nanoparticle is likely to influence the antimicrobial efficacy more than the shape of the nanoparticle.

4.4.3 pH

pH is a measurement of hydrogen ion concentration. The logarithmic pH scale expands from 0 to 14, with 14 being most alkaline with least concentration of hydrogen ions. In the middle, pH 7 is regarded as neutral [302]. Nanoparticles have the ability to form ions when suspended in water, which can influence the pH of the suspension. Ag nanoparticles are known to undergo oxidative dissolution in water where the nanoparticles are oxidised by oxygen and then react with hydrogen ions to form Ag ions (Equation 3). The overall reaction is shown in Equation 4 [76]. Due to the reduction of hydrogen ions, the acidity of the suspension decreases and therefore the pH increases. A similar reaction can occur with Cu nanoparticles to form their corresponding ions [303].

$$4Ag_{(s)} + O_2 \rightarrow 2Ag_2O_{(s)}$$

$$Ag_2O_{(s)} + 2H^+ \rightarrow 2Ag^+ + H_2O$$

Equation 3: Oxidative dissolution of Ag nanoparticles in water

$$4Ag_{(s)} + O_2 + 4H^+ \rightarrow 4Ag^+ + H_2O$$

Equation 4: Overall oxidative dissolution of Ag nanoparticles in water

The immediate pH measurement of nanoparticle suspension supernatant showed that Ag nanoparticle suspension had the greatest pH, followed by AgCu nanoparticle suspension, whilst Cu10 nanoparticle suspension had pH close to that of the water control. To improve the dispersion of Ag and AgCu nanoparticles, the alkaline compound NH_4OH was added to the suspension. This compound itself increased the pH via dissociation to produce hydroxide ions as shown in Equation 5. Corresponding concentration controls of NH_4OH were measured to elucidate the influence on pH. Since very low concentrations were used in the nanoparticle suspensions, the pH of the NH_4OH controls was similar to the pH of water and therefore did not affect the results for Ag and AgCu.

$$NH_4OH_{(aq)} \rightarrow {NH_4}^+{}_{(aq)} + {OH^-}_{(aq)}$$

Equation 5: Dissociation of NH_4OH

The formation of ions is one of the main mechanisms of action theorised for nanoparticles. Positive ions are attracted to the negative cell walls of microbes. Ions in a solution can interact with microbial cell walls and penetrate inside to cause damage including cellular disruption, inhibition of enzyme function and inactivation of DNA replication [21]. It has been found that the antimicrobial activity of nanoparticles is proportional to the concentration of ions released [139]. In this study, the release of ions of the nanoparticle suspensions was measured indirectly through the change of pH over 14 days, where a higher increase of pH corresponds to a higher release of ions. Ag nanoparticles had the greatest increase in pH after 14 days in all tested concentrations and higher concentrations resulted in larger pH increase. The highest tested concentration (1000 μg/ml) had an increase of 1.8 in pH, whilst the lowest tested concentration (10 μg/ml) had an increase of 1.1 in pH. AgCu nanoparticles had the same trend, but slightly less increase in pH was measured. At the same concentration, an increase of 1.2 and 1.0 pH, respectively, was measured. On the other hand, only higher tested concentrations of Cu10 had a slight increase of up to 0.9 pH. This suggests that Ag nanoparticles had the largest release of ions, which correlates with some of the MIC values in Chapter 3. In comparison, Cu10 nanoparticles had less increase in pH, and subsequently a greater MIC value. However, AgCu nanoparticles had similar MIC values in comparison to Ag, but a slightly lower increase pH. This suggests that ions contributes to the mechanism of action but it is not the only mechanism as AgCu nanoparticles had higher antimicrobial efficacy towards certain microbes but was found to have less ions released.

4.4.4 Summary

To summarise, optical investigation found that Ag and AgCu nanoparticles had unique SPR, did not contain anisotropic features and correlated with absorbance reported in published journals. In contrast the UV absorbance of Cu10 nanoparticles could not be detected and may have been caused by agglomeration. This was further confirmed by SEM and TEM imaging where agglomerations were observed, despite sonication to disperse the nanoparticles in water suspension. The ζ- potential measurement showed that AgCu and Ag nanoparticles were in the stable range thus less likely to form agglomerates, whilst the ζ- potential of Cu10 nanoparticles was within the unstable range and they were very likely to form agglomerates.

Furthermore, the hydrodynamic size of the nanoparticles was measured using DLS and found that AgCu nanoparticles were the smallest, with a diameter of 170.6 nm at 250 μg/ml and the size of the particles reduced with an increase in concentration as a result of surface charge repulsion. In correlation to the ζ- potential, Cu10 had larger hydrodynamic sizes (716.0 nm at 250 μg/ml) which may have been a result of agglomerations within the suspension. In comparison to the MIC results from Chapter 3, it is possible that the hydrodynamic size of the nanoparticles influenced the antimicrobial activity of the nanoparticles, with smaller nanoparticles exhibiting higher antimicrobial efficacy. The ζ- potential was also used to predict the attraction between microbes and nanoparticles. It showed that Cu10 nanoparticles were most likely to form attraction to pathogens in comparison to Ag and AgCu as it was positive and microbes have a negative surface charge; however, this does not agree with the MIC values from Chapter 3. The TEM observations showed that all nanoparticles were spherical; however some Cu10 nanoparticles were cuboid. In addition to the size of the nanoparticles, the shape may also influence their antimicrobial activity due to their compatibility to microbes and surface area which can contribute to the release rate of ions. The release of ions, which was indirectly measured by suspension pH, showed that Ag nanoparticles released greater number of ions, followed by AgCu nanoparticles. Therefore, this suggests that many properties of nanoparticles contribute to their antimicrobial activity, with small hydrodynamic size and high ion release showing the most effect.

Chapter 5 Mechanisms of action of AgCu nanoparticles

5.1 Introduction

Certain nanoparticles have shown to exhibit excellent antimicrobial activity and may provide alternative mechanisms to combat antibiotic resistance in bacteria, including bacteria protected by their biofilms. As a result, certain nanoparticles have been utilised for various antimicrobial applications, however, the mechanisms of action of antimicrobial nanoparticles are still unclear. It has been theorised that nanoparticles have several mechanisms of action and multiple mechanisms can occur simultaneously, which decreases the potential of microbes to develop resistance of the nanoparticles [138-140, 304].

The mechanism of action is different for each type of nanoparticle; currently, the common theorised mechanisms of action include oxidative stress, the release of ions, cell membrane interactions and enzyme inhibition [138, 139, 144]. Oxidative stress is one of the most common contributors to nanoparticles antibacterial mechanisms. Nanoparticles can anticipate the production of reactive oxygen species (ROS) in microbial cells, which induces oxidative stress. Bacterial cells can establish a ROS equilibrium within the cells; however, with excess production, it leads to damage in cell membrane, DNA, ribosome, and proteins, which subsequently inhibits the electron transport chain, enzymes, and DNA transcription and translation, and eventually leads to cell death. Furthermore, nanoparticles can attach onto the cell membrane and cause damage, which may result in the leakage of cellular content and/or blockage of transport channels. Additionally, nanoparticles can form ions in suspension which can be transported through the cell membrane. Ions can bind to functional groups and interfere with protein and DNA synthesis [305, 306]. Nanoparticles and ions can also interact with enzymes and inhibit them which leads to disruption of essential cellular processes [144].

The physical properties of nanoparticles also contribute to the mechanism of action. For instance, smaller sized NPs are more able to diffuse through the bacterial cell wall and interact with bacteria [307]. Similarly, the shape of NPs can contribute to the antibacterial efficacy and mechanism of action. Cha *et al.* (2015) reported that ZnO nanopyramids produce the greatest antimicrobial activity by inhibiting essential

bacterial enzymes due to their shape compatibility with the enzyme active site in methicillin resistant *S. aureus.*

Both Ag and Cu nanoparticles have been reported with antimicrobial properties and have been developed for biomedical applications such as substrate coatings [308]. Reyes *et al.* (2020) found that bimetallic AgCu nanoparticles exhibited stronger antimicrobial activity than the single elements; however, their mechanism of action was not investigated. Therefore, investigations on the mechanism of action of AgCu nanoparticles are essential.

Outline of the research work:

This chapter aims to explore the possible mechanism of action of AgCu nanoparticles through physical observations of microbes and fluorescent assays against a fungus (*C. albicans*), a Gram-negative bacteria (*E. coli*) and a Gram-positive bacteria (*S. aureus*). Microscopic techniques, including electron microscopes and light microscopes, were used to observe physical morphology changes and interactions between AgCu nanoparticles and microbes. Several assays were used to determine the effects of AgCu against microbes at a cellular level, such as oxidative stress, changes to DNA production and leakage of protein. Additionally, the relationship between characteristic properties (investigated in Chapter 4) was also considered to explain their antimicrobial behaviour towards the tested microbes.

5.2 Materials and methods

The preparation of AgCu nanoparticle suspension and microbes (*E.coli, S. aureus* and *C. albicans*) can be found in Chapter 2. For all experiments, microbes were grown 24 hours prior to experiment in broth (nutrient broth for bacteria and YPD broth for fungi) and diluted to ~3x10^7 CFU/ml using a spectrometer at 600 nm. For Gram stain, SEM and TEM, samples were further diluted to ~3x10^4 CFU/ml. Microbial samples were treated with AgCu nanoparticle suspension at ½ MIC concentrations (MIC value can be found in Chapter 3, Table 3.5), samples were incubated for 24 hours at 37°C in a MaxQ8000 incubated shaker set at 180 rpm. For assay experiments, microbes were treated with AgCu nanoparticle suspensions at 150 µg/ml, 100 µg/ml and MIC value and were incubated at 37°C in a MaxQ8000 incubated shaker set at 180 rpm. Samples were taken hourly for 4 hours and all samples were performed in triplicate. Results are displayed as percentage in comparison to control without AgCu nanoparticle treatment with error bars to denote the standard deviation. Controls of AgCu nanoparticles at several concentrations without presence of microbes were performed to prove that the nanoparticles did not affect the assay.

5.2.1 Gram stain

After incubation, 100 µl of sample was pipetted onto a clean glass slide and left to dry under a Bunsen burner. Once dried, the samples were heat fixed, and then underwent the gram staining procedure. Samples were treated with crystal violet for one minute and then briefly washed with tap water. Iodine solution was then used to treat the samples for 30 seconds and then briefly washed with tap water followed by ethanol wash. Lastly, samples were treated with carbol fuchsin for 5 mintues and then briefly washed with tap water. Excess water was carefully shaken off and samples were left to dry under a Bunsen burner. When dry, samples were viewed under a microscope (GT Vision Ltd, UK) and images were taken at magnifications of x400 and x1000.

5.2.2 SEM

After 24 hour of AgCu nanoparticle treatment, microbes underwent an SEM preparation method developed by Staniszewska *et al.* (2013). In summary, 15 µl of sample was pipetted onto a clean glass slide cover and fixed with 2.5% glutaraldehyde (in 0.1M phosphate buffer, pH 7.2) for 18 hour at 4^{o}C. Each sample

was then washed with phosphate-buffered saline (PBS) until clear, followed by a final wash with pure water. Osmium tetroxide (2%) was added to the sample for 2 hour and then it was washed with an increasing alcohol gradient (from 50% to 100%) and acetone [309]. When dry, samples were gold sputtered for 45 seconds and imaged on the SEM CarryScope JCM-5700 (JEOL, UK).

5.2.3 TEM

After 24 hours of AgCu nanoparticles treatment, microbes underwent a TEM preparation method as described by Hermansen *et al.* (2018), with slight modification. In summary, 10 µl of sample was pipetted onto a carbon-supported TEM mesh grid for 2 minutes. Then the grid was gently tapped on a piece of filter paper to remove excess sample and washed with water three times by pipetting 10 µl of water onto the grid and gently tapping away the water on the filter paper. After washing, the grid was stained with phosphotungstic acid (0.125%) for 30 seconds and then excess was tapped away on the filter paper. Grids were left to dry before being imaged on the TEM JEOL-1400 (JEOL, UK).

5.2.4 ζ- potential of microbes

Freshly grown microbial cells at ~3x10^7 CFU/ml were washed three times with sterile distilled water; this was done by centrifuging cells at 2000 rpm for 5 minutes, gently pouring away the supernatant and suspending the cell pellet in sterile distilled water. Washed microbes were then measured for the ζ- potential using settings reported in Chapter 4**.**

5.2.5 Oxidative stress assay

The generation of oxidative stress after AgCu nanoparticle treatment was measured using an assay described by Quinteros *et al.* (2016) with slight modification. In summary, 200 µl of AgCu nanoparticle treated microbial sample was taken and incubated with 20 µl of 2', 7'-dichlorodihydrofluorescein diacetate (H_2-DCFDA) (20 µM) for 30 minutes. The fluorescent intensity of the samples was then measured with a spectrometer (CLARIOstar, BMG) set at 480 nm excitation and 520 nm emission.

5.2.6 Bradford assay

The protein leakage of microbes after AgCu nanoparticle treatment was measured using the Bradford assay, as described by Reddy *et al.* (2014) with slight

modifications. In summary, 250 µl of AgCu nanoparticle treated sample was taken and centrifuged at 600 rpm for 15 minutes. Then 200 µl of the supernatant was incubated with 800 µl of Bradford reagent for 10 minutes in the dark. The optical density of the samples was then measures with a spectrometer (CLARIOstar, BMG) at 595nm.

5.2.7 DNA production assay

The production of DNA of microbes after AgCu nanoparticle treatment was measured using an assay described by Ojkic *et al.* (2020) with slight modification. In summary, 600 µl of AgCu nanoparticle treated sample was treated with 150 µl of 1.2% formaldehyde (in PBS). Then 50 µl of 4', 6'-diamidino-2-phenylindole (DAPI) was added to make a final concentration of 2 µg/ml and incubated for 30 minutes. The samples were then washed with PBS for three times by centrifuging cells at 2000 rpm for 5 minutes, gently pouring away the supernatant and suspending the cell pellet in PBS. The fluorescent intensity of the samples was measured with a spectrometer (CLARIOstar, BMG) set at 358 nm excitation and 461 nm emission.

5.3 Results

To investigate the mechanism of action of antimicrobial AgCu nanoparticles, three methods were used to observe the physical changes of microbes: *E. coli* (to represent Gram-negative bacteria), *S. aureus* (to represent Gram-positive bacteria) and *C. albicans* (to represent fungi). The overall differences between AgCu nanoparticle treated and untreated microbes were firstly observed using Gram staining technique. At x400 and x1000 magnification, a reduction in cells was seen after treatment. Secondly, SEM technique was used to visualise the physical changes and found damage to the microbial cell membrane. Lastly, the final physical observation of microbial change after AgCu nanoparticle treatment was visualised through the TEM technique which provided the highest magnification and higher power to observe through the microbial cells. Breakage of the cell membrane and changes to the surface topography were observed. In addition to physical changes, assays found that AgCu nanoparticle treatment affected internal processes leading to changes in oxidative stress levels, DNA production and presence of overall protein. Furthermore, all tested microbes had negative surface charge.

5.3.1 *E. coli* (Gram-negative bacteria)

The Gram staining technique showed that the AgCu nanoparticle treatment at ½ MIC value resulted in a reduction of cell abundance, as shown in Figure 5.1. Although the interaction between AgCu nanoparticle and *E. coli* was hard to observe at x1000 magnification, the treatment resulted in 53.4% reduction of cells compared to the untreated control. At a higher magnification, images taken through the SEM technique showed damage to the cell membrane and smears of possible leakage through the damaged area (Figure 5.2). Size analysis through ImageJ showed slight increase in the length size of *E. coli* cells, where control cells were an average length of 2.0 µm, in comparison to treated cells with an average length of 3.1 µm. The last observational technique visualised physical changes to the surface of the bacterial membrane using TEM. As shown in Figure 5.3, in comparison to the control cells, the treated cells look wrinkled and dehydrated with black dots surrounding the cells that could possibly be cell membrane fragments. ImageJ analysis found that treated cells decreased by 28.6% in width size, from an average of 0.7 µm to 0.5 µm.

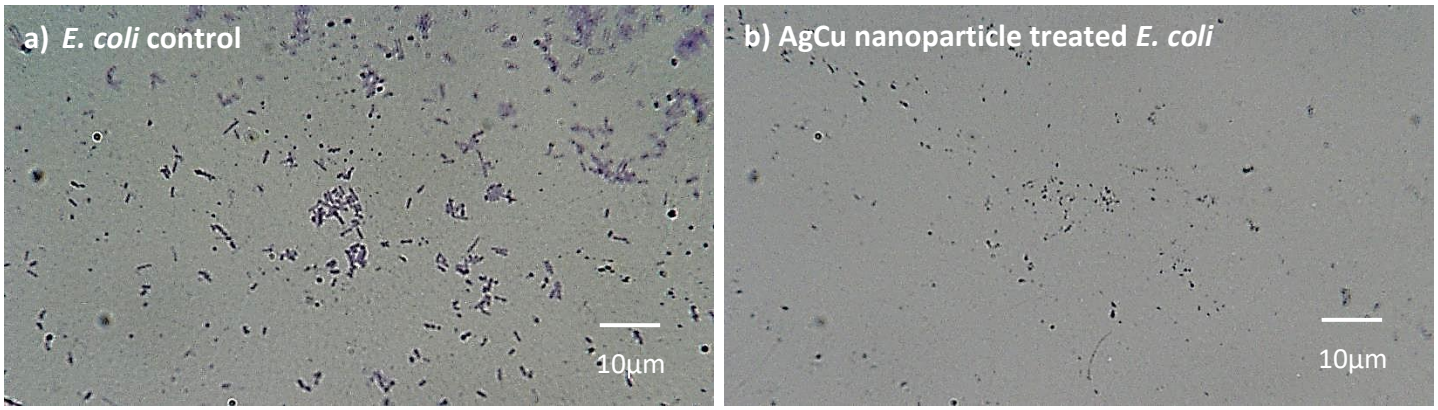

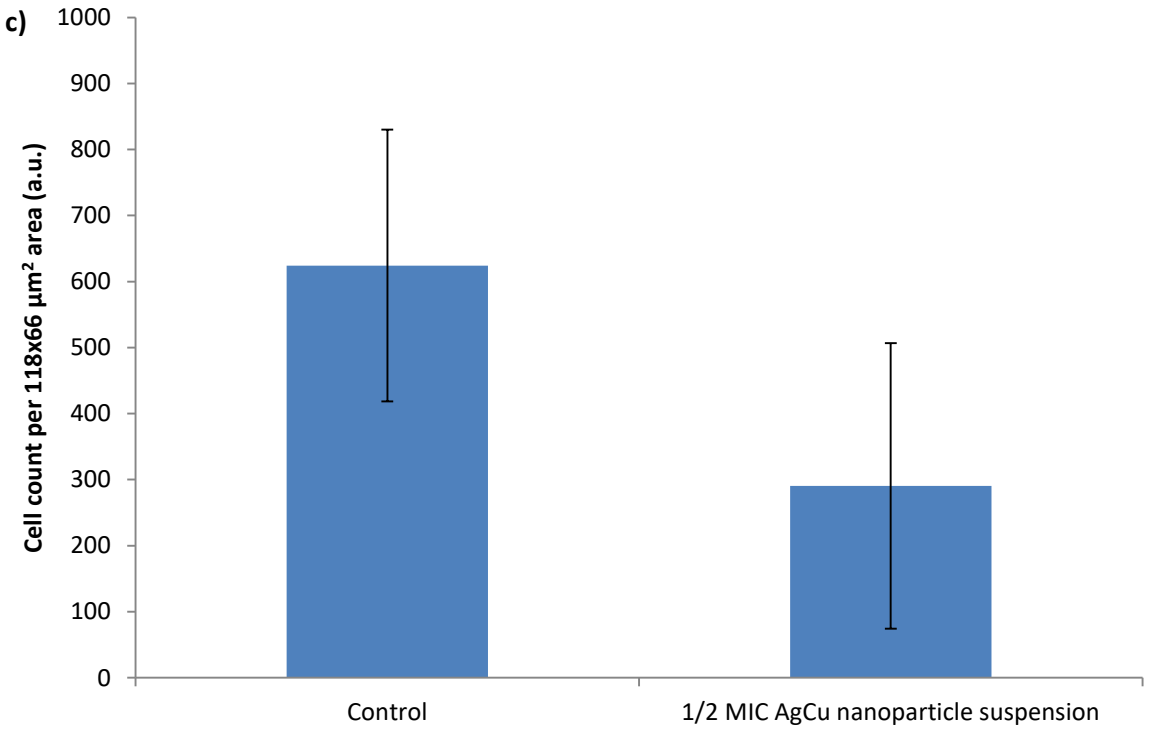

Figure 5.1: Gram stain images and analysis of *E. coli* before and after AgCu nanoparticle treatment at 1/2 MIC value. a) Gram stain of *E. coli* control, b) Gram stain of treated *E. coli* and c) change in abundance of *E. coli* cells after AgCu nanoparticle treatment, as analysed by ImageJ.

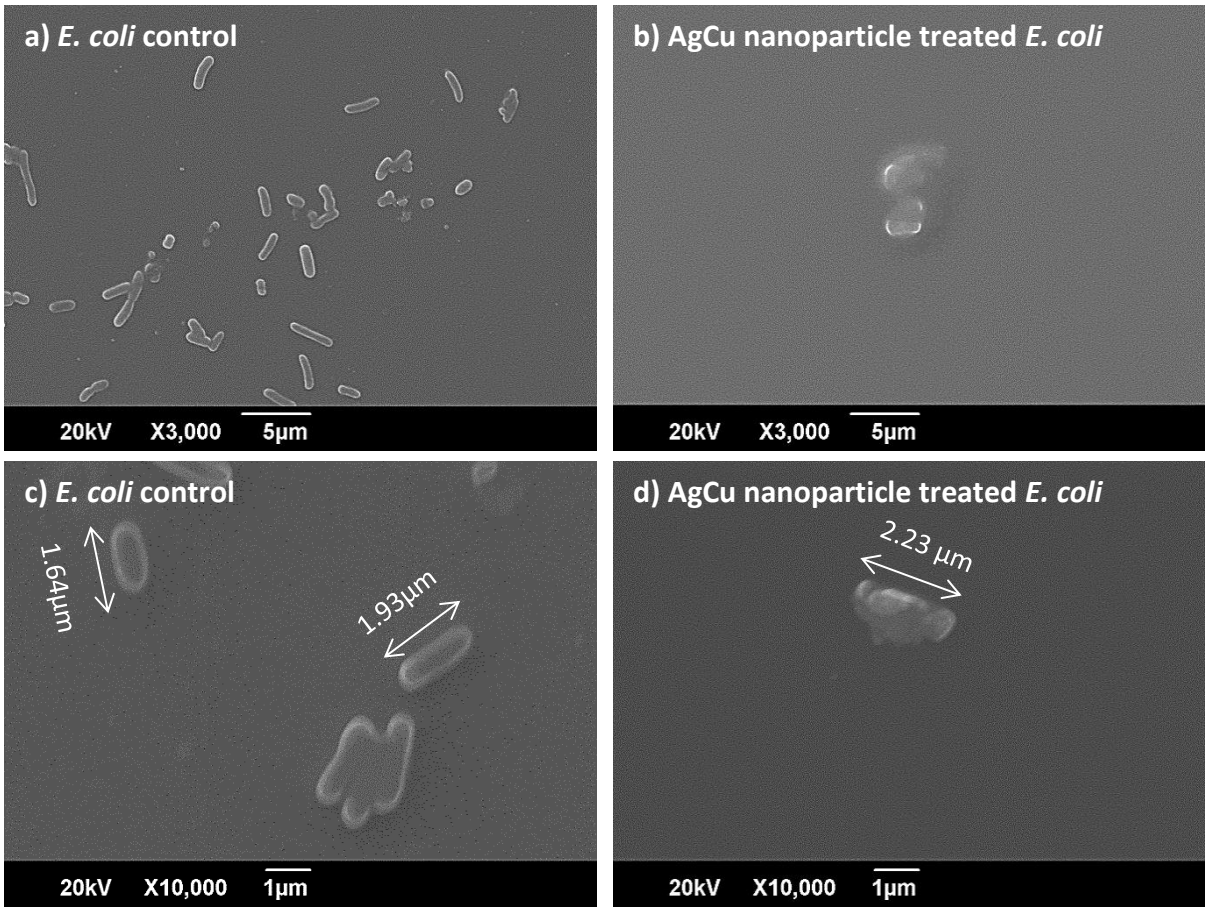

Figure 5.2: SEM images of AgCu nanoparticle treated and untreated *E. coli.* a) *E. coli* control (x3000 magnification), b) treated *E. coli* (x3000 magnification), c) *E. coli* control (x10000 magnification), d) treated *E. coli* (x10000). The sizes of the bacteria were measured using ImageJ and annotated onto the image.

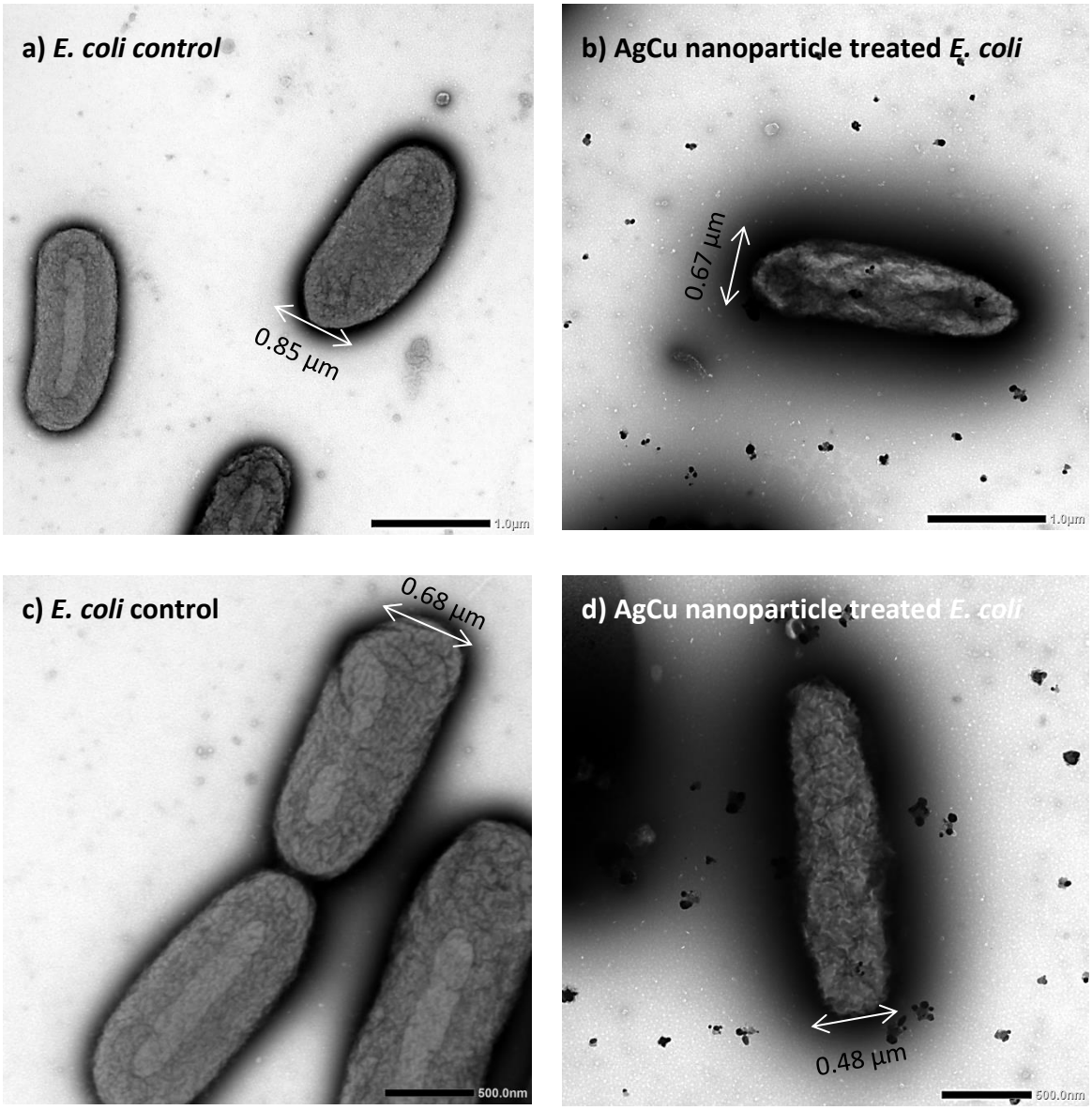

Figure 5.3: TEM images of AgCu nanoparticle treated and untreated *E. coli*. a) E. coli control (x8000 magnification), b) treated E. coli (x8000 magnification), c) E. coli control (x12000 magnification), d) treated E. coli (x12000). The sizes of the bacteria were measured using ImageJ and annotated onto the image.

In addition to physical changes, AgCu nanoparticle suspension had an effect on the internal cellular processes of *E. coli*. Assuming that the control *E. coli* cells had 0% oxidative stress, an increase was found after a period of incubation with AgCu nanoparticle suspension. As shown in Figure 5.4 (a), the H_2-DCFDA assays showed an immediate decrease in oxidative stress, followed by an increase of up to 318% after 2 hours of incubation when treated with high concentrations of AgCu nanoparticle suspension. However, after 2 hours of incubation, the level of oxidative stress began to reduce. On the other hand, this trend was not seen when treated with the MIC concentration; an immediate decrease in oxidative stress was found that continued to increase. Moreover, the increase in oxidative stress in *E. coli* was not concentration related, as 100 µg/ml concentration caused the highest increase in oxidative stress.

Assuming the control *E. coli* cells had 100% protein, incubation with AgCu nanoparticle suspension resulted in decrease in detected protein over time, as shown in Figure 5.4 (b). The higher concentrations of AgCu nanoparticle suspension reduced the protein levels faster, with an immediate reduction at 150 µg/ml concentration. In contrast, at 100 µg/ml and at MIC value, the reduction in protein level began after 2 hours and after 4 hours of incubation, respectively.

The DNA production was monitored using fluorescent DAPI dye and found that AgCu nanoparticle suspension resulted in a decrease of DNA. Assuming the control *E. coli* cells had 100% DNA, AgCu nanoparticle suspension at concentrations of 150 µg/ml and 100 µg/ml resulted in a DNA reduction to 56.2% and 69.1%, respectively. As shown in Figure 5.4 (c), less reduction of DNA was found at lower concentrations; after 4 hours of incubation with the AgCu nanoparticle suspension, less than 10% of DNA was detected in both 150 µg/ml and 100 µg/ml, however at MIC value 93% of DNA was detected. Furthermore, at MIC value, the reduction began after 1 hour of incubation.

The surface charge of *E. coli,* as measured by ζ- potential, was found to be -44.3 mV (+/- 0.2). Out of the tested microbes, *E. coli* was the most negative.

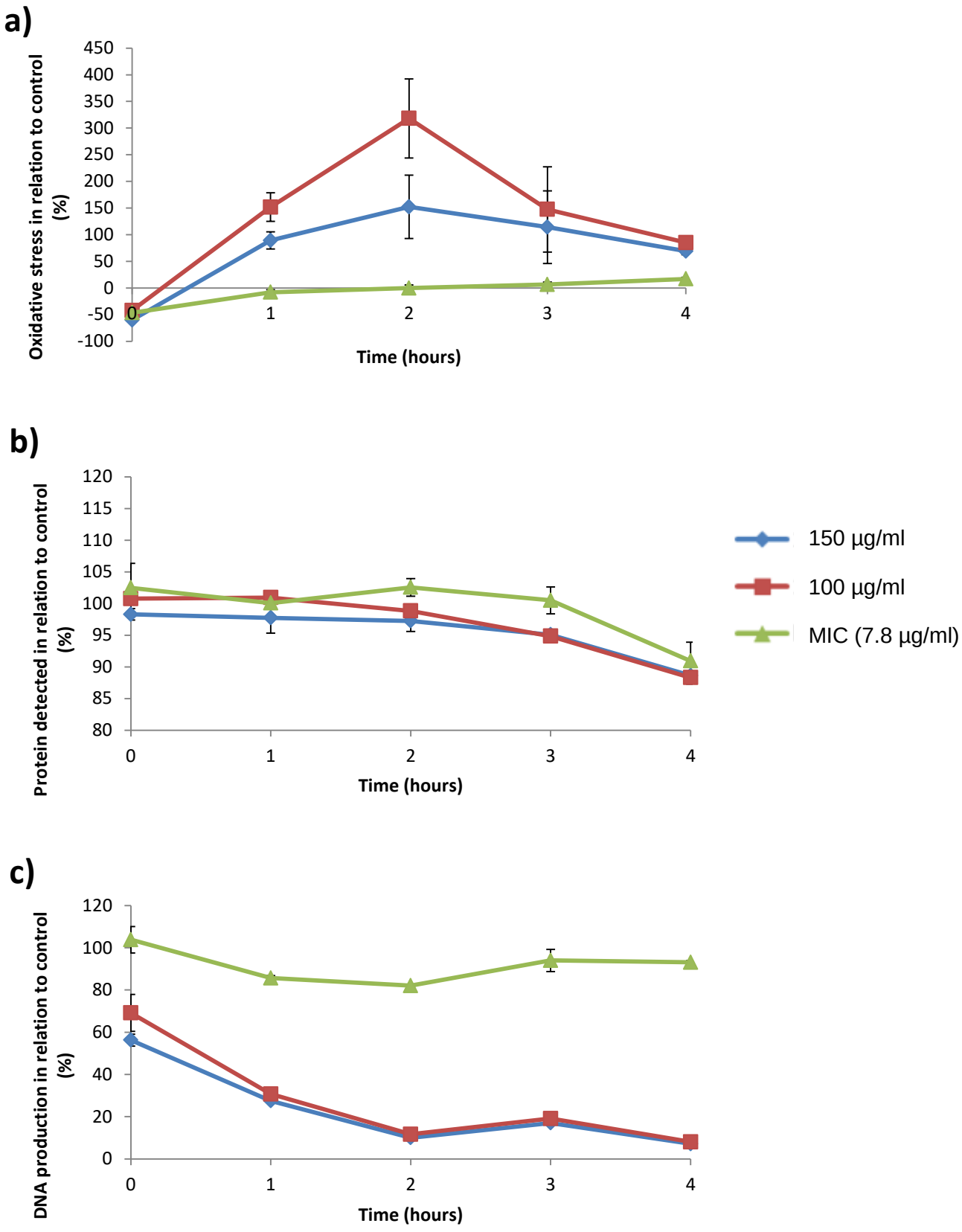

Figure 5.4: Internal cellular changes to *E. coli* after incubation with several concentrations of AgCu nanoparticle suspensions over a 4 hour time period. Graphs are used to display the changes to a) oxidative stress, b) overall protein and c) DNA production. AgCu nanoparticle suspensions were at concentrations of 150 µg/ml (represented in blue), 100 µg/ml (represented in red) and MIC value 7.8 µg/ml (represented in green). Error bars are used to denote the standard deviations of 3 replicates.

5.3.2 *S. aureus* (Gram-positive bacteria)

S. aureus was used to represent Gram-positive bacteria. Similar to *E. coli,* the Gram staining technique showed that the AgCu nanoparticle treatment at ½ MIC value resulted in a reduction of cell abundance, as shown in Figure 5.5. However the interaction between the nanoparticles and cells were unclear due to the low magnification of x1000. Analysis using ImageJ found that the AgCu nanoparticle treatment resulted in 52.8% reduction of cells, compared to the untreated control. At a higher magnification of x3000 and x10,000, images taken through the SEM technique showed fragmentation to the cell membrane as shown in Figure 5.6. In addition, possible leakage of intracellular material can be seen through the smears of the treated cells. Size analysis through ImageJ showed decrease of 35.2% in size of *S. aureus* cells, where control cells were an average diameter of 1.1 µm, in comparison to treated cells with an average diameter of 0.7 µm. Furthermore, many control cells were observed undergoing cell division; however, this was not seen in the treated samples.

TEM was used as the last observational technique to visualise physical changes to *S. aureus* cells after AgCu nanoparticle suspension treatment. As shown in Figure 5.7, AgCu nanoparticles (black circles) can be observed attached on to and possibly inside the bacteria cells. In comparison to the control cells, some of the treated cells have burst and deflated, with internal material leaking from the cell. ImageJ analysis found that some treated cells significantly decreased in diameter size. The burst cells decreased to 0.4 µm in diameter, whilst treated *S. aureus* cells with intact cell membrane had an average diameter of 0.7 µm. Control cells varied between 1.2 µm to 0.7 µm in diameter.

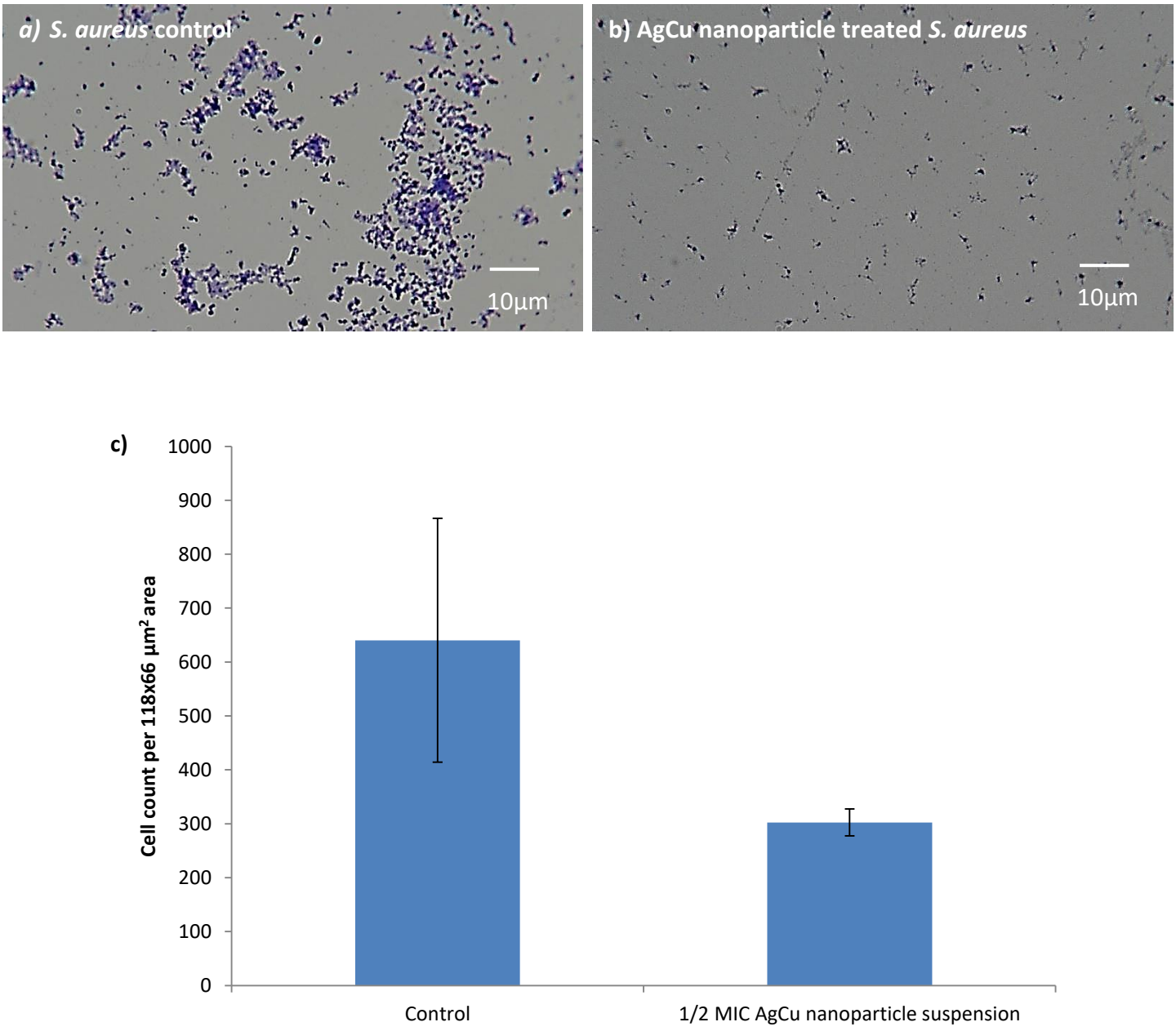

Figure 5.5: Gram stain images and analysis of *S. aureus* before and after AgCu nanoparticle treatment at 1/2 MIC value. a) Gram stain of *S. aureus* control, b) Gram stain of treated *S. aureus* and c) change in abundance of *S. aureus* cells after AgCu nanoparticle treatment, as analysed by ImageJ.

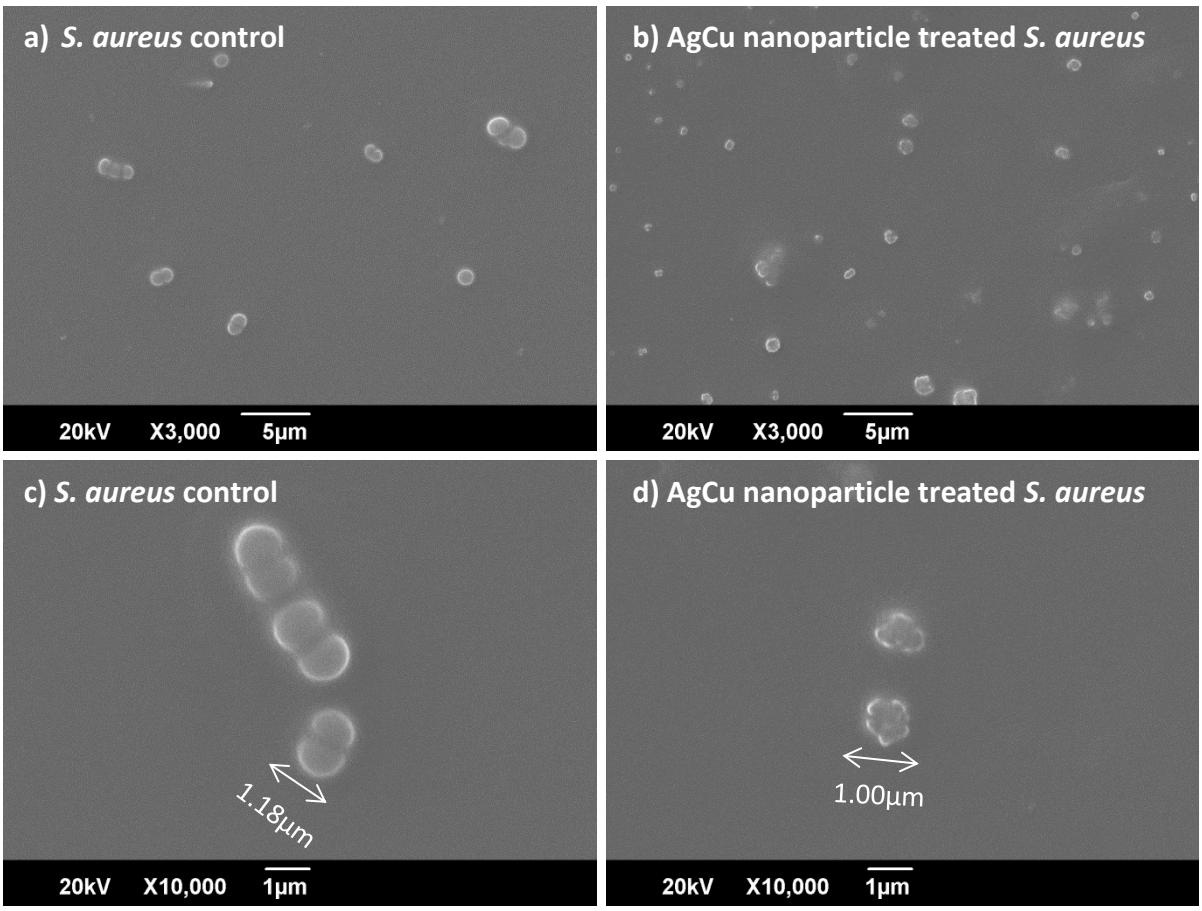

Figure 5.6: SEM images of AgCu nanoparticle treated and untreated *S. aureus*. a) *S. aureus* control (x3000 magnification), b) treated *S. aureus* (x3000 magnification), c) *S. aureus* control (x10000 magnification), d) treated *S. aureus* (x10000). The sizes of the bacteria were measured using ImageJ and annotated onto the images.

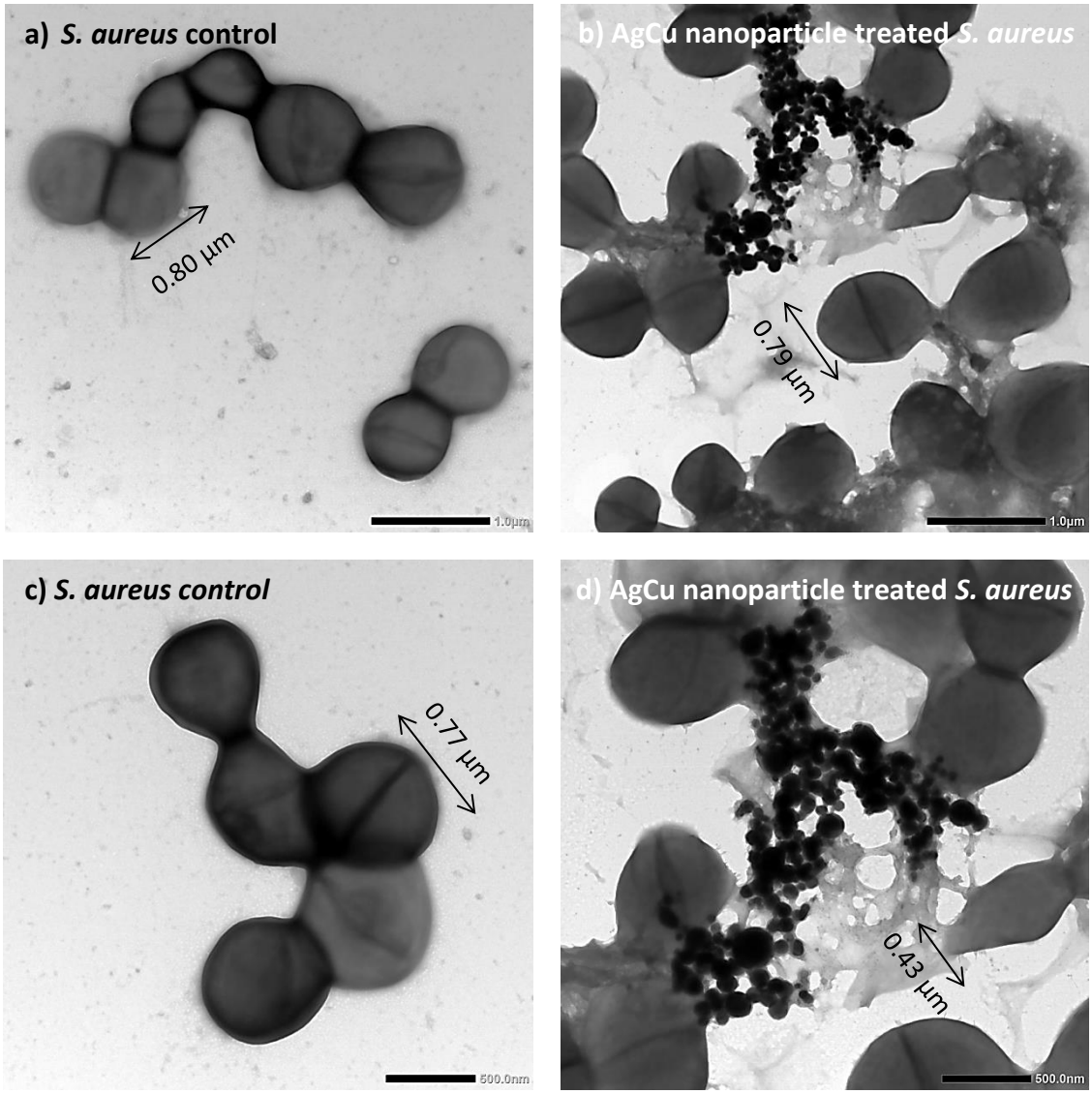

Figure 5.7: TEM images of AgCu nanoparticle treated and untreated *S. aureus*. a) *S. aureus* control (x8000 magnification), b) treated *S. aureus* (x8000 magnification), c) *S. aureus* control (x12000 magnification), d) treated *S. aureus* (x12000). AgCu nanoparticles (smaller black spheres) can be seen in b and d. The sizes of the bacteria were measured using ImageJ and annotated onto the images.

Similar to *E. coli,* AgCu nanoparticle suspension had an effect on the internal cellular processes of *S. aureus*. Assuming that the control cells had 0% oxidative stress, AgCu nanoparticle suspension resulted in an initial decrease in oxidative stress by up to 57%. However, after 2 hours of incubation, the oxidative stress increased and continued to increase up to the final reading point; after 4 hours of incubation, 100 µg/ml of AgCu nanoparticle suspension had the highest increase in oxidative stress towards *S. aureus*, with an increase of 155.8%. As shown in Figure 5.8 (a), all three concentrations of AgCu nanoparticles resulted in a similar trend line of increase in oxidative stress. Likewise to *E. coli*, the increase in oxidative stress was not concentration related, as 100 µg/ml resulted in higher levels of oxidative stress compared to 150 µg/ml and 31.3 µg/ml (MIC).

Assuming the control *S. aureus* cells had 100% protein, incubation with AgCu nanoparticle suspension resulted in decrease in detected protein over time, as shown in Figure 5.8 (b). The reduction in protein seems concentration linked with higher concentrations resulting in higher levels of reduction after a shorter period of incubation time. At 150 µg/ml and 100 µg/ml AgCu nanoparticle concentrations, the reduction of detected protein began after 2 hours of incubation, with 150 µg/ml concentration resulting in the highest decrease (13.0%) of protein after 4 hours of incubation. In contrast, the MIC value began to reduce protein after 3 hours of incubation.

AgCu nanoparticle suspension also resulted in a decrease of DNA in *S. aureus* cells. Assuming the control *S. aureus* cells had 100% DNA, AgCu nanoparticle suspension at concentrations of 150 µg/ml and 100 µg/ml immediately reduced DNA to 63.8% and 69.2%, respectively. As shown in Figure 5.8 (c), in the first hour of incubation, the MIC value had less DNA reduction in comparison to the higher concentrations of AgCu nanoparticles. However, after 4 hours of incubation, all three concentrations reduced the DNA to 13.2 to 12.1%.

The surface charge of *S. aureus,* was found to be less negative in comparison *E. coli*, with a reading of -31.2 mV (+/- 1.6).

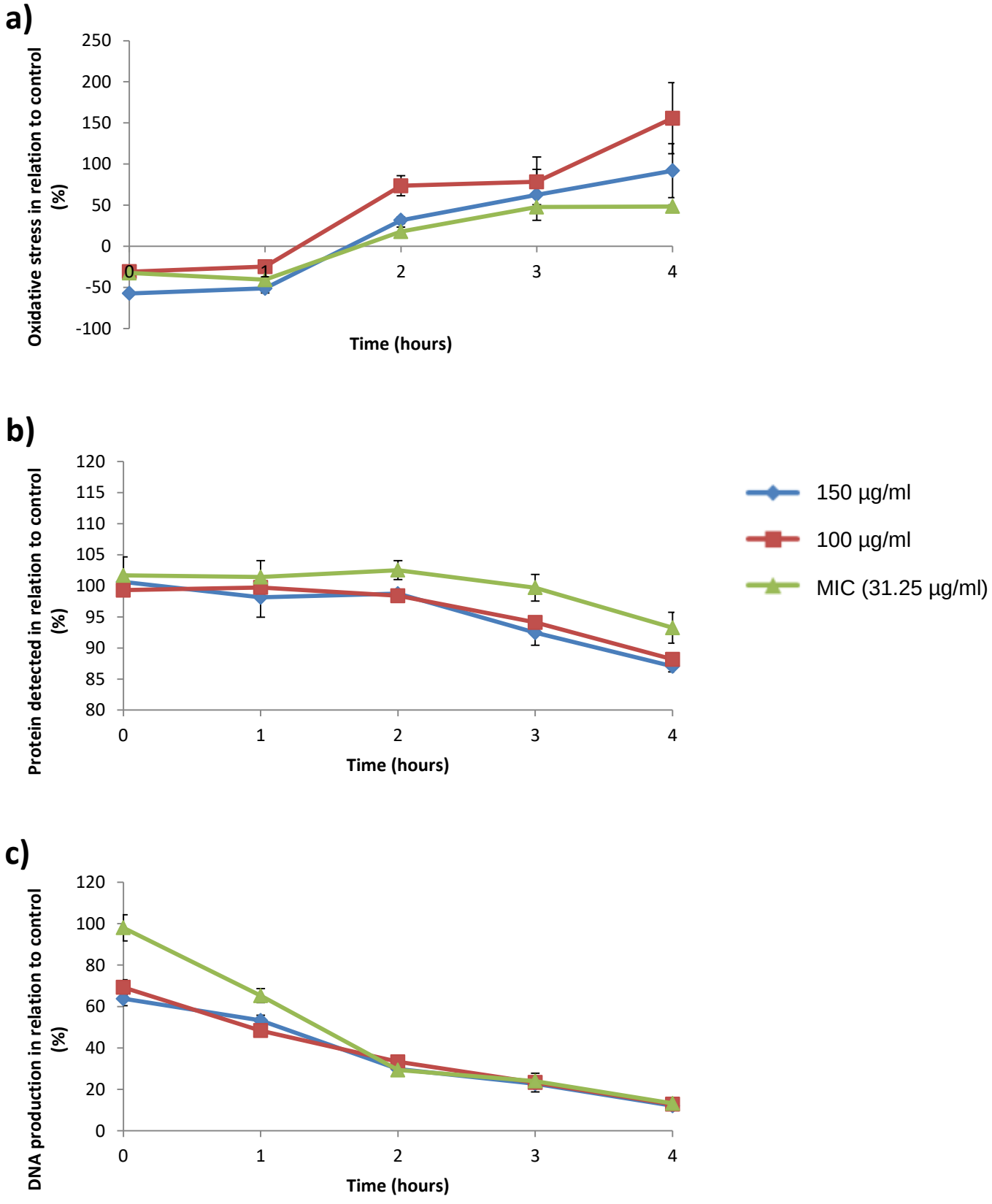

Figure 5.8: Internal cellular changes to *S. aureus* after incubation with several concentrations of AgCu nanoparticle suspension over a 4 hour time period. Graphs are used to display the changes to a) oxidative stress, b) overall protein and c) DNA production. AgCu nanoparticle suspensions were at concentrations of 150 µg/ml (represented in blue), 100 µg/ml (represented in red) and MIC value 31.25 µg/ml (represented in green). Error bars are used to denote the standard deviations of 3 replicates.

5.3.3 *C. albicans* (Fungi)

Lastly, *C. albicans* was used to represent fungi. Due to the larger size of *C. albicans* cells, Gram staining technique was able to visualise the overall interaction between AgCu nanoparticles and fungi cells. As shown in Figure 5.9, AgCu nanoparticles were observed to be attached onto *C. albicans* cells and their hyphae. At ½ MIC of AgCu nanoparticle suspension, it was found that the treatment resulted in 80.0% reduction of cells in comparison to untreated control.

Using the SEM, higher magnification of x3000 and x10,000 observed the physical changes of cell shrinkage and cell membrane damage after incubation with AgCu nanoparticle suspension. As shown in Figure 5.10, the uniform spherical shape of *C. albicans* was lost after treatment; instead the cells had increase cell wall roughness and irregular shape that inverted inwards in the centre. Furthermore, the attachment of some AgCu nanoparticles can be seen on the surface of *C. albicans* (Figure 5.10 (e)). Size analysis through ImageJ showed a 29.4% decrease in diameter of *C. albicans* cells, where control cells were an average diameter of 4.1 µm, in comparison to treated cells with an average diameter of 2.9 µm.

TEM imaging observed similar morphology changes to SEM of *C. albicans* after AgCu nanoparticle suspension treatment. As shown in Figure 5.11, AgCu nanoparticles (black circles) can be observed attached on to the surface of *C. albicans*. In comparison to the control cells, the treated cells have increased roughness and texture to the cell membrane. Additionally, some *C. albicans* cells look deflated and invert inwards. ImageJ analysis found that treated cells overall decreased in size by 10%; control cells had an average diameter of 4.2 µm in contrast to treated cells with a diameter of 3.8 µm.

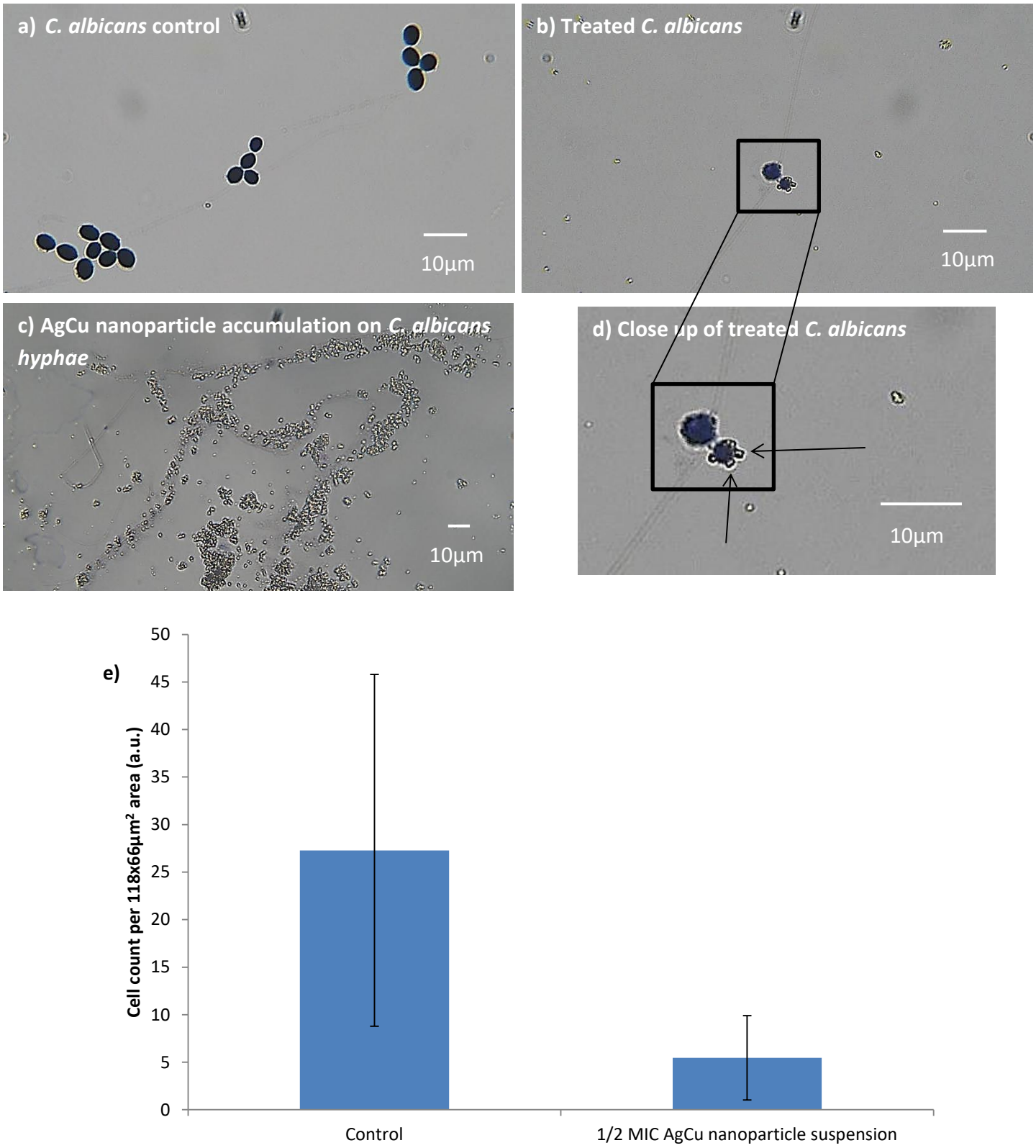

Figure 5.9: Gram stain images and analysis of *C. albicans* before and after AgCu nanoparticle treatment at 1/2 MIC value. a) *C. albicans* control, b) treated *C. albicans*, c) AgCu nanoparticle accumulation on *C. albican* hyphae at x400 magnification, d) closer observation of treated *C. albicans* with arrows pointing at AgCu nanoparticle attachment to fungal cell, and e) change in abundance of *C. albicans* cells after AgCu nanoparticle treatment, as analysed by ImageJ.

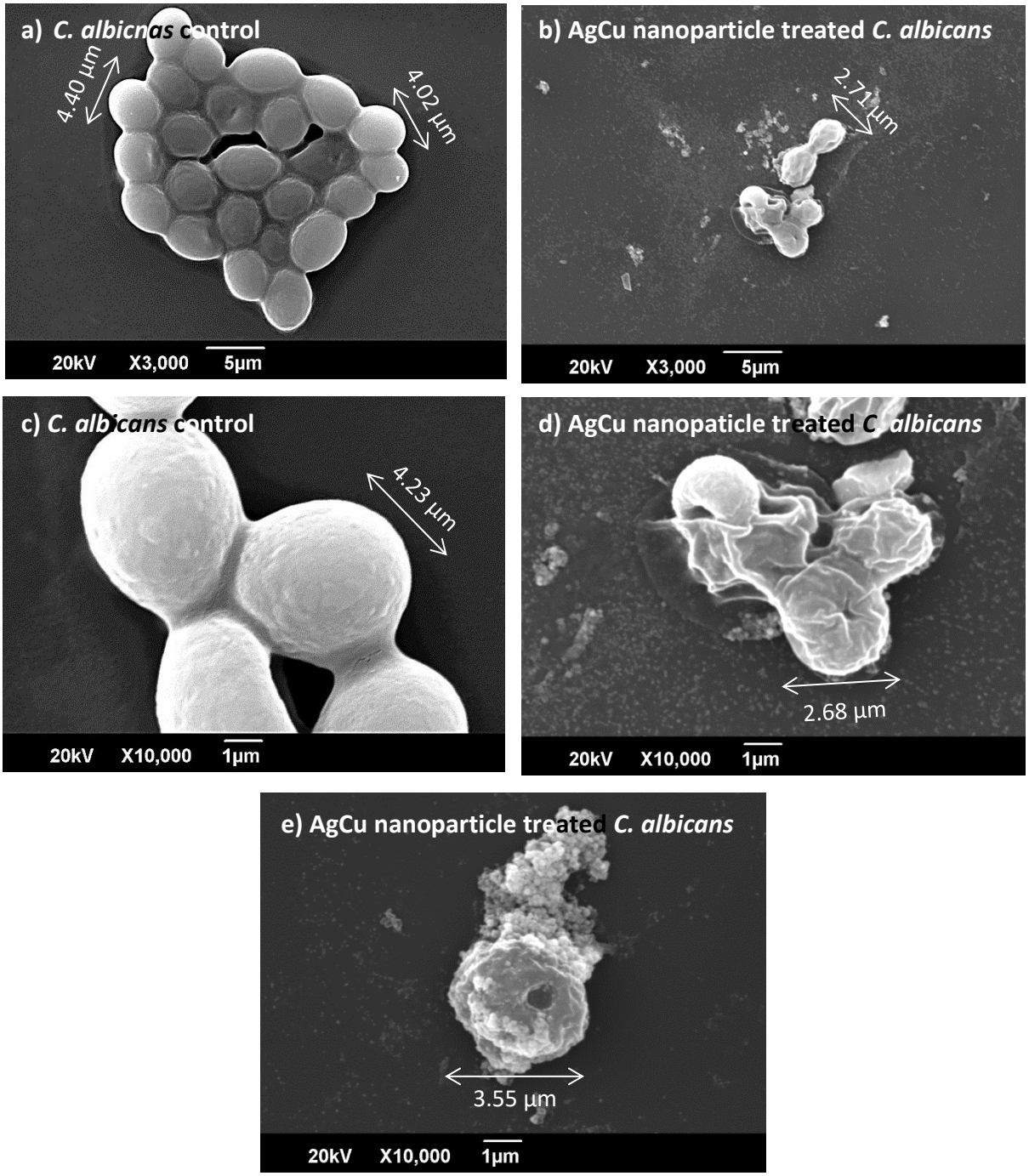

Figure 5.10: SEM images of AgCu nanoparticle treated and untreated *C. albicans*. a) C. albicans control (x3000 magnification), b) treated C. albicans (x3000 magnification), c) C. albicans control (x10000 magnification), d) treated C. albicans (x10000 magnification) and e) treated C. albicans with attachment of AgCu nanoparticles (x10,000 magnification).The sizes of the fungi were measured using ImageJ and annotated onto the images.

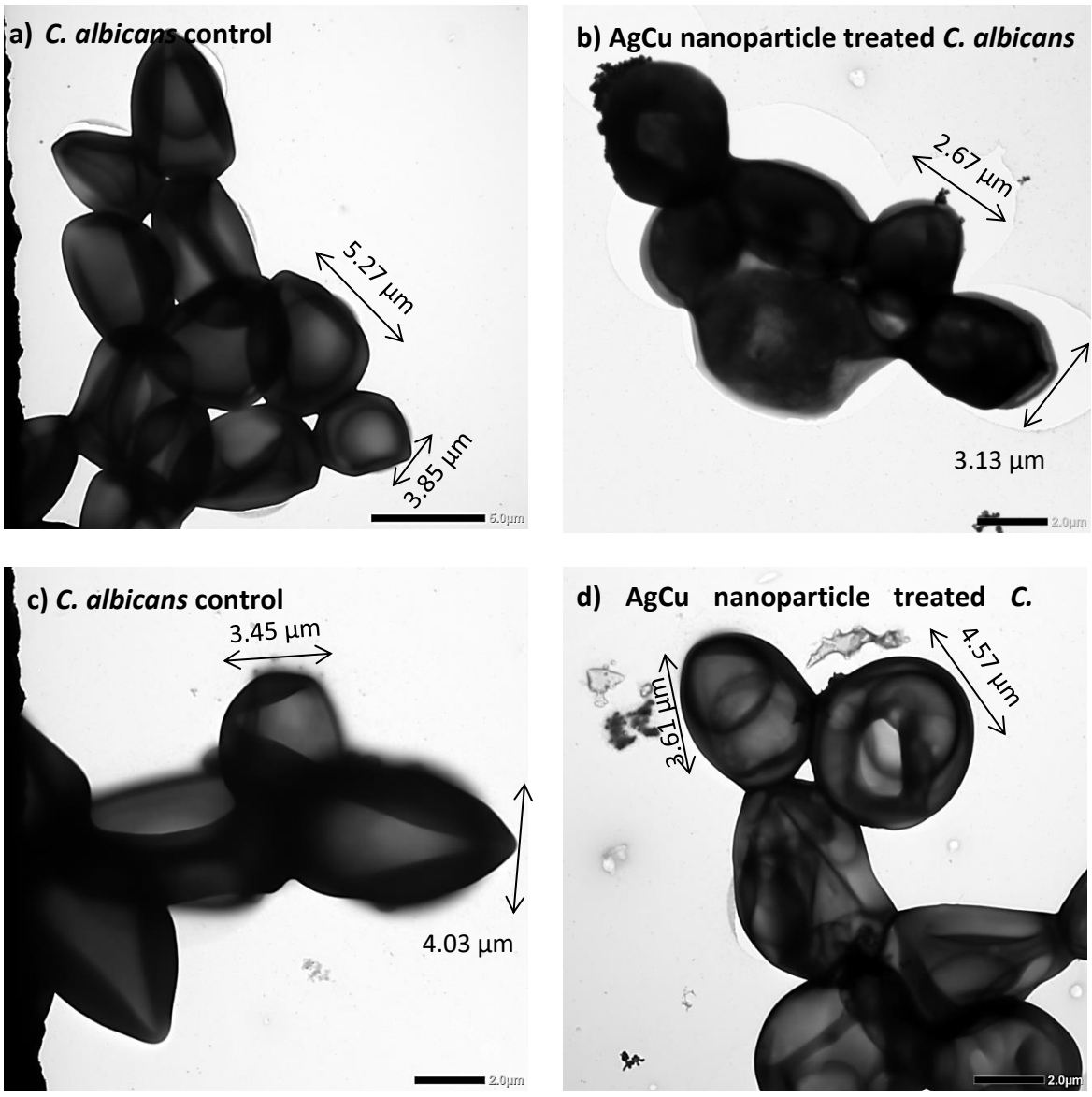

Figure 5.11: TEM images of AgCu nanoparticle treated and untreated *C. albicans.* a) *C. albicans* control (x1500 magnification), b) treated *C. albicans* (x2500 magnification), c) *C. albicans* control (x2500 magnification), d) treated *C. albicans* (x2500). AgCu nanoparticles (smaller black spheres) can be seen in b and d. The sizes of the fungi were measured using ImageJ and annotated onto the images.

AgCu nanoparticle suspension had less effect on the internal cellular processes of *C. albicans* in comparison to the bacteria cells. Assuming that the control cells had 0% oxidative stress, AgCu nanoparticle suspension resulted in a decrease in oxidative stress, with an immediate reduction of 25.8% to 23.0% in all concentrations. Although, less reduction was seen after incubation, the oxidative stress level did not exceed the control, as shown in Figure 5.12 (a).

Assuming the control *C. albicans* cells had 100% protein, incubation with AgCu nanoparticle suspension resulted in an immediate increase in detected protein. The MIC value resulted in the highest increase in protein at 107.7%. However, protein levels decreased slightly over time. As shown in Figure 5.12 (b), all three concentrations resulted in a slight reduction of protein, but the detected percentage was close to the control.

AgCu nanoparticle suspension also caused a change in the level of DNA in *C. albicans* cells. Assuming the control *C. albicans* cells had 100% DNA, AgCu nanoparticle suspension treatment resulted in an immediate decrease in DNA, followed by an increase which peaked at 2 and 3 hours of incubation, before decreasing again. As shown in Figure 5.12 (c), the MIC value of AgCu nanoparticle suspension resulted in the highest decrease (29.9% reduction in comparison to the control) in DNA immediately after treatment. The percentage of detected DNA then increased until 2 hours after incubation, where it reached 127.1%, then decreased to 77.5% at the final reading. The higher concentrations peaked after 3 hours of incubation, with 150 μg/ml concentration resulting in an increase of 147.0%. Both concentrations then decreased.

The surface charge of *C. albicans,* was found to be least negative in comparison to the tested microbes, with a reading of -28.5 mV (+/- 0.2).

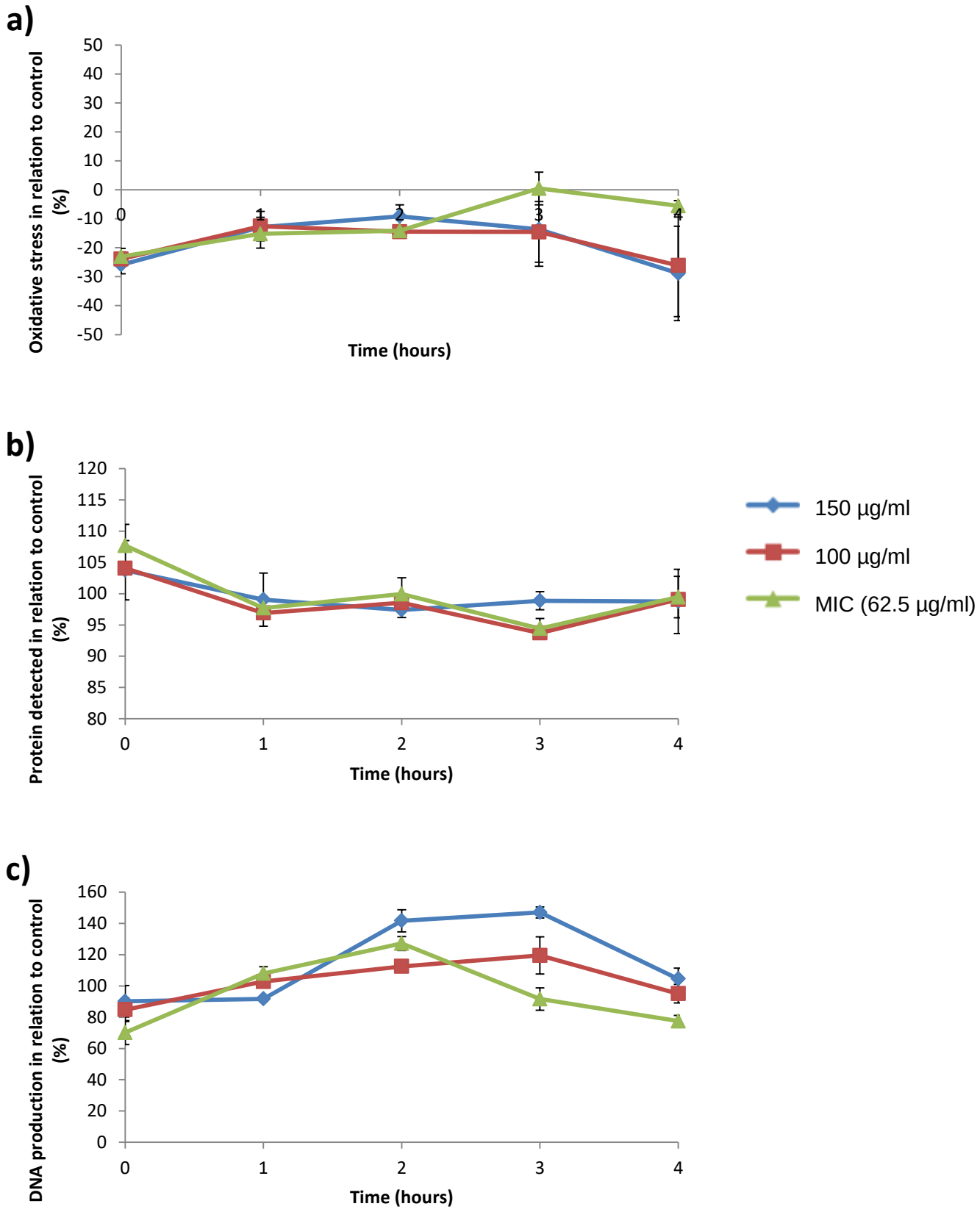

Figure 5.12: Internal cellular changes to *C. albicans* after incubation with several concentrations of AgCu nanoparticle suspensions over a 4 hour period. Graphs are used to display the changes to a) oxidative stress, b) overall protein and c) DNA production. AgCu nanoparticle suspensions were at concentrations of 150 µg/ml (represented in blue), 100 µg/ml (represented in red) and MIC value 62.5 µg/ml (represented in green). Error bars are used to denote the standard deviations of 3 replicates.

5.4 Discussion

The antimicrobial properties of nanoparticles are well known, however the mechanisms of action is still theorised and unclear. Based on these theories, experiments have been conducted in this chapter to investigate the possible mechanisms of action of AgCu nanoparticles. Furthermore, the properties of silver copper nanoparticles characterised in Chapter 4 will be used to link and help elucidate their antimicrobial activities against microbes.

5.4.1 Bacteria (*E. coli* and *S. aureus*)

One of the most supported theorised mechanisms of action of metallic nanoparticles is the physical interaction with microbial cell surface leading to cell membrane damage and ultimately cell death [139, 310]. Through three visualisation techniques (Gram staining, SEM and TEM), the physical interactions and changes to the morphology of microbes after AgCu nanoparticle treatment were observed. Firstly, Gram stain was used to view the samples at x1000 magnification. This gave an overall observation of multiple cells; however due to the small size of bacterial cells, a reduction of cells was seen after the treatment but details of interaction was unclear (Figure 5.1 and Figure 5.5). A reduction in cells was expected as a result of the antimicrobial properties of AgCu nanoparticles. As investigated by the growth rate experiment in Chapter 3, the addition of AgCu nanoparticle suspension at ½ MIC value significantly reduced the growth of microbes after 24 hours. In regards to *E. coli* and *S. aureus,* the growth rate experiment found a reduction of 48.7% and 53.4%, respectively, after 24 hours of treatment at ½ MIC, which is similar to the reduction observed through the Gram stain technique of 53.4% and 52.8%, respectively. The reduction in bacterial growth is due to cell death as a result of the presence of AgCu nanoparticles. The MIC is defined as the lowest concentration of an antimicrobial sample required to inhibit the growth of a microbe after overnight incubation [311]. As ½ of the MIC value was used in these experiments, the microbial sample was roughly reduced by half, and due to the low dosage certain microbes will be unaffected, thus growth of cells were still observed.

Using higher magnification, attachment of a few AgCu nanoparticles to the surface of *S. aureus* can be observed in the TEM images (Figure 5.7). The attachment of nanoparticles to the cell membrane of microbes has been reported to be due to the electrostatic attraction between the surface of nanoparticles and microbe [312, 313].

El Badawy *et al.* (2011) found that there is a direct correlation between the ζ-potential of nanoparticles and antimicrobial efficacy, with positive nanoparticles exhibiting more antimicrobial activity [314]. Microbial cell surface typically has a negative surface charge due to the presence of negatively charged components such as phospholipids, lipopolysaccharides and phosphatidylglycerol in bacterial cell wall [315-318]. However, in Chapter 4, it was found that AgCu nanoparticles also had a negative surface charge of -20.9 mV and -21.3 mV at corresponding MIC values to *E. coli* and *S. aureus*. In this case, it is believed that the repulsive forces are overcome when microbial cells and nanoparticles are at close distances, leading to the presence of strong attraction forces [319]. Others have also reported antimicrobial activity of nanoparticles involving the interactions between negatively charged nanoparticles and microbial cells. For example, Mailard *et al.* (2018) found that their negatively surface charged Ag nanoparticle interacted with the surface of *E. coli* membrane which contributed to the antimicrobial effect [320]. Furthermore, it has been reported that negatively charged nanoparticles can interact with negative microbial surfaces as a result of molecular crowding at high nanoparticle concentrations [321].

On the other hand, AgCu nanoparticle attachment was not seen in the TEM images for the *E. coli* samples (Figure 5.3). Gram-negative bacteria generally have a more negative surface charge, due to the presence of lipopolysaccharides in the cell wall, compared to Gram-positive bacteria, with less negative phospholipids in the cell wall [112, 322]. This was confirmed by measuring the surface charge via ζ- potential. *E. coli* was found to be more negative than *S. aureus,* with a measurement of -44.3 mV (±0.2) and -31.2 mV (±1.6), respectively. As a result of a more negative surface charge, *E. coli* would have less attraction to AgCu nanoparticles. Moreover, the attachment of AgCu nanoparticles was not seen in the SEM observations in either *S. aureus* or *E. coli.* A reason for this could be the difference in staining between the techniques. The SEM procedure involved more steps and washing of the sample in comparison to TEM procedure, which may have cause the detachment of nanoparticles with weak attraction force.

In addition to nanoparticle interaction, the negative surface charge of microbes can attract positive ions released by the AgCu nanoparticles. Metallic nanoparticles are known to release ions, with smaller sized particles having a higher release rate as a

result of the larger surface area [323]. In Chapter 4, the pH experiment found AgCu nanoparticles increased the pH of water and thus suggesting the release of AgCu ions. Once positively charged ions have attached onto negatively charged components on the surface of the microbes via electrostatic interactions, they can neutralise the charge of the surface of the microbe [322]. Therefore, negatively charged AgCu nanoparticles can physically interact with the neutralised microbial surface without electrostatic repulsion and cause cell membrane damage. Furthermore, metal ions themselves have been reported to exhibit antimicrobial activity and are one of the theorised mechanisms of action of nanoparticles. It is believed that the metal ions can interact with the cell surface, alter the membrane permeability and disrupt the cell wall [249, 322-324]. Interestingly, the more negatively charged bacteria, *E. coli*, had a lower MIC, in comparison to the less negatively charged bacteria, *S. aureus.* It seems logical that the microbes with more negativity have a higher affinity for positive metal ions which can neutralise the cell faster, resulting in nanoparticle interactions, and interact with more ions, thus requiring less concentration to inhibit the cells.

It is believed that once nanoparticles make physical contact with the bacterial cells, the interaction can damage the bacterial cell wall. This can lead to changes to the morphology, as a result of leakage of cellular material, electrolyte imbalance, disruption of membrane function, and eventually lead to cell death [22]. In terms of AgCu nanoparticles, the attachment onto the bacterial cell surface caused structural changes and degradation of the cell wall, eventually leading to cell death. SEM images (Figure 5.2 (a and c) and Figure 5.6 (a and c)) show the cell surfaces of untreated control cells are intact with no visible damage. In contrast, SEM images of both bacterial strains after AgCu nanoparticle treatment (Figure 5.2 (b and d) and Figure 5.6 (b and d)) clearly showed cell lysis with changes to the morphology and cell membrane damage, including cell membrane fragmentation. The cell wall is designed to protect the cell from mechanical damage and to maintain osmotic balance [105, 325]. As a result, the breakage of the cell wall can result in the leakage of cellular material. This was visualised as blurry smears in the SEM images (Figure 5.2 (b and d) and Figure 5.6 (b and d)) and more clearly in the TEM images of *S. aureus* (Figure 5.7 (b and d)). Despite the TEM images of treated *E. coli* not showing leakage (Figure 5.3 (b and d)), observations of shrinkage and cell surface wrinkles

suggests dehydration through loss of cytoplasmic material. Similar observations of cell membrane damage and internal component leakage were also reported by Sabira *et al.* (2020) where they treated microbes with AgCu and CuAg nanoparticles. Additionally, results of disruption to the cell membrane, cell shrinkage and release of intercellular membrane were seen in microbes tested against Cu and Ag nanoparticles [324, 326, 327].

Analysis of the observational images showed a change in bacterial sizes after incubation with AgCu nanoparticles. In *E. coli*, an increase in length was visualised using SEM. The average length of the control cells were 2.0 μm, whilst the treated cells were on average 3.1 μm. As the AgCu nanoparticles resulted in fragmentation of the cell membrane, the fragments have spread with leakage of internal material smearing away from the cell leading to an increase in length. At close magnification, TEM images showed a decrease in the width of *E. coli* cells from 0.7 μm to 0.5 μm – this supports the leakage of internal components hence deflation and shrinkage of the cell. Deflation and reduction in cell size was also seen in *S. aureus* cells after treatment, particularly in TEM images (Figure 5.7 (b and d)). Average control cells of *S. aureus* varied between 1.2 to 0.7 μm; on average treated *S. aureus* cells with visually intact membrane were 0.7 μm which is similar to the control cells. However, cells with ruptured membrane were much smaller with an average size of 0.4 μm as a result of the outflow of cellular material. Similar reports of intracellular material leakage and shrinkage of cells were also reported when bacteria cells were treated with Ag nanoparticles [328].

Although it has been reported that nanoparticles can be internalised into microbial cells due to their small size, this was not observed in the AgCu nanoparticle treated *E. coli* cells [329]. On the other hand, TEM images of *S. aureus* (Figure 5.7 (b and d)) showed internalisation of AgCu nanoparticles. It has been reported that nanoparticles below 80 nm can be transported through the cell membrane into the cell [330]. In Chapter 4, hydrodynamic size measurements found that AgCu nanoparticles were on average 181 nm in diameter, nevertheless particle sizes of below 80 nm were also measured within the suspension. This suggests that smaller sized particles within the AgCu nanoparticles suspension may have been transported into the *S. aureus* cells or alternatively, AgCu nanoparticles entered

through areas of broken cell membrane. However, it is also unclear whether the AgCu nanoparticles have entered the microbial cell or is on the surface, as schematically illustrated in Figure 5.13.

In addition to structural changes, assays have shown that AgCu nanoparticles affected the levels of oxidative stress, overall protein and DNA in bacterial cells. Using Bradford assay, the protein of AgCu nanoparticle treated cells were monitored and compared to the control cells. The Bradford assay was used to monitor the protein level of microbes when incubated with AgCu nanoparticles. In this colorimetric assay, the protein concentration can be determined through the change in colour of Coomassie blue G-250 dye at 595 nm. Under acidic conditions, the cationic dye is red, however in the presence of protein, the dye is stabilised to the anionic form which is blue [331, 332].

In both bacterial samples, it was found that the protein decreased with incubation time. Furthermore, the reduction in protein was concentration related, with higher concentration of AgCu nanoparticle causing a higher percentage of reduction. Bacterial protein can be found throughout the cell including in the cell membrane and in the cytoplasm [333-335]. Both Ag and Cu nanoparticles have been reported to cause protein damage [59, 336-338]. Furthermore, Cu ions are reported to strongly interact with sulphur containing amino acids and the interaction between Ag ions and thiol groups of proteins lead to their inactivation [338, 339]. As a result, the reduced protein percentage is likely to be caused by the AgCu nanoparticle denaturing the protein. Roughly 25 to 30% of bacterial proteins are located in the cell envelope or exterior of the cell [333]. Thus the ability of AgCu nanoparticles to denature proteins may have contributed to the observed damage to the cell membrane.

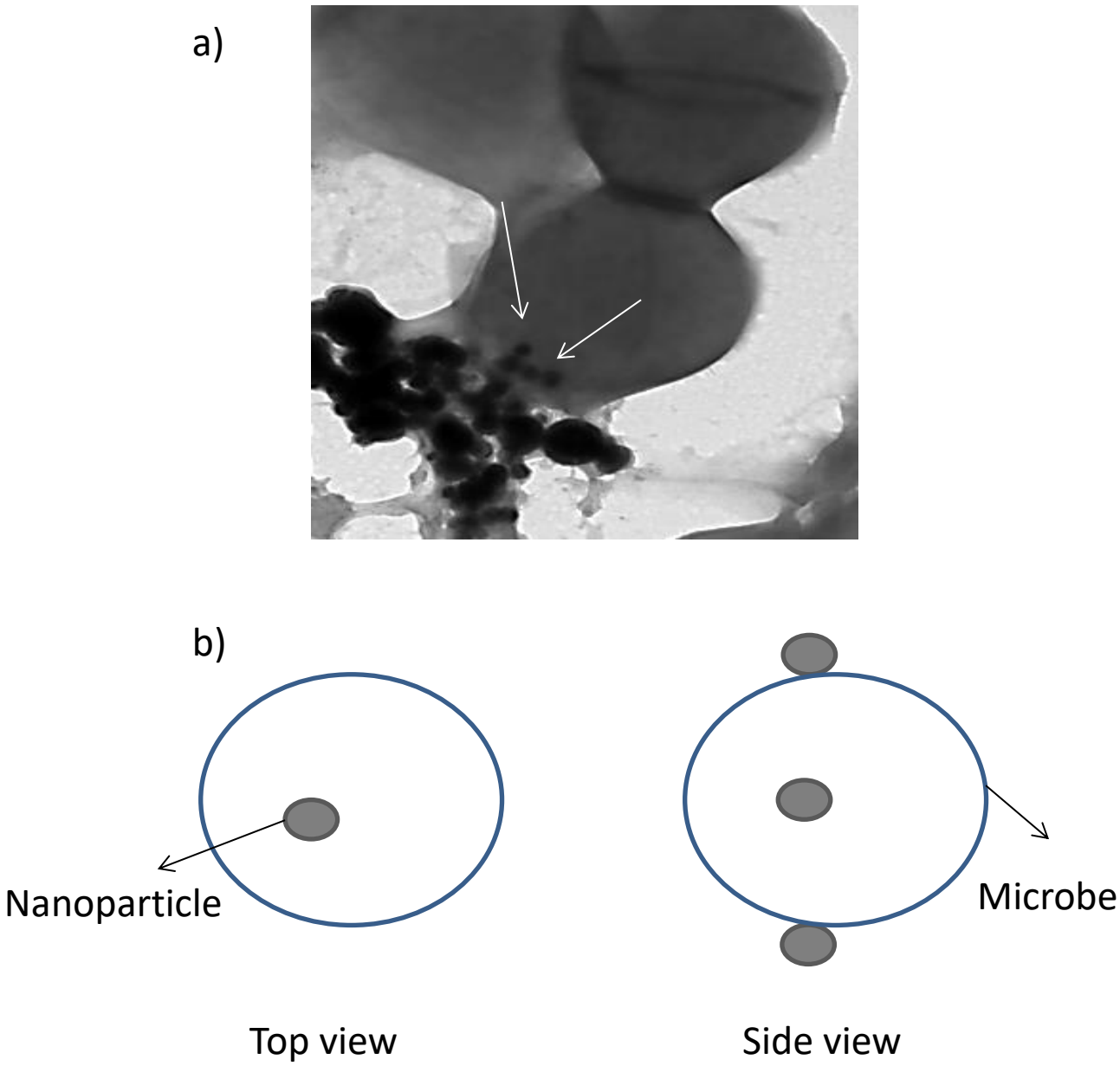

Figure 5.13: Nanoparticle position observation. a) TEM image of treated *S. aureus* cell with arrows to highlight the AgCu nanoparticle. TEM imaging is observed through one angle. As shown in b, the top view represents what we see from the TEM image (blue circle representing the microbial cell and grey circle representing the AgCu nanoparticle). However, the side view shows that the nanoparticle can be located on top of the microbe, inside the microbe or underneath the microbe, thus from the TEM image it is unclear whether the nanoparticle is internalised or outside of the microbe.

On the other hand, Siddique *et al.* (2020) and Gunalan *et al.* (2012) detected an increase in protein after microbial incubation with Ag nanoparticles and ZnO nanoparticles, respectively. It was suggested that the increase in protein was a result of cytoplasmic protein leakage due to the cell membrane damage caused by the nanoparticles. Although the same protein measuring reagent was used, the increase in protein was detected after 6 and 12 hours of incubation [340, 341]. As the experiment in this chapter stopped after 4 hours, it is possible that the cell membrane was still intact and leakage of protein began at a later time period, or the leaked protein was denatured by the AgCu nanoparticles thus unable to be detected.

Moreover, when nanoparticles make physical contract with the microbial cell membrane, the nanoparticles can interfere with the electron transport chain, resulting in formation of ROS [139, 342]. ROS are highly reactive unstable molecules that contain an oxygen atom, e.g. superoxides and hydroxyl radicals [343]. They are produced naturally in microbial cells as a response to metabolism of oxygen, with an importance in cell signalling and homeostasis. The exposure of nanoparticles can induce the excess production of ROS, also known as oxidative stress, which can lead to cytotoxicity [343-345]. ROS can react with lipids in the microbial cell membrane, resulting in membrane lipid peroxidation. This increases the cell permeability and the transport of particles become uncontrolled [346]. Furthermore, the ions released by nanoparticles can enter microbial cells and induce the generation of intracellular ROS which damages internal components [342, 345].

The generation of ROS can be detected by oxidative stress assay using H_2-DCFDA. Mechanistically, H_2-DCFDA diffuses into the microbial cells and where it gets deacetylated by esterase to form H_2DCF. In the presence of ROS, H_2DCF is oxidised to DCF which emits green fluorescence at excitation and emission wavelengths of 485 nm and 530 nm, respectively [347, 348]. In terms of AgCu nanoparticles, the H_2-DCFDA assay detected a significant increase of oxidative stress in the bacterial samples after 2 hours of incubation. Upon immediate addition of the AgCu nanoparticles, drop in oxidative stress was measured in both samples. Bacteria contain defence mechanisms to help protect and regulate oxidative stress. In particular, *Staphylococci* species contain carotenoid pigments that can protect the cell by quenching single oxygen molecules, whilst both *E. coli* and *S. aureus* can produce enzymes such as superoxide dismutase that can detoxify the ROS [349,

350]. The reduction in oxidative stress levels could be the bacteria's response to the production of ROS caused by the AgCu nanoparticles. However, over time the bacteria's defence mechanisms were unable to cope with the excess production of ROS, thus an increase in oxidative stress level was measured.

For *E. coli*, an increase in oxidative stress was measured after an hour of incubation with AgCu nanoparticles (at 100 μg/ml and 150 μg/ml) and peaked after 2 hours of incubation, with over 318% increase at 100 μg/ml concentration of AgCu nanoparticle in comparison to the control. Afterwards in the following hours, the oxidative stress level was still elevated in comparison to the control, however, it began to reduce. A reason for this could be the death of cells, thus resulting in a reduction of bacteria for AgCu nanoparticles to interact with. In Chapter 3, the fluorescent cell viability experiment found that after 2 hours of incubation with AgCu nanoparticles at 100 μg and corresponding MIC, less than 1% of *E. coli* cells were viable. Therefore, the production of new ROS was prevented due to the lack of viable cells to interact with AgCu nanoparticles.

In regards to *S. aureus,* the oxidative stress levels started to increase after 2 hours of incubation and continued to increase in the following hours. The fluorescent cell viability test in Chapter 3 showed that more cells were viable in comparison to *E. coli*, thus viable cells were still able to react with AgCu nanoparticles to continue the increase in oxidative stress. The fluorescent cell viability assay also found that membrane damage and cell death of bacterial cells began immediately, with a reduction of 23.9% and 72.2% viability in *S. aureus* and *E. coli*, respectively, after 100 μg/ml AgCu nanoparticle treatment. In contrast, an increase in oxidative stress was only detected after 2 and 1 hour of treatment, respectively. Additionally, the increase in oxidative stress did not correlate with increasing concentration of AgCu nanoparticles in both bacteria; 100 μg/ml of AgCu nanoparticle resulted in the highest increase of oxidative stress followed by at 150 μg/ml and lowest increase at MIC value. This suggests that oxidative stress increased with increasing concentration of AgCu nanoparticles until a certain concentration where bacterial cell death exceeded the production of oxidative stress. Therefore, this indicates that the increase in oxidative stress level contributed to bacterial cell death; however it is not the main mechanism of action of AgCu nanoparticles.

The last assay was used to monitor the DNA levels in bacteria after incubation with AgCu nanoparticles. DNA contains the genetic information of the microbe, thus providing important information for cell replication [351]. Upon damage to the DNA, bacterial cells can undergo programmed cell death [352]. DAPI is a cell permeable DNA-specific probe. Once internalised, it has an affinity towards the minor grove of A-T sequences in DNA which results in the formation of fluorescent complex with an excitation and emission wavelength of 358 nm and 461 nm, respectively [353, 354]. In both bacterial strains, the DNA decreased after incubation with AgCu nanoparticles; immediate reduction was seen in higher AgCu nanoparticle concentrations (100 μg/ml and 150 μg/ml), however at MIC level, reduction was seen after 1 hour of treatment. It has been reported that both Ag and Cu nanoparticle can bind to and damage DNA, including breaking the bonds between nucleotides [355-357]. Furthermore, nanoparticle ions, including Ag and Cu, were found to damage DNA [358-360].

DNA is heavily comprised of sulphur and phosphorous. The affinity of Ag nanoparticles towards phosphorous and sulphur compounds contributes to their ability to damage DNA. Ag and Cu nanoparticles can interact with the compounds, thus react with and damage the DNA [59, 281, 339, 361-363]. The reaction has been reported to result in disruptions to DNA replication, damage and denaturing of the DNA, and ultimately causing cell death [361, 363, 364]. Likewise, the ions released by Ag nanoparticles can also interact with the phosphorous and sulphur areas in DNA and result in cell death. Similar to the nanoparticles, the interaction of ions and DNA can disrupt the DNA structure, inactivate the ability of DNA to replicate, bind to nucleotide bases which displace hydrogen bonds and denatures the DNA, [339, 361, 363, 365].

The reduction trend of DNA in *E. coli* cells after AgCu nanoparticle incubation corresponded with the fluorescent cell viability test (Chapter 3); however, the reduction in DNA was not as significant as cell death, especially at when incubated at the MIC. This suggests that AgCu nanoparticles can damage DNA of *E. coli* cells, which contribute to cell death, but it is not the main cause. On the other hand, the decrease in cell viability of *S. aureus* cells was more closely related to the reduction of DNA. As mentioned previously, internalisation of AgCu nanoparticles was possibly seen in *S. aureus* cells through TEM imaging. Bacterial DNA is contained in a

nucleoid located in the cytoplasm of the cell [351]. Since AgCu nanoparticles can enter *S. aureus* cells, they can damage the DNA prior to the breakage of the cell membrane, thus the cell viability and DNA levels were more closely linked in comparison to *E. coli.*

Although the effects of AgCu ions were not separately tested in this thesis, it has been reported that ions themselves can interact with bacterial cells and result in structural changes [139, 339, 366]. AgCu nanoparticles have been found to release ions through the pH experiment in Chapter 4. Additionally, the agar well diffusion method suggests that ions contributed to the antimicrobial activity of AgCu nanoparticles. As both AgCu nanoparticles and microbial membrane have a negative surface charge, it might be possible that the ions produced by the nanoparticles were the preliminary mechanism of action as a result of electrostatic interaction [310]. It has been reported that metal ions can be absorbed through the microbial cell membrane or are directly transported by membrane proteins [22]. Through observational techniques, experiments have found that Ag ion treatment caused the separation between cell wall and cell membrane of bacteria, followed by the release of cellular material. Similar observations of cell shrinkage and blurry areas were reported [366, 367]. Additionally, both silver nanoparticles and ions have been reported to react with sulphur containing proteins on the cell membrane and consequently causing cell membrane damage and morphology change [361, 362, 367]. However, further experiments are required to confirm the mechanisms of action of AgCu ions.

5.4.2 Fungi (*C. albicans)*

Observations and assays have shown that the mechanism of action towards fungi, which was represented by *C. albicans,* was slightly different than towards bacteria. Fungal cell wall, in particular *C. albicans,* consists of a two layers: outer mannoprotein layer and an inner β-Glucan and chitin layer. Overall, fungal cell wall has a negative charge due to the presence of negatively charged molecules, including melanin [318, 368]. By measuring the ζ- potential, it was found that *C. albicans* had the least negative charge out of the microbes tested at -28.5 mV (+/- 0.2). Despite AgCu nanoparticles also having a negative charge, *C. albicans* was found to have AgCu nanoparticles attached onto the surface of the microbe in all observational techniques. Likewise to the interaction between AgCu nanoparticles

and negatively charged bacteria, it is believed that the repulsion forces were overcome through molecular crowding and close distance between the nanoparticle and microbe [319, 321]. Since *C. albicans* had the least negative charge, the attraction to nanoparticles is likely to be stronger than that to bacterial cells, thus attachment of nanoparticles were visualised in all three observational techniques despite washing during the preparation procedure.

In addition to nanoparticle attachment, agglomerations were visualised on the hyphae (Figure 5.9 (c)) using the Gram stain technique. Hyphae are networks produced by filamentous fungi through tip growth; they are formed as essential aspects for colonisation, pathogenicity and nourishment [369-371]. Certain antifungal agents, including nanoparticles, have shown to inhibit the growth of hyphae and decrease the metabolic activity of hyphae clumps [372-374]. In comparison to control cells, less hyphae observations were visualised. This suggests that AgCu nanoparticles were able to inhibit the formation of fungal hyphae. Furthermore, Chen *et al.* (2020) and Chen *et al.* (2016) found that the direct contact between the nanoparticle and fungal hyphae led to damage to the hyphae including disruptions to cell surface protein structures. Although the damage to the hyphae after AgCu nanoparticle is unclear in the Gram stain images, there are no *C. albicans* cells in Figure 5.9 (c). This suggests that AgCu nanoparticles may have inhibited the formation of yeast cells. It was also found the cells were reduced by 80.0% after 24 hours incubation. However, in Chapter 3, the growth rate experiment found no change in cell density when incubated with AgCu nanoparticles at ½ MIC value after 24 hours. This suggests that despite AgCu nanoparticles at concentrations below the MIC could not kill the fungi as they were still viable (as confirmed by the MIC experiment in section 3.4.3), the nanoparticles had great inhibitory properties as the fungi did not multiple.

When observed at a higher concentration, both SEM and TEM images show that the attachment AgCu nanoparticles caused significant structural change. The cell inverted inwards with a more wrinkled surface and certain parts of the cell wall was ruptured. The changes to the fungal cell morphology were similar to those described when *C. albicans* was treated with Ag and Cu nanoparticles. The interaction between the fungal cell and Ag nanoparticle resulted in distortions to the morphology and disruptions to the cell membrane, which led to intercellular leakage and cell death

[371, 375-378]. It was reported that the increase in surface roughness was an indicator of outer cell wall damage. Therefore, the attachment of AgCu nanoparticles onto the fungal cell caused damage to the surface which resulted in an increase in surface roughness and wrinkles. Whilst all AgCu nanoparticles treated *C. albicans* cells exhibited this change in surface morphology, one cell in Figure 5.10 (b and d) showed rupture of the cell wall which revealed a cell of the same shape but with a smooth surface. Through TEM, Lara *et al.* (2015) found that Ag nanoparticle treatment caused separation of the cell wall and cell membrane. This suggests that AgCu nanoparticles might also cause the separation of the cell wall and membrane, and when the cell wall ruptured, the cell membrane was visible. However, Lara *et al.* (2015) reported an increase in cell size as a result of the separation, whereas TEM and SEM measurements in this thesis showed a decrease in diameter after incubation with AgCu nanoparticle suspension. On the other hand, it has been found that Ag and Cu nanoparticles caused pits in the cell wall which resulted in leakage of intercellular components and compounds [375, 378]. SEM and TEM images (Figure 5.10 (b, d and e) and Figure 5.11 (b and d), respectively) both showed the formation of pits in AgCu nanoparticle treated cells, thus the reduction in size of *C. albicans* may have been a result of cellular leakage.

In addition to effects on morphology, assays were used to investigate other mechanisms of action of AgCu nanoparticles which involved internal damage of *C. albicans* cells. Unlike the bacterial cells, AgCu nanoparticles did not induce an increase of oxidative stress in *C. albicans*. Throughout the 4 hour period that was monitored, the oxidative stress level of AgCu nanoparticle treated *C. albicans* was below the control level. The reasons for this could be due *C. albicans'* transcriptional response to ROS. As fungi are eukaryotic microbes, their response to ROS is more developed than prokaryotic bacteria [379]. *C. albicans* has been reported to have a higher resistance to oxidative stress in comparison to other species of fungal yeast cells, despite having the same transcriptional response to oxidative stress. Once ROS are detected, *C. albicans* can upregulate the genes that encode antioxidants that can detoxify oxidative stress and repair proteins [379, 380]. On the other hand, Radhakrishnan *et al.* (2017) reported an increase in ROS levels when *C. albicans* was treated with Ag nanoparticles; however, it was found that the increase in ROS contributed to the cell death, but it was not the main mechanism of action.

Although a slight reduction in fungal protein was seen at certain time points after AgCu nanoparticle incubation, the level of protein was close to that of the control. Ag nanoparticles have been reported to inhibit protein synthesis of *C. albicans* and reduce the ergosterol content, which plays a critical role in protein synthesis [376, 381]. However, it was also reported that Ag nanoparticles enhanced the production of trehalose in *C. albicans,* which can protect protein from inactivation or denaturation [375]. From this experiment, it is unclear whether AgCu nanoparticles did not target the fungal protein, or the protective mechanism of *C. albicans* was able to overcome the inhibitive and denaturing ability of AgCu nanoparticles. Regardless, denaturing of protein was not the main mechanism of action of AgCu nanoparticles against fungi.

Lastly, the level of DNA in *C. albicans* after AgCu nanoparticle treatment was investigated and found an immediate decrease in DNA. However, unlike bacteria where the DNA levels continued to decrease, the level of DNA increased and decreased throughout the initial 4 hours of treatment, ranging from 77.5 to 147.0%. A reason for this is the structural difference between bacterial and fungal DNA. In eukaryotic fungal cells, DNA is part of a complex that forms a chromatin within the nucleus. This provides more protection than prokaryotic bacterial cells, where the DNA is found in the nucleoid which does not have a membrane [351, 382]. The death rate (cell viability test in Chapter 3) of *C. albicans* was slower in comparison to the bacterial cells, which may have been a result of the better DNA protection. It is possible that DNA damage happened later on as the AgCu nanoparticle treatment required more time to penetrate and interact with the DNA. The last reading at 4 hours showed a reduction, however more readings is required to confirm the trend.

Any damage to the DNA might lead to cellular mutation or cell death; therefore cells have defensive mechanisms to protect their DNA. It was suggested that chromatin condensation was a defence mechanism to protect the DNA from harm [339, 383]. DNA specific fluorescent dye, DAPI, can be used to quantify DNA [353]. However, it has been found that the intensity of the fluorescent dye can increase when chromatins are condensed, thus the increase in detected DNA might have been contributed by condensed chromatins of *C. albicans* rather than an increase in DNA production [384]. NiO nanoparticles have also been reported to result in initial chromatin condensation of fungal cells, then followed by DNA damage and cell death

[385]. Furthermore, Ag nanoparticles were found to enhance the staining of DAPI in *C. albicans* cells as a result of nucleus damage when they interacted with DNA; this lead to DNA fragmentation, cell division failure and cell death [386].

5.4.3 Summary

To summarise, the common hypothesised mechanisms of action of AgCu nanoparticles were investigated through visual observations and assays. It was found that the AgCu nanoparticles were able to make direct physical contact with *S. aureus* and *C. albicans*, although the attraction might have been weak due to a negative ζ- potential in both the microbe and nanoparticle. Morphology changes were clearly observed in all samples, which indicated damage to the cell membrane after incubation with AgCu nanoparticles. Leakage of internal material was seen through blurs around the damaged cell and also supported by shrinkage of cells. Using Bradford assay, an immediate increase in detected protein was found which supports the finding of internal cellular leakage. The assay also indicated that AgCu nanoparticles were able to reduce and denature bacterial proteins after a few hours of treatment. Other assays have shown that AgCu nanoparticles can damage or inhibit DNA production and induce oxidative stress of bacterial cells. However, in fungal cells, there was no increase in oxidative stress and the percentage of DNA fluctuated. In comparison to the cell viability test in Chapter 3, the changes to oxidative stress and DNA production occurred after cell death began. Therefore, this suggests that AgCu nanoparticles and their ions are the primary mechanism of action, particularly in fungal cells, whilst the production of ROS contributes to the antimicrobial activity against bacteria, but is not essential. Figure 5.14 and Figure 5.15 schematically illustrates a summary of possible mechanisms of action of AgCu nanoparticles.

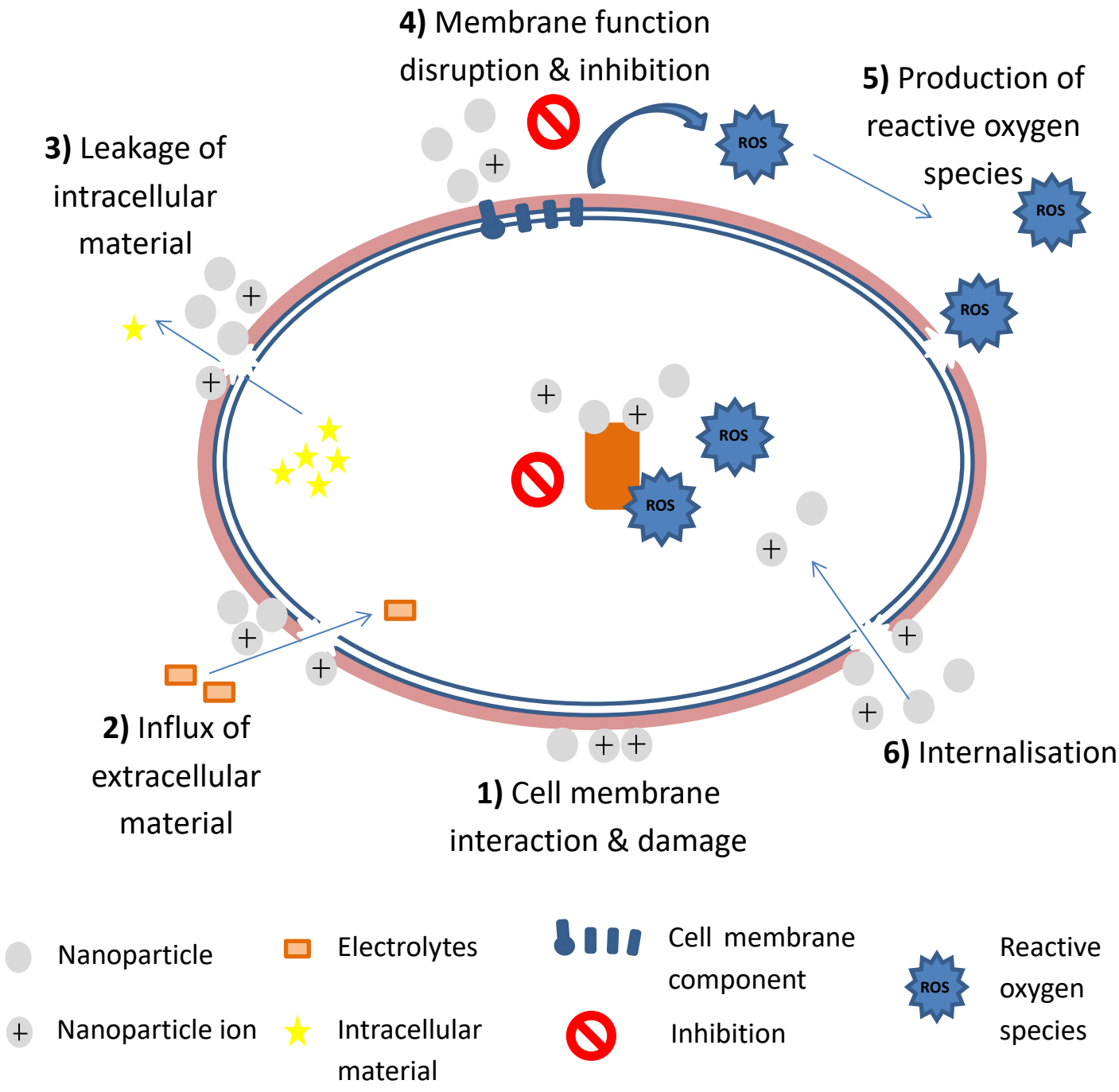

Figure 5.14: Schematic illustration of possible mechanism of actions of AgCu nanoparticles. Observations and assays have shown that more than one mechanism of action occurs when microbes are treated with AgCu nanoparticles. In no particular order, 1) AgCu nanoparticles and ions interact with the cell membrane which can result in damage to the cell membrane. 2) The damaged cell membrane can results in electrolyte imbalance due to extracellular material entering cell. 3) The damaged cell membrane can also result in leakage of intracellular material. 4) AgCu nanoparticles and ions can inhibit and disrupt membrane function. 5) The interaction of AgCu nanoparticles and ions with the cell membrane causes production of reactive oxygen species (ROS) which can also damage the cell through oxidative stress. 6) AgCu nanoparticles and ions can enter the cell and cause internal cell damage.

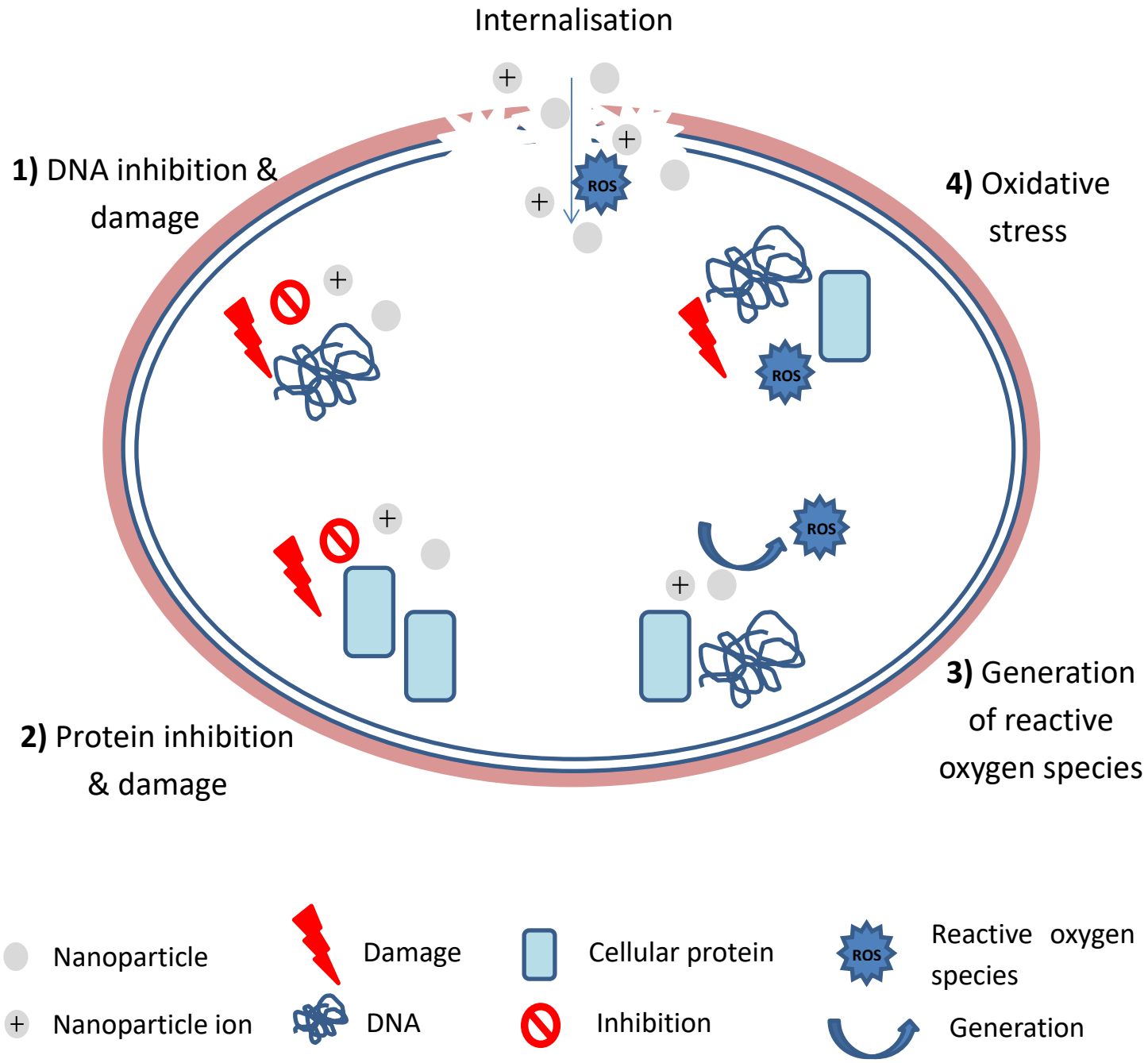

Figure 5.15: Schematic illustration of possible internal cellular mechanism of action of AgCu nanoparticles. Assays have shown that AgCu nanoparticles can affect internal components of microbial cells. Once internalised, AgCu nanoparticles and its ions have shown to 1) inhibit and damage cellular DNA. 2) Inhibit and damage cellular protein. 3) Induce the production of reactive oxygen species through the interaction with cellular protein and DNA, of which 4) ROS themselves can damage DNA and cellular protein through oxidative stress.

Chapter 6 Engineering antimicrobial film: Fabrication of AgCu nanoparticles into PDMS polymer

6.1 Introduction

Invasive devices and contaminated environments are strongly associated with nosocomial infections and their transmission [13, 104]. Over 50% of nosocomial infections are related to invasive devices as open wounds and insertion sites allow microbes to gain access into the body and the surface of devices allow microbial attachment [177, 387]. The most common nosocomial infections were reported to be urinary tract infections and primary bloodstream infections, both of which require the use of catheters. These plastic implantable devices are used to transport liquids, such as urine or medication, in or out of the body. Although catheters can improve the therapeutic outcome of patients, pathogens can colonise both the outer and inner surfaces thus leading to infections for the patient [177].

There are existing methods to reduce the risk of infection caused by contaminated catheters. These include use of disinfectants on skin prior to insertion, the wearing of sterile gloves and sterile clothing and the replacement of catheter tubing after recommended periods of use. However, even with these methods in place, infections still occur with urinary catheters responsible for up to 95% of nosocomial urinary tract infections [388, 389]. Furthermore, there is evidence that use of biocidal agents can enhance the antibiotic resistance of Gram-negative bacterial species, thus resulting in infections with limited effective treatment [390]. As a result, research is required into alternative solutions to produce antimicrobial polymers for the use as catheters.

As discussed in Chapter 3, certain nanoparticles, in particularly AgCu, exhibit antimicrobial properties [61]. Nanoparticles can be incorporated into materials for antimicrobial applications, such as biocompatible polymers that are already used in biomedical applications. Polydimethlsiloxane (PDMS) is a polymer that has been approved by the US Food and Drug Administration for medical applications due its biocompatibility. Many biomedical applications, including catheters, are manufactured using PDMS polymers and the incorporation of antimicrobial nanoparticles has been reported to enhance the properties of PDMS for these applications [391]. Catheters with antimicrobial activity may provide an alternative solution to reduce the risk of infection caused by contamination at the site of the

invasive device. Therefore, the incorporation of AgCu nanoparticles into PDMS to produce antimicrobial films was investigated.

Outline of the research work:

This chapter investigates the incorporation of AgCu nanoparticles into PDMS polymer to produce films and their antimicrobial activity was tested against a fungus (*C. albicans*), a Gram-negative bacteria (*E. coli*) and a Gram-positive bacteria (*S. aureus*), which were used to represent a broad range of microbes that cause nosocomial infections. Additionally, UV light surface treatment was explored to aid the antimicrobial activity of the polymer films. The physical properties of the nanoparticle incorporated PDMS polymer film were characterised using SEM, tensiometer and pH probe to help understand the antimicrobial activity.

6.2 Materials and methods

The preparation and information of microbes (*E.coli, S. aureus* and *C. albicans*) can be found in Chapter 2, section 2.2 and Chapter 3, section 3.2, respectively. For antimicrobial experiments, microbes were grown 24 hours prior to experiment in broth (nutrient broth for bacteria and YPD broth for fungi) in a shaking incubator set at 37°C. Microbes were then diluted to ~$3x10^7$ CFU/ml using a spectrometer at 600 nm and then further diluted to desired concentration.

6.2.1 Fabrication of AgCu nanoparticle PDMS films

AgCu nanoparticle powder (Sigma-Aldrich, UK) was weighed using scales and added to corresponding volume of Sylgard™ 184 silicone elastomer curing agent (Sigma-Aldrich, UK). The sample was vortexed and then a few drops of chloroform were added to aid dispersion of nanoparticles. The sample was then sonicated for 20 seconds (20% amp, 5 secs pulse on, 5 secs pulse off). In plastic holders, Sylgard™ 184 silicone elastomer base (Sigma-Aldrich, UK) was measured and the curing agent was added in the ratio of 10:1 silicon: curing agent to produce final concentration of AgCu nanoparticle at 0.1 w/v% and 1 w/v%. The samples were then mixed for 4 minutes using a mechanical stirrer (starting at 0 rev/min and slowly increased to 200 rev/min). The mixture was degassed under vacuum (375 mmHg) for 1 hour to remove bubbles. The degassed mixture was then dispensed into film moulds using a syringe. The film mould was pressed firmly and held together using Clarex® PMMA plates and large bulldog clips. The sample was then placed into a 65^{o}C oven overnight. Each batch produces 24 films. An example of the process and end products are shown in Figure 6.1. Control PDMS was produced in the same way without the addition of AgCu nanoparticles, chloroform and sonication to the curing agent. A separate mould of the same dimensions was used to produce the control PDMS films. To remove the films from the mould, the cover was gently removed and aseptic forceps were used to gently peel off a film. The moulds were cleaned using industrial methylated spirit (IMS) and reused to fabricate films when required. Fabricated films were stored at room temperature and used within a week of production. Film samples from each batch were weighed on scales for consistency and AgCu nanoparticle content calculation. The film moulds and Clarex® PMMA plates were kindly laser cut to size by Richard Kaye.

The PDMS mixtures were mixed using mechanical stirrer

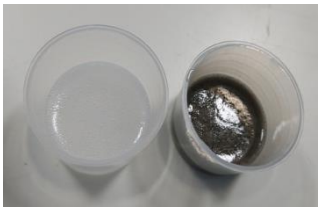

The mixtures were vacuumed to remove bubbles created during mixing

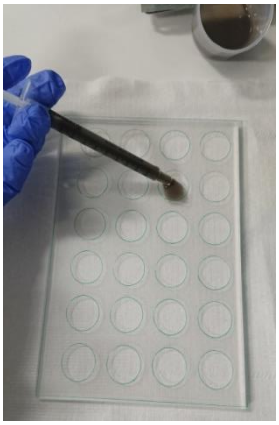

The vacuumed PDMS mixtures were dispensed into film mould

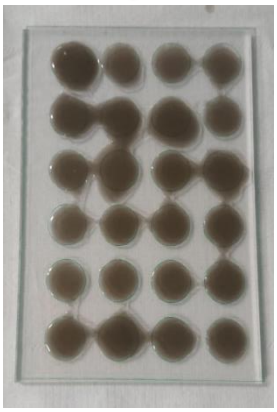

Each mould is able to produce 24 films

The mould cover is placed on and pressed to remove bubbles

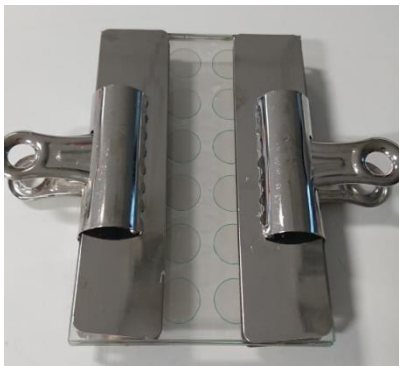

Clamps are used to hold the mould together and then incubated at 65°C

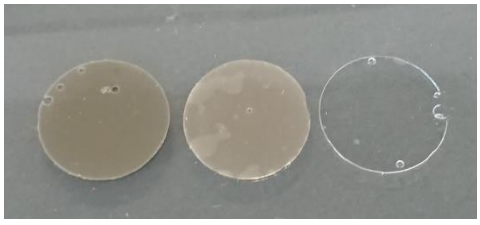

Circular films were produced

Figure 6.1: Flow diagram of the engineering of AgCu nanoparticle incorporated PDMS films. PDMS mixtures were mixed using a mechanical stirrer for 4 minutes at 200 rev/min and then placed in a vacuum for 1 hour to remove bubbles. Using a syringe, the mixtures are dispensed into a film mould. The mould cover is placed on and pressed firmly to remove any bubbles. Then the mould is held together by clamps and placed into an oven at 65°C. Circular films are produced; darker colours correspond to higher concentration of AgCu nanoparticles with colourless films as the PDMS control.

6.2.2 UV treatment

Prior to tests, some samples were UV treated using a compact UV lamp (UVP, USA), at 365 nm and 254 nm wavelength. Samples were placed 2 cm away from the lamp face and each treatment lasted for 15 minutes. For further details on the UV lamp, the UV spectrum of the lamp was kindly measured by Professor William Martin. The compact UV lamp (UVP, USA) was warmed up for 15 minutes. Using a spectrograph, the lamp face was placed at roughly 160nm away from the detector and the irradiance and the wavelength emittance spectra were measured for both wavelength bands. As shown in Figure 6.2, it was found that at 254 nm wavelength, the source had a narrow band (with intensity peak between 252 nm and 255 nm); in contrast at 365 nm wavelength, the source had a broader band (with intensity peak between 352 nm and 387 nm). The power irradiance was 80 uW and 95 uW at 254 nm and 365 nm wavelength, respectively.

Following the same method as the MIC test in Chapter 3, section 3.2.2, the effects of UV treatment on the MIC was investigated. In brief, AgCu nanoparticle suspension was pipetted into a 96 well plate in 2-fold reducing concentration from 500 μg/ml to 1.95 μg/ml and UV treated. Samples without UV treatment were used as controls. Microbes diluted to 3 x 10^4 CFU/ml in MH broth was added to the wells and incubated at 37°C. After 24 hours of incubation, resazurin dye (0.02%) was added to all wells and further incubated at 37°C. The colour change of the dye was observed and compared.

Similarly, the heat generation after UV treatment was measured. In a 12 well plate, 1 ml of AgCu nanoparticle suspension (0.1 w/v% and 0.01 w/v%) was placed into a well and UV treated. Pure water was used as a control. After treatment, the heat of the suspension was monitored using a compact thermal camera (FLIR C5, UK). The same method was conducted to test the film samples.

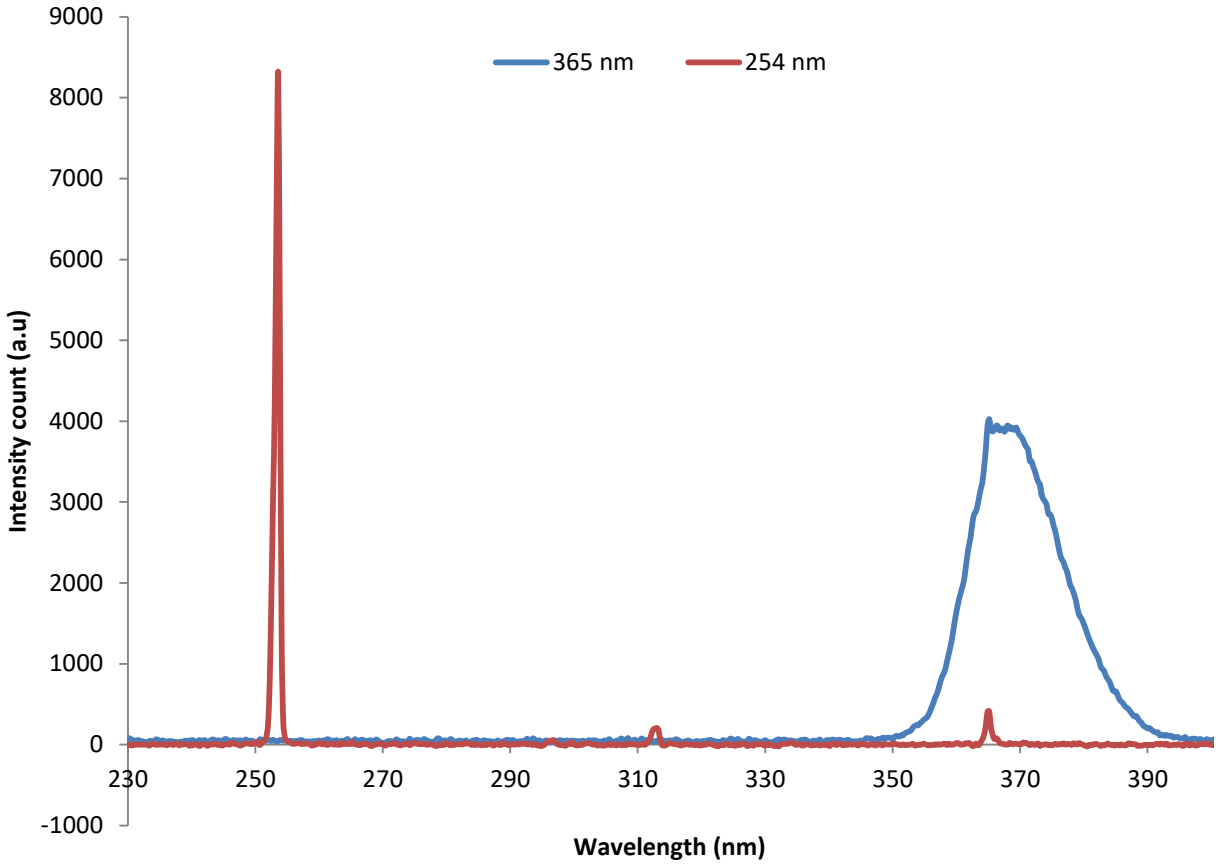

Figure 6.2: UV lamp wavelength emission spectra. The emission spectra and intensity count of the UVP compact UV lamp detected by spectrograph. Red represents the 254 nm wavelength band and blue represents the 365 nm wavelength band.

6.2.3 Antimicrobial activity of polymers

Antimicrobial activity of the film samples was measured through the disk diffusion method. Using a sterile swab, microbes at ~1-3x 10^7 CFU/ml were spread onto separate MH agar plate, following the spreading method in Chapter 3, section 3.2.1. The UV treated and original films were cut into 4mm circles using a sterile corker and placed onto the inoculated agar plates. The plates were then incubated at 37°C for 24 hours in triplicate and the antimicrobial activity of the samples was observed through zones of inhibition.

Additionally, the film samples were placed into a 24 well plate to conduct kinetic growth measurements. Certain film samples were UV treated for 15 minutes and then 400 µl of microbes at 3x10^4 CFU/ml were added. Separate experiments were conducted for microbes *E. coli, S. aureus* and *C. albicans* and UV wavelengths. Using a plate reader (CLARIOstar, BMG), the UV absorbance was measured at 600nm every hour for 24 hours. The plate reader was programmed to incubate the samples at 37^{o}C and shake the plate at 60 rpm immediately prior to each UV absorbance measurement. The initial absorbance was considered as a blank and taken away from all data points. The growth kinetics was presented as a regression graph. Furthermore, the final growth percentage after 24 hours of incubation was calculated following Equation 6 and presented as a bar graph with data expressed as the mean value (mean value of both experiments if the same samples were tested in both e.g. PDMS control and AgCu PDMS without UV treatment) with error bars to denote the standard deviations. Unpaired student t test function embedded in Excel was used as statistical analysis to compare each growth percentage with the untreated PDMS control. A value of p <0.05 was considered as a significant difference and was indicated by * in the bar graph.

$$Growth\ (\%) = \frac{Final\ absorbance\ of sample - initial\ sample\ absorbance}{Final\ asorbance\ of\ control - inital\ control\ absorbance}\ x100$$

Equation 6: Growth percentage calculation

6.2.4 Characterisation of AgCu nanoparticle PDMS films

For physical observation, the film samples were coated in gold for 45 seconds and then observed using SEM CarryScope JCM-5700 (JEOL, UK) at x1000 magnification. ImageJ was used to adjust the colour threshold on the obtained SEM image and then the number of nanoparticles present in an 86 μm x 128 μm area of polymer. Additionally, the diameter and frequency of the nanoparticles were analysed. Three areas of three different polymer films were tested.

The hydrophobicity of film samples were measured using Theta Lite Optical Tensiometer (Biolin Scientific, UK). The sessile drop function was used to measure the contact angle of 5 μl pure water with image recording settings on 3.8 fps for 10 seconds to produce 38 contact angle measurements per run. Three repeats were performed for each sample type. The mean average of the repeats was presented in a graph with error bars to denote the standard deviations. One-way ANOVA function embedded in Excel was used to statistically analyse the results. A value of p <0.05 was considered as significant difference.

The film samples were also tested for release of ions by measuring the pH; samples were immersed in 5 ml of deionised water in a universal tube for 14 days at room temperature. The pH was measured using a pH meter (Jenway, UK). Three repeats were performed and results were presented in a graph as mean average with error bars to denote the standard deviation. The one-way ANOVA function embedded in Excel was used to statistically analyse the results. A value of p <0.05 was considered as significant difference.

6.3 Results

6.3.1 Antimicrobial activity

The disk diffusion agar method was used to investigate antimicrobial activity by observing for zones of inhibition. As shown in Figure 6.3, no zones of inhibition were produced by the samples.

Growth kinetics were also investigated by using a plate reader to measure the hourly UV absorbance at 600 nm of microbial samples incubated with various PDMS films to create a 24 hour regression growth curve. As shown in Figure 6.4, Figure 6.6 and Figure 6.8, only UV treated 0.1 w/v% AgCu PDMS polymer films showed antimicrobial activity where the same growth trend line was produced, however at a lower absorbance which indicates less cells. Due to the dark colour of 1 w/v% AgCu nanoparticle incorporated PDMS films, disturbance was observed in the absorbance readings and therefore was not included in this Chapter; however, results can be found in Appendix.

The percentage of growth after 24 hours of incubation with the PDMS polymer films was calculated in relation to the microbe control (growth of microbes without presence of any PDMS film) and displayed in Figure 6.5, Figure 6.7 and Figure 6.9. The 0.1 w/v% AgCu nanoparticle incorporated PDMS film was most effective against *C. albicans* with 71.8% reduction in microbial growth when treated with 365 nm UV light, followed by 254 nm treatment with 55.9% reduction. *E. coli* also showed a reduction in microbial growth of 26.5% and 22.9%, respectively. Less antimicrobial activity was seen towards *S. aureus* with a reduction in microbial growth of 9.8% and 11.5%, respectively. Using unpaired student t test analysis, it was found that there was a statistically significant difference in microbial growth, where $P < 0.05$, for both UV wavelength treated AgCu PDMS films, as indicated by the asterisk on the bar graph.

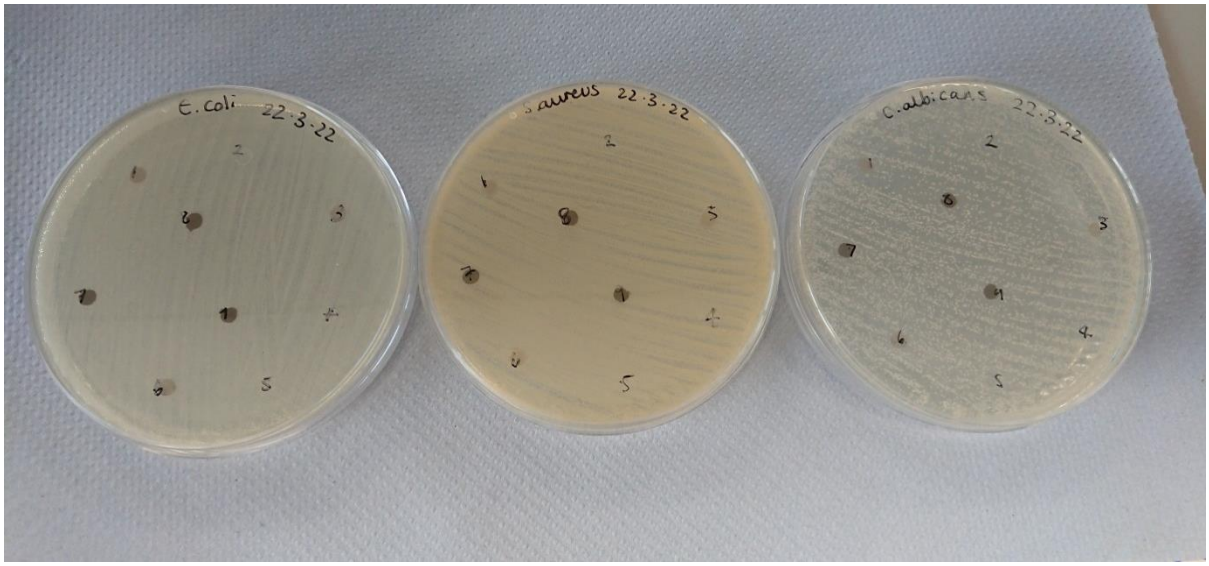

Figure 6.3: Disk Diffusion agar plates of PDMS film samples. PDMS samples were cut into small disks using a sterile 4 mm corker and placed onto inoculated Mueller Hinton agar plates. PDMS samples are labelled as 1) 254 mn UV treated AgCu nanoparticle incorporated PDMS film, 2) 254 nm UV treated PDMS control film, 3) 365 nm UV treated 0.1 w/v% AgCu nanoparticle incorporated PDMS film, 4) 365 nm UV treated PDMS control film, 5) PDMS control film with no treatment, 6) 0.1 w/v% AgCu nanoparticle incorporated PDMS film with no treatment, 7) 365 nm UV treated 1 wt/v% AgCu nanoparticle incorporated PDMS film, 8) 254 nm UV treated 1 w/v% AgCu nanoparticle incorporated PDMS film, and 9) 1 w/v% AgCu nanoparticle incorporated PDMS film with no treatment. As labelled on the plates, microbes *E. coli, S. aureus* and *C. albicans* (from left to right) were used.

a) *E. coli* 365 nm

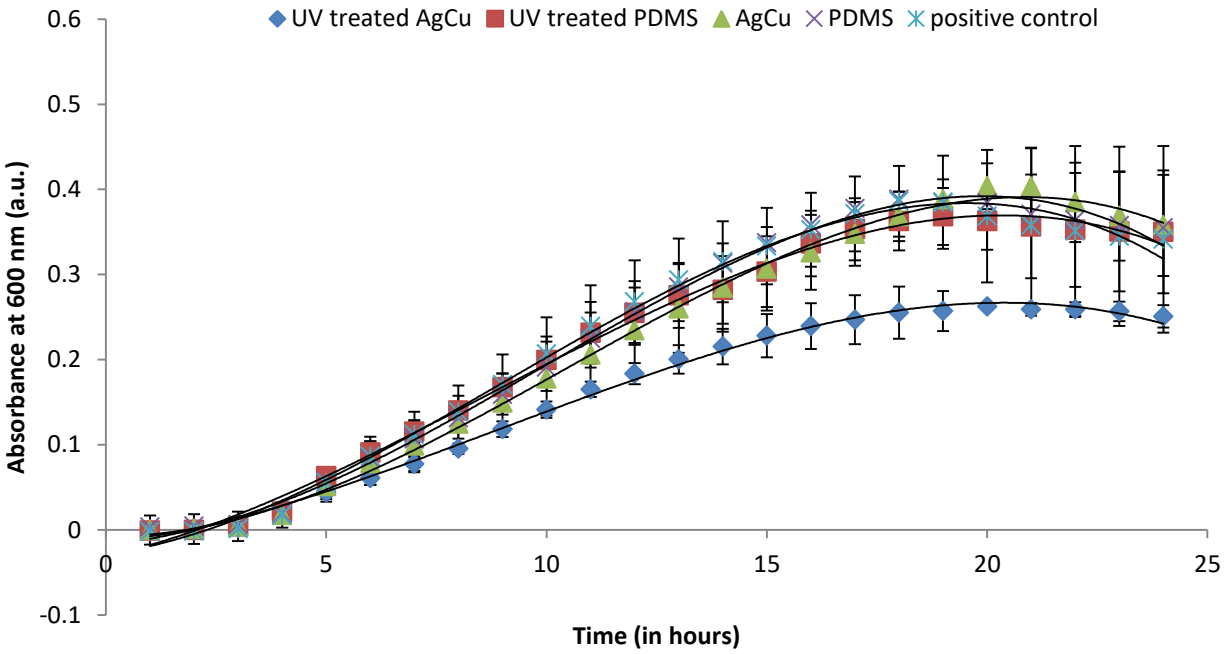

b) *E. coli* 254 nm

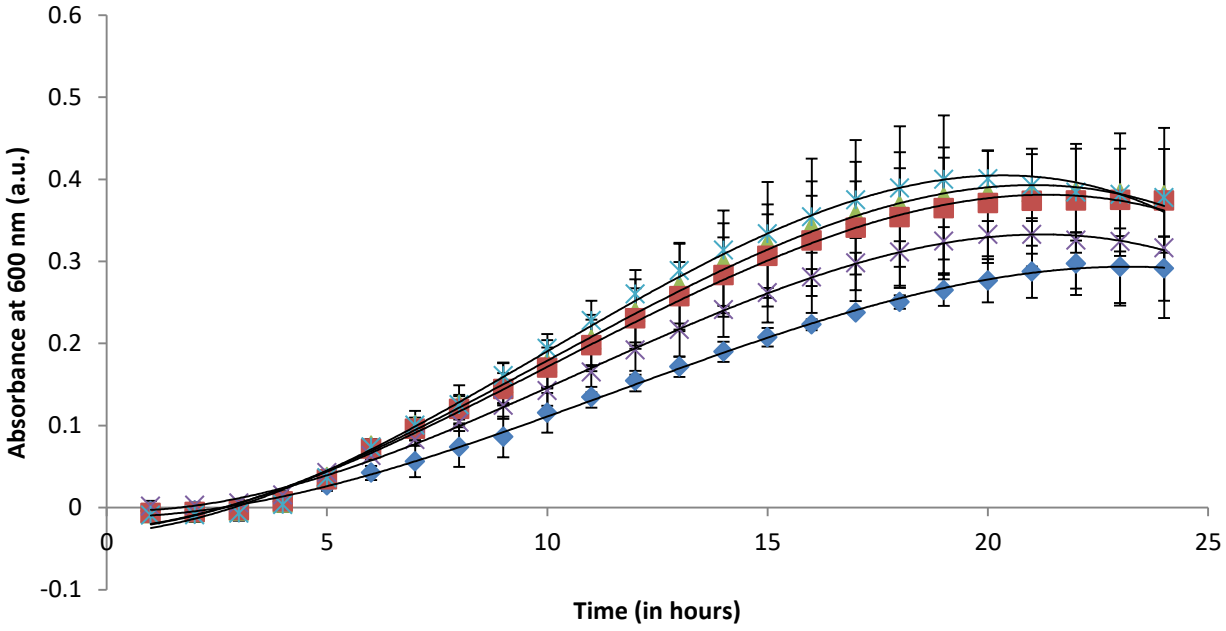

Figure 6.4: 24 hour growth curve of *E. coli* on 0.1 w/v% of AgCu nanoparticle incorporated and control PDMS film, with UV treatment at a) 254 nm and b) 365 nm. Data points are absorbance measurements at 600 nm at hourly intervals. As shown in the legend, 5 samples are included in each experiment, with blue diamond and red square respectively representing UV treated 0.1 w/v% AgCu nanoparticle incorporated PDMS film and PDMS film; green triangle and purple cross respectively representing 0.1 w/v% AgCu nanoparticle incorporated PDMS film and PDMS film without UV treatment; and blue asterisk representing positive control (without any films present). Polynominal regression line, with 3 orders, was used to display the line of best fit and error bars denote standard deviations of results.

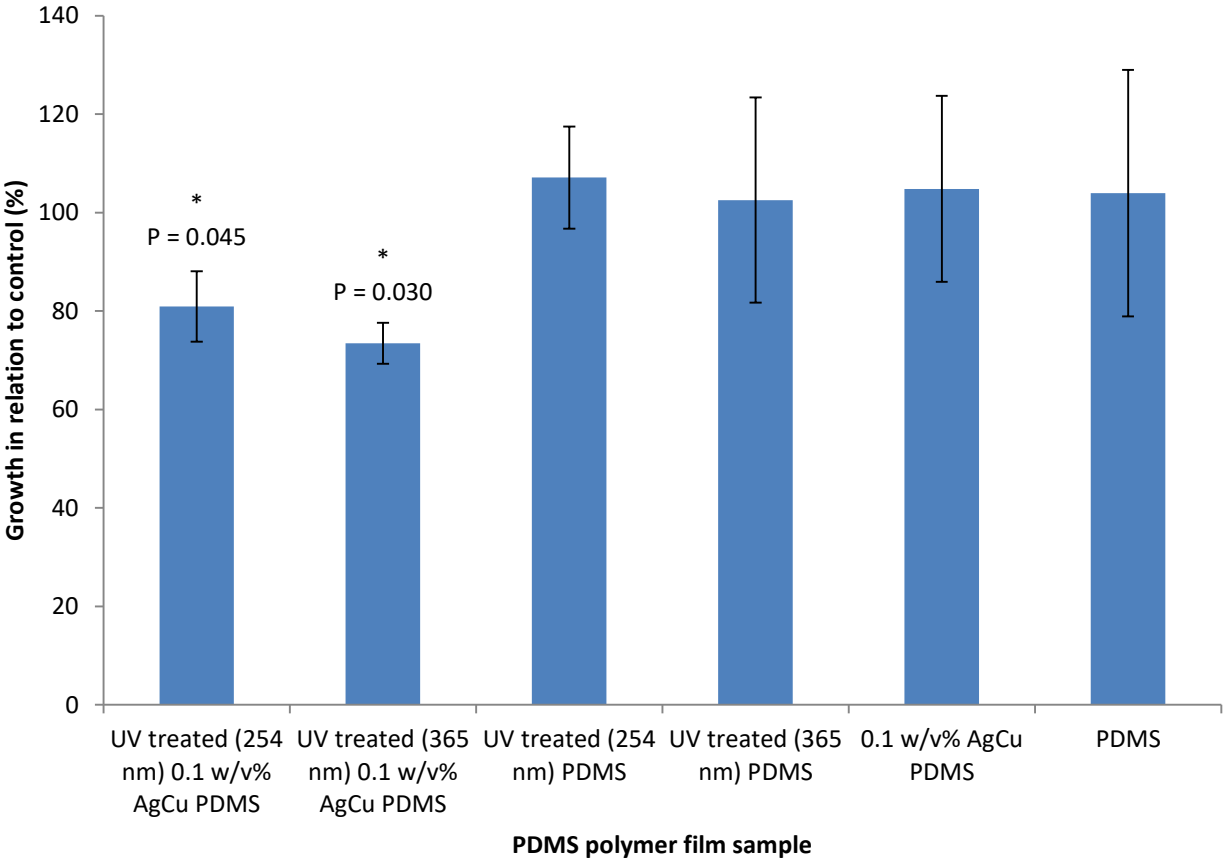

Figure 6.5: Percentage growth of *E. coli* after 24 hour incubation with 0.1 w/v% AgCu nanoparticle incorporated and control PDMS films. Absorbance at 600 nm was measured after 24 hours and percentage of growth was calculated in relation to control sample (growth of *E. coli* without polymer film present). Unpaired student t test was used to statistically analyse the growth of microbes in comparison to the PDMS control and showed that UV treated AgCu incorporated PDMS film results were significant (* $P < 0.05$). Error bars denote standard deviations of results.

a) *S. aureus* 365 nm

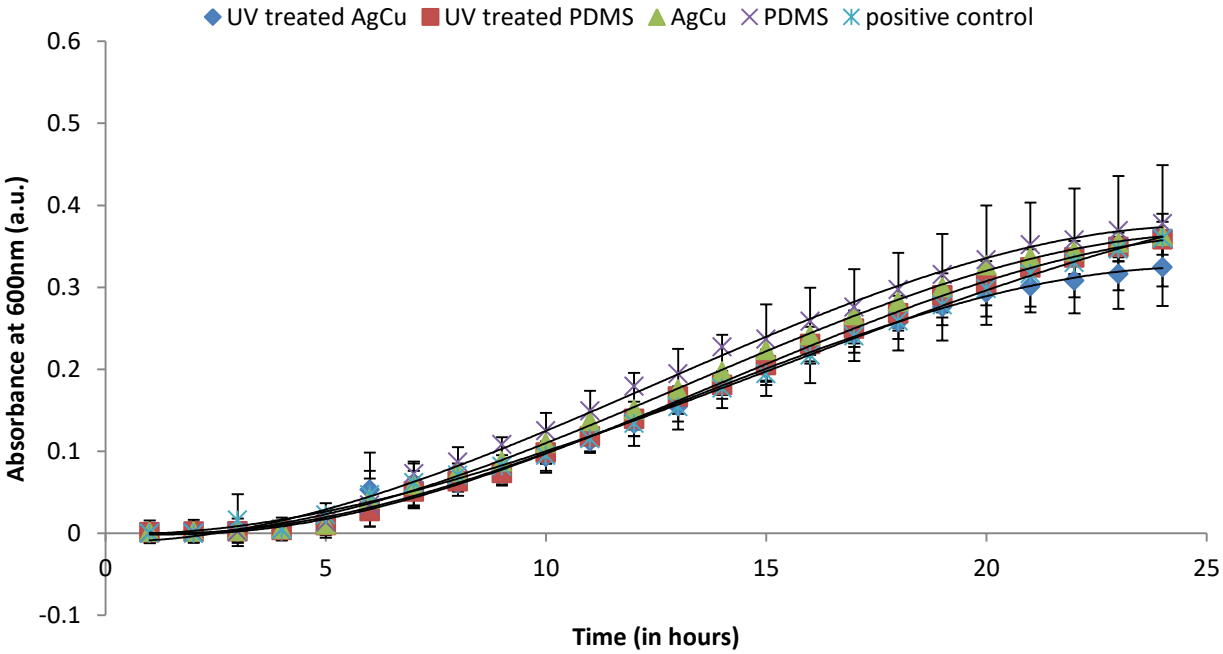

b) *S. aureus* 254 nm

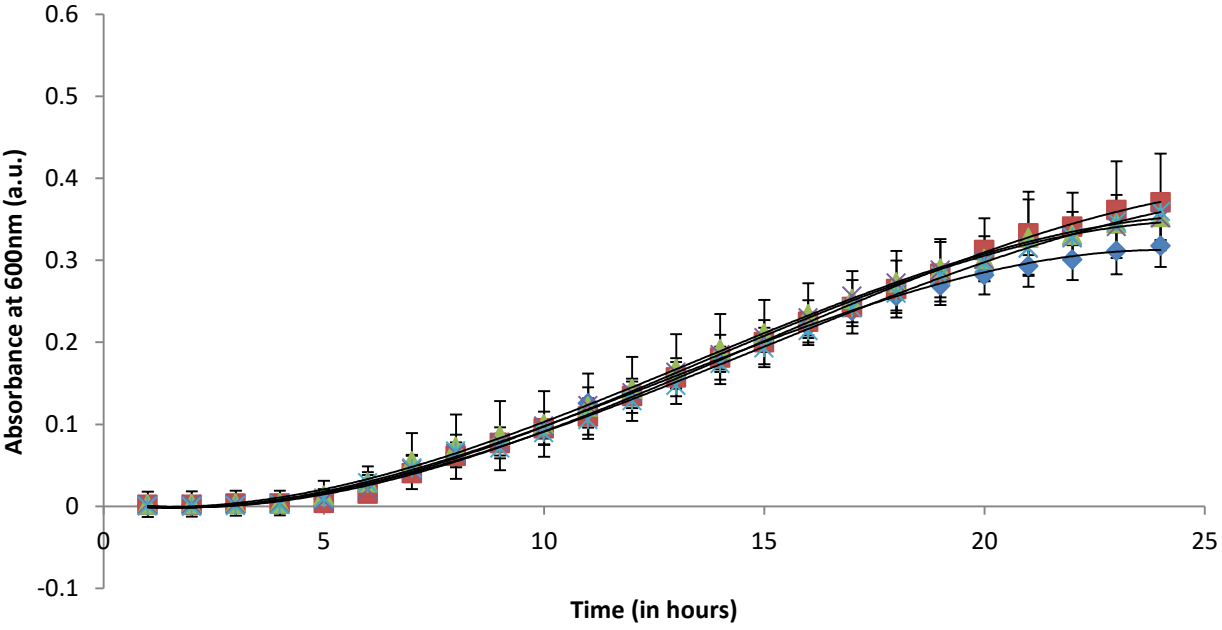

Figure 6.6: 24 hour growth curve of *S. aureus* on 0.1 w/v% AgCu nanoparticle incorporated and control PDMS film, with UV treatment at a) 254 nm and b) 365 nm. Data points are absorbance measurements at 600 nm at hourly intervals. As shown in the legend, 5 samples are included in each experiment, with blue diamond and red square respectively representing UV treated 0.1 w/v% AgCu nanoparticle incorporated PDMS film and PDMS film; green triangle and purple cross respectively representing 0.1 w/v% AgCu nanoparticle incorporated PDMS film and PDMS film without UV treatment; and blue asterisk representing positive control (without any films present). Polynominal regression line, with 3 orders, was used to display the line of best fit and error bars denote standard deviations of results.

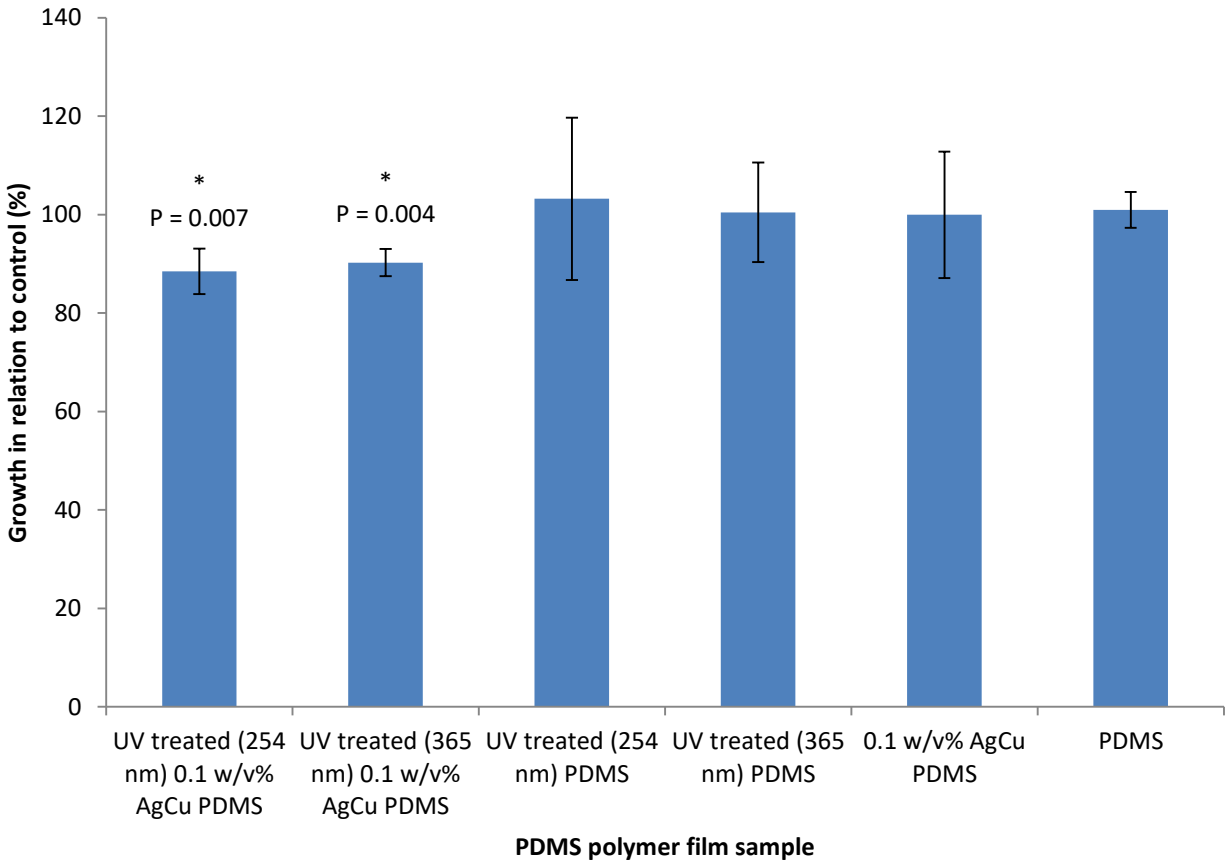

Figure 6.7: Percentage growth of *S. aureus* after 24 hour incubation with 0.1 w/v% AgCu nanoparticle incorporated and control PDMS films. Absorbance at 600 nm was measured after 24 hours and percentage of growth was calculated in relation to control sample (growth of *S. aureus* without polymer film present). Unpaired student t test was used to statistically analyse the growth of microbes in comparison to the PDMS control and showed that UV treated AgCu incorporated PDMS film results were significant (* $P < 0.05$). Error bars denote standard deviations of results.

a) *C. albicans* 365 nm

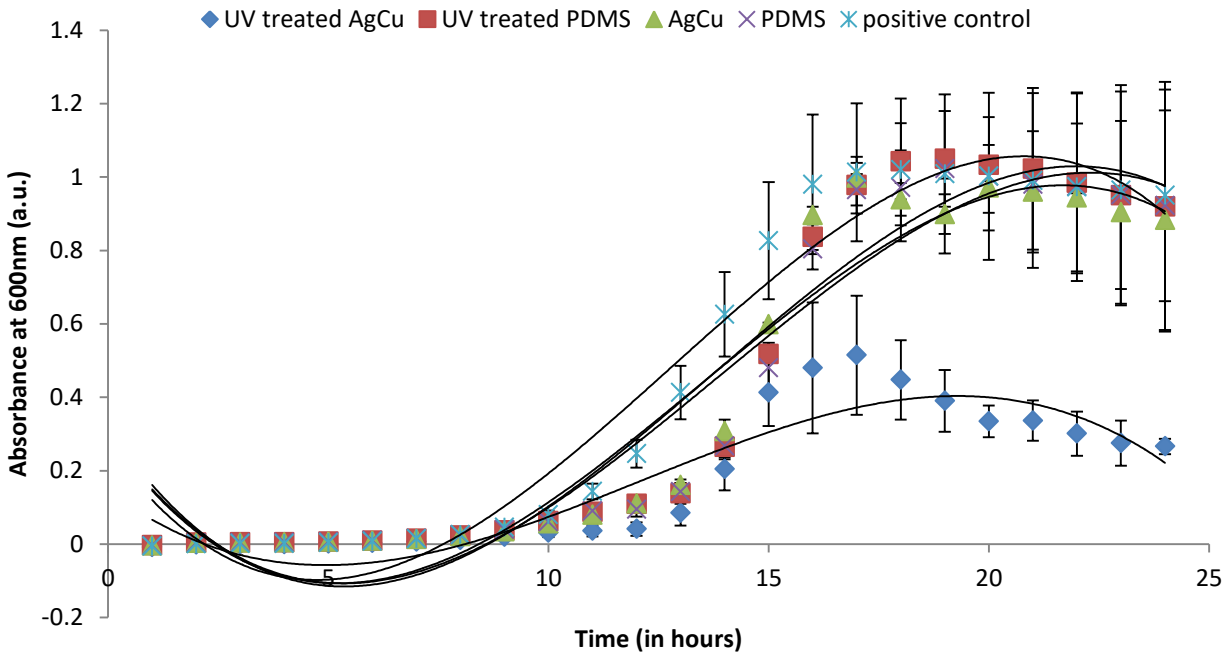

b) *C. albicans* 254 nm

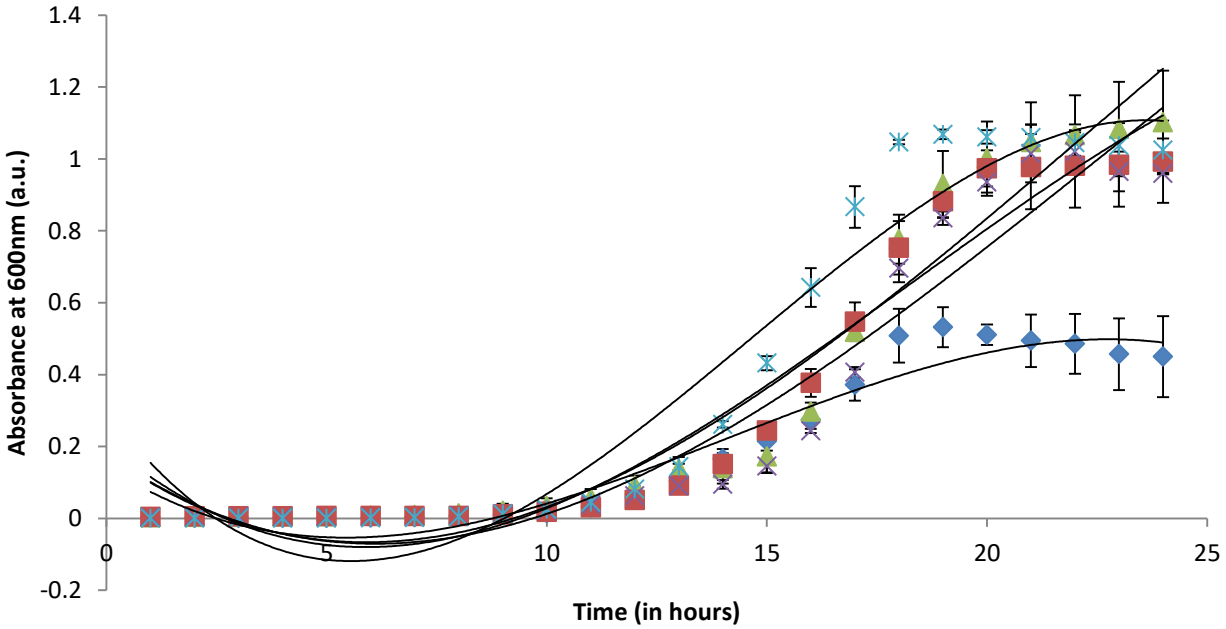

Figure 6.8: 24 hour growth curve of *C. albicans* on 0.1 w/v% AgCu nanoparticle incorporated and control PDMS film, with UV treatment at a) 254 nm and b) 365 nm. Data points are absorbance measurements at 600nm at hourly intervals. As shown in the legend, 5 samples are included in each experiment, with blue diamond and red square respectively representing UV treated 0.1 w/v% AgCu nanoparticle incorporated PDMS film and PDMS film; green triangle and purple cross respectively representing 0.1 w/v% AgCu nanoparticle incorporated PDMS film and PDMS film without UV treatment; and blue asterisk representing positive control (without any films present). Polynominal regression line, with 3 orders, was used to display the line of best fit and error bars denote standard deviations of results.

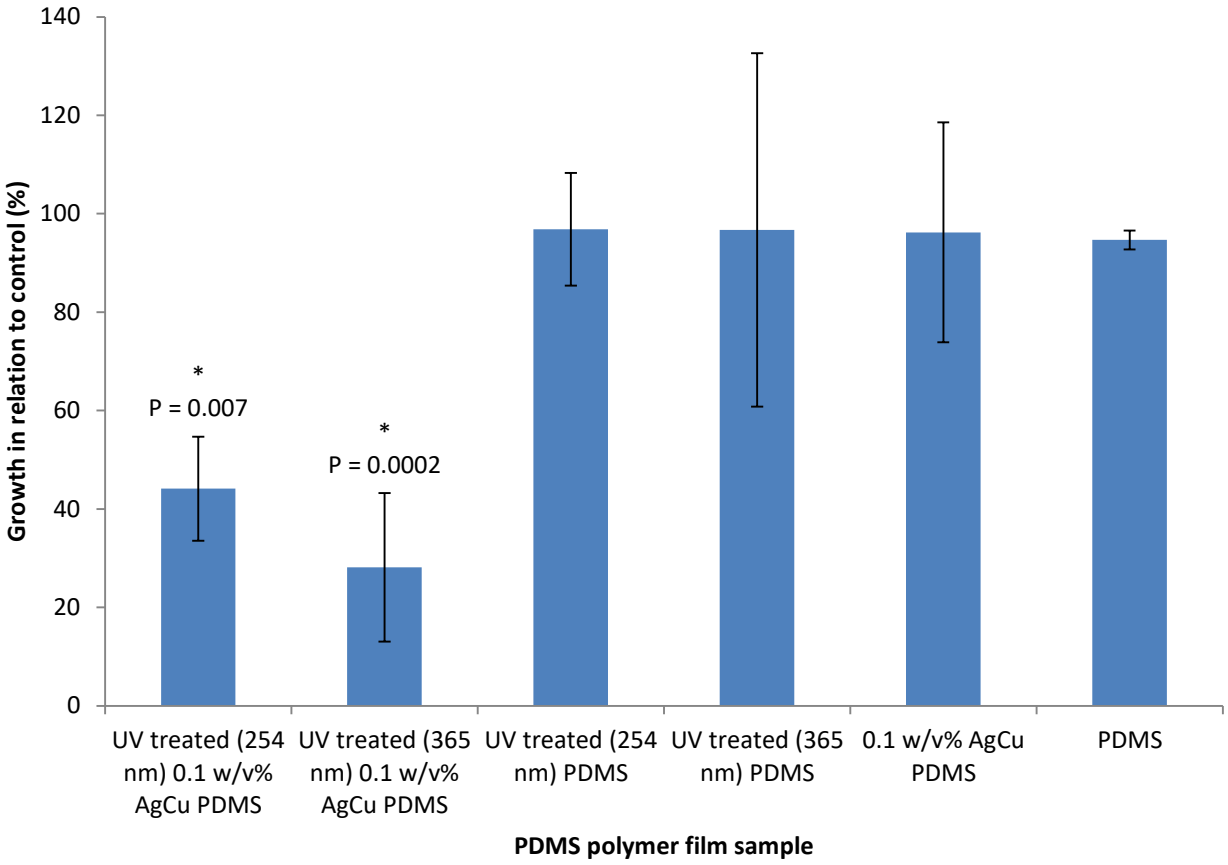

Figure 6.9: Percentage growth of *C. albicans* after 24 hour incubation with 0.1 w/v% AgCu nanoparticle incorporated and control PDMS films. Absorbance at 600 nm was measured after 24 hours and percentage of growth was calculated in relation to control sample (growth of *C. albicans* without polymer film present). Unpaired student t test was used to statistically analyse the growth of microbes in comparison to the PDMS control and showed that UV treated AgCu incorporated PDMS film results were significant (* $P < 0.05$). Error bars denote standard deviations of results.

6.3.2 Characterisation of AgCu nanoparticle PDMS film and UV treatment

The average weight of the films was 0.039 g across all film types. Hence at 0.1 w/v% the AgCu nanoparticle content would be 39.35 µg/ml and 393.5 µg/ml at 1 w/v%.

A tensiometer was used to measure the contact angle of water on the AgCu nanoparticle incorporated PDMS films, control PDMS films and the films after UV treatment to investigate the hydrophobicity properties. As shown in Figure 6.10, the contact angle of water on the films ranged from 108.73° to 104.47°, with an example of each of the contact angle image captured by the tensiometer. Statistical analysis using one way ANOVA showed that the UV treatment and addition of AgCu nanoparticles into the PDMS film only resulted in a very small difference in contact angle as the *p* value was higher than 0.05 (df =8, *p-value* = 0.84).

To investigate the distribution of AgCu nanoparticles in PDMS, SEM images were taken at x1000 magnification. The number of nanoparticles and the diameter (in nm) were calculated using ImageJ, by analysing three spots of area (86 µm x 128 µm) from three separate films. Examples of the SEM images and ImageJ colour threshold adjustment to identify particles can be seen in Figure 6.11. The number of AgCu nanoparticles increased with the UV treatments, with 365 nm wavelength showing the highest number of AgCu nanoparticles in the film, as shown in Figure 6.12. Furthermore, despite a tenfold difference of AgCu nanoparticles between 0.1 w/v% AgCu nanoparticle incorporated films and 1 w/v% AgCu nanoparticle incorporated films, the increase in observed AgCu nanoparticles was between 16.9% - 53.6 %. The diameters of the AgCu nanoparticles were calculated and displayed as a histogram in Figure 6.13 (a and b). Similar diameter size distribution was seen in both concentrations of AgCu nanoparticle incorporated PDMS films and the UV treatment did not affect the AgCu nanoparticle diameter. As shown, the most frequent diameter size was between 101-150 nm, with 1 w/v% AgCu nanoparticle incorporated PDMS films showing the presence of larger sized particles that reached up to 501-550 nm in diameter. However, Figure 6.13 (c) shows that the average diameter (in nm) was similar across all samples.

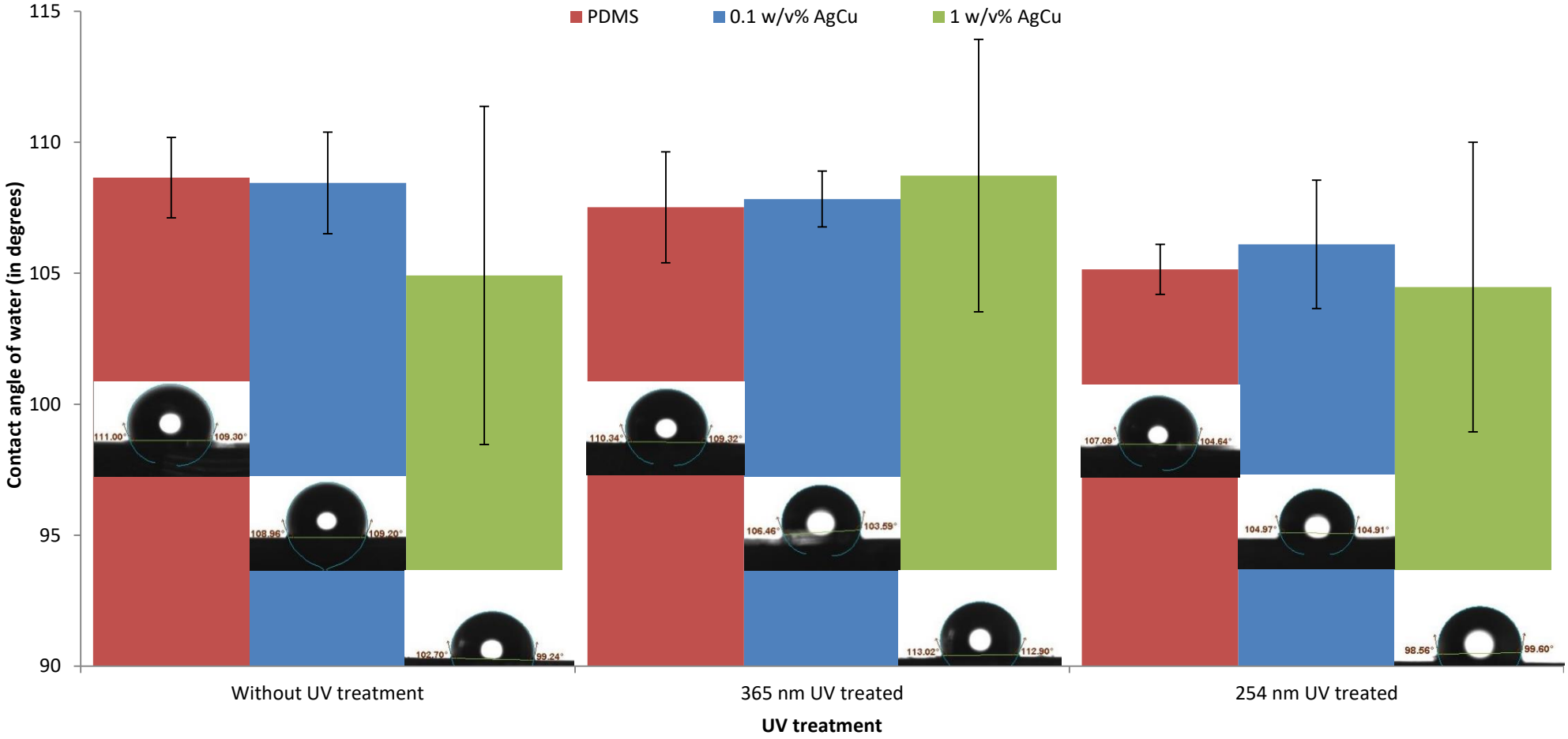

Figure 6.10: Contact angle of PDMS films before and after UV treatment. Data are presented as the average contact angle of three samples. Blue bars represent 0.1 w/v% AgCu nanoparticle incorporated PDMS films; red bars represent PDMS films; and green bars represents 1 w/v% AgCu nanoparticle incorporated PDMS films. Error bars denote the standard deviation. An example of the contact angle is also shown for each sample; the circle is 5 µl drop of pure water pipetted onto the film sample (rectangle on the bottom). Theta Lite Optical Tensiometer (Biolin Scientific, UK) was used to capture and analyse the contact angle as shown on each of the examples.

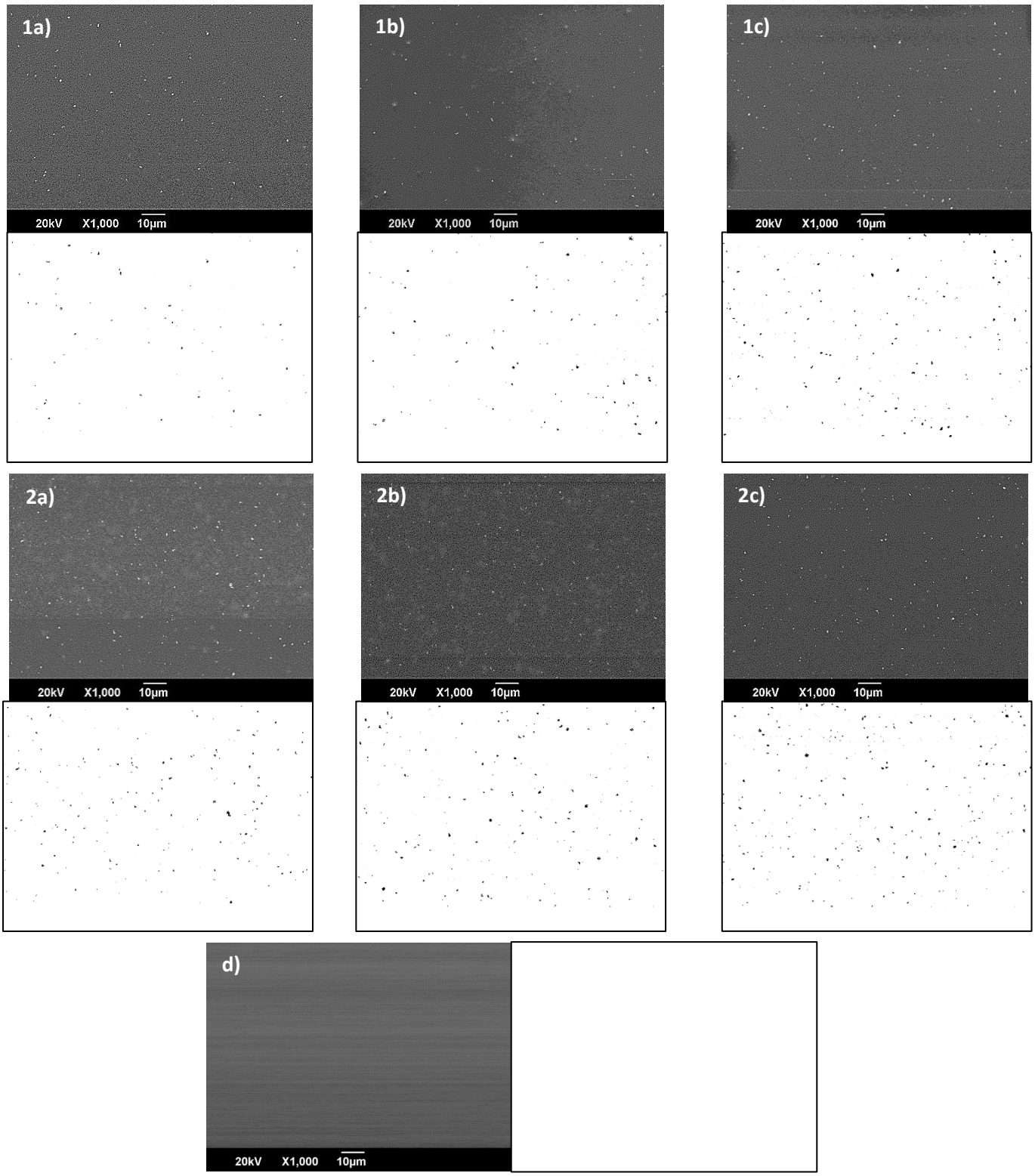

Figure 6.11: SEM observations and ImageJ adjustment of AgCu nanoparticle incorporated PDMS films before and after UV treatment. Examples of the SEM images (above) and corresponding ImageJ threshold adjustment for analysis (below) are shown. (a) Samples without treatment, (b) with 254 nm UV treatment and (c) 365 nm UV treatment are presented respectively for 1) 0.1 w/v% AgCu nanoparticle incorporated PDMS films and 2) 1 w/v% AgCu nanoparticle incorporated PDMS films, and lastly d) control PDMS film with no incorporated AgCu nanoparticles (SEM image on left and ImageJ on right).

a)

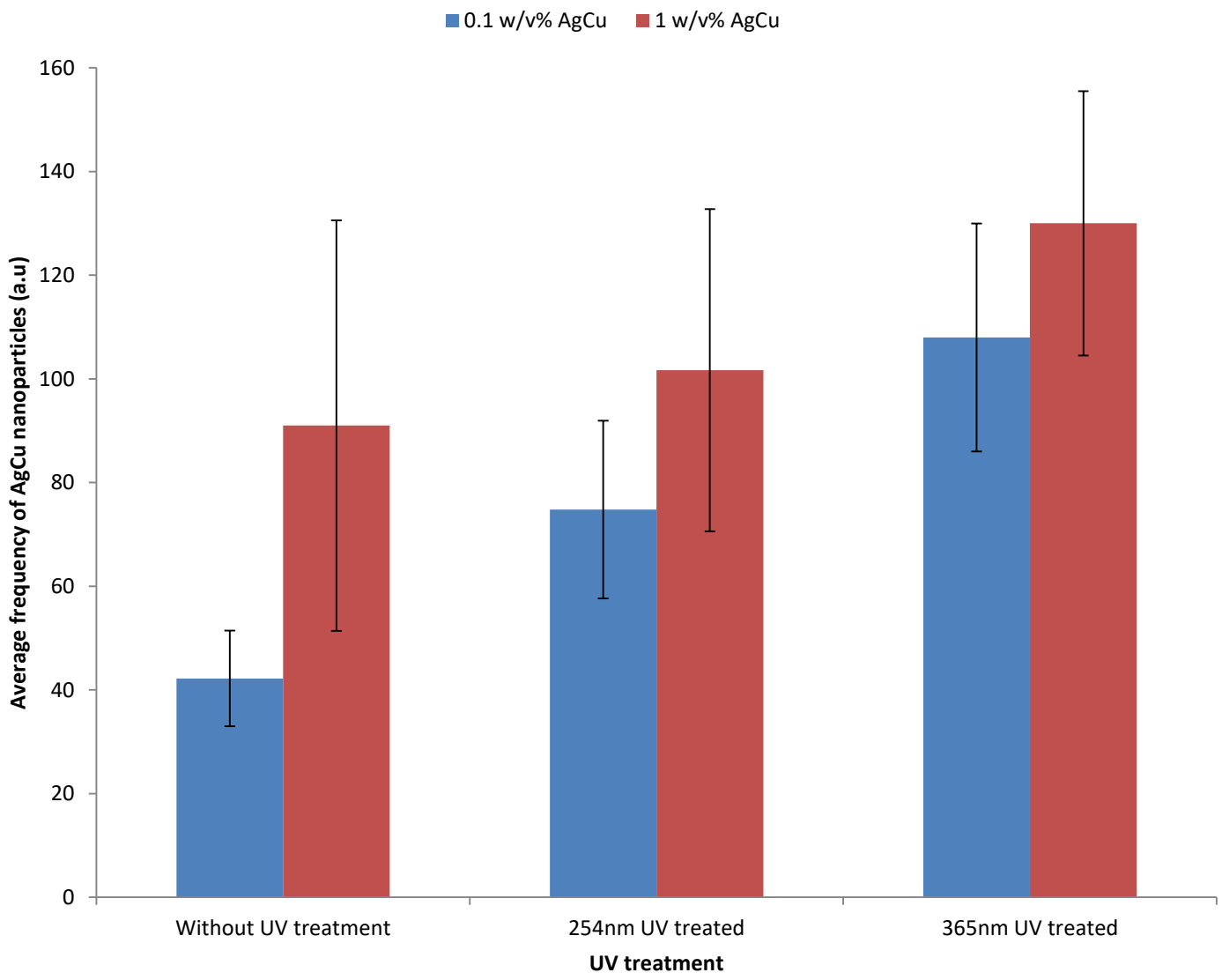

Figure 6.12: Frequency of AgCu nanoparticle observed in AgCu nanoparticle incorporated PDMS films before and after UV treatment. The average number of AgCu nanoparticles in the 0.1 w/v% and 1 w/v% AgCu nanoparticle incorporated PDMS film was observed using SEM and analysed using ImageJ. Results include three areas of three different AgCu nanoparticle incorporated PDMS films with error bars to denote the standard deviations.

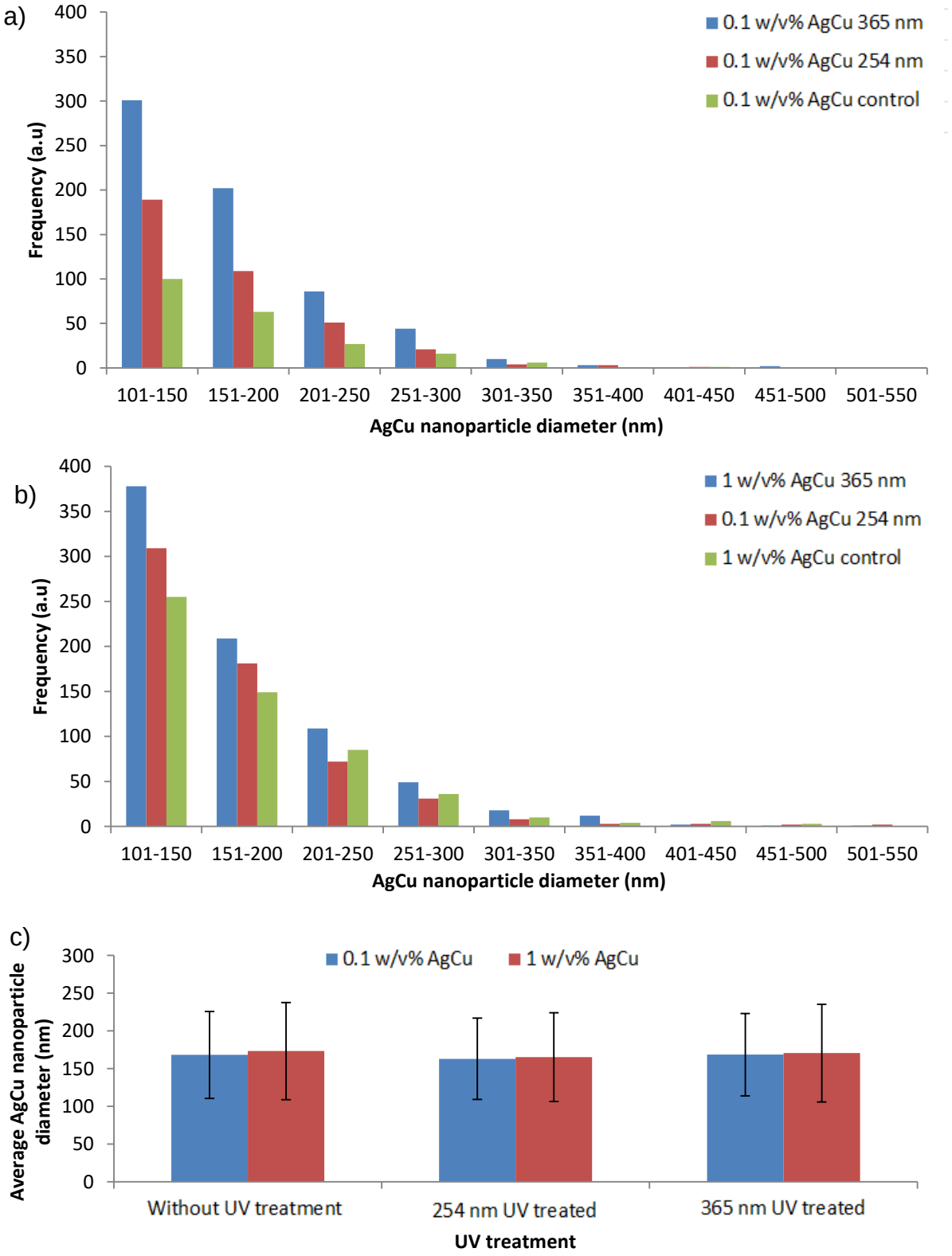

Figure 6.13: AgCu nanoparticle size distribution in AgCu nanoparticle incorporated PDMS films. Both (a) 0.1 w/v% and (b) 1 w/v% AgCu nanoparticle incorporated PDMS films before and after UV treatment were observed using SEM. ImageJ was used to measure the diameter size and frequency of the nanoparticles. c) The average diameter in nm of the films, with error bars to denote the standard deviations. Results include three areas of three different AgCu nanoparticle incorporated PDMS films.

To investigate the release of ions from the AgCu nanoparticle incorporated films, the film samples were immersed in water and the pH was monitored. As shown in Figure 6.14, the pH of the immersed PDMS samples were slightly lower than the samples incorporated with AgCu nanoparticles. Furthermore, at 1 w/v% AgCu nanoparticle concentration, the increase in pH was higher than at a lower concentration of 0.1 w/v% AgCu nanoparticles. The pH in all samples was between pH 6.6 to pH 7, which is within the average pH of water (6.8). Statistical analysis using one way ANOVA found that there was a significant difference as the *p* value was lower than 0.05 (df =8, *p-value* = 0.007).

The UV treatment was investigated for its potential effect in antimicrobial enhancement and heat generation in AgCu nanoparticles. After 15 minutes of UV treatment, the AgCu nanoparticle suspension was tested for the MIC and compared to AgCu nanoparticle suspension without UV treatment. Both wavelengths showed no effect on the antimicrobial activity of AgCu nanoparticle suspension as the MIC value was the same as the untreated AgCu nanoparticles - the MIC was 7.5 μg/ml against *E. coli,* 31.25 μg/ml against *S. aureus* and 62.5 μg/ml against *C. albicans.* Similarly, the temperature of the samples after 15 minutes of UV treatment was tested using an infrared camera. The UV treatment showed no changes in temperature between the UV treated samples and controls of both suspension and PDMS films. In regard to the suspensions, both the water control and AgCu suspension (0.1 w/v% and 1 wt/v%) were at 24.5°C before and after UV treatment. For the PDMS samples, the temperature of the control films and AgCu nanoparticle incorporated films (0.1 w/v% and 1 wt/v%) increased by 2.8°C after UV treatment and then cooled down to the original temperature within 10 minutes. However, no temperature difference was seen between the control PDMS and the AgCu nanoparticle incorporated films.

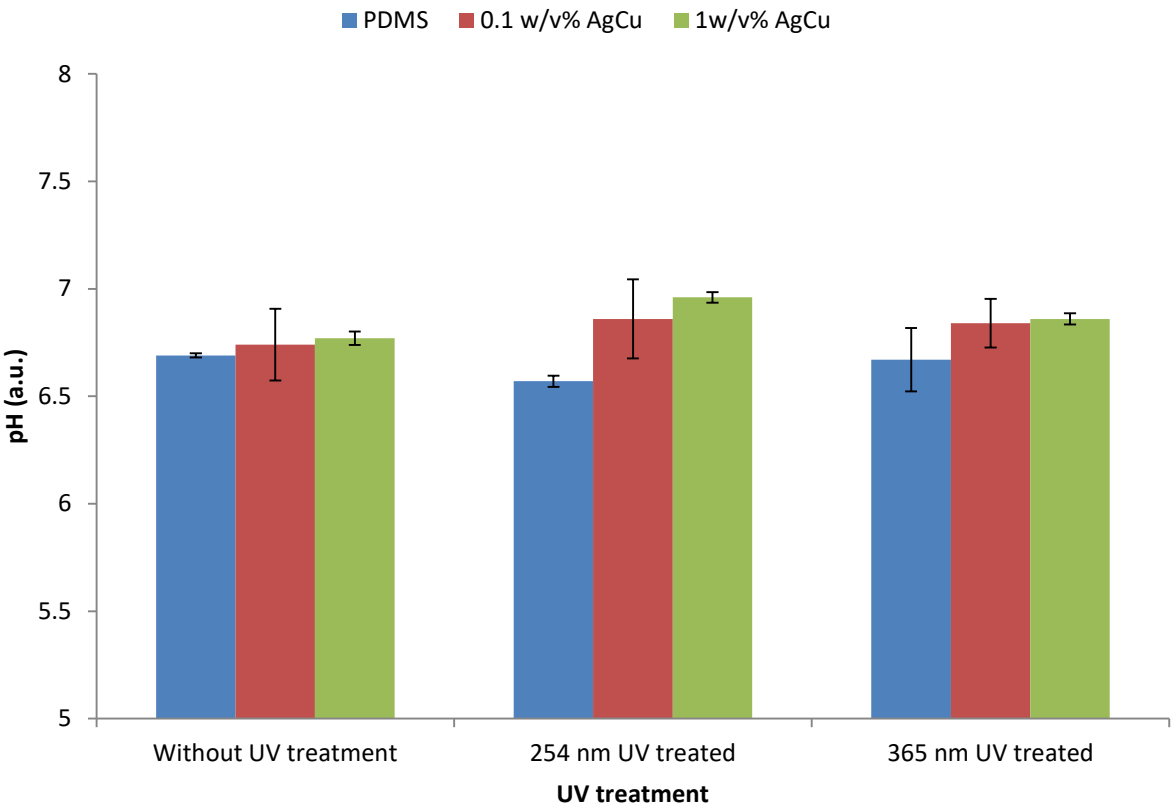

Figure 6.14: pH of PDMS film samples immersed in water for 14 days. The UV treated (at 254 nm and 365 nm wavelength) and untreated PDMS film samples (pure PDMS, 0.1 w/v% AgCu nanoparticle incorporated PDMS and 1 w/v% AgCu nanoparticle incorporated PDMS) were immersed in 5 ml of water for 14 days and the pH was measured. Three repeats were performed for each sample and the average was represented. Error bars denote the standard deviations of the repeats.

6.4 Discussion

The contamination and growth of microbes on biomedical polymers are a health issue to patients in hospitals, especially those that are immunocompromised. Since AgCu nanoparticles have been shown to exhibit a wide range of antimicrobial activity against HAI microbes, they were incorporated into a biocompatible PDMS polymer with aims to produce antimicrobial film. Therefore, the antimicrobial properties of these films were investigated along with physical and chemical properties.

6.4.1 AgCu nanoparticle PDMS film antimicrobial properties

The antimicrobial properties of the AgCu nanoparticle incorporated PDMS films were investigated by monitoring the change in turbidity at 600nm, which directly correlates to the CFU of microbes [238, 239]. However, due to the dark colour of AgCu nanoparticles, the PDMS films with 1 w/v% AgCu nanoparticles was unable to be investigated using this method as a result of absorbance disturbances. The incorporation of AgCu nanoparticles (0.1 w/v%) into PDMS films did not have a significant effect on microbial growth, as the growth curve and growth percentage in relation to the control after 24 hours was similar to that of PDMS control and positive control. The inability for the AgCu nanoparticles to exhibit their antimicrobial activity, as reported for a suspension, may have been due to the PDMS forming a layer covering the nanoparticles which prevented the physical contact between the microbe and nanoparticles and the release of ions.

Although the mechanisms of action of nanoparticles are still not fully elucidated, experiments in Chapter 5 and several reported hypotheses agree that direct contact is required for antimicrobial activity [22]. For example, Raffi *et al.* (2008) reported that Ag nanoparticles adhered to the cell wall surface of *E. coli* bacteria which lead to damage to the membrane morphology, changes in permeability and ultimately cell death [360]. Furthermore, Chapter 5 section 5.3, observed physical interaction between microbes and AgCu nanoparticles, which was suggested to have contributed to the disfiguration of the microbial morphology through membrane damage. It is logical that AgCu nanoparticles require physical contact with microbial cells to exhibit antimicrobial activity and therefore the findings of AgCu nanoparticle incorporated PDMS producing no significant microbial reduction was likely to have been a result of the PDMS layer forming a barrier which prevented physical contact with the microbes.

In order to reduce the problem of the PDMS layer preventing the physical contact between microbial cells and AgCu nanoparticles, the films were exposed to UV treatment at 254 nm and 365 nm wavelength. As found in Chapter 4, AgCu nanoparticles possess unique SPR properties, with a λ_{max} at 410 nm. UV radiation, especially at λ_{max} wavelength, can result in excitation of nanoparticles which leads to heat and radical generation that may degrade the polymer [392, 393]. Additionally, UV irradiation can generate radicals on the surface of silicone, which leads to degradation of the polymer [394]. Subsequently, the UV exposure can decreases the thickness of PDMS [395]. Therefore, the exposure of UV treatment may lead to an increase in exposure of AgCu nanoparticles on the surface of the PDMS film that was previously covered by a layer of PDMS.

Through SEM observations, it was found that the AgCu nanoparticles were evenly distributed in the PDMS films with similar average diameters of the AgCu nanoparticles across all samples, regardless of UV treatment and concentration of AgCu. This suggests that the mechanical stir process and sonication of the AgCu nanoparticles in the curing agent was efficient in dispersing the AgCu nanoparticles, and minimal agglomeration occurred as diameters were similar to those of AgCu suspension in Chapter 4. In contrast, it was found that the UV treatment resulted in an increase of observed AgCu nanoparticles which corresponds to the antimicrobial activity exhibited after UV treatment. As schematically illustrated in Figure 6.15, the UV treatment may have degraded the surface of the PDMS, particularly at the AgCu nanoparticle location, and thus exposed AgCu nanoparticles that were covered by the PDMS layer. Therefore, the exposed AgCu nanoparticles enabled physical contact with microbes which resulted in microbial cell damage and cell death.

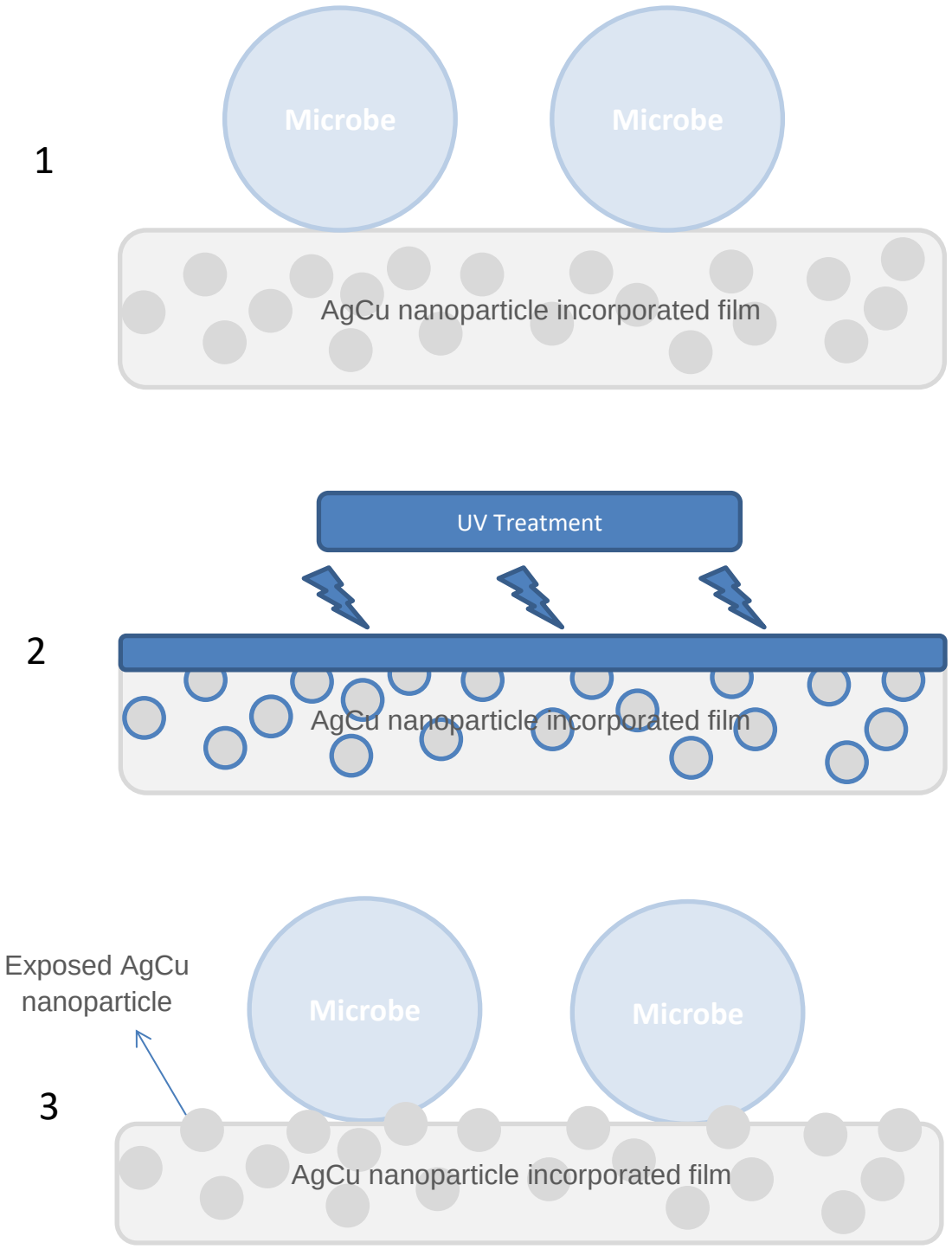

Figure 6.15: Schematic illustration of possible antimicrobial enhancement of AgCu nanoparticle incorporated PDMS film through UV surface treatment. The AgCu nanoparticle incorporated PDMS film is represented by the grey rectangle, with AgCu nanoparticles as darker grey circles inside. As shown in 1) the microbes cannot make physical contact with the AgCu nanoparticles due to the PDMS layer acting as a barrier. 2) The UV treatment affects the surface of the PDMS sample and excites the AgCu nanoparticles. After treatment 3) the AgCu nanoparticles are partly exposed, which enables some physical contact with microbes.

Interestingly, the longer UV wavelength (365 nm) exposed more AgCu nanoparticles in the film (255.9% and 142.9% in 0.1 w/v% and 1 w/v% AgCu nanoparticle incorporated PDMS, respectively, in relation to the corresponding untreated film) than the shorter UV wavelength (254 nm) (177.3% and 111.8%, respectively). However, it has been found that shorter wavelengths (UVB (280 - 340 nm)) caused more degradation in PDMS in comparison to longer wavelengths (UVA (300 – 380 nm)) [396]. The degradation of PDMS is related to the photon energy. Shorter wavelengths have higher photon energy; the higher the photon energy, the more easily chemical bonds can be broken which results in the degradation of the polymer.

In this case, the UV lamp analysis showed that the longer wavelength had a power irradiance of 95 µW, which was higher in comparison to the shorter wavelength with a power irradiance of 80 µW. This will have resulted in more Watts per area, thus increased the energy of the wavelength. Furthermore, as previously mentioned, AgCu had a λ_{max} UV absorbance at 410 nm. The longer tested wavelength was closer to the λ_{max} of AgCu. Whilst 365 nm is the wavelength with the highest emittance, the wavelength spectrum showed that the lamp also produced wavelength between 352 to 387 nm. This may have resulted in higher excitation of the SPR in comparison to the shorter wavelength, which was between 252 to 255 nm [397]. Excitation of the SPR can be dissipated as heat [398]. Therefore, the heat caused by the excitation may have contributed to the degradation of the PDMS via thermal degradation. However, high temperatures are required for PDMS to degrade; it has been found that the degradation of PDMS begins at 250°C [399]. Moreover, the temperature of the AgCu incorporated PDMS films and AgCu nanoparticle suspensions were the same temperatures as their controls after UV treatment. This suggests that the UV irradiation was unlikely to have caused enough heat to degrade the PDMS polymer.

In addition to heat generation, it has been found that Ag nanoparticles can also generate hydroxyl radicals when irradiated with UV light [400]. As a highly reactive molecular species, hydroxyl radicals can react with and degrade PDMS [401]. Although the generation of hydroxyl radicals from UV radiation on Ag nanoparticles has not been fully investigated, it is hypothesised that the generation of hydroxyl

radicals is linked to specific UV wavelengths and may be associated with the SPR [400]. In terms of this study, the 365 nm UV wavelength was closer to the λ_{max} of AgCu than the 254 nm UV wavelength. Therefore, it is hypothesised that during the 365 nm UV treatment the AgCu nanoparticles incorporated in the PDMS polymer generated more hydroxyl radicals, than during 254 nm UV treatment. Thus, with more generated hydroxyl radicals, more of the PDMS surround the nanoparticle would be degraded, which resulted in higher exposure of the AgCu nanoparticles on the surface of the PDMS films.

Reports have shown that the visible light radiation (<450 nm) can enhance the antimicrobial properties of silver modified titania through induced photocatalytic activity [402]. Similarly, da Silva *et al.* (2020) found that treating citrate-coated silver nanoparticles (which had 436 nm λ_{max}) with 448 nm radiation increased the antimicrobial activity by 50%, based on MIC results. The interaction of light radiation excited silver electrons and the heat transfer encouraged the release of ROS [403]. Enhanced generation of ROS can lead to antimicrobial activity as excess ROS can damage DNA, induce oxidative stress and interfere with metabolic pathways [404]. To investigate whether the UV treatment increased the antimicrobial activity of the AgCu nanoparticles, the MIC of UV treated AgCu nanoparticle suspension was tested. However, the results showed that the UV treatment did not increase in antimicrobial activity as the MIC value was the same as non-UV treated suspensions. Furthermore, there was no temperature difference between the AgCu nanoparticle suspension and water control, and between the AgCu nanoparticle incorporated PDMS and control PDMS after 15 minutes of UV treatment. Moreover, as investigated in Chapter 5, an increase in oxidative stress contributed to the mechanisms of action of AgCu nanoparticles towards bacterial cells; however, an increase in oxidative stress was not seen in *C. albicans* cells, thus if the UV irradiation encouraged the release of ROS, it was not the main factor that resulted in increased antimicrobial activity. This suggests that the ability of the UV treatment to enhance antimicrobial activity of the AgCu nanoparticle incorporated films were due to the degradation effect on PDMS which resulted in increased exposure of AgCu nanoparticles.

As analysed using a tensiometer, the films were hydrophobic with high contact angles that ranged between 108.72° to 104.91°. Generally, materials with poor wettability prevent bacterial colonisation as the contact between bacterium and surface are prevented [405, 406]. However, in this case, the contact between microbes and the AgCu nanoparticles in the PDMS film were also prevented, thus the antimicrobial mechanism of action of physical contact was limited and sometimes could not be exhibited. Although UV exposure can cause PDMS to undergo chain scission and degrade the main backbone and side groups of the polymer, it has been reported that the wetting properties of PDMS that was UV treated for less than an hour, were very similar to untreated PDMS [407]. However, when treated for longer, UV radiation can result in hydrophilisation of the PDMS surface. Tsuzuki *et al.* (2022) found that three hours of UV treatment at 254 nm and 185 nm resulted in the formation of a stiff thin silica layer on top of the PDMS. This new layer was hydrophilic; immediately after UV treatment the contact angle was 0° and then increased to approximately 40° five hours after the treatment [408]. In this study, the UV treatment was for 15 minutes which did not result in much change in the hydrophilicity of the PDMS. Although the contact angle increased by up to 3.81°, the statistical analysis showed that the change was not significant. Thus, the incorporation of AgCu nanoparticles and UV treatment did not affect the hydrophilicity of the PDMS films and the change in hydrophilicity did not contribute towards the increase antimicrobial activity after UV treatment. However, the hydrophobicity of the films may have contributed to the weak antimicrobial properties of AgCu nanoparticle incorporated PDMS films due to the lack of physical contact between the film surface and the microbes in broth.

Although there was a significant difference (*P*-Value = 0.007 and 0.004 for 254 nm and 365 nm UV treatment, respectively) in the reduction of *S. aureus* growth, the reduction was the least within the tested microbes, despite having a lower MIC value than *C. albicans.* A possible reason for this is the difference in cell wall composition and structure between the microbes. Generally, fungi and Gram-negative bacteria have thinner cell walls which range from 20-50 nm and 1.5-10 nm thickness, respectively. On the other hand, Gram-positive bacteria have thicker cell walls that range from 20-80 nm [409, 410]. It has been found that the thicker peptidoglycan cell wall of Gram-positive *S. aureus* provides more protection from Ag nanoparticles and

Ag ions in contrast to thinner peptidoglycan cell wall of Gram-negative *E. coli* [139, 339, 366]. Therefore, AgCu nanoparticles had a lower MIC value towards *E. coli* than *S. aureus,* as investigated in Chapter 3 and the UV treated AgCu nanoparticle incorporated PDMS films were more effective towards *E. coli*. Since the AgCu nanoparticles are stationary in the PDMS rather than a free suspension, the exposed part of the AgCu nanoparticle may not have been enough to penetrate through the full thickness of the cell wall, thus unable to produce antimicrobial activity against *S. aureus*, as illustrated in Figure 6.16.

In comparison to the kinetic growth curve in Chapter 3, it was found that higher concentrations of AgCu nanoparticles were required to inhibit the growth of *S. aureus* than *E. coli* and *C. albicans*, which correlates with the antimicrobial trend of the AgCu nanoparticle incorporated films. The kinetic growth behaviour of *E. coli* and *C. albicans* showed that when *E. coli* and *C. albicans* was incubated with AgCu nanoparticles at concentrations of 7.8 μg and 15.6 μg, respectively, or higher, cell inhibition occurred as there was no change in cell turbidity as detected by absorbance. In contrast, for *S. aureus,* concentrations of 31.3 μg or higher was required for cell inhibition. Although each film at 0.1 w/v% AgCu has an average of 39.35 μg of AgCu nanoparticles, as calculated by the weight, the AgCu nanoparticles were imbedded within the polymer. Therefore, only a limited number of AgCu nanoparticles within the 39.35 μg were able to contact the microbes unlike the free suspension. As a result, the exposed AgCu nanoparticles in the film were able to inhibit a percentage of microbes. For example, in Chapter 3, the kinetic growth curve showed that AgCu nanoparticle suspensions at 3.9 μg/ml concentration were able to inhibit 51.3% of *E. coli* growth and 62.7% of *C. albicans* growth; however, 0% of *S. aureus* was inhibited. This suggests that higher concentrations of AgCu nanoparticles are required for the AgCu nanoparticle incorporated PDMS film to produce more effective antimicrobial activity.

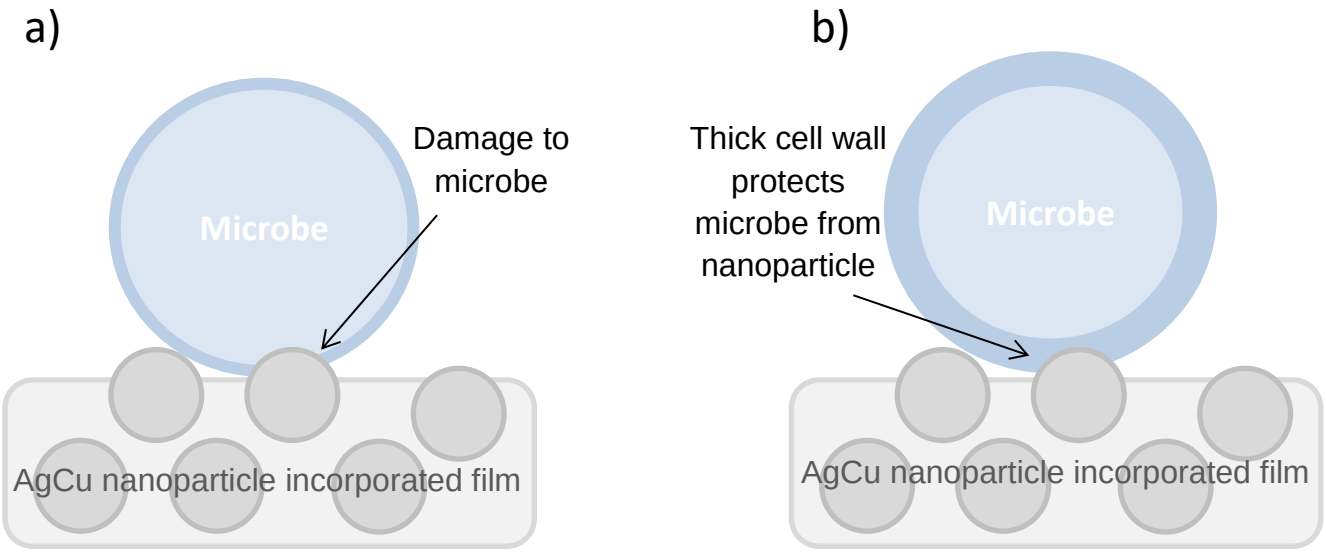

Figure 6.16: Schematic illustration of how cell wall thickness can prevent antimicrobial activity of AgCu incorporated PDMS films. The UV treated AgCu incorporated PDMS films were found to exhibit antimicrobial activity towards *E. coli* and *C. albicans*, however, no effect towards *S. aureus*. It is possible that the cell thickness plays a role in this. As shown in a) the exposed part of the AgCu nanoparticle was able to penetrate through the cell wall (as represented by the darker coloured ring around the microbe). However, with microbes that have a thicker cell wall, b), the exposed part of the AgCu nanoparticle was able to come in contact but not able to fully penetrate through the whole thickness of the cell wall, thus the remaining cell wall can maintain the integrity of the cell.

Additionally, the AgCu nanoparticles are attached to the PDMS film and therefore they are stationary, unlike the initial antimicrobial experiments where the AgCu nanoparticles were free to move in broth. In Chapter 5 section 5.3.2, TEM images showed possible internalisation of AgCu nanoparticles in *S. aureus* cells which was not seen in *E. coli* and *C. albicans* cells. It may be possible that the AgCu nanoparticle mechanism of action towards *S. aureus* requires free AgCu nanoparticles to fully damage the cell wall and internalise the cell. Therefore, partly exposed AgCu nanoparticles that are stationary within the incorporated PDMS films had less antimicrobial effect towards *S. aureus* as they could not be internalised by the *S. aureus* cells.

Despite showing slight antimicrobial activity in broth, when using the disk diffusion method, no samples showed antimicrobial activity as there were no zones of inhibition. As investigated in Chapter 3, testing antimicrobial activity of nanoparticles on agar has limitations due to limited physical contact between the nanoparticles and microbes. Nevertheless, AgCu nanoparticle suspension showed antimicrobial activity towards all tested microbes which was suggested to have been caused by the release of AgCu ions that were able to travel through the agar matrix. Although the mechanism of action of AgCu ions were not separately tested in this thesis, metallic ions are found to be toxic to microbial cells [139]. However, the cross linking of PDMS has be found to supress ion migration [411]. Thus, the AgCu nanoparticles within the PDMS were unable to release ions to cause antimicrobial effect and hence zones of inhibition were not produced when tested with the disk diffusion method.

The PDMS films were submerged in water and investigated for change in pH, which can be used to identify the release of ions through the reduction of hydrogen ions as detected by an increase in pH. After 14 days of submersion, the pH of the water in AgCu nanoparticle incorporated samples was higher than the PDMS control, with one way ANOVA showing a statistical significance. The increase in pH could have been the result of released ions from the AgCu nanoparticle incorporated samples. Furthermore, the UV treatment resulted in a higher increase in pH. This suggests that the UV treatment was able to result in PDMS degradation to expose the covered AgCu nanoparticles, thus the AgCu ions were released. However, the AgCu incorporated PDMS films, including UV treated samples, did not exhibit antimicrobial activity through the disk diffusion method, and therefore the release of ions from the

AgCu nanoparticle incorporated PDMS films may have been too low in concentration to exhibit antimicrobial activity and produce zones of inhibition.

Further investigations can be conducted to improve the antimicrobial activity of AgCu nanoparticle incorporated films. Longer periods of UV treatment may decrease the PDMS layer further, thus exposing more AgCu nanoparticles, and increasing the hydrophilicity leading to increased contact between exposed nanoparticles and microbes. Alternative surface treatments could also be considered including plasma treatment. Furthermore, the concentration of AgCu nanoparticles can be increased, which would also lead to increased chances of interaction between nanoparticles and microbes. For example, antimicrobial PDMS has been produced using a similar method by incorporating TiO_2 nanoparticles. At 13 wt% TiO_2 nanoparticles, the films were able to reduce *E. coli* and *B. cereus* by 99.97% and 99.99%, respectively; at lower concentration (7 wt% TiO_2 nanoparticles), the reduction was less, at 20% and 25%, respectively [412]. In comparison to the PDMS films made in this thesis, the AgCu nanoparticle concentration was much lower at 0.1 wt/v% and 1 wt/v%. Although higher concentrations were not tested, it is possible that the antimicrobial activity will increase with the concentration. However, the increase of nanoparticles causes concerns of toxicity. In excess, copper can induce cellular toxicity leading to hepatic disorder and neurodegenerative changes [413]. Similarly, the excess exposure of silver can lead to the cumulative toxicity with accumulation in organs and rare cases of argyria [414, 415]. Prior to the use as biomedical applications, the AgCu nanoparticle incorporated PDMS films will need to be tested for cytotoxicity and biocompatibility.

6.4.2 Summary

To summarise, AgCu nanoparticles were incorporated into PDMS films through the dispersion of nanoparticles in the curing agent prior mixing with silicone base and curing at 65^{o}C. When the antimicrobial activity was tested through the change in microbial turbidity, it was found that the AgCu incorporated PDMS films did not exhibit antimicrobial activity. On the other hand, after the films were irradiated with UV at 254 nm and 365 nm wavelength, they were able to significantly reduce the growth of *E. coli, S. aureus* and *C. albicans* ($P < 0.05$). The films were characterised to understand the lack of antimicrobial activity. Through SEM observation, it was found that the UV treatment resulted in an increase of observed AgCu nanoparticles

on the surface of the films which might have been responsible for the increase in antimicrobial activity. Furthermore, all of the film samples were hydrophobic, which may have limited the contact between the AgCu nanoparticles and the microbes in broth. Lastly, the disk diffusion agar method found the films produced no zones of inhibition which was likely to have been a result of the crosslinking within PDMS preventing ion migration, although UV treatment showed a slight increase in pH which suggested the release of AgCu ions. Further studies are required to investigate the enhancement of antimicrobial activity in AgCu nanoparticle incorporated PDMS films included extended UV exposure, alternative surface treatment and increase of AgCu concentration. In addition, toxicity tests are required to research the suitability of these PDMS films for biomedical applications.

Chapter 7 Engineering antimicrobial film: Fabrication of AgCu nanoparticles into PCL/PEO polymer

7.1 Introduction

Infections can develop in surgical incisions and wounds, which can increase hospital stay by 14 days, delay the healing process and in some cases cause death [416]. In 2017/2018, the UK's National Health Service treated an estimated 3.8 million patients with a wound. It was found that only 59% of chronic wounds were healed and the percentage dropped to 45% in the presence of an infection [417]. General hygiene, sterile operation and efficient wound treatment can prevent up to 60% of surgical site infections and patients with infections can be treated with prescribed antibiotics [416]. However, it has been found that 70% of wound infection bacteria had resistance against at least one commonly used antibiotic, thus resulting in an imperative need for alternative treatments [418].

Wounds are physically managed through dressing products, which include gauze, plasters and bandages. These are commonly made of natural fibres such as cotton and cellulose, or synthetic materials such as polyamide and polyesters [419]. Conventionally, wound dressings provide a shield to protect the wound from external contaminations [418]. However, infections can occur through the improper use and infrequent changes of bandage [420]. In this respect, the development of wound dressings functionalised with antimicrobial agents has been researched. The addition of antibiotics such as amoxicillin and tetracycline into biocompatible materials has shown to provide effective antimicrobial activity in vitro and in vivo [421, 422]. Although these new wound dressings might prevent infections, the increased use of antibiotics may enhance the development of antibiotic resistance [17, 232]. As a result, the incorporation of alternative antimicrobial agents, such as nanoparticles and natural agents, into wound dressings have sparked interested in researchers and wound dressing companies.

Since 1920s, the FDA has approved colloidal silver for wound treatment. In the 1960s, topical agents containing silver nitrate and silver sulfadiazine were used to treat burn wounds. However, these treatments were labour intensive as they required frequent reapplication and dressing changes. New formulations of silver incorporated into wound dressing have shown improvement with sustained

antibacterial activity [423, 424]. Currently, there are few medically approved and commercialised wound dressings that are manufactured with silver, for example Acticoat™ [418]. It was found that Acticoat™ had excellent antimicrobial properties and were able to protect the wound with a physical barrier, however, their antibacterial properties were less effective in comparison to topical antimicrobial agents containing antibiotics [425]. Hence further research into nanoparticle incorporated wound dressing is required.

As shown in Chapter 3, AgCu nanoparticles exhibited broad antimicrobial properties and were the most effective nanoparticle out of the tested samples. Furthermore, copper has shown ability to enhance wound healing by promoting angiogenesis [426]. Research has shown that the incorporation of antimicrobial agents into biodegradable polyethylene oxide (PEO) and polycaprolactone (PCL) have shown potential as wound dressing. The incorporation of natural antimicrobial agents, such as chitosan and olive oils, into PCL/PEO have shown antimicrobial activity against *E. coli* and *S. aureus* [427]. Additionally, the incorporation of silver nanoparticles with aloe vera into PCL/PEO was also effective against *E. coli* [428]. Therefore, the incorporation of AgCu nanoparticles into PCL/PEO to produce antimicrobial material was investigated.

Outline of the research work:

This chapter investigates the incorporation of AgCu nanoparticles into PCL/PEO polymer. The produced sheet was tested against a Gram-negative bacteria (*E. coli*), Gram-positive bacteria (*S. aureus*) and a fungus (*C. albicans*), which are reported to commonly cause nosocomial infections and wound infections. The physical properties of the nanoparticle incorporated PCL/PEO sheet was characterised to help understand the antimicrobial activity.

7.2 Materials and methods

The preparation and information of microbes (*E.coli, S. aureus* and *C. albicans*) can be found in Chapter 2, section 2.2 and Chapter 3, section 3.2, respectively. For antimicrobial experiments, microbes were grown 24 hours prior to experiment in broth (nutrient broth for bacteria and YPD broth for fungi) in a shaking incubator set at 37°C. Microbes were then diluted to ~3x10^7 CFU/ml using a spectrometer at 600 nm and then further diluted to desired concentration.

7.2.1 Engineering of AgCu nanoparticle incorporated PCL/PEO polymers

AgCu nanoparticle incorporated PCL/PEO polymers were kindly made by Hessah Alotaibi from the department of mechanical engineering, University College London. PCL, PEO and dichloromethane (DCM; stabilised with 0.002% 2-methyl-2-butene) was purchased from Sigma-Aldrich, UK.

PCL and PEO (1:1 ratio) were weighed using scales and dissolved in 5 ml of DCM at a concentration of 5 w/v% for each. Then, AgCu nanoparticles were weighed using scales and added to the solution at different concentrations (0.1, 1, 5 and 10 w/w%). Pure PCL/PEO control samples were made following the same protocol but without the addition of AgCu nanoparticles. The solution was mixed in a tightly closed beaker at 250 rpm for 30 minutes at room temperature. When a homogenous solution was obtained, the solution was cast into a 4 cm glass petri dish and left overnight to dry. The polymer samples were peeled from the dish and stored at room temperature until required.

Examples of the AgCu nanoparticle incorporated PCL/PEO polymers are shown in Figure 7.1. The polymers were measured and cut into desired shape and size by using clean scissors or as stated; examples of the cut polymers are shown in the Appendix. The samples were then handled with forceps when used in the experiments.

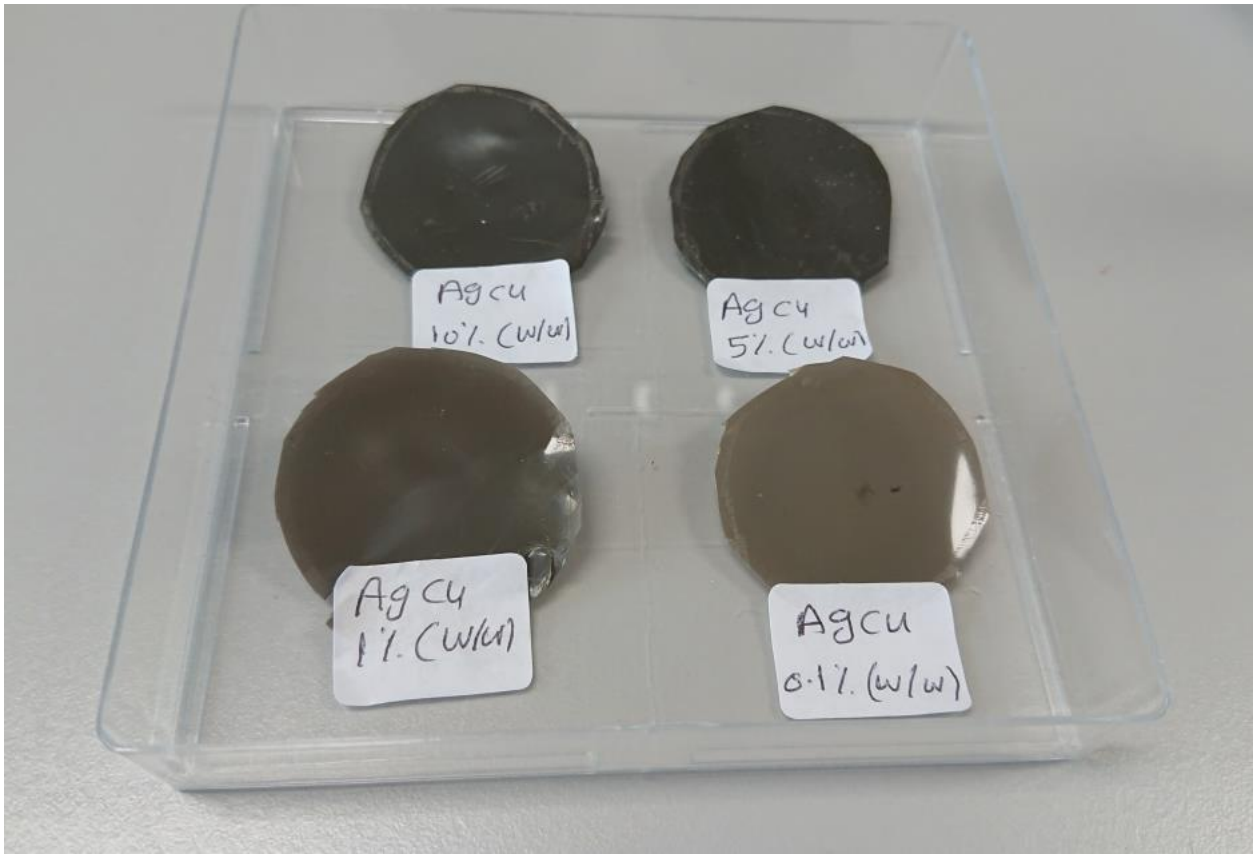

Figure 7.1: Physical observation of AgCu nanoparticle incorporated PCL/PEO polymers. As labelled, 4 concentrations of AgCu nanoparticle incorporated PCL/PEO polymers were produced. Films were stored in square petri dish at room temperature until required.

7.2.2 Antimicrobial activity of PCL/PEO polymers

Following the disk diffusion method in Chapter 6, section 6.2.3, the antimicrobial activity of the PCL/PEO samples was investigated. In brief, microbes at ~1-3 x10^7 CFU/ml were inoculated onto MH agar plate. Using a sterile corker, 4 mm circle templates were pressed into the sample and then the circles were cut out using clean scissors. The circular disks were then placed onto the inoculated agar plates and incubated at 37°C for 24 hours in triplicates. Pure PCL/PEO was used as a control. The antimicrobial activity was observed through zones of inhibition and the diameters of the zones were measured in cm.

7.2.3 Characterisation of AgCu incorporated PCL/PEO polymers

The same methods as Chapter 6, section 6.2.4 were used to characterise the PCL/PEO polymers. In brief, the physical observation of PCL/PEO samples and controls were observed using the SEM and ImageJ was used to adjust the colour threshold on the obtained SEM image and then to calculate the presence of pores. The hydrophobicity of PCL/PEO polymers and control were measured using Theta Lite Optical Tensiometer. The release of ions from the PCL/PEO polymers was investigated through the change in pH. The PCL/PEO samples were cut into 1 cm^2 squares, weighed and immersed in 5 ml of deionised water in a small glass tube. The pH of the solution was measured 14 days after initial immersion.

Similarly, the release of AgCu nanoparticles was investigated through UV-Vis spectrometry. The PCL/PEO samples were cut roughly into 1 cm^2 squares, weighed and immersed in 5 ml of deionised water in a small glass tube. The tube was inverted three times and then 3 ml of the supernatant was measured following the same protocol as Chapter 4, section 4.2.3. After measurement, the sample was carefully poured back into the glass tube with the immersed polymer. Supernatant was taken hourly for four hours and then at 24 hours, with glass tube inverted three times prior to the extraction of the supernatant. Sterile distilled water was used as a blank control. Three repeats were performed for each sample type and cuvette was cleaned with acetone and dried with compressed air between each sample. Standard curve of AgCu nanoparticle suspension from 50 to 10 μg/ml was measured using the same protocol.

7.3 Results

7.3.1 Antimicrobial activity

The contact between the PCL/PEO polymers and the inoculated agar resulted in the polymer edges curling away from the agar and started to produce a little bit of liquid. After 5 minutes of contact with the inoculated agar, the polymers became flat against the inoculated agar and started to swell. This resulted in an increase of 2 mm in diameter after 20 minutes. The production of liquid can be seen surrounding the PCL/PEO polymer sample; the liquid remained around the polymer and did not seem to increase after 20 minutes. Furthermore, the colour of the polymer changed from a dark grey to a lighter grey over time.

The disk diffusion method was used to investigate antimicrobial activity of AgCu incorporated PCL/PEO films by observing for zones of inhibition. As shown in Figure 7.2 (a), after 24 hours of incubation with the inoculated agar plate, all concentrations of AgCu nanoparticle incorporated PCL/PEO showed antimicrobial activity towards all tested microbes. Despite the same curling and production of liquid seen within 10 minutes of contact with the inoculated agar plate, the control PCL/PEO had no effect towards the tested microbes.

Furthermore, the antimicrobial activity increased with the concentration of AgCu, as shown in Figure 7.2 (b). At the lowest concentration of 0.1 w/w% AgCu, the average zone of inhibition was 1.0 cm, 2.1 cm and 1.7 cm towards *E. coli, S. aureus* and *C. albicans*, respectively, whilst at the highest concentration of 10 w/w% AgCu, the average zone of inhibition was 1.9 cm, 3.3 cm and 4.2 cm, respectively. The AgCu nanoparticle incorporated PCL/PEO polymers had the largest zone of inhibition in diameter towards *C. albicans* and the smallest zone of inhibition towards *E. coli*.

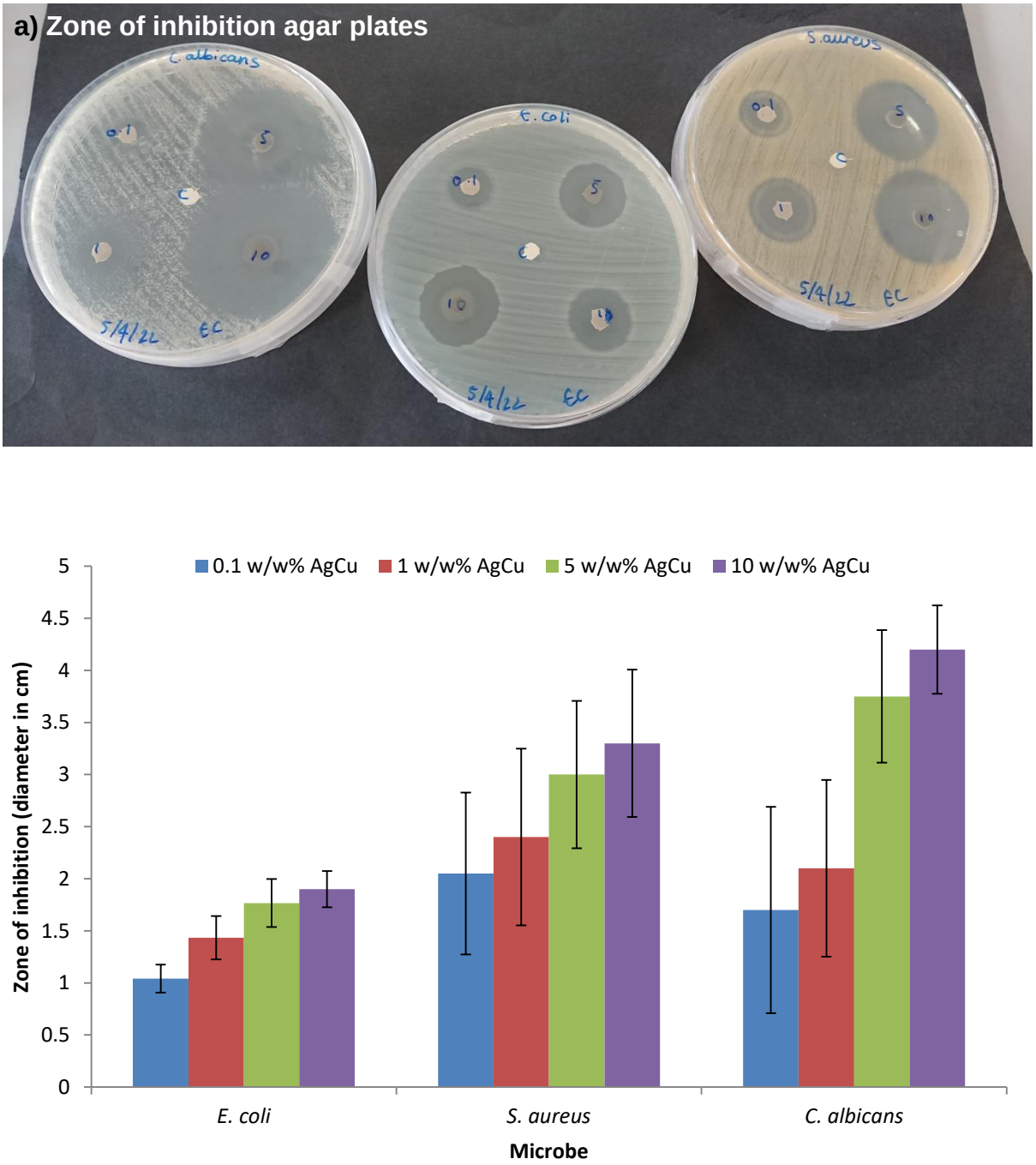

Figure 7.2: Zone of inhibition produced by AgCu nanoparticle incorporated PCL/PEO polymer films after 24 hours incubation. a) Image of the agar plates with zones of inhibition where microbe cells did not grow. The PCL/PEO samples are labelled by the concentration of AgCu nanoparticle percentage and the control is labelled as 'c'. b) Bar graph to compare the zones of inhibition (diameter in cm) produced by the AgCu nanoparticle incorporated PCL/EPO films from 0.1 to 10 w/w%. Error bars are used to denote the standard deviations of three replicates.

7.3.2 Characterisation of AgCu nanoparticle incorporated PCL/PEO polymers

The hydrophobicity of the AgCu nanoparticle incorporated PCL/PEO polymer and control PCL/PEO polymer was investigated using a Tensiometer. As shown in Figure 7.3, the contact angle ranged from 67.26° to 72.85°, with pure PCL/PEO control having the highest contact angle degree and 1 w/w% AgCu nanoparticle incorporated PCL/PEO having the lowest. However, a few minutes after contact with the water droplet, the area of the PCL/PEO sample swelled up and the water droplet was absorbed. Statistical analysis using one way ANOVA showed that the addition of AgCu nanoparticles into the PCL/PEO polymers had no significant difference and did not affect the hydrophobicity of the films as the *p* value was higher than 0.05 (df =4, *p-value* = 0.09).

A SEM was used to observe the surface of the polymer samples at x1000 magnification. The images were then analysed using ImageJ to calculate the number and size (diameter in nm) of the pores present in the surface of the polymers within a 86 μm x 128 μm area. Examples of the SEM images and ImageJ threshold adjustment to identify the pores can be seen in Figure 7.4. It was found that the surface of the PCL/PEO polymers had pores, which increased with the concentration of AgCu nanoparticle. As shown in Figure 7.5, the pure PCL/PEO control had an average of 75.7 pores per area. In contrast, within the same measured area, the addition of AgCu nanoparticles at the lowest tested concentration (0.1 w/w%) had an average of 95.5 pores and the highest tested concentration (10 w/w%) had an average of 1038.8 pores. The diameters of the pores were found to be most frequent at 600 to 699 nm in all samples; however, the size of the pore reached up to 2000 nm.

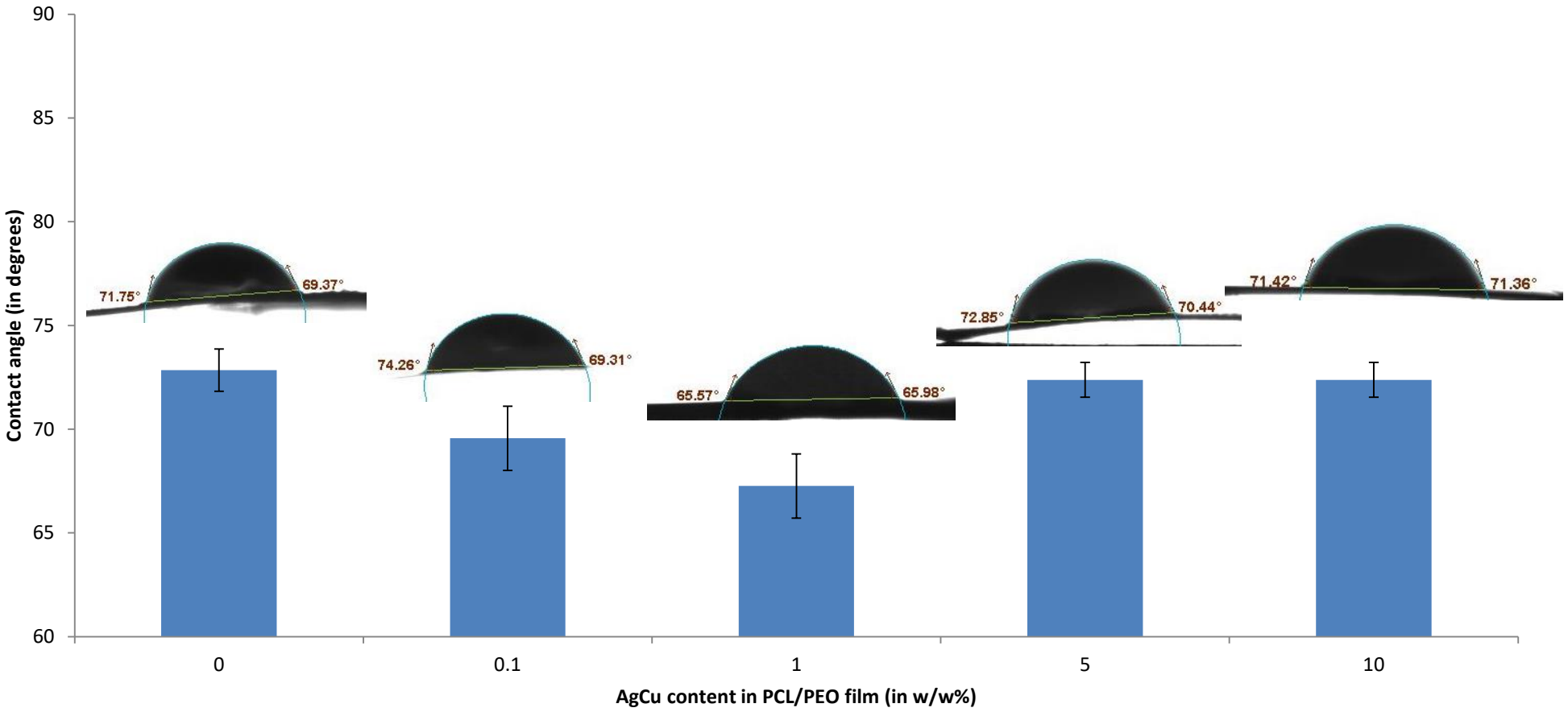

Figure 7.3: Contact angle of PCL/PEO polymers. Data are presented as the average contact angle of three samples. Error bars denote the standard deviations. An example of the contact angle is also shown for each sample; the circle is 5 µl drop of pure water pipetted onto the film sample (rectangle on the bottom). Theta Lite Optical Tensiometer (Biolin Scientific, UK) was used to capture and analyse the contact angle as shown on each of the examples.

a) control

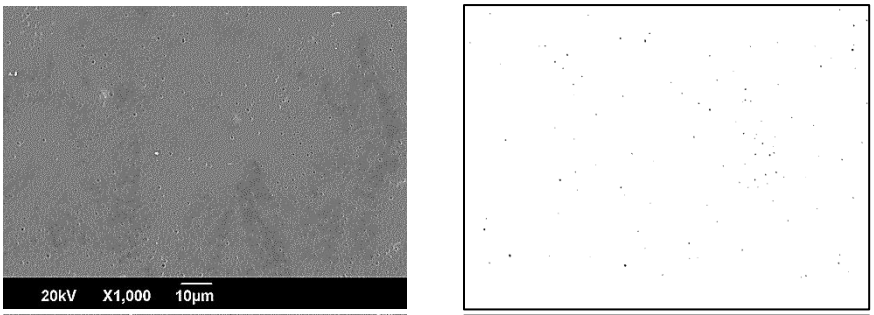

b) 0.1 w/w% AgCu nanoparticles

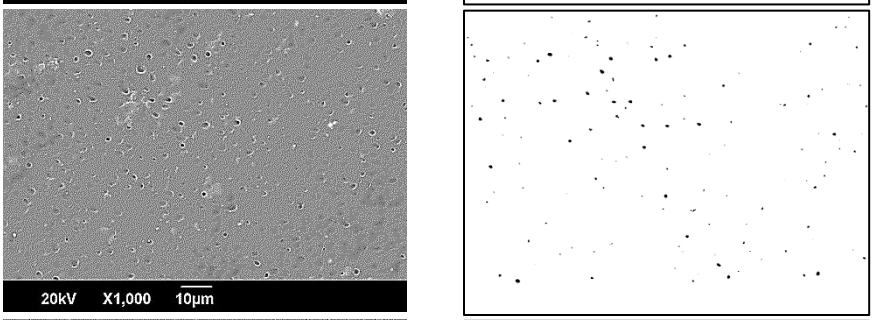

c) 1 w/w% AgCu nanoparticles

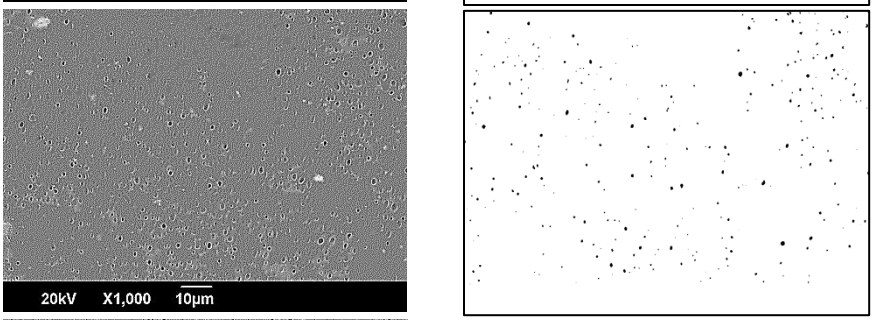

d) 5 w/w% AgCu nanoparticles

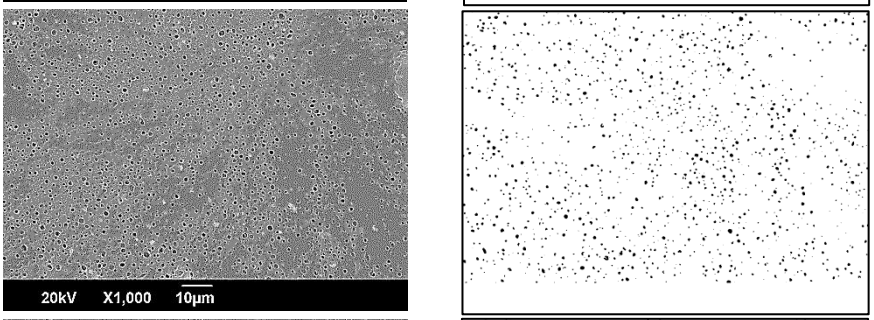

e) 10 w/w% AgCu nanoparticles

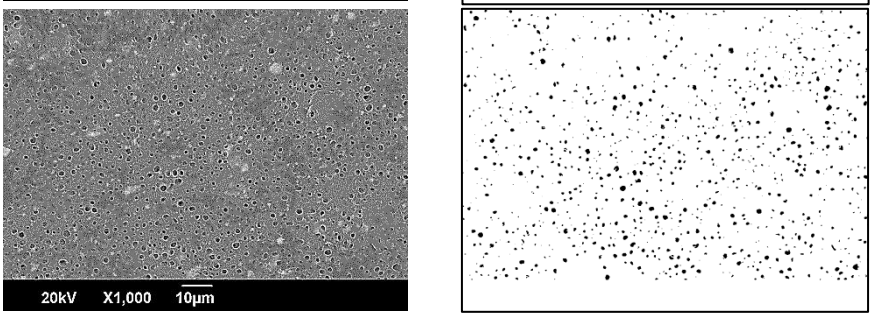

Figure 7.4: SEM images and corresponding ImageJ threshold adjustment of PCL/PEO polymers. The SEM images show the porosity on the surface of the PCL/PEO polymers. Images on the left are SEM images and images on the right are the corresponding ImageJ threshold adjustments. a) control PCL/PEO polymer, b) 0.1 w/w% AgCu nanoparticle incorporated PCL/PEO polymer, c) 1 w/w% AgCu nanoparticle incorporated PCL/PEO polymer, d) 5 w/w% AgCu nanoparticle incorporated PCL/PEO polymer and e) 10 w/w% AgCu nanoparticle incorporated PCL/PEO polymer

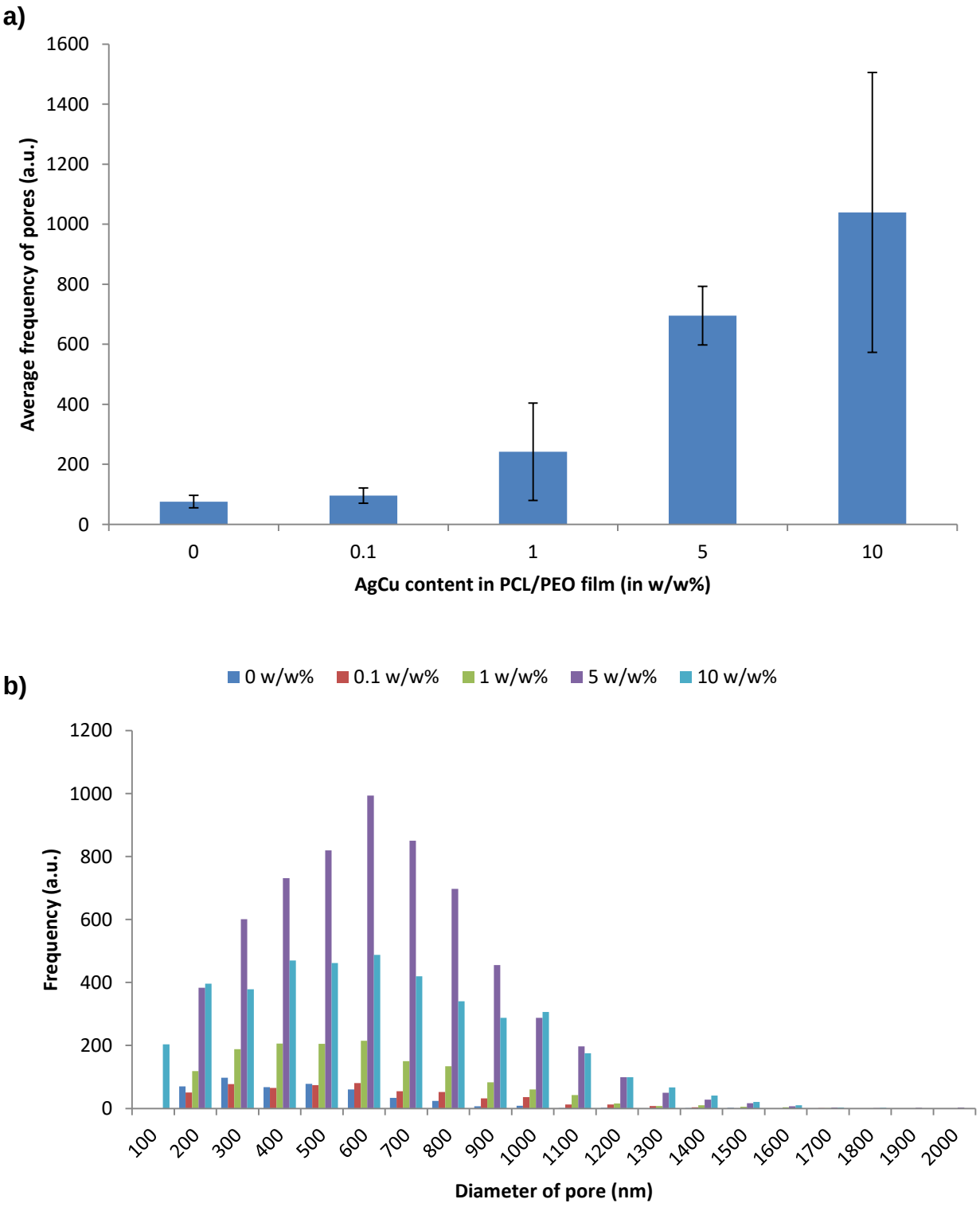

Figure 7.5: Size distribution of pores in PCL/PEO polymer samples. The AgCu nanoparticle incorporated PCL/PEO polymers were observed to contain pores using SEM. ImageJ was used to analyse the a) frequency of the pores and b) size distribution of the diameter of the pores. Results include three areas of three different of the AgCu nanoparticle incorporated PCL/PEO polymers.

The average weight of the cut 1 cm^2 films was measured and the AgCu content was calculated from the weight percentage of incorporated AgCu nanoparticles. As shown in Table 7.1, the mass of AgCu ranged from 2023.3 μg to 19.2 μg. Since the cut films were immerse in 5 ml for characterisation, the concentration of AgCu nanoparticles per 5 ml were also calculated, which ranged from 404.7 to 3.8 μg per 5 ml.

The release of AgCu nanoparticles from the AgCu nanoparticle incorporated PCL/PEO polymers over 24 hours was measured using UV-Vis. As shown in Figure 7.6, detectable absorbance was found in higher concentrations (5 w/w% and 10 w/w%). There was no detectable absorbance of the supernatant measured immediately after the polymers were immersed in water. However, after 1 hour of immersion in water an absorbance was detected in 10 w/w% AgCu samples, whilst an absorbance in 5 w/w% AgCu sample was detected 2 hours after immersion. In contrast, no absorbance was detected in lower concentrations (0.1 w/w% and 1 w/w%) and pure PCL/PEO control samples throughout the 24 hours of measurement. As immersion time increased, the absorbance of the supernatant increased. Samples at 10 w/w% AgCu nanoparticle concentration had higher absorbance (between 0.14 to 0.19 abs) in comparison to samples at a lower concentration of 5 w/w% (between 0.04 to 0.05 abs). The detected absorbance was between 413 to 419 nm in wavelength.

The release of ions from the AgCu nanoparticle incorporated PCL/PEO polymers was measured by monitoring the pH after the polymers were immersed in water for 14 days. As shown in Figure 7.7, there was a positive correlation between the pH and the AgCu nanoparticle concentration incorporated into the polymers - as the concentration increased, the pH also increased. At the highest concentration (10 w/w% AgCu), the highest pH value was observed (at 7.69), whilst the pure PCL/PEO had the lowest pH value (at 7.16) after 14 days of immersion. Water control had a pH measurement of 7.2 after 14 days of storage in the small glass tube under the same conditions.

Table 7.1: Weight and calculated AgCu nanoparticle content of AgCu nanoparticle incorporated PCL/PEO polymers

AgCu nanoparticle concentration in PCL/PEO polymer (w/w%)	**Average weight of 1 cm^2 cut AgCu nanoparticle incorporated polymer (g)**	**AgCu nanoparticle content (µg)**	**AgCu nanoparticle content (µg) in 5 ml water**
0	0.022	-	-
0.1	0.019	19.17	3.83
1	0.016	155.67	31.13
5	0.018	903.33	180.67
10	0.020	2023.33	404.67

a)

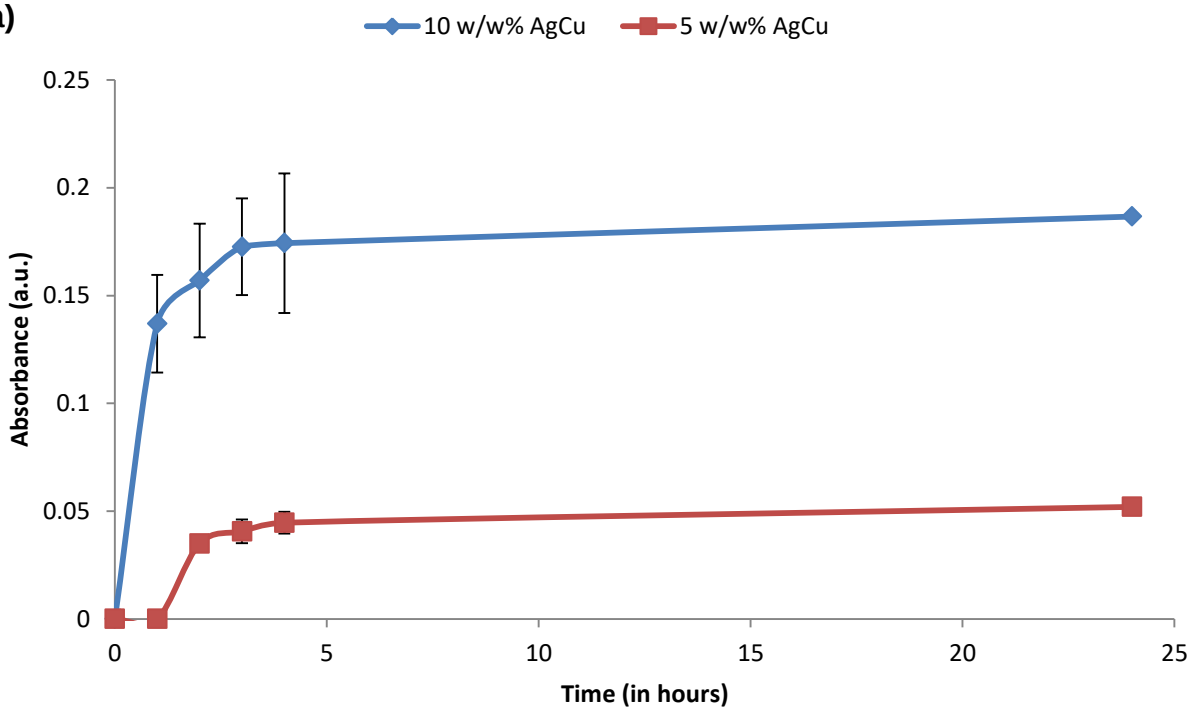

b)

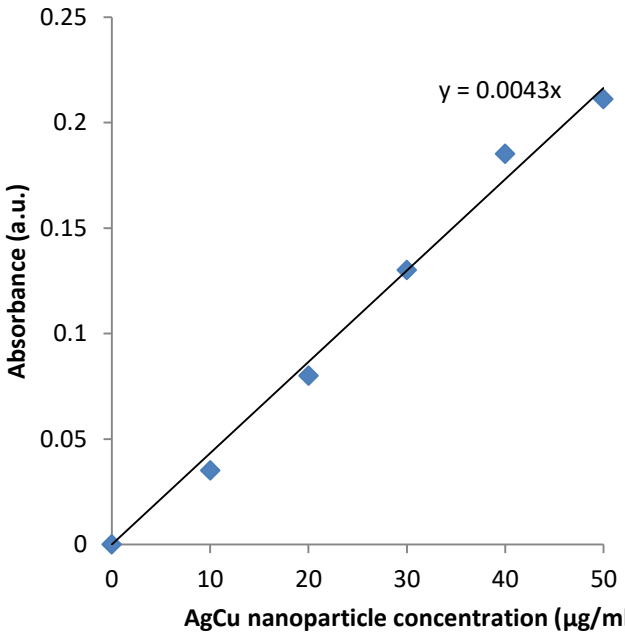

Immersion time (in hours)	Released % of AgCu	
	10 w/w%	5 w/w%
0	0	0
1	7.87	0
2	9.02	4.50
3	9.92	5.23
4	10.02	5.75
24	10.73	6.69

Figure 7.6: Release of AgCu nanoparticles from the AgCu nanoparticle incorporated PCL/PEO polymers. The AgCu nanoparticle incorporated PCL/PEO polymers were immersed in water and the supernatant was measured for a) release of AgCu nanoparticles over 24 hours through UV-Vis. Error bars denote the standard deviations of three replicates. b) Standard curve of AgCu nanoparticle absorbance was used to calculate c) the percentage of AgCu nanoparticle release from the AgCu nanoparticle incorporated PCL/PEO polymer samples.

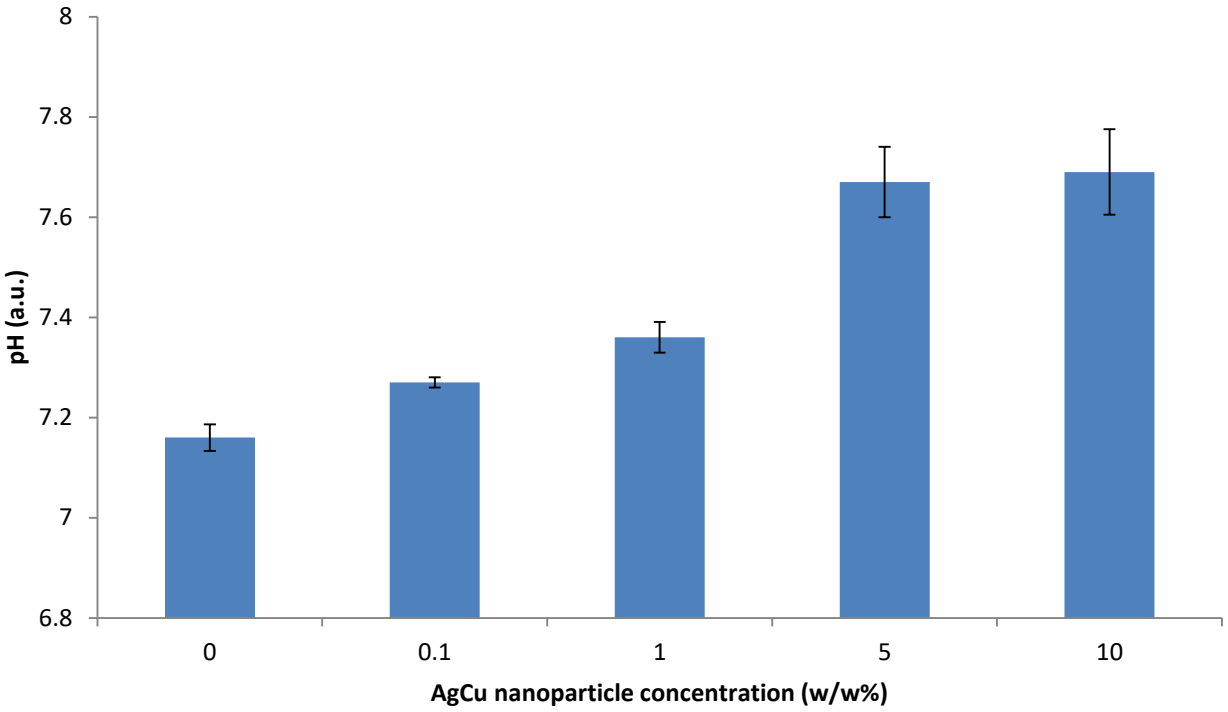

Figure 7.7: Release of AgCu ions from the AgCu nanoparticle incorporated PCL/PEO polymers. The AgCu nanoparticle incorporated PCL/PEO polymers were immersed in water and the pH of the supernatant was measured after 14 days of immersion. Error bars denote the standard deviations of three replicates.

7.4 Discussion

Contamination of wounds and surgical sites can result in colonisation of microorganisms due to their favourable environment. This can delay the healing period and sometimes result in death of the infected patient. Wound dressings are used to protect the wounds from external contaminations. However, infrequent changes and improper use can lead to infections. Thus, the functionalisation of wound dressing with antimicrobial properties might reduce infections in wounds. From experiments in Chapter 3, AgCu nanoparticles have shown antimicrobial activity towards a wide range of nosocomial microbes. Therefore, AgCu nanoparticles were incorporated into PCL/PEO polymer and their physical, chemical and antimicrobial properties were investigated.

7.4.1 Antimicrobial properties

The disk diffusion method was used to investigate the antimicrobial properties of the AgCu nanoparticles incorporated PCL/PEO polymers. It was found that all samples that were incorporated with AgCu nanoparticles had antimicrobial activity, with higher concentrations showing larger zones of inhibition and no antimicrobial activity with pure PCL/PEO polymers. It was suggested in Chapter 5 that the release of ions by the AgCu nanoparticles and interaction between the microbes and AgCu nanoparticles contributed to the mechanism of action. Furthermore, in Chapter 3, section 3.4.1, it was found that the interaction between the sample and the microbes are limited in the disk diffusion agar method as the diffusion of nanoparticles was restricted by the agar matrix, hence the inhibition of microbes were likely to have been caused by the ions produced by AgCu nanoparticles. Despite testing samples with the same concentration of AgCu nanoparticle, the PDMS films (from Chapter 6) did not produce zones of inhibition which was suggested to be caused by the PDMS preventing ion migration and hydrophobic properties restricting the physical contact between incorporated AgCu nanoparticles and microbes. On the other hand, the AgCu nanoparticle incorporated PCL/PEO polymers allowed contact between microbes and the AgCu nanoparticles through the release of AgCu nanoparticles from the polymer. Although PCL is hydrophobic, PEO is a hydrophilic and can dissolve in water [428, 429]. At 1:1 PCL:PEO ratio, the contact angle was measured to be between 67.26° to 72.85°, which is hydrophilic as the contact angle is below 90° [430]. As found in Chapter 5, physical interaction between AgCu nanoparticles

and microbes were observed, particularly in *S. aureus* and *C. albicans,* which was suggested to have contributed to the mechanism of action. The hydrophilic properties of PCL/PEO allow physical contact between the polymer and microbes suspensions, which contributed to the antimicrobial activity as the incorporated AgCu nanoparticles were able to make physical contact with the microbes.

Furthermore, when the PCL/PEO samples contact the agar, the moisture in the agar can dissolve the PEO thus releasing AgCu nanoparticles and ions from within the polymer. Subsequently, the dissolution of PEO resulted in swelling of the sample and water retention [428, 429]. The process of this is seen in Figure 7.8, where the samples swelled and grew by 2 mm in diameter followed by a surrounding of liquid after contact with the agar plate. The samples also resulted in reduction of colour, which may have been a result of the release of AgCu nanoparticle from the PCL/PEO polymer during the dissolution of PEO. This was confirmed through UV-Vis spectrometry. Detectable levels of AgCu nanoparticles were found in polymer samples with higher concentrations of AgCu (5 w/w% and 10 w/w% AgCu) after 1 hour of immersion in water and continued to increase over time, which may have been established by the dissolution rate of PEO. This shows that the dissolution of PEO in the polymers resulted in the release of AgCu nanoparticles from the polymer, which contributed to the antimicrobial activity, as the released AgCu nanoparticles were able to make physical contact with the microbes and produce ions. Using the standard curve of AgCu nanoparticle UV-Vis absorbance, it was found that after 24 hours of immersion in water, 43.4 µg/ml and 12.1 µg/ml of AgCu nanoparticles were released from the 10 w/w% and 5 w/w% AgCu nanoparticle incorporated PCL/PEO polymer, respectively. This shows that low concentrations of AgCu nanoparticles were able to produce antimicrobial activity and low leaching rate of AgCu nanoparticles will have minimal cell toxicity, although toxicity tests are still required.

Figure 7.8: Inoculated agar with PCL/PEO samples prior to incubation. AgCu nanoparticle incorporated PCL/PEO polymers were cut into 4mm circles and placed onto an inoculated agar plate. The sample was flat against the agar during initial contact, however as time progressed, the sample curled and started to swell. After 20 minutes of contact with the agar, the sample was flat against the agar again, increased by 2 mm in diameter with a surrounding of liquid and the colour of the sample got lighter overtime. The example showed contained 0.1 w/w% AgCu nanoparticles.

In comparison to the total content of AgCu nanoparticles, the release of AgCu nanoparticles into the immersion water was quite low. At 10 w/w% AgCu, 10.7% of AgCu nanoparticles were released, whilst at 5 w/w% AgCu, 6.7% was released after 24 hours of immersion. Additionally, in the lower concentrations (0.1 w/w% and 1 w/w% AgCu nanoparticle) there was no detectable level of AgCu nanoparticle release in the immersion water after 24 hours. A reason for this is the dissolution rate of the polymer. Although the AgCu nanoparticles were not clearly observed in the incorporated PCL/PEO polymers when imaged using the SEM, it was found that the polymers contained pores. Interestingly, the number of pores present in the surface of the polymer had a positive correlation with the concentration of AgCu nanoparticle incorporated. Within the polymer blend, PEO is responsible for the pore formation and it has been found that increasing the ratio of PEO to PCL can increase the pore density [431]. Furthermore, the decrease in crystallinity of PEO can lead to the increase in porosity [432]. Reports have shown that the addition of nanoparticles, such as Al_2O_3 and CdO, into PEO can reduce the crystallinity and as a result increase the porosity [433, 434]. Consequently, this was observed when the increase in AgCu nanoparticles resulted in an increase in porosity in the PCL/PEO polymers; however, the size of the pores was unaffected. An increase in porosity, with the same sized pores, increases the dissolution of a material as a result of increased surface area ratio [435]. As the polymers with higher concentration of AgCu nanoparticles had higher porosity, the dissolution rate of the PCL/PEO was faster than the samples with lower concentrations of AgCu nanoparticles, thus more AgCu nanoparticles were released and detected via UV-Vis spectrometry. The release of AgCu nanoparticles could potentially be controlled by the PCL to PEO ratio which influences the porosity of the polymer. However, further investigation is required as it has been reported that the change in PCL to PEO ratio also affects the size of pores and hydrophobicity of the polymer, with an increase in PCL causing larger pore size and increased hydrophobicity [436].

Although the level of AgCu release was undetectable in lower incorporated concentrations, antimicrobial activity was still observed. This suggests that the unreleased AgCu nanoparticles attached onto the PCL/PEO samples were able to exhibit antimicrobial activity and the release of ions from the nanoparticles were able to contribute as well. The release of ions was detected through the increase in pH

when the polymers were immersed in water for 14 days. A positive correlation was found between the increase in concentration of incorporated AgCu nanoparticles and the increase in pH. This shows that in addition to the release of AgCu nanoparticles from the polymers, AgCu ions were also released, of which higher concentrations of incorporated AgCu nanoparticles released more ions. As mentioned in Chapter 5, ions are theorised to contribute to the mechanism of action. Hence, the release of AgCu ions from the PCL/PEO polymers contributed towards the antimicrobial activity by their ability to travel through agar and produce a zone of inhibition.

In comparison to the agar well diffusion experiment in Chapter 3, section 3.4.1, the AgCu nanoparticle incorporated polymers showed more antimicrobial activity via a larger zone of inhibition towards *S. aureus* and *C. albicans*. A reason for this might be due to the swelling properties of the polymers; the swelling resulted in a growth of 2mm in diameter and hence the new polymer size would have been larger than the cut well. The water retention properties resulted in a surrounding of liquid may have carried the diffused AgCu nanoparticles thus allowed the nanoparticles to travel. Therefore, AgCu nanoparticles were able to interact with more microbes leading to a larger zone of inhibition. However, the antimicrobial activity towards *E. coli* was lower compared to the AgCu nanoparticle suspension result from the agar well diffusion method. As found in Chapter 5, *S. aureus* and *C. albicans* were observed to have AgCu nanoparticle attachment to the surface of the cells which was suggested to have contributed to the mechanism of action. In contrast, no physical contact between AgCu nanoparticles and *E. coli* was observed; instead it was suggested that the ions produced by AgCu nanoparticles contributed more to the mechanism of action due to the more negative charge of the *E. coli* cells attracting the positive ions. The reduction of antimicrobial activity may have been a result of decreased ion contact. It has been found that the ionic conductivity is restricted by the high crystallinity structure of PEO [437]. Therefore, fewer ions may have been released from the AgCu nanoparticle incorporated PCL/PEO polymer samples to inhibit *E. coli,* in comparison to the AgCu nanoparticle suspension at the same concentration, leading to a smaller zone of inhibition.

The increase in porosity of the PCL/PEO polymer after incorporation of AgCu nanoparticles is beneficial to wound dressing applications. Oxygen is essential for wound healing as it is triggers healing responses and is involved in many biological

processes such as protein synthesis and cell proliferation [438, 439]. The gas permeability of a polymer is related to its porosity [440]. Thus, an increase in porosity would allow more diffusion of oxygen through the polymer to the wound which will contribute to the healing. Furthermore, in addition to the antimicrobial properties, it has been found that Cu encourages wound healing by promoting angiogenesis and skin formation [426, 441]. However, investigation of the cell toxicity of AgCu nanoparticles incorporated PCL/PEO polymer is required before being employed in biomedical applications.

Similar to the AgCu nanoparticle incorporated PCL/PEO polymer, Dubey *et al.* (2015) produced a nanofiber with potential for wound dressing applications by incorporating Ag nanoparticles into PEO PCL (4:1 wt%). The nanofiber showed antimicrobial activity towards *E. coli* at Ag nanoparticle concentrations of 1, 2 and 3 wt%. It was found to exhibit antimicrobial activity towards *E. coli* and continuously released Ag nanoparticle when immersed in phosphate buffered saline. It was suggested that the sustained released of antimicrobial nanoparticles would be useful for wound dressings as they provide long term antimicrobial properties [442]. In comparison, the antimicrobial results in this study showed to be more effective as lower concentrations of nanoparticles were able to have antimicrobial activity towards a broad range of microbes, including *E. coli*.

In summary, AgCu nanoparticles were successfully incorporated into PCL/PEO polymers at concentrations from 0.1 w/w% to 10 w/w%. All of the concentrations produced antimicrobial activity towards *E. coli*, *S. aureus* and *C. albicans,* whilst the control of pure PCL/PEO had no effect. The incorporated polymers were hydrophilic, however, after a few minutes of contact, the water would be absorbed and the polymer would swell and degrade. Polymer degradation resulted in the sustained release of AgCu nanoparticles and ions, whilst the swelling effect of the polymer may have helped to transport the AgCu nanoparticles further, thus increasing the antimicrobial activity. Moreover, literature has shown that Cu promotes wound healing. Thus AgCu nanoparticle incorporated PCL/PEO polymers could be potentially used as wound dressings, however, further investigations including cell toxicity is required.

Chapter 8 General conclusion

8.1 Conclusion

The prevalence of nosocomial pathogens highlights a cause of global concern towards public health, in particular with pathogens developing multiple resistances against current antibiotic agents. Although the discovery and development of new antibiotics are being intensively researched, it is slow and risk future resistance. Therefore, antimicrobial nanoparticles may provide an alternative approach to reduce infections through the application of biomedical applications such as catheters and wound dressing.

The studies in this thesis were performed using various nanoparticles and methods to produce polymers with potential to improve current biomedical applications. The results are summarised as below:

In summary, 26 different commercial and engineered nanoparticles, with various compositions, including metals, oxides and carbon based materials, were initially screened against 10 common nosocomial pathogens to identify ones with antimicrobial activity. It was found that metallic nanoparticles contained the most antimicrobial activity when comparing to the carbon based ones. Bimetallic AgCu nanoparticles were found to have the broadest and highest efficacy against all strains. Through different methods, it was found that AgCu nanoparticles were able to immediately produce antimicrobial effects and low concentrations were able to delay and reduce growth rates. These results demonstrate that AgCu nanoparticles have potential for antimicrobial applications.

The correlation between the antimicrobial effects of AgCu nanoparticles and their physical and chemical properties were evaluated. By comparing their properties to the single element nanoparticles (Ag and Cu), it was found that the hydrodynamic size and release of ions (as measured by the pH of supernatant nanoparticle suspension) had the largest influence on the antimicrobial properties of the nanoparticles. Ag and AgCu nanoparticles had similar antimicrobial efficacies; however AgCu nanoparticles showed antimicrobial activity towards all strains tested, including those which were not effective by Ag nanoparticles alone. The antimicrobial activity of Ag and AgCu were contributed by their smaller hydrodynamic size and

their higher pH value suggested a release of ions. In contrast, Cu nanoparticles had less antimicrobial efficacy and had a larger hydrodynamic size with a pH that was similar to the water control suggesting little or no ion release. In addition, it was found that the ζ- potential of the nanoparticle suspensions was linked to the hydrodynamic size, with ζ- potential in the unstable region having a larger hydrodynamic size. Despite Cu nanoparticles having a smaller raw particle size (between 28-43 nm in comparison to AgCu nanoparticles which was between 86 to 36 nm), the hydrodynamic size was much larger than Ag and AgCu nanoparticles. This was a result of Cu having larger surface area to volume, hence more surface exposure for aggregation and agglomeration, and having a ζ- potential in the unstable region at certain concentrations (ζ-potential of 5.1 to 18.9 mV at concentrations of 31.25 to 125 µg/ml). In contrast Ag and AgCu nanoparticles had ζ-potential of -20.9 to -33.0 mV, which is part of the stable region, for all concentrations measured. In theory, nanoparticles with positive surface charge should have a higher attraction towards microbes as they have an overall negative cell wall. However, it was found that both Ag and AgCu nanoparticles had a negative charge and had a higher antimicrobial efficacy in comparison to Cu nanoparticles which had a positive charge. Hence the surface charge has less contribution towards the antimicrobial efficacy. Although the correlation to the antimicrobial activity is unknown, Ag and AgCu nanoparticles tested in this study possessed a unique SPR (UV-vis λ_{max} 410 nm) whilst Cu nanoparticles did not, which may have been caused by agglomerations of Cu nanoparticles preventing detection. These results suggest that many nanoparticle properties can influence their antimicrobial efficacy, but hydrodynamic size and release of pH had the largest influence.

To further elucidate the understanding between nanoparticles and their antimicrobial activity, their mechanisms of action was investigated through qualitative analysis and assays. It was found that the mechanisms of action of AgCu nanoparticles towards bacteria were different to that of fungi. It was physically observed that AgCu nanoparticles made direct contact with *C. albicans* cells and resulted in morphology changes. Typically an increase in surface roughness, shrinkage of cell and leakage of internal material was observed. Although similar morphology changes were observed in the bacterial cells, it was also found that the AgCu nanoparticles

resulted in protein denaturation, DNA production inhibition and an increase in oxidative stress, which was not found in fungal cells.

Furthermore, in comparison to the cell viability test over time, it was found that cell death began before the changes to oxidative stress and DNA production. This suggests that the physical interaction between AgCu nanoparticles and microbes were the primary mechanisms of action, whilst the increase in oxidative stress and decrease in DNA production were the secondary mechanisms of action and not essential for cell death since it was only observed in bacterial cells. Therefore, in terms of application, the AgCu nanoparticles within the material are required to make physical contact with the microbes to produce antimicrobial activity.

With a clearer understanding of the antimicrobial and physio-chemical properties of AgCu nanoparticles, biocompatible polymers were fabricated with AgCu nanoparticles as potential antimicrobial polymers for biomedical applications.

AgCu nanoparticles were fabricated with two different polymers for different potential biomedical applications. As can be seen in Chapter 6, AgCu nanoparticles were incorporated into PDMS with the aims of producing antimicrobial polymers for biomedical uses such as catheters. However the polymers did not exhibit antimicrobial activity, whilst the fabricated material was hydrophobic, which is perfect for the delivery or removal of fluid, it limited physical contact between nanoparticles and microbes. Furthermore, it was found that crosslinking of PDMS prevented the release of AgCu ion. For the above reasons, the AgCu-PDMS hybrid were UV surface treated which had led to increases in the exposure of AgCu nanoparticles, as observed by the SEM. This resulted in antimicrobial activity, thus it was suggested that the increase in release of AgCu ions and physical contact between exposed AgCu nanoparticles with microbes was responsible for the inhibitory effect and antimicrobial activity. However, the antimicrobial activity was still relatively low and inconsistent. Therefore, further investigations on enhancing the antimicrobial activity of the AgCu nanoparticle in hybridised polymers are required.

In Chapter 7, AgCu nanoparticles were fabricated into PCL/PEO polymer with aims of producing antimicrobial effects in wound dressing. The fabricated polymers produced antimicrobial activity through the disk diffusion method. PCL/PEO is a hydrophilic polymer which is partly degradable in water. This enabled physical

contact with microbes and the release of AgCu nanoparticles from the polymer. In comparison to the AgCu nanoparticle suspension (0.1 wt/v%), the AgCu nanoparticle incorporated PCL/PEO polymers (0.1 w/w%) had increased antimicrobial activity towards *S. aureus* and *C. albicans.* It was suggested that the swelling and water retention properties of the PCL/PEO was responsible for the increased antimicrobial activity as it enable the diffused AgCu nanoparticles and ions to travel further. Additionally, Cu has been reported with wound healing properties. Therefore antimicrobial AgCu nanoparticle incorporated PCL/PEO polymers have potential applications as wound dressing and/or other biomedical consumables.

8.2 Future work

The research in this thesis has demonstrated that certain metallic nanoparticles exhibited antimicrobial properties and could be fabricated into polymers for potential biomedical applications. Although the antimicrobial efficacy and broadness has been tested, further investigations on the long term effectiveness of the nanoparticles should be studied. It would be interesting to explore the length of time nanoparticles can exhibit antimicrobial activity and how the storage conditions can affect the antimicrobial efficacy. By researching this, nanoparticles can be potentially used for long term applications and the risk of microbes developing antimicrobial resistance can be determined.

Whilst some of the mechanisms of action of AgCu nanoparticles were investigated, further elucidation such as specific genetic damage and enzyme active site interaction should also be studied. This will increase the understanding of the antimicrobial properties of AgCu nanoparticles and their mechanisms of action. Moreover, the interactions between AgCu nanoparticles and mammalian cells are required to be researched to ensure they are safe, in terms of cytotoxicity and genotoxicity, for use in biomedical applications.

The AgCu nanoparticle incorporated polymers have shown potential as for antimicrobial biomedical applications, in particularly the PCL/PEO as they showed great release and antimicrobial properties. Although the polymers are biocompatible, the addition of AgCu nanoparticles require cytotoxicity and genotoxicity tests on the fabricated materials to ensure that they have no adverse effects towards mammalian cells.

Finally, the AgCu nanoparticle incorporated PDMS films have shown slight antimicrobial activity. Samples that were surface treated showed enhanced antimicrobial activity. In this thesis, UV surface treatment was used to increase the exposure of AgCu nanoparticles on the surface of the PDMS film. It was suggested that the UV wavelength was able to excite the AgCu nanoparticles leading to the generation of hydroxyl radicals which degraded the PDMS. Other surface treatments, such as plasma treatment, can be investigated along with the plasmonic and photothermal effect which may potentially improve the antimicrobial activity. Furthermore, the fabrication process can be altered; the current method involves curing the polymer sandwiched in Perspex glass to produce a thin film. Alternative methods such as spin coating can be studied where thinner films can be produced which might exposure more incorporated nanoparticles.

In summary, this thesis has presented work that clearly shows that bimetallic AgCu nanoparticles have a wide spectrum of antimicrobial properties against all 10 strains tested in this study. It can also be utilised and incorporated into polymers with potential applications in biomedical consumables. The physiochemical properties can influence the efficacy of the nanoparticle and has helped to understand of their mechanisms of action. However, further research, such as the molecular docking of AgCu nanoparticles on the surface of microbial cells and deactivation of certain enzymes, can be performed to fully elucidate their mechanisms of action towards microbial cells. Moreover, studies are required to investigate their interactions towards mammalian cells and their cytotoxicity as biomedical applications. These research outcomes will increase the understanding of the antimicrobial properties of AgCu nanoparticles and help to fabricate antimicrobial biomedical applications to help combat the antibiotic resistant microbes.

References

[1] R. Csepregi *et al.*, "Complex Formation of Resorufin and Resazurin with B-Cyclodextrins: Can Cyclodextrins Interfere with a Resazurin Cell Viability Assay?," (in eng), *Molecules (Basel, Switzerland),* vol. 23, no. 2, p. 382, 2018, doi: 10.3390/molecules23020382.

[2] J. S. Uzarski, M. D. DiVito, J. A. Wertheim, and W. M. Miller, "Essential Design Considerations for the Resazurin Reduction Assay to Noninvasively Quantify Cell Expansion within Perfused Extracellular Matrix Scaffolds," *Biomaterials,* vol. 129, pp. 163-175, 2017, doi: 10.1016/j.biomaterials.2017.02.015.

[3] S. Singh, A. Bharti, and V. Meena, "Green synthesis of multi-shaped silver nanoparticles: optical, morphological and antibacterial properties," *Journal of Materials Science: Materials in Electronics,* vol. 26, 06/01 2015, doi: 10.1007/s10854-015-2881-y.

[4] R. D. Rivera-Rangel, A. Navarro-Segura Me Fau - Arizmendi-Morquecho, M. Arizmendi-Morquecho A Fau - Sánchez-Domínguez, and M. Sánchez-Domínguez, "Electrodeposition of plasmonic bimetallic Ag-Cu nanodendrites and their application as surface-enhanced Raman spectroscopy (SERS) substrates," (in eng), *Nanotechnology,* vol. 31, no. 46, pp. 1361-6528 (Electronic), 2020.

[5] L.-u. Rahman, R. Qureshi, M. M. Yasinzai, and A. Shah, "Synthesis and spectroscopic characterization of Ag-Cu alloy nanoparticles prepared in various ratios," *Comptes Rendus Chimie,* vol. 15, no. 6, pp. 533-538, 2012/06/01/ 2012, doi: 10.1016/j.crci.2012.03.012.

[6] S. Laurent *et al.*, "Magnetic Iron Oxide Nanoparticles: Synthesis, Stabilization, Vectorization, Physicochemical Characterizations, And Biological Applications," *Chemical Reviews,* vol. 110, no. 4, p. 2574, 2010.

[7] R. P. Feynman, "There's plenty of room at the bottom," *California institute of technology journal of engineering and science,* vol. 4, pp. 23-36, 1960.

[8] A. Junk and F. Riess, "From an idea to a vision: there's plenty of room at the bottom," *American journal of physics,* vol. 74, p. 825, 2006.

[9] S. Kathirvelu, L. D'Souza, and B. Dhurai, "UV Protection Finishing Of Textiles Using ZnO Nanoparticles," *Indian Journal Of Fibre & Textile Research,* vol. 34, pp. 267-273, 2008.

[10] G. Y. Bae, B. G. Min, Y. G. Jeong, S. C. Lee, J. H. Jang, and G. H. Koo, "Superhydrophobicity of cotton fabrics treated with silica nanoparticles and water-repellent agent," *Journal of colloid and interface science,* vol. 337, pp. 170-175, 2009.

[11] T. G. Smijs and S. Pavel, "Titanium Dioxide And Zinc Oxide Nanoparticles In Sunscreens: Focus On Their Safety And Effectiveness," *Nanotechnology Science And Applications,* vol. 4, pp. 95-112, 2011.

[12] S. Mourdikoudis, R. M. Pallares, and N. T. K. Thanh, "Characterization techniques for nanoparticles: comparison and complementarity upon studying nanoparticle properties," *Nanoscale,* vol. 10, no. 27, pp. 12871-12934, 2018, doi: 10.1039/C8NR02278J.

[13] H. A. Khan, F. K. Biag, and R. Mehboob, "Nosocomial infections: Epidemiology, prevention, control and surveillance," *Asian Pacific Journal of Tropcial biomedicine,* vol. 7, no. 5, pp. 478-482, 2017.

[14] B. Haley and E. Frenkel, "Nanoparticles for drug delivery in cancer treatment," *Urologic Oncology: Seminars and Original Investigations,* vol. 26, no. 1, pp. 57-64, 2008.

[15] N. Palanisamy *et al.*, "Antibiofilm properties of chemically synthesized silver nanoparticles found against Pseudomonas aeruginosa," *Journal of Nanobiotechnology,* vol. 12, no. 2, p. . 2014.

[16] "'No Time to Wait: Securing the Future from drug-resistant infections'," Interagency Coordination Group (IACG) on Antimicrobial Resistance, 2019.

[17] M. Frieri, K. Kumar, and A. Boutin, "Antibiotic resistance," *Journal of Infection and Public Health,* vol. 10, no. 4, pp. 369-378, 2017.

[18] C. f. D. C. a. Prevention, "Antibiotic resistance threats in the United States," (in eng), Report 2019, doi: 10.15620/cdc:82532.
[19] J. O'Neill, "Antimicrobial Resistance: Tackling a crisis for the health and wealth of nations," *Review on Antimicrobial Resistance,* 2014.
[20] S. Fernando, T. Gunasekara, and J. Holton, "ntimicrobial nanoparticles: applications and mechanisms of action," *Sri Lankan Journal of Infectious Diseases,* vol. 8, pp. 2-11, 2018.
[21] A. Brandelli, A. C. Ritter, and F. F. Veras, "Antimicrobial Activites of Metal Nanoparticles," in *Metal Nanoparticles in Pharma*, M. Rai and S. R. Eds.: Springer, Cham, 2017, pp. 337-363.
[22] L. Wang, C. Hu, and L. Shao, "The antimicrobial activity of nanoparticles: present situation and prospects for the future," *International Journal of Nanomedicine,* vol. 12, pp. 1227-1249, 2017.
[23] P. A. Sabatier, "Top-Down And Bottom-Up Approaches To Implementation Research: A Critical Analysis And Suggested Synthesis," *Journal Of Public Policy,* vol. 6, pp. 21-48, 1986.
[24] V. M. Arole and S. V. Munde, "Fabrication of nanomaterials by top-down and bottom-up approaches - an overview.," *Jaast: material science,* vol. 1, pp. 89-93, 2014.
[25] N. Salah *et al.*, "High-Energy Ball Milling Technique For Zno Nanoparticles As Antibacterial Material," *International Journal Of Nanomedicine,* vol. 6, pp. 861-869, 2011.
[26] D. P. Macwan, C. Balasubramanian, P. N. Dave, and S. Chaturvedi, "Thermal Plasma Synthesis Of Nanotitania And Its Characterization," *Journal Of Saudi Chemical Society,* vol. 18, pp. 234-244, 2014.
[27] G. Ren, D. Hu, E. W. C. Cheng, M. A. Vargas-Reus, P. Reip, and R. P. Allaker, "Characterisation Of Copper Oxide Nanoparticles For Antimicrobial Applications," *International Journal Of Antimicrobial Agents,* vol. 33, pp. 587-590, 2009.
[28] L. Zhi and K. Müllen, "A Bottom-Up Approach From Molecular Nanographenes To Unconventional Carbon Materials," *Journal Of Materials Chemistry,* vol. 18, pp. 1472-1484, 2008.
[29] C. Raab, M. Simko, U. Fiedeler, M. Netwich, and A. Gazso, "Production Of Nanoparticles And Nanomaterials," *Nano Trust Dossier,* vol. 6, pp. 1-4, 2011.
[30] J.-G. Mattei *et al.*, "Gas-Phase Synthesis Of Trimetallic Nanoparticles," *Chemistry Of Materials,* vol. 31, pp. 2151-2163, 2019.
[31] H. Rashid, M. A. Mansoor, B. Haider, R. Nasir, S. B. Abd Hamid, and A. Abdulrahman, "Synthesis and characterization of magnetite nano particles with high selectivity using in-situ precipitation method," *Separation Science And Technology,* vol. 55, no. 6, pp. 1207-1215, 2020.
[32] I. Dörner *et al.*, "Cost-effective sol-gel synthesis of porous cuo nanoparticle aggregates with tunable specific surface area," *Scientific reports,* vol. 9, p. 11758, 2019.
[33] B. Ajitha, A. K. Reddy, and P. S. Reddy, "Enhanced antimicrobial activity of silver nanoparticles with controlled particle size by pH variation," *Powder Technology,* vol. 269, pp. 110-117, 2015.
[34] K. S. Butler, D. J. Peeler, B. J. Casey, and B. J. E. Dair, R. K., "Silver nanoparticles: correlating nanoparticle size and cellular uptake with genotoxicity," *Mutagenesis,* vol. 30, no. 4, pp. 577-591, 2015.
[35] S. Karthik, R. Suriyaprabha, K. S. Balu, P. Manivasakan, and V. Rajendran, "Influence of ball milling on the particle sizeand antimicrobial properties of Tridaxprocumbens leaf nanoparticles," *IET Nanobiotechnology,* vol. 11, no. 1, pp. 12-17, 2017.
[36] P. Zhang, B. Chen, and J. F. Banfield, "Particle Size and pH Effects on Nanoparticle Dissolution," *The Journal of Physical Chemistry,* vol. 114, no. 35, pp. 14876-14884, 2010.
[37] A. M. Fayaz, K. Balaji, P. T. Kalaichelvan, and R. Venkatesan, "Fungal based synthesis of silver nanoparticles—An effect of temperature on the size of particles," *Colloids and Surfaces B: Biointerfaces,* vol. 74, no. 1, pp. 123-126, 2009.

[38] D. H. Kim, J. C. Park, G. E. Jeon, C. S. Kim, and J. H. Seo, "Effect Of The Size And Shape Of Silver Nanoparticles On Bacterial Growth And Metabolism By Monitoring Optical Density And Fluorescence Intensity," *Biotechnology And Bioprocess Engineering,* vol. 22, pp. 210-217, 2017.

[39] Y. Jeong, D. W. Lim, and J. Choi, "Assessment of size-dependent antimicrobial and cytotoxic properties of silver nanoparticles," *Advances in materials science and engineering,* vol. 1, p. 6, 2014.

[40] X. Deng, Z. Huang, W. Wang, and R. N. Dave, "Investigation of nanoparticle agglomerates properties using monte carlo simulations," *Advanced power technology,* vol. 27, pp. 1971-1979, 2016.

[41] C. Liao, Y. Li, and S. Tjong, "Bactericidal and Cytotoxic Properties of Silver Nanoparticles," *International Journal of Molecular Sciences,* vol. 20, no. 2, p. 449, 2019.

[42] A. M. E. Badawy, R. G. Silva, B. Morris, K. G. Sheckel, M. T. Suidan, and T. M. Tolaymat, "Surface Charge-Dependent Toxcitity Of Silver Nanoparticles," *Environmental Science and Technology,* vol. 45, pp. 283-287, 2011.

[43] Y. Guo, Y. Zhao, S. Wang, C. Jiang, and J. Zhang, "Relationship between the zeta potential and the chemical agglomeration efficiency of fine particles in flue gas during coal combustion," *Fuel,* vol. 215, pp. 756-765, 2018.

[44] S. Shukla *et al.*, "The Impact Of Aspect Ratio On The Biodistribution And Tumor Homing Of Rigid Soft-Matter Nanorods," *Advanced Healthcare Materials,* vol. 4, pp. 874-882, 2015.

[45] C. Buzea, I. I. Pacheco, and K. Robbie, "Nanomaterials and nanoparticles: sources and toxicity," *Biointerphases,* vol. 2, pp. 17-71, 2007.

[46] M. Bouloudenine and M. Bououdina, "Toxic effects of engineered nanoparticles on living cells," in *Pharmaceutical Sciences: Breakthroughs in Research and Practice*: IGI Global, 2016, ch. 2, pp. 35-68.

[47] S. Pal, Y. K. Tak, and J. M. Song, "Does The Antibacterial Activity Of Silver Nanoparticles Depend On The Shape Of The Nanoparticle? A Study Of The Gram-Negative Bacterium Escherichia Coli," *Applied And Environmental Microbiology,* vol. 73, pp. 1712-1720, 2007.

[48] J. Y. Cheon, S. J. Kim, Y. H. Rhee, O. H. Kwon, and W. H. Park, "Shape-dependent antimicrobial activities of silver nanoparticles," *International Journal of Nanomedicine,* vol. 14, pp. 2273-2780, 2019.

[49] S. Pothukuchi, Y. Li, and C. P. Wong, "Shape controlled synthesis of nanoparticles and their incorporation into polymers," in *2004 Proceedings/ 54th Electronic Components and Technology Conference*, Las Vegas, 2004, vol. 2: IEEE, pp. 1965-1967.

[50] G. Sharma *et al.*, "Novel Development Of Nanoparticles To Bimetallic Nanoparticles And Their Composites: A Review," *Journal Of King Saud University -Science,* vol. 31, pp. 257-269, 2019.

[51] K. A. Abd-Elsalam, A. F. Hashim, and M. A. Alghuthaymi, "Bimetallic nanoparticles as antimicrobials," *Journal of Nanotechnology and Materials Science,* vol. 3, no. 1, pp. 1-2, 2016.

[52] M. Shoeb *et al.*, "Ros-Dependent Anticandidal Activity Of Zinc Oxide Nanoparticles Synthesized By Using Egg Albumen As A Biotemplate," *Advances In Natural Sciences: Nanoscience And Nanotechnology,* vol. 4, p. 11, 2013.

[53] J. A. Garza-Cervantes *et al.*, "Synergistic Antimicrobial Effects of Silver/Transition-metal Combinatorial Treatments," *Scientific Reports,* vol. 7, no. 1, p. 903, 2017/04/18 2017, doi: 10.1038/s41598-017-01017-7.

[54] P. Kumar, P. Huo, R. Zhang, and B. Liu, "Antibacterial Properties Of Graphene-Based Nanomaterials," *Nanomaterials,* vol. 9, p. 737, 2019.

[55] S. Varghese, S. Kuriakose, and S. Jose, "Antimicrobial Activity of Carbon Nanoparticles Isolated from Natural Sources against Pathogenic Gram-Negative and Gram-Positive Bacteria," *Journal of Nanoscience,* p. 5, 2013.

[56] L. Pang, C. Dai, L. Bi, Z. Guo, and J. Fan, "Biosafety and Antibacterial Ability of Graphene and Graphene Oxide In Vitro and In Vivo," *Nanoscale Research Letters,* vol. 12, no. 1, p. 564, 2017.
[57] R. C. Muthiah, K. Eswaran, S. Shankar, and A. Kumaraguru, "Antibacterial Effects Of Ag, Au And Bimetallic (Ag-Au) Nanoparticles Synthesized From Red Algae," *Solid State Phenomena,* vol. 201, pp. 211-230, 2013.
[58] A. S. Lozhkomoev, M. I. Lerner, A. V. Pervikov, S. O. Kazantsev, and A. N. Fomenko, "Development Of Fe/Cu And Fe/Ag Bimetallic Nanoparticles For Promising Biodegradable Materials With Antimicrobial Effect," *Nanotechnologies In Russia,* vol. 13, pp. 18-25, 2018.
[59] M. Raffi *et al.*, "Investigations Into The Antibacterial Behavior Of Copper Nanoparticles Against Escherichia Coli," *Annals Of Microbiology,* vol. 60, pp. 75-80, 2010.
[60] A. K. Chatterjee, R. K. Sarkar, S. P. Chattopadhyay, P. Aich, R. Chakraborty, and T. Basu, "A simple robust method for synthesis of metallic copper nanoparticles of high antibacterial potency against e. Coli," *Nanotechnology,* vol. 23, p. 11, 2012.
[61] G. M. Nazeruddin, N. R. Prasad, Y. I. Shaikh, and A. A. Shaikh, "Synergetic Effect Of Ag-Cu Bimetallic Nanoparticles On Antimicrobial Activity," *Der Pharmacia Lettre,* vol. 6, pp. 129-136, 2014.
[62] A. Alonso *et al.*, "Environmentally-safe Bimetallic Ag@Co Magnetic Nanocomposites with Antimicrobial Activity.," *Chemical Communications,* pp. 10464-10466, 2011.
[63] N. V. Savarovskaya *et al.*, "Chemical Behaviour Of Al/Cu Nanoparticles In Water," *Progress in Natural Science: Materials International,* vol. 25, no. 1, pp. 1-5, 2015.
[64] S. Jadhav, S. Gaikwad, M. Nimse, and A. Rajbhoj, "Copper oxide nanoparticles: synthesis, characterization and their antibacterial activity," *Journal of cluster science,* vol. 22, pp. 121-129, 2011.
[65] O. Yamamoto, "Influence Of Particles Size On The Antibacterial Activity Of Zinc Oxide," *International Journal Of Inorganic Materials,* vol. 3, pp. 643-646, 2001.
[66] W. A. Daoud, J. H. Xin, and Y. H. Zhang, "Surface functionalization of cellulose fibers with titanium dioxide nanoparticles and their combined bactericidal activities," *Surface science,* vol. 599, pp. 69-75, 2005.
[67] A. N. Fomenko, O. V. Bakina, S. O. Kazantsev, and A. M. Kondranova, "Synthesis of iron oxide based nanostructures with antimicrobial activity," *Materials science and engineering,* vol. 447, pp. 1-4, 2018.
[68] M. A. Raza, Z. Kanwal, A. Rauf, A. N. Sabri, S. Riaz, and S. Naseem, "Size- and Shape-Dependent Antibacterial Studies of Silver Nanoparticles Synthesized by Wet Chemical Routes," *Nanomaterials,* vol. 6, no. 4, p. 74, 2016.
[69] O. I. Olubiyi, F.-K. Lu, D. Calligris, F. A. Jolesz, and N. T. Agar, "Chapter 17 - Advances in Molecular Imaging for Surgery," in *Image-Guided Neurosurgery*, A. J. Goldby Ed. Boston: Academic Press, 2015, pp. 407-439.
[70] "Raman Spectroscopy for Chemical Analysis," ed. Cambridge, MA: JoVE, 2020.
[71] F. Sima, C. Ristoscu, L. Duta, O. Gallet, K. Anselme, and I. N. Mihailescu, "3 - Laser thin films deposition and characterization for biomedical applications," in *Laser Surface Modification of Biomaterials*, R. Vilar Ed. Duxford: Woodhead Publishing, 2016, pp. 77-125.
[72] "X-ray Diffraction," ed. Cambridge, MA: JoVE, 2020.
[73] J. P. Patel and P. H. Parsania, "3 - Characterization, testing, and reinforcing materials of biodegradable composites," in *Biodegradable and Biocompatible Polymer Composites*, N. G. Shimpi Ed. Santa Cruz: Woodhead Publishing, 2018, pp. 55-79.
[74] S. Karastogianni, S. Girousi, and S. Sotiropoulos, "pH: Principles and Measurement," in Encylopedia of Food and Health, S. Caballero, P. M. Finglas, and F. Toldrá Eds. Oxford: Academic Press, 2016, pp. 333-338.

[75] A. Medveďová and L. Valík, "Staphylococcus aureus: Characterisation and Quantitative Growth Description in Milk and Artisanal Raw Milk Cheese Production," in *Structure and Function of Food Engineering*, A. A. Eissa Ed. Rijeka: IntechOpen, 2012, pp. 71-102.
[76] I. Z. Fernando, Y., "Impact of pH on the stability, dissolution and aggregation kinetics of silver nanoparticles," *Chemosphere,* vol. 216, pp. 297-305, 2019.
[77] T. S. Peretyazhko, Q. Zhang, and V. L. Colvin, "Size-Controlled Dissolution of Silver Nanoparticles at Neutral and Acidic pH Conditions: Kinetics and Size Changes," *Environmental Science and Technology,* vol. 48, no. 20, pp. 11954-11961, 2014.
[78] J. Lui, D. A. Sonshine, S. Shervani, and R. H. Hurt, "Controlled Release of Biologically Active Silver from Nanosilver Surfaces," *ACS Nano,* vol. 4, no. 11, pp. 6903-6913, 2010.
[79] M. N. Hang *et al.*, "Influence of Nanoparticle Morphology on Ion Release and Biological Impact of Nickel Manganese Cobalt Oxide (NMC) Complex Oxide Nanomaterials," *ACS Applied Nano Materials,* vol. 1, no. 4, pp. 1721-1730, 2018.
[80] J. Nölte, *ICP Emission Spectrometry: A Practical Guide*. Weinheim: WILEY-VCH, 2003.
[81] W. W. Wilson, M. M. Wade, S. C. Holman, and F. R. Champlin, "Status of methods for assessing bacterial cell surface charge properties based on zeta potential measurements," *Journal of Microbiological Methods,* vol. 43, no. 3, pp. 153-164, 2001.
[82] V. Selvamani, "Chapter 15 - Stability Studies on Nanomaterials Used in Drugs," in *Characterization and Biology of Nanomaterials for Drug Delivery*, S. S. Mohapatra, S. Ranjan, N. Dasgupta, R. K. Mishra, and S. Thomas Eds. Amsterdam: Elsevier, 2019, pp. 425-444.
[83] A. Kumar and C. K. Dixit, "3 - Methods for characterization of nanoparticles," in *Advances in Nanomedicine for the Delivery of Therapeutic Nucleic Acids*, S. Nimesh, R. Chandra, and N. Gupta Eds. Duxford: Woodhead Publishing, 2017, pp. 43-58.
[84] E. J. Chung, L. Leon, and C. Rinaldi, *Nanoparticles for Biomedical Applications: Fundamental Concepts, Biological Interactions and Clinical Applications*. Amsterdam: Elsevier, 2019.
[85] E. Arroyo, L. Enríquez, A. Sánchez, M. Ovalle, and A. Olivas, "Scanning Electron Microscopy of Bacteria Tetrasphaera Duodecadis," *Scanning,* vol. 36, no. 5, pp. 547-550, 2014.
[86] S. Sharma, *Handbook of Materials Characterization*. Cham: Springer International Publishing, 2018.
[87] L. E. Franken, K. Grünewald, E. J. Boekeman, and M. C. A. Stuart, "A Technical Introduction to Transmission Electron Microscopy for Soft-Matter: Imaging, Possibilities, Choices, and Technical Developments," *Small,* vol. 16, no. 14, 2020.
[88] G. Alberti and G. Nuzzaci, "1.6.5 SEM and TEM techniques," in *World Crop Pests*, E. E. Lindquist, M. W. Sabelis, and J. Bruin Eds. Amsterdam: Elsevier Science, 1996, pp. 399-410.
[89] C. M. Maguire, M. Rösslein, P. Wick, and A. Prina-Mello, "Characterisation of particles in solution - a perspective on light scattering and comparative technologies," (in eng), *Science and technology of advanced materials,* vol. 19, no. 1, pp. 732-745, 2018, doi: 10.1080/14686996.2018.1517587.
[90] J. Stetefeld, S. A. McKenna, and T. R. Patel, "Dynamic light scattering: a practical guide and applications in biomedical sciences," *Biophysical Reviews,* vol. 8, no. 4, pp. 409-427, 2016.
[91] P. M. Carvalho, M. R. Felicio, N. C. Santos, S. Goncalves, and M. M. Domingues, "Application of Light Scattering Techniques to Nanoparticle Characterization and Development," *Frontiers in Chemistry,* vol. 6, p. 237, 2018.
[92] J. Hou *et al.*, "Nanoparticle tracking analysis versus dynamic light scattering: Case study on the effect of Ca2+ and alginate on the aggregation of cerium oxide nanoparticles," *Jounral of Hazardous Materials,* vol. 360, pp. 319-328, 2018.
[93] L. D. S. Yadav, "Ultraviolet (UV) and Visible Spectroscopy," in *Organic Spectroscopy*, L. D. S. Yadav Ed.: Springer, Dordrecht, 2005, pp. 7-51.
[94] Q. Abbas, "Understanding the UV-Vis Spectroscopy for Nanoparticles," *Journal of Nanomaterials and Molecular Nanotechnology,* vol. 8, no. 3, 2019.

[95] E. J. Beard, G. Sivaraman, Á. Vázquez-Mayagoitia, V. Vishwanath, and J. M. Cole, "Comparative dataset of experimental and computational attributes of UV/vis absorption spectra," *Sci Data,* vol. 6, p. 307, 2019.
[96] V. Shinde, P. Jadhav, J. H. Kim, and P. S. Patil, "One-step synthesis and characterization of anisotropic silver nanoparticles: Application for enhanced antibacterial activity of natural fabric," *Journal of Materials Science,* vol. 48, no. 24, pp. 8393-8401, 2013.
[97] D. Acharya, B. Mohanta, S. Deb, and A. K. Sen, "Theoretical prediction of absorbance spectra considering the particle size distribution using Mie theory and their comparison with the experimental UV–Vis spectra of synthesized nanoparticles," *Spectroscopy Letters,* vol. 51, no. 3, pp. 139-143, 2018.
[98] X. Huang and M. A. El-Sayed, "Gold nanoparticles: Optical properties and implementations in cancer diagnosis and photothermal therapy," *Journal of Advanced Research,* vol. 1, no. 1, pp. 13-28, 2010.
[99] M. Quinten, *Optical Properties of Nanoparticle Systems: Mie and Beyond*. Singapore: Wiley-VCH, 2011.
[100] N. Kandel, S. Chungong, A. Omaar, and J. Xing, "Health security capacities in the context of COVID-19 outbreak: an analysis of International Health Regulations annual report data from 182 countries," *The Lancet,* vol. 395, no. 10229, pp. 1047-1053, 2020.
[101] F. Balloux and L. Van Dorp, "Q&A: What are pathogens, and what have they done to and for us?," *BMC Biology,* vol. 15, p. 91, 2017.
[102] J. Bourn, "The Management and Control of Hospital Aqcuired Infection in Acute NHS Trusts in England," National Audit Office, London, 2000.
[103] R. Mertens, "Methodologies And Results Of National Surveillance," *Bailieres Clinical Infectious Diseases,* vol. 3, pp. 159-178, 1996.
[104] K. Inweregbu, J. Dave, and A. Pittard, "Nosocomial infections," *Continuing Educationin Anaesthesia Critical Care & Pain,* vol. 5, no. 1, pp. 14-17, 2005.
[105] T. J. Silhavy, D. Kahne, and S. Walker, "The Bacterial Cell Envelope," *Cold Spring Harbor Perspectives in Biology,* vol. 2, no. 5, 2010, doi: 10.1101/cshperspect.a000414.
[106] A. Revelas, "Healthcare - associated infections: A public health problem," *Nigerian Medical Journal,* vol. 53, no. 2, pp. 59-64, 2012, doi: 10.4103/0300-1652.103543.
[107] P. D. Cani, "Human gut microbiome: hopes, threats and promises," *Gut,* vol. 67, no. 9, p. 1716, 2018, doi: 10.1136/gutjnl-2018-316723.
[108] A. Elbourne, J. Chapman, A. Gelmi, D. Cozzolino, R. J. Crawford, and V. K. Truong, "Bacterial-nanostructure interactions: The role of cell elasticity and adhesion forces," *Journal of Colloid and Interface Science,* vol. 546, pp. 192-210, 2019, doi: 10.1016/j.jcis.2019.03.050.
[109] B. Mehrad, N. M. Clark, G. G. Zhanel, and J. P. Lynch, "Antimicrobial Resistance In Hospital-Acquired Gram-Negative Bacterial Infections," *Chest,* vol. 147, pp. 1413-1421, 2015.
[110] R. A. Weinstein, R. Gaynes, J. R. Edwards, and N. N. I. S. System, "Overview Of Nosocomial Infections Caused By Gram-Negative Bacilli," *Clinical Infectious Diseases,* vol. 41, pp. 848-854, 2005.
[111] A. H. Delcour, "uter membrane permeability and antibiotic resistance," *Biochim biophys acta,* vol. 1794, pp. 808-816, 2008.
[112] T. J. Beveridge, "Structures of gram-negative cell walls and their derived membrane vesicles," *Journal of bacteriology,* vol. 181, pp. 4725-4733, 1999.
[113] G. D. Shockman and J. F. Barrett, "Structure, Function, And Assembly Of Cell Walls Of Gram-Positive Bacteria," *Annual Review Of Microbiology,* vol. 37, pp. 501-527, 1983.
[114] C. Eades, S. Hughes, K. Heard, and I. S. Moore, "Antimicrobial therapies for gram-positive infections," *Cliinical Pharmacist,* vol. 9, no. 9, pp. 1-19, 2017.
[115] L. J. Piddock, "The Crisis Of No New Antibiotics-What Is The Way Forward?," *The Lancet Infectious Diseases,* vol. 12, pp. 249-253, 2012.

[116] X. H. Fu, F. I. Meng, Y. Hu, and J. Q. Zhou, "Candida albicans, a distinctive fungal model for cellular aging study," *Aging Cell,* vol. 7, pp. 746-757, 2008.
[117] J. Perlroth, B. Choi, and B. Spellberg, "osocomial Fungal Infections: Epidemiology, Diagnosis, And Treatment," *Medical Mycology,* vol. 45, pp. 321-346, 2007.
[118] L. Wang and X. Lin, "Morphogenesis In Fungal Pathogenicity: Shape, Size, And Surface.," *Plos Pathogens,* vol. 8, p. E1003027, 2012.
[119] F. Kong *et al.*, "Possible Mechanisms Of The Antimicrobial Effects Of Polypeptide-Enriched Gastrodia Elata Blume Extracts," *Molecular Medicine Reports,* vol. 20, pp. 723-730, 2019.
[120] C. Spampinato and D. Leonardi, "Candida Infections, Causes, Targets, And Resistance Mechanisms: Traditional And Alternative Antifungal Agents," *Biomed Research International,* vol. 2013, p. 204237, 2013.
[121] C. G. Golding, I. L. Lamboo, D. R. Beniac, and T. F. Booth, "The scanning electron microscope in microbiology and diagnosis of infectious disease," *Scientific reports,* vol. 6, p. 26516, 2016.
[122] I. Almansour, M. Alhagri, R. Alfares, M. Alshehri, R. Bakhashwain, and A. Maarouf, "IRAM: virus capsid database and analysis resource.," *Database,* vol. 2019, no. baz079, 2019.
[123] S. Sengupta, M. K. Chattopadhyay, and H. P. Grossart, "The Mulitfaceted Roles Of Antibiotics And Antibiotic Resistance In Nature," *Frontiers In Microbiology,* vol. 4, p. 47, 2013.
[124] G. Kapoor, S. Saigal, and A. Elongavan, "Action and resistance mechanisms of antibiotics: a guide for clinicians," *Journal of anaesthesiology clincal pharmacology,* vol. 33, pp. 300-305, 2017.
[125] S. Dzidic, J. Suskovic, and B. Kos, "Antibiotic resistance mechanisms in bacteria: biochemical and genetic aspects," *Food technology and biotechnology,* vol. 46, pp. 11-21, 2008.
[126] P. A. Lambert, "Bacterial Resistance To Antibiotics: Modified Target Sites," *Advanced Drug Delivery Reviews,* vol. 57, pp. 1471-1485, 2005.
[127] S. M. Hamilton *et al.*, "High-level resistance of staphylococcus aureus to β-lactam antibiotics mediated by penicillin-binding protein 4 (pbp4)," *Antimicrobial agents and chemotherapy,* vol. 61, pp. e02727-16, 2017.
[128] L. Scorzoni *et al.*, "Antifungal Therapy: New Advances In The Understanding And Treatment Of Mycosis," *Frontiers In Microbiology,* vol. 8, p. 36, 2017.
[129] R. R. Morubagal, S. G. Shivappa, R. P. Mahale, and S. M. Neelambike, "Study Of Bacterial Flora Associated With Mobile Phones Of Healthcare Workers And Non-Healthcare Workers," *Iranian Journal Of Microbiology,* vol. 9, pp. 143-151, 2017.
[130] J. Koscova, Z. Hurnikova, and J. Pistl, "Degree Of Bacterial Contamination Of Mobile Phone And Computer Keyboard Surfaces And Efficacy Of Disinfection With Chlorhexidine Digluconate And Triclosan To Its Reduction," *International Journal Of Enviromnental Research And Public Health,* vol. 15, no. 10, p. 2238, 2018.
[131] A. K. Al-Ghamdi, S. M. A. Abdelmalek, A. M. Ashshi, H. Faidah, H. Shukri, and A. A. Jiman-Fatani, "Bacterial contamination of computer keyboards and mice, elevator buttons and shopping carts," *African Journal of Microbiology Research,* vol. 5, pp. 3998-4003, 2011.
[132] K. A. Reynolds, P. M. Watt, S. A. Boone, and C. P. Gerba, "Occurence Of Bacteria And Biochemical Markers On Public Surfaces," *International Journal Of Enviromnental Health Research,* vol. 15, pp. 225-234, 2005.
[133] S. Doron, "Bacterial Infections: Overview," *International Encyclopedia of Public HEalth,* pp. 273-282, 2008.
[134] J. F. Timsit *et al.*, "New materials and devices for preventing catheter-related infections," *Annals of Intensive Care,* vol. 1, p. 34, 2011.
[135] E. Cheung, M. O. Baerlocher, M. Asch, and A. Myers, "Venous access: a practical review for 2009," *Canadian family physician Medecin de famille canadien,* vol. 55, no. 5, pp. 494-496, 2009.

[136] H. Al-Hazmi, "Role of duration of catheterization and length of hospital stay on the rate of catheter-related hospital-acquired urinary tract infections," *Research and Reports in Urology,* vol. 7, pp. 41-47, 2015.
[137] B. W. Trautner and R. O. Darouiche, "Catheter-Associated Infections: pathogenesis affects prevention," *Archives of internal medicine,* vol. 164, no. 8, pp. 842-850, 2004.
[138] S. Cheeseman *et al.*, "Antimicrobial Metal Nanomaterials: From Passive to Stimuli-Activated Applications," *Advanced Science,* vol. 7, no. 10, p. 1902913, 2020.
[139] Y. N. Slavin, J. Asnis, U. O. Häfeli, and H. Bach, "Metal nanoparticles: understanding the mechanisms behind antibacterial activity," *Journal of Nanobiotechnology,* vol. 15, no. 1, p. 65, 2017.
[140] P. Nisar, N. Ali, L. Rhman, M. Ali, and Z. K. Shinwari, "Antimicrobial activities of biologically synthesized metal nanoparticles: an insight into the mechanism of action," *JBIC Journal of Biological Inorganic Chemistry,* vol. 24, pp. 929-941, 2019.
[141] K. Gold, B. Slay, M. Knackstedt, and A. K. Gaharwar, "Antimicrobial Activity of Metal and Metal-Oxide Based Nanoparticles," *Advanced Therapeutics,* vol. 1, no. 3, 2018.
[142] L. Zhang, L. Wu, Y. Si, and K. Shu, "Size-dependent cytotoxicity of silver nanoparticles to Azotobacter vinelandii: Growth inhibition, cell injury, oxidative stress and internalization," *PLoS ONE,* vol. 13, no. 12, p. e0209020, 2018.
[143] O. M. Bondarenko, M. Sihtmäe, J. Kuzmičiova, L. K. Ragelienė, A., and R. Daugelavičius, "Plasma membrane is the target of rapid antibacterial action of silver nanoparticles in Escherichia coli and Pseudomonas aeruginosa," *International Journal of Nanomedicine,* vol. 13, pp. 6779-6790, 2018.
[144] S. Shaikh *et al.*, "Mechanistic Insights into the Antimicrobial Actions of Metallic Nanoparticles and Their Implications for Multidrug Resistance," *International Journal of Molecular Sciences,* vol. 20, no. 10, p. 2468, 2019, doi: 10.3390/ijms20102468.
[145] Y. Kaneko, M. Thoendel, O. Olakanmi, B. Britigan, and P. K. Singh, "The transition metal gallium disrupts Pseudomonas aeruginosa iron metabolism and has antimicrobial and antibiofilm activity," *The Journal of Clinical Investigation,* vol. 117, no. 4, pp. 877-888, 2007.
[146] C. R. Chitambar, "Gallium and its competing roles with iron in biological systems," *Biochimica et Biophysica Acta (BBA) - Molecular Cell Research,* vol. 1863, no. 8, pp. 2044-2053, 2016.
[147] W.-R. Li, X.-B. Xie, Q.-S. Shi, H.-Y. Zeng, Y.-S. OU-Yang, and Y.-B. Chen, "Antibacterial activity and mechanism of silver nanoparticles on Escherichia coli," *Applied Microbial and Cell Physiology,* vol. 85, pp. 1115-1122, 2010.
[148] I. Mukha *et al.*, "Antimicrobial Activity of Stable Silver Nanoparticles of a Certain Size," *Applied Biochemistry and Microbioilogy,* vol. 49, no. 2, pp. 199-206, 2013.
[149] C. Marambio-Jones and E. M. V. Hoek, "A review of the antibacterial effects of silver nanomaterials and potential implications for human health and the environment," *Journal of Nanoparticle Research,* vol. 12, pp. 1531-1551, 2010.
[150] K. Holt and A. Bard, "Interaction of silver(I) ions with the respiratory chain of Escherichia coli: an electrochemical and scanning electrochemical microscopy study of the antimicrobial mechanism of micromolar Ag," *Biochemistry,* vol. 44, pp. 13214-13223, 2005.
[151] H. Park *et al.*, "Silver-ion-mediated reactive oxygen species generation affecting bactericidal activity," *Water Research,* vol. 43, pp. 1027-1032, 2009.
[152] B. Ezraty, A. Gennaris, F. Barras, and J.-F. Collet, "Oxidative stress, protein damage and repair in bacteria," *Nature Reviews Microbiolgy,* vol. 15, pp. 385-396, 2017.
[153] S. Ranjan and C. Ramalingam, "Titanium dioxide nanoparticles induce bacterial membrane rupture by reactive oxygen species generation," *Environmental Chemistry Letters,* vol. 14, pp. 487-494, 2016.
[154] K. Zheng, M. I. Setyawati, D. T. Leong, and J. Xie, "Antimicrobial Gold Nanoclusters," *ACS Nano,* vol. 11, no. 7, pp. 6904-6910, 2017.

[155] Z. Yu *et al.*, "Reactive Oxygen Species-Related Nanoparticle Toxicity in the Biomedical Field," *Nanoscale Research Letters,* vol. 15, p. 115, 2020.
[156] O. Bondarenko, K. Juganson, A. Ivask, K. Kasemets, M. Mortimer, and A. Kahru, "Toxicity of ag, CuO and ZnO nanoparticles to selected environmentally relevant test organisms and mammalian cells in vitro: a critical review," *Archives of toxicology,* vol. 87, pp. 1181-1200, 2013.
[157] M. Muzslay, S. Ali, and P. Wilson, "Antimicrobial efficacy of Corning® Gorilla® Glass 3 under laboratory condition," *Open Forum Infectious Diseases,* vol. 1, p. S363, 2014.
[158] K. Hodges and R. Gill, "Infectious diarrhea," *Gut microbes,* vol. 1, pp. 4-21, 2010.
[159] J. Ahmed, Y. Arfat, A. Bher, M. Mulla, H. Jacob, and R. Auras, "Active Chicken Meat Packaging Based on Polyactide Films and Bimetallic Ag-Cu Nanoparticles and Essential Oil," *Journal of food sciences,* vol. 83, pp. 1299-1310, 2018.
[160] A. Emamifar, M. Kadivar, M. Shahedi, and S. Soleimanian-Zad, "Effect of nanocomposite packaging containing ag and zno on inactivation of lactobacillus plantarum in orange juice," *Food Control,* vol. 22, pp. 408-413, 2010.
[161] J. An, M. Zhang, S. Wang, and J. Tang, "Physical, chemical and microbiological changes in stored green asparagus spears as affected by coating of silver nanoparticles-pvp.," *Swiss society of food science and technology,* vol. 41, pp. 1100-1107, 2008.
[162] K. Lem *et al.*, "Use Of Nanosilver In Consumer Products.," *Recent Patents On Nanotechnology,* vol. 6, pp. 60-72, 2012.
[163] C. Callewaert, E. D. Maeseneire, F. M. Kerckhof, A. Verliefde, T. V. D. wWele, and N. Boon, "Microbial odor profile of polyester and cotton clothes after a fitness session," *Applied and environmental microbiology,* vol. 80, pp. 6611-6619, 2014.
[164] L. B. Baker, "Sweating Rate And Sweat Sodium Concentration In Athletes: A Review Of Methodology And Intra/Interindividual Variability," *Sports Medicine,* vol. 47, pp. 111-128, 2017.
[165] M. Troccaz, C. Strakkenman, Y. Niclass, M. V. D. Waal, and A. J. Clark, "3-Methly-3-Sulfanylhexan-1-Ol As A Major Descriptor For The Human Axilla-Sweat Odour Profile," *Chemistry & Biodiversity,* vol. 1, pp. 1022-1035, 2004.
[166] C. Ozeki and O. Moro, "A Study Of The Suppression Of Body Odour In Elderly Subjects By Anti-Fungal Agents," *International Journal Of Cosmetic Sciences,* vol. 38, pp. 312-318, 2015.
[167] I. C. Gerber *et al.*, "Incorporation of reactive silver-tricalcium phosphate nanoparticles into polyamide 6 allows preparation of self-disinfecting fibers," *Polymer engineering & science,* vol. 51, pp. 71-77, 2011.
[168] Y. Zhang, Y. Li, and Q. Hu, "Colourless Antibacterial Cotton Fabrics Based On Silver Nanoparticles And Chitosan Complexes," *International Journal Of Clothing Science And Technology,* vol. 24, pp. 118-128, 2012.
[169] U. E. Illangakoon *et al.*, "Gyrospun antimicrobial nanoparticle loaded fibrous polymeric filters," *Materials science and engineering,* vol. 74, pp. 315-324, 2017.
[170] D. Weber, D. Anderson, and W. Rutala, "The Role Of The Surface Environment In Healthcare-Associated Infections," *Current Opinion In Infectious Diseases,* vol. 26, pp. 338-344, 2013.
[171] A. Kramer, I. Schwebke, and G. Kampf, "How Long Do Nosocomial Pathogens Persist On Inanimate Surfaces? A Systematic Review," *BMC Infectious Diseases,* vol. 6, p. 130, 2006.
[172] A. Kumar, P. K. Vemula, P. M. Ajayan, and G. John, "Silver-Nanoparticle-Embedded Antimicrobial Paints Based On Vegetable Oil," *Nature Materials,* vol. 7, pp. 236-241, 2008.
[173] M. Gunell *et al.*, "Antimicrobial characterization of silver nanoparticle-coated surfaces by "touch test" method," *Nanotechnology, science and applications,* vol. 10, pp. 137-145, 2017.
[174] C. D. Valle *et al.*, "A Novel Antibacterial Modification Treatment Of Titanium Capable To Improve Osseointegration," *The International Journal Of Artificial Organs,* vol. 35, pp. 864-875, 2012.

[175] W. Xia, K. Grandfield, A. Hoess, A. Ballo, Y. Cai, and H. Enggvist, "Mesoporous Titanium Dioxide Coating For Metallic Implants," *Journal Of Biomedical Materials Research Part B Applied Biomaterials,* vol. 100, no. 1, pp. 82-93, 2012.
[176] U. Samuel and J. P. Guggenbichler, "Prevention Of Catheter-Related Infections: The Potential Of A New Nano-Silver Impregnated Catheter," *Antimicrobial Agents,* vol. 23, pp. 75-78, 2004.
[177] J. P. Guggenbichler, O. Assadian, M. Boeswald, and A. Kramer, "Incidence and clinical implication of nosocomial infections associated with implantable biomaterials – catheters, ventilator-associated pneumonia, urinary tract infections," *GMS Krankenhhygiene Interdisziplinar,* vol. 6, no. 1, 2011.
[178] J. Wu *et al.*, "In Situ Synthesis Of Silver-Nanoparticles/Bacterial Cellulose Composites For Slow-Released Antimicrobial Wound Dressing," *Carbohydrate Polymers,* vol. 102, pp. 762-771, 2014.
[179] R. Augustine, N. Kalarikkal, and S. Thomas, "Electrospun PCL Membranes Incorporated With Biosynthesized Silver Nanoparticles As Antibacterial Wound Dressings," *Applied Nanoscience,* vol. 6, pp. 337-344, 2016.
[180] M. Tanaka, K. Sato, E. Kitakami, S. Kobayashi, T. Hoshiba, and K. Fukushima, "Design of biocompatible and biodegradable polymers based on intermediate water concept," *Polymer Journal,* vol. 47, pp. 114-121, 2015.
[181] B. D. Ratner, "Chapter 3 - The Biocompatibility of Implant Materials," in *Host Response to Biomaterials*, S. F. Badylak Ed. United States: Academic Press, 2015, pp. 37-51.
[182] A. Teo, A. Mishra, I. Park, Y.-J. Kim, W.-T. Park, and Y.-J. Yoon, "Polymeric Biomaterials for Medical Implants and Devices," *ACS Biomeaterials Science & Engineering,* vol. 2, no. 4, pp. 454-472, 2016.
[183] M. N. Helmus, D. F. Gibbsons, and D. Cebon, "Biocompatibility: Meeting a Key Functional Requirement of Next-Generation Medical Devices," *Toxicologic Pathology,* vol. 36, no. 1, pp. 70-80, 2008.
[184] D. Leaper *et al.*, "Healthcare associated infection: novel strategies and antimicrobial implants to prevent surgical site infection," *Annals of the Royal College of Surgeons of England,* vol. 92, no. 6, pp. 453-458, 2010.
[185] M. Merola and S. Affatato, "Materials for Hip Prostheses: A Review of Wear and Loading Considerations," *Materials (Basel),* vol. 12, no. 3, p. 495, 2019.
[186] K. Ramachandran, "Breast augmentation," *Indian Journal of Plastic Surgery,* vol. 41 (Suppl), pp. 41-47, 2008.
[187] V. E. Del Bene, "Chapter 218Temperature," in *Clinical Methods: The History, Physical, and Laboratory Examinations*, H. Walker, W. Hall, and J. Hurst Eds. Boston: Butterworths, 1990.
[188] A. Souza, J. Ribeiro, and F. Araújo, "Study of PDMS characterization and its applications in biomedicine: A review," *Journal of Mechanical Engineering and Biomechanics,* vol. 4, no. 1, pp. 1-9, 2019.
[189] N. P. D. Tran and M. C. Yang, "Synthesis and Characterization of Silicone Contact," *Polymers,* vol. 11, no. 6, p. 944, 2019.
[190] J. H. Kim, H. W. Park, and S. W. Seo, "In situ synthesis of silver nanoparticles on the surface of PDMS with high antibacterial activity and biosafety toward an implantable medical device," *Nano Convergence,* vol. 4, no. 1, p. 33, 2017.
[191] P. Veluchamy, P. M. Sivakumar, and M. Doble, "Immobilization of Subtilisin on Polycaprolactam for Antimicrobial Food Packaging Applications," *Journal of Agricultural and Food Chemistry,* vol. 59, no. 20, pp. 10869-10878, 2011.
[192] S. Huda, S. Smoukov, H. Nakanishi, B. Kowalczyk, K. Bishop, and B. Grzybowski, "Antibacterial nanoparticle monolayers prepared on chemically inert surfaces by Cooperative Electrostatic Adsorption (CELA)," *ACS Applied Materials Interfaces,* vol. 2, no. 4, pp. 1206-1210, 2010.

[193] A. Goyal *et al.*, "In situ Synthesis of Metal Nanoparticle Embedded Free Standing Multifunctional PDMS Films," *Macromolecular Rapid Communications,* vol. 30, no. 13, pp. 1116-1122, 2099.
[194] B. Bera and M. Sarkar, "Piezoelectricity in PVDF and PVDF Based Piezoelectric," *IOSR Journal of Applied Physics,* vol. 9, no. 3, pp. 95-99, 2017.
[195] H.-F. Guo *et al.*, "Piezoelectric PU/PVDF electrospun scaffolds for wound healing applications," *Colloids and Surfaces B: Biointerfaces,* vol. 96, pp. 29-36, 2012.
[196] A. Toor, "Gold nanoparticle/PVDF polymer composite with improved particle dispersion," Rome, 2015: IEEE International Conference on Nanotechnology.
[197] M. Zrilic, V. Panic, D. Stamenkovic, S. Seslija, and S. Velickovic, "The Mechanical Properties of a Poly(methyl methacrylate) Denture Base Material Modified with Dimethyl Itaconate and Di-n-butyl Itaconate," *International Journal of Polymer Science,* p. 9, 2015.
[198] J. Fang, C. Wang, Y. Li, Z. Zhao, and L. Mei, "Comparison of Bacterial Adhesion to Dental Materials of Polyethylene," *Scanning,* vol. 38, pp. 665-670, 2016.
[199] E. Ng, G. Barrett, and R. Bowman, "In vitro bacterial adherence to hydrogel and poly(methyl methacrylate) intraocular lenses," *Journal of Cataract & Refractive Surgery,* vol. 22, no. 2, pp. 1331-1335, 1996.
[200] A. Alrahlah, H. Fouad, M. Hashem, A. Niazy, AlBadah, and A., "Titanium Oxide (TiO2)/Polymethylmethacrylate (PMMA) Denture Base Nanocomposites: Mechanical, Viscoelastic and Antibacterial Behavior," *Materials (Basel),* vol. 11, no. 7, p. 1096, 2018.
[201] S. Swar, V. Zajícová, M. Rysová, I. Lovětinská-Šlamborová, L. Voleský, and I. Stibor, "Biocompatible surface modification of poly(ethylene terephthalate) focused on pathogenic bacteria: Promising prospects in biomedical applications," *Journal of Applied Polymer Science,* vol. 134, p. 44990, 2017.
[202] T. Çaykara, M. Sande, N. Azoia, L. Rodrigues, and C. Silva, "Exploring the potential of polyethylene terephthalate in the design of antibacterial surfaces," *Medical Microbiology and Immunology,* vol. 209, pp. 363-372, 2020.
[203] M. Lam and J. Wu, "Biomaterial applications in cardiovascular tissue repair and regeneration," *Expert review of cardiovascular therapy,* vol. 10, no. 8, pp. 1039-1049, 2012.
[204] R. Dwivedi *et al.*, "Polycaprolactone as biomaterial for bone scaffolds: Review of literature," (in eng), *Journal of oral biology and craniofacial research,* vol. 10, no. 1, pp. 381-388, 2020, doi: 10.1016/j.jobcr.2019.10.003.
[205] O. S. Manoukian *et al.*, "Biodegradable Polymeric Injectable Implants for Long-Term Delivery of Contraceptive Drugs," (in eng), *Journal of applied polymer science,* vol. 135, no. 14, 2018, doi: 10.1002/app.46068.
[206] X. Yang, Y. Wang, Y. Zhou, J. Chen, and Q. Wan, "The Application of Polycaprolactone in Three-Dimensional Printing Scaffolds for Bone Tissue Engineering," *Polymers,* vol. 13, no. 16, 2021, doi: 10.3390/polym13162754.
[207] J. Caplin and A. García, "Implantable Antimicrobial Biomaterials for Local Drug Delivery in Bone Infection Models," *Acta Biomaterialia,* vol. 93, 07/01 2019, doi: 10.1016/j.actbio.2019.01.015.
[208] T. Fang, J. Wen, J. Zhou, Z. Shao, and J. Dong, "Poly (ε-caprolactone) coating delays vancomycin delivery from porous chitosan/β-tricalcium phosphate composites," *Journal of Biomedical Materials Research Part B: Applied Biomaterials,* vol. 100B, no. 7, pp. 1803-1811, 2012, doi: 10.1002/jbm.b.32747.
[209] A. Muñoz-Escobar, Á. d. J. Ruíz-Baltazar, and S. Y. Reyes-López, "Novel Route of Synthesis of PCL-CuONPs Composites With Antimicrobial Properties," *Dose-Response,* vol. 17, no. 3, p. 1559325819869502, 2019, doi: 10.1177/1559325819869502.
[210] Y. Yamaguchi, Z. Li, X. Zhu, C. Liu, D. Zhang, and X. Dou, "Polyethylene Oxide (PEO) and Polyethylene Glycol (PEG) Polymer Sieving Matrix for RNA Capillary Electrophoresis," *PLOS ONE,* vol. 10, no. 5, p. e0123406, 2015, doi: 10.1371/journal.pone.0123406.

[211] A. G. B. Pereira, A. T. Paulino, A. F. Rubira, and E. C. Muniz, "Polymer-polymer miscibility in PEO/cationic starch and PEO/hydrophobic starch blends," *Express Polymer Letters,* vol. 4, pp. 488-499, 2010.
[212] M.-Y. Wong, B. Amini Horri, and B. Salamatinia, "Chapter 8 - Grafted Copolymerized Chitosan and Its Applications as a Green Biopolymer," in *Biopolymer Grafting*, V. K. Thakur Ed.: Elsevier, 2018, pp. 285-333.
[213] K. Tokuda, M. Noda, T. Maruyama, M. Kotera, and T. Nishino, "A low-fouling polymer surface prepared by controlled segregation of poly(ethylene oxide) and its functionalization with biomolecules," *Polymer Journal,* vol. 47, no. 4, pp. 328-333, 2015/04/01 2015, doi: 10.1038/pj.2014.131.
[214] A. Roosjen, H. C. van der Mei, H. J. Busscher, and W. Norde, "Microbial Adhesion to Poly(ethylene oxide) Brushes: Influence of Polymer Chain Length and Temperature," *Langmuir,* vol. 20, no. 25, pp. 10949-10955, 2004/12/01 2004, doi: 10.1021/la048469l.
[215] C. D. Saquing *et al.*, "Alginate–Polyethylene Oxide Blend Nanofibers and the Role of the Carrier Polymer in Electrospinning," *Industrial & Engineering Chemistry Research,* vol. 52, no. 26, pp. 8692-8704, 2013/07/03 2013, doi: 10.1021/ie302385b.
[216] L. Carvalho *et al.*, "Doxycycline release and antibacterial activity from PMMA/PEO electrospun fiber mats," *Journal of Applied Oral Science,* vol. 27, 10/07 2019, doi: 10.1590/1678-7757-2018-0663.
[217] O. Neděla, P. Slepička, and V. Švorčík, "Surface Modification of Polymer Substrates for Biomedical Applications," *Materials (Basel),* vol. 10, no. 10, p. 1115, 2017.
[218] S. K. Nemani *et al.*, "Surface Modification of Polymers: Methods and Applications," *Advanced Materials Interfaces,* vol. 5, no. 24, pp. 1-26, 2018.
[219] Q. F. Xu, B. Mondal, and A. M. Lyons, "Fabricating superhydrophobic polymer surfaces with excellent abrasion resistance by a simple lamination templating method," *ACS Applied Material Interfaces,* vol. 3, no. 9, pp. 3508-3514, 2011.
[220] Y. Yuan, M. P. Hays, P. R. Hardwidge, and J. Kim, "Surface characteristics influencing bacterial adhesion to polymeric substrates," *RSC Advances,* vol. 7, pp. 14254-14261, 2017.
[221] S. L. Fávaro, A. F. Rubira, E. C. Muniz, and E. Radovanovic, "Surface modification of HDPE, PP, and PET films with KMnO4/HCl solutions," *Polymer Degradation and Stability,* vol. 92, no. 7, pp. 1219-1226, 2007.
[222] D. Schaubroeck, J. De Baets, T. Desmet, S. Van Vlierberghe, E. Schacht, and A. Van Calstera, "Introduction of amino groups on the surface of thin photo definable epoxy resin layers via chemical modification," *Applied Surface Science,* vol. 255, no. 21, pp. 8780-8787, 2009.
[223] Masruroh and D. Santjojo, "Surface Modification of Polystyrene by Nitrogen Plasma Treatment," in *Coatings and Thin-Film Technologies*, J. A. P. Taborda and A. G. A. Bernal Eds. Croatia: IntechOpen, 2018, pp. 69-86.
[224] W. Chen, R. Lam, and J. Fu, "Photolithographic surface micromachining of polydimethylsiloxane (PDMS)," *Lab on a chip,* vol. 12, no. 2, pp. 391-395, 2012.
[225] G. Toworfe, R. Composto, C. Adams, I. Shapiro, and P. Ducheyne, "Effect of surface activated poly(dimethylsiloxane) on fibronectin adsorption and cell function," Philadelphia, 2003: Materials Research Society.
[226] F. Formosa *et al.*, "UV-O3-treated and protein-coated polymer surfaces facilitate endothelial cell adhesion and proliferation mediated by the PKCα/ERK/cPLA2 pathway," *Microvascular Research,* vol. 75, no. 3, pp. 330-342, 2008.
[227] D. Vadas, Z. Nagy, I. Csontos, G. Marosi, and K. Bocz, "Effects of thermal annealing and solvent-induced crystallization on the structure and properties of poly(lactic acid) microfibres produced by high-speed electrospinning," *Journal of Thermal Analysis and Calorimetry,* 2020.
[228] P. Frontini and A. Fave, "The effect of annealing temperature on the fracture performance of isotactic polypropylene," *Journal of Materials Science,* vol. 30, no. 9, pp. 2446-2454, 1995.

[229] E. R. M. Sydnor and T. M. Perl, "Hospital Epidemiology and Infection Control in Acute-Care Settings," *Clinical Microbiology Reviews,* vol. 24, no. 1, pp. 141-173, 2011.
[230] R. M. Klevens *et al.*, "Estimating Health Care-Associated Infections and Deaths in U.S. Hospitals, 2002," *Public Health Reports,* vol. 122, no. 2, pp. 160-166, 2007.
[231] "Healthcare-associated infections," in *Health at a Glance: Europe 2018: State of Health in the EU Cycle*, E. Union Ed. Brussels: OECD Publishing, 2018, p. 166.
[232] S. F. Hormozi, N. Vasei, M. Aminianfar, M. Darvishi, and A. A. Saeedi, "Antibiotic resistance in patients suffering from nosocomial infections in Besat Hospital," *European Journal of Translational Myology,* vol. 28, no. 3, p. 7594, 2018.
[233] A. Cortegiani, G. Misseri, T. Fasciana, A. Giammanco, A. Giarratano, and A. Chowdhary, "Epidemiology, clinical characteristics, resistance, and treatment of infections by Candida auris," *Journal of Intensive care,* vol. 6, p. 69, 2018.
[234] "Prioritization of pathogens to guide discovery, research and development of new antibiotics for drug resistant bacterial infections, including tuberculosis," World Health Organisation, Geneva, 2017.
[235] J. K. Martin *et al.*, "A Dual-Mechanism Antibiotic Kills Gram-Negative Bacteria and Avoids Drug Resistance," *Cell,* vol. 181, no. 7, pp. 1518-1532e.14, 2020.
[236] N. Niño-Martínez, M. F. Orozco, G.-A. Martínez-Castañón, F. T. Méndez, and F. Ruiz, "Molecular Mechanisms of Bacterial Resistance to Metal and Metal Oxide Nanoparticles," *International Journal of Molecular Sciences,* vol. 20, p. 2808, 2019.
[237] G. Ren, J. S. Oxford, P. W. Reip, R. Lambkin-Williams, and A. Mann, "Anti-viral formulations nanomaterials and nanoparticles," United States Patent US 2013/00916611 A1, 2013.
[238] R. L. Cihlar and R. A. Calderone, *Candida albicans. Methods and protocols*. New York: Humana press, 2009.
[239] Eppendorf, "Od600 measurements using different photometers," *White paper,* vol. 28, pp. 1-4, 2015.
[240] S. N. Rampersad, "Multiple Applications Of Alamar Blue As An Indicator Of Metabolic Function And Cellular Health In Cell Viability Bioassays," *Sensors (Basel),* vol. 12, pp. 12347-12360, 2012.
[241] M. Balouiri, M. Sadiki, and S. K. Ibnsouda, "Methods for in vitro evaluating antimicrobial activity: A review," *Journal of Pharmaceutical Analysis,* vol. 6, no. 2, pp. 71-79, 2016.
[242] R. Toy, E. Hayden, C. Shoup, H. Baskaran, and E. Karathanasis, "The effects of particle size, density and shape on margination of nanoparticles in microcirculation," (in eng), *Nanotechnology,* vol. 22, no. 11, pp. 115101-115101, 2011, doi: 10.1088/0957-4484/22/11/115101.
[243] J. Khetan, M. Shahinuzzaman, S. Barua, and D. Barua, "Quantitative Analysis of the Correlation between Cell Size and Cellular Uptake of Particles," *Biophysical Journal,* vol. 116, no. 2, pp. 347-359, 2019/01/22/ 2019, doi: 10.1016/j.bpj.2018.11.3134.
[244] B. Bonev, J. Hooper, and J. Parisot, "Principles of assessing bacterial susceptibility to antibiotics using the agar diffusion method," *Journal of Antimicrobial Chemotherapy,* vol. 61, no. 6, pp. 1295-1301, 2008, doi: 10.1093/jac/dkn090.
[245] S. Liu *et al.*, "Antibacterial Activity Of Graphite, Graphite Oxide, Graphene Oxide, And Reduced Graphene Oxide: Membrane And Oxidative Stress," *ACS Nano,* vol. 5, pp. 6971-6980, 2011.
[246] S. Gurunathan *et al.*, "Antibacterial activity of dithiothreitol reduced graphene oxide," *Journal of Industrial and Engineering Chemistry,* vol. 19, no. 4, pp. 1280-1288, 2013/07/25/ 2013, doi: 10.1016/j.jiec.2012.12.029.
[247] M. T. H. Aunkor, T. Raihan, S. H. Prodhan, H. S. C. Metselaar, S. U. F. Malik, and A. K. Azad, "Antibacterial activity of graphene oxide nanosheet against multidrug resistant superbugs isolated from infected patients," *Royal Society Open Science,* vol. 7, no. 7, p. 200640, doi: 10.1098/rsos.200640.

[248] L. Devi and S. R. Joshi, "Evaluation of the Antimicrobial Potency of Silver Nanoparticles Biosynthesized by Using an Endophytic Fungus, Cryptosporiopsis ericae PS4," *The Journal of Microbiology,* vol. 52, 07/04 2014, doi: 10.1007/s12275-014-4113-1.
[249] I. X. Yin, J. Zhang, I. S. Zhao, M. L. Mei, Q. Li, and C. H. Chu, "The Antibacterial Mechanism of Silver Nanoparticles and Its Application in Dentistry," (in eng), *International journal of nanomedicine,* vol. 15, pp. 2555-2562, 2020, doi: 10.2147/IJN.S246764.
[250] R. Salomoni, P. Leo, A. F. Montemor, B. G. Rinaldi, and M. F. A. Rodrigues, "Antibacterial Effect Of Silver Nanoparticles In Pseudomonas Aeruginosa," *Nanotechnology Science And Applications,* vol. 10, pp. 115-121, 2017.
[251] S. Magaldi *et al.*, "Well Diffusion For Antifungal Susceptibility Testing," *International Journal Of Infectious Diseases,* vol. 8, pp. 39-45, 2004.
[252] B. Bonev, J. Hooper, and J. Parisot, "Principles of assessing bacterial susceptibility to antibiotics using the agar diffusion method," *Journal of antimicrobial chemotherapy,* vol. 61, pp. 1295-1301, 2008.
[253] T. L. Riss *et al.*, "Cell Viability Assays," in *Assay Guidance Manual [Internet]*, S. Markossian, A. Grossman, and K. e. a. Brimacombe Eds.: National Center for Advancing Translational Sciences (NCATS), 2013.
[254] F. L. Mayer, D. Wilson, and B. Hube, "Candida Albicans Pathogenicity Mechanisms," *Virulence,* vol. 4, pp. 119-128, 2013.
[255] D. A. Cooksey, "Copper uptake and resistance in bacteria," *Molecular microbiology,* vol. 7, pp. 1-5, 1994.
[256] P.-C. Wu *et al.*, "Graphene Oxide Conjugated With Polymers: A Study Of Culture Condition To Determine Whether A Bacterial Growth Stimulant Or An Antimicrobial Agent?," *Journal Of Nanobiotechnology,* vol. 16, no. 1, p. 1, 2018.
[257] N. Jones, B. Ray, K. T. Ranjit, and A. C. Manna, "Antibacterial activity fo zno nanoparticle suspensions on a broad spectrum of microorganisms," *Fems microbiology letters,* vol. 279, pp. 71-76, 2008.
[258] L. Ma, A. Terwilliger, and A. W. Maresso, "Iron And Zinc Exploitation During Bacterial Pathogenesis," *Metallomics,* vol. 7, pp. 1541-1554, 2015.
[259] A. Gaballa and J. D. Helmann, "Identification of a zinc-specific metalloregulatory protein, zur, controlling zinc transport operons in bacillus subtilis," *Journal of bacteriology,* vol. 180, pp. 5815-5821, 1998.
[260] M. E. Levison and J. H. Levison, "Pharmacokinetics and pharmacodynamics of antibacterial agents," (in eng), *Infectious disease clinics of North America,* vol. 23, no. 4, pp. 791-vii, 2009, doi: 10.1016/j.idc.2009.06.008.
[261] B. Kowalska-Krochmal and R. Dudek-Wicher, "The Minimum Inhibitory Concentration of Antibiotics: Methods, Interpretation, Clinical Relevance," (in eng), *Pathogens (Basel, Switzerland),* vol. 10, no. 2, p. 165, 2021, doi: 10.3390/pathogens10020165.
[262] J. Ruparelia, A. Chatterjee, S. Duttagupta, and S. Mukherji, "Strain specificity in antimicrobial activity of silver and copper nanoparticles," *Acta Biomaterialia,* vol. 4, no. 3, pp. 707-716, 2008.
[263] A. Kalińska, S. Jaworski, M. Wierzbicki, and M. Gołębiewski, "Silver and Copper Nanoparticles—An Alternative in Future Mastitis Treatment and Prevention?," *International Journal of Molecular Sciences,* vol. 20, no. 7, p. 1672, 2019.
[264] M. Valodkar, S. Modi, A. Pal, and S. Thakore, "Synthesis and anti-bacterial activity of Cu, Ag and Cu–Ag alloy nanoparticles: A green approach," *Materials Research Bulletin,* vol. 46, no. 3, pp. 384-389, 2011.
[265] H. L. Jorgensen and E. Schulz, "Turbidimetric measurement as a rapid method for the determination of the bacteriological quality of minced meat," *International Journal of Food Microbiology,* vol. 2, pp. 177-183, 1985.

[266] W. K. Lack, B. Becker, J. Kramer, and W. H. Holzapfel, "Turbidimetry as a rapid method for enumeration of microorganisms in raw vegetables," *Arch Lebensmittelhyg,* vol. 50, pp. 136-140, 1999.

[267] S. Hona, R. Dangol, J. Ghatane, D. Giri, and R. R. Pradhananga, "Antimicrobial Effect of Copper Nanoparticles Synthesized by Chemical Method," *International Journal of Applied Sciences and Biotechnology,* vol. 7, no. 4, pp. 421-428, 12/28 2019, doi: 10.3126/ijasbt.v7i4.26295.

[268] T. Chatterjee, B. K. Chatterjee, D. Majumdar, and P. Chakrabarti, "Antibacterial effect of silver nanoparticles and the modeling of bacterial growth kinetics using a modified Gompertz model," *Biochimica et Biophysica Acta (BBA) - General Subjects,* vol. 1850, no. 2, pp. 299-306, 2015/02/01/ 2015, doi: 10.1016/j.bbagen.2014.10.022.

[269] S. Agnihotri, S. Mukherji, and S. Mukherji, "Size-controlled silver nanoparticles synthesized over the range 5–100 nm using the same protocol and their antibacterial efficacy," *RSC Advances,* 10.1039/C3RA44507K vol. 4, no. 8, pp. 3974-3983, 2014, doi: 10.1039/C3RA44507K.

[270] I. Sondi and B. Salopek-Sondi, "Silver nanoparticles as antimicrobial agent: a case study on E. coli as a model for Gram-negative bacteria," *Journal of Colloid and Interface Science,* vol. 275, no. 1, pp. 177-182, 2004/07/01/ 2004, doi: 10.1016/j.jcis.2004.02.012.

[271] Y. Chisti, "Fermentation (Industrial) | Basic Considerations," in *Encyclopedia of Food Microbiology (Second Edition)*, C. A. Batt and M. L. Tortorello Eds. Oxford: Academic Press, 2014, pp. 751-761.

[272] A. Hecht, D. Endy, M. Salit, and M. S. Munson, "When Wavelenths Collide: Bias in Cell Abundance Measurements Due to Expressed Fluorescent Proteins," *ACS Synthetic Biology,* vol. 5, pp. 1024-1027, 2016.

[273] J. Beal *et al.*, "Robust estimation of bacterial cell count from optical density," *Communications Biology,* vol. 3, no. 512, 2020.

[274] P. Stiefel, S. Schmidt-Emrich, K. Maniura-Weber, and Q. Ren, "Critical aspects of using bacterial cell viability assays with the fluorophores SYTO9 and propidium iodide," *BMC Microbiology,* vol. 15, no. 1, p. 36, 2015, doi: 10.1186/s12866-015-0376-x.

[275] L. Boulos, M. Prevost, B. Barbeau, J. Coallier, and R. Desjardins, "LIVE/DEAD® BacLight™: Application of a new rapid staining method for direct enumeration of viable and total bacteria in drinking water," *Journal of Microbiological Methods,* vol. 37, no. 1, pp. 77-86, 1999.

[276] Y. Deng, L. Wang, Y. Chen, and Y. Long, "Optimization of staining with SYO 9/propidium iodide: interplay, kinetics and impact on Brevibacillus brevis," *BioTechniques,* vol. 69, no. 2, 2020.

[277] M. Reyes, N. Maldonado-Luna, C. Rivera-Quiñones, A. Vega-Avila, F. Roman-Velazquez, and O. Perales-Perez, "Single Step Microwave Assisted Synthesis and Antimicrobial Activity of Silver, Copper and Silver-Copper Nanoparticles," *Journal of Materials Science and Chemical Engineering,* vol. 08, pp. 13-29, 01/01 2020, doi: 10.4236/msce.2020.88002.

[278] N. A. R. Gow and B. Hube, "Importance of the Candida albicans cell wall during commensalism and infection," *Current Opinion in Microbiology,* vol. 15, no. 4, pp. 406-412, 2012/08/01/ 2012, doi: https://doi.org/10.1016/j.mib.2012.04.005.

[279] T. Hanawa, "Research and development of metals for medical devices based on clinical needs," (in eng), *Science and technology of advanced materials,* vol. 13, no. 6, pp. 064102-064102, 2012, doi: 10.1088/1468-6996/13/6/064102.

[280] A. Nanda and M. Saravanan, "Biosynthesis of silver nanoparticles from Staphylococcus aureus and its antimicrobial activity against MRSA and MRSE," *Nanomedicine: Nanotechnology, Biology and Medicine,* vol. 5, no. 4, pp. 452-456, 2009.

[281] S. Prabhu and E. Poulose, K., "Silver nanoparticles: mechanism of antimicrobial action, synthesis, medical applications, and toxicity effects," *International nano letters,* vol. 2, no. 32, 2012, doi: 10.1186/2228-5326-2-32.

[282] D. A. Montero *et al.*, "Antimicrobial properties of a novel copper-based composite coating with potential for use in healthcare facilities," *Antimicrobial Resistance & Infection Control,* vol. 8, no. 1, p. 3, 2019/01/05 2019, doi: 10.1186/s13756-018-0456-4.

[283] N. M. Zain, A. G. F. Stapley, and G. Shama, "Green synthesis of silver and copper nanoparticles using ascorbic acid and chitosan for antimicrobial applications," *Carbohydrate Polymers,* vol. 112, pp. 195-202, 2014.

[284] N. Durán, P. D. Marcato, R. D. Conti, O. L. Alves, F. T. M. Costa, and M. Brocchi, "Potential use of silver nanoparticles on pathogenic bacteria, their toxicity and possible mechanisms of action," *Journal of Brazilian Chemcial Society,* vol. 21, no. 6, pp. 949-959, 2010.

[285] O. Erdogan *et al.*, "Green synthesis of silver nanoparticles via Cynara scolymus leaf extracts: The characterization, anticancer potential with photodynamic therapy in MCF7 cells," *PLOS ONE,* vol. 14, no. 6, p. e0216496, 2019, doi: 10.1371/journal.pone.0216496.

[286] A. T. M. Saeb, A. S. Alshammari, H. Al-Brahim, and K. A. Al-Rubeaan, "Production of Silver Nanoparticles with Strong and Stable Antimicrobial Activity against Highly Pathogenic and Multidrug Resistant Bacteria," *The Scientific World Journal,* vol. 2014, p. 704708, 2014/06/30 2014, doi: 10.1155/2014/704708.

[287] W.-L. Du, S.-S. Niu, Y.-L. Xu, Z.-R. Xu, and C.-L. Fan, "Antibacterial activity of chitosan tripolyphosphate nanoparticles loaded with various metal ions," *Carbohydrate Polymers,* vol. 75, no. 3, pp. 385-389, 2009.

[288] S. Al Tamimi *et al.*, "Synthesis and analysis of silver–copper alloy nanoparticles of different ratios manifest anticancer activity in breast cancer cells," *Cancer Nanotechnology,* vol. 11, no. 1, p. 13, 2020/11/25 2020, doi: 10.1186/s12645-020-00069-1.

[289] Q. Luo, R. A. Mackay, and S. V. Babu, "Copper Dissolution in Aqueous Ammonia-Containing Media during Chemical Mechanical Polishing," *Chemistry of Materials,* vol. 9, no. 10, pp. 2101-2106, 1997/10/01 1997, doi: 10.1021/cm970168s.

[290] P. Singh *et al.*, "Particle size analyses of polydisperse liposome formulations with a novel multispectral advanced nanoparticle tracking technology," *International Journal of Pharmaceutics,* vol. 566, pp. 680-686, 2019/07/20/ 2019, doi: 10.1016/j.ijpharm.2019.06.013.

[291] V. Filipe, A. Hawe, and W. Jiskoot, "Critical Evaluation of Nanoparticle Tracking Analysis (NTA) by NanoSight for the Measurement of Nanoparticles and Protein Aggregates," *Pharmaceutical Research,* vol. 27, no. 5, pp. 796-810, 2010/05/01 2010, doi: 10.1007/s11095-010-0073-2.

[292] A. Wal, W. Norde, S. Zehnder, and J. Lyklema, "Determination of the total charge in the cell walls of Gram-positive bacteria," *Colloids and Surfaces B: Biointerfaces,* vol. 9, no. 1-2, pp. 81-100, 1997.

[293] J. I. Ibeas *et al.*, "Fungal cell wall phosphomannans facilitate the toxic activity of a plant pr-5 protein," *The plant journal,* vol. 23, no. 3, pp. 375-83, 2001.

[294] D. Acharya, B. Mohanta, S. Deb, and A. K. Sen, "Theoretical prediction of absorbance spectra considering the particle size distribution using Mie theory and their comparison with the experimental UV–Vis spectra of synthesized nanoparticles," *Spectroscopy Letters,* p. 5, 2018.

[295] F. Dong, E. Valsami-Jones, and J.-U. Kreft, "New, rapid method to measure dissolved silver concentration in silver nanoparticle suspensions by aggregation combined with centrifugation," *Journal of Nanoparticle Research,* vol. 18, p. 259, 2016.

[296] M. Paszkiewicz, A. Gołąbiewska, Ł. Rajski, E. Kowal, A. Sajdak, and A. Zaleska-Medynska, "Synthesis and Characterization of Monometallic (Ag, Cu) and Bimetallic Ag-Cu Particles for Antibacterial and Antifungal Applications," *Journal of Nanomaterials,* vol. 2016, p. 2187940, 2016/02/29 2016, doi: 10.1155/2016/2187940.

[297] J. Ashraf, M. Ansari, H. Khan, M. Alzohairy, and I. Choi, "Green synthesis of silver nanoparticles and characterization of their inhibitory effects on AGEs formation using biophysical techniques," *Scientific Reports,* vol. 6, p. 20414, 2016.

[298] P. Khanna, P. More, J. Jawalkar, Y. Patil, and N. K. Rao, "Synthesis of hydrophilic copper nanoparticles: Effect of reaction temperature," *Journal of Nanoparticle Research,* vol. 11, no. 4, pp. 793-799, 2009.

[299] S. Cha, J. Hong, M. McGuffie, B. Yeom, J. VanEpps, and N. Kotov, "Shape-Dependent Biomimetic Inhibition of Enzyme by Nanoparticles and Their Antibacterial Activity," *ACS Nano,* vol. 9, no. 9, pp. 9097-91105, 2015.

[300] J. Helmlinger *et al.*, "Silver nanoparticles with different size and shape: equal cytotoxicity, but different antibacterial effects," *RSC Advances,* 10.1039/C5RA27836H vol. 6, no. 22, pp. 18490-18501, 2016, doi: 10.1039/C5RA27836H.

[301] X. Hong, J. Wen, X. Xiong, and Y. Hu, "Shape effect on the antibacterial activity of silver nanoparticles synthesized via a microwave-assisted method," *Environmental Science and Pollution Research,* vol. 23, no. 5, pp. 4489-4497, 2016/03/01 2016, doi: 10.1007/s11356-015-5668-z.

[302] E. Proksch, "pH in nature, humans and skin," *The Journal of Dermatology,* vol. 45, no. 9, pp. 1044-1052, 2018.

[303] H. S. Salapare *et al.*, "Cupric Oxide Nanostructures from Plasma Surface Modification of Copper," *Biomimetics,* vol. 4, no. 2, p. 42, 2019.

[304] D. Benoit, K. Sims, and D. Fraser, "Nanoparticles for oral biofilm treatments," *ACS Nano,* vol. 13, no. 5, pp. 4869-4875, 2019.

[305] S. Shahzadi, N. Zafar, and R. Sharif, "Chapter 3: Antibacterial Activity of Metallic Nanoparticles," in *Bacterial Pathogenesis and Antibacterial Control*, S. Kırmusaoğlu Ed. London: IntechOpen, 2018, pp. 51-72.

[306] S. Shaikh *et al.*, "Mechanistic Insights into the Antimicrobial Actions of Metallic Nanoparticles and Their Implications for Multidrug Resistance," *International Journal of Molecular Sciences,* vol. 20, no. 10, p. 2468, 2019.

[307] Z. Lu, K. Rong, J. Li, H. Yang, and R. Chen, "Size-dependent antibacterial activities of silver nanoparticles against oral anaerobic pathogenic bacteria," *Journal of materials science. Materials in medicine,* vol. 24, no. 6, pp. 1465-1471, 2013.

[308] X. Fan, L. H. Yahia, and E. Sacher, "Antimicrobial Properties of the Ag, Cu Nanoparticle System," (in eng), *Biology,* vol. 10, no. 2, p. 137, 2021, doi: 10.3390/biology10020137.

[309] M. Staniszewska, M. Bondaryk, E. Swoboda-Kopec, K. Siennicka, G. Sygitowicz, and W. Kurzatkowski, "*Candida albicans* morphologies revealed by scanning electron microscopy analysis," *Brazilian Journal of Microbiology,* vol. 44, no. 3, pp. 813-821, 2013.

[310] E. O. Mikhailova, "Silver Nanoparticles: Mechanism of Action and Probable Bio-Application," (in eng), *Journal of functional biomaterials,* vol. 11, no. 4, p. 84, 2020, doi: 10.3390/jfb11040084.

[311] J. M. Andrews, "Determination of minimum inhibitory concentrations," *Journal of Antimicrobial Chemotherapy,* vol. 48, no. suppl_1, pp. 5-16, 2001, doi: 10.1093/jac/48.suppl_1.5.

[312] A. Thill *et al.*, "Cytotoxicity of CeO2 Nanoparticles for Escherichia coli. Physico-Chemical Insight of the Cytotoxicity Mechanism," *Environmental Science & Technology,* vol. 40, no. 19, pp. 6151-6156, 2006/10/01 2006, doi: 10.1021/es060999b.

[313] M. J. Hajipour *et al.*, "Antibacterial properties of nanoparticles," *Trends in Biotechnology,* vol. 30, no. 10, pp. 499-511, 2012/10/01/ 2012, doi: 10.1016/j.tibtech.2012.06.004.

[314] A. M. El Badawy, R. G. Silva, B. Morris, K. G. Sheckel, M. T. Suidan, and T. M. Tolaymat, "Surface Charge-Dependent Toxcitity Of Silver Nanoparticles," *Environmental Science and Technology,* vol. 45, no. 1, pp. 283-287, 2011, doi: 10.1021/es1034188.

[315] J. S. Dickson and M. Koohmaraie, "Cell surface charge characteristics and their relationship to bacterial attachment to meat surfaces," (in eng), *Applied and environmental microbiology,* vol. 55, no. 4, pp. 832-836, 1989, doi: 10.1128/aem.55.4.832-836.1989.

[316] M. J. Wilhelm *et al.*, "Determination of bacterial surface charge density via saturation of adsorbed ions," *Biophysical Journal,* vol. 120, no. 12, pp. 2461-2470, 2021, doi: 10.1016/j.bpj.2021.04.018.

[317] N. Malanovic and K. Lohner, "Gram-positive bacterial cell envelopes: The impact on the activity of antimicrobial peptides," *Biochimica et Biophysica Acta (BBA) - Biomembranes,* vol. 1858, no. 5, pp. 936-946, 2016/05/01/ 2016, doi: 10.1016/j.bbamem.2015.11.004.

[318] N. A. R. Gow, J. P. Latge, and C. A. Munro, "The Fungal Cell Wall: Structure, Biosynthesis, and Function.," (in eng), *Microbiology Spectrum,* vol. 5, no. 3, 2021.

[319] R. Jones, R. Draheim, and M. Roldo, "Silver Nanowires: Synthesis, Antibacterial Activity and Biomedical Applications," *Applied Sciences,* vol. 8, p. 673, 04/26 2018, doi: 10.3390/app8050673.

[320] A. P. V. Ferreyra Maillard, P. R. Dalmasso, B. A. López de Mishima, and A. Hollmann, "Interaction of green silver nanoparticles with model membranes: possible role in the antibacterial activity," *Colloids and Surfaces B: Biointerfaces,* vol. 171, pp. 320-326, 2018/11/01/ 2018, doi: 10.1016/j.colsurfb.2018.07.044.

[321] M. Arakha *et al.*, "Antimicrobial activity of iron oxide nanoparticle upon modulation of nanoparticle-bacteria interface," (in eng), *Scientific reports,* vol. 5, pp. 14813-14813, 2015, doi: 10.1038/srep14813.

[322] N. Arora, K. Thangavelu, and G. N. Karanikolos, "Bimetallic Nanoparticles for Antimicrobial Applications," (in eng), *Frontiers in chemistry,* vol. 8, pp. 412-412, 2020, doi: 10.3389/fchem.2020.00412.

[323] B. Reidy, A. Haase, A. Luch, K. A. Dawson, and I. Lynch, "Mechanisms of Silver Nanoparticle Release, Transformation and Toxicity: A Critical Review of Current Knowledge and Recommendations for Future Studies and Applications," (in eng), *Materials (Basel, Switzerland),* vol. 6, no. 6, pp. 2295-2350, 2013, doi: 10.3390/ma6062295.

[324] S. Liao *et al.*, "Antibacterial activity and mechanism of silver nanoparticles against multidrug-resistant *Pseudomonas aeruginosa*," *International Journal of Nanomedicine,* vol. 14, pp. 1469-1487, 2019, doi: 10.2147/IJN.S191340.

[325] S. F. Sabira, A. M. Kasabe, P. C. Mane, R. D. Chaudhari, and P. V. Adhyapak, "Selective antifungal and antibacterial activities of Ag-Cu and Cu-Ag core–shell nanostructures synthesizedin-situPVA," *Nanotechnology,* vol. 31, no. 48, p. 485705, 2020/09/15 2020, doi: 10.1088/1361-6528/ab9da5.

[326] G. Cárdenas, J. Díaz V, M. F. Meléndrez, C. Cruzat C, and A. García Cancino, "Colloidal Cu nanoparticles/chitosan composite film obtained by microwave heating for food package applications," *Polymer Bulletin,* vol. 62, no. 4, pp. 511-524, 2009/04/01 2009, doi: 10.1007/s00289-008-0031-x.

[327] N. El-Deeb *et al.*, "Biogenically Synthesized Polysaccharides-Capped Silver Nanoparticles: Immunomodulatory and Antibacterial Potentialities Against Resistant Pseudomonas aeruginosa," *Frontiers in Bioengineering and Biotechnology,* vol. 8, 07/21 2020, doi: 10.3389/fbioe.2020.00643.

[328] A. Al-Sharqi, K. Apun, M. Vincent, D. Kanakaraju, and L. M. Bilung, "Enhancement of the Antibacterial Efficiency of Silver Nanoparticles against Gram-Positive and Gram-Negative Bacteria Using Blue Laser Light," *International Journal of Photoenergy,* vol. 2019, p. 2528490, 2019/05/30 2019, doi: 10.1155/2019/2528490.

[329] A. Lesniak, A. Salvati, M. J. Santos-Martinez, M. W. Radomski, K. A. Dawson, and C. Åberg, "Nanoparticle Adhesion to the Cell Membrane and Its Effect on Nanoparticle Uptake Efficiency," *Journal of the American Chemical Society,* vol. 135, no. 4, pp. 1438-1444, 2013/01/30 2013, doi: 10.1021/ja309812z.

[330] X.-H. N. Xu, W. J. Brownlow, S. V. Kyriacou, Q. Wan, and J. J. Viola, "Real-Time Probing of Membrane Transport in Living Microbial Cells Using Single Nanoparticle Optics and Living Cell Imaging," *Biochemistry,* vol. 43, no. 32, pp. 10400-10413, 2004/08/01 2004, doi: 10.1021/bi036231a.

[331] P. N. Brady and M. A. Macnaughtan, "Evaluation of colorimetric assays for analyzing reductively methylated proteins: Biases and mechanistic insights," *Analytical Biochemistry,* vol. 491, pp. 43-51, 2015/12/15/ 2015, doi: 10.1016/j.ab.2015.08.027.

[332] L. S. Reddy, M. M. Nisha, M. Joice, and P. N. Shilpa, "Antimicrobial activity of zinc oxide (ZnO) nanoparticle against Klebsiella pneumoniae," *Pharmaceutical Biology,* vol. 52, no. 11, pp. 1388-1397, 2014/11/01 2014, doi: 10.3109/13880209.2014.893001.

[333] A. J. M. Driessen and N. Nouwen, "Protein Translocation Across the Bacterial Cytoplasmic Membrane," *Annual Review of Biochemistry,* vol. 77, no. 1, pp. 643-667, 2008/06/01 2008, doi: 10.1146/annurev.biochem.77.061606.160747.

[334] R. E. Dalbey and A. Kuhn, "Protein Traffic in Gram-negative bacteria – how exported and secreted proteins find their way," *FEMS Microbiology Reviews,* vol. 36, no. 6, pp. 1023-1045, 2012, doi: 10.1111/j.1574-6976.2012.00327.x.

[335] W. W. Navarre and O. Schneewind, "Surface proteins of gram-positive bacteria and mechanisms of their targeting to the cell wall envelope," (in eng), *Microbiology and molecular biology reviews : MMBR,* vol. 63, no. 1, pp. 174-229, 1999, doi: 10.1128/MMBR.63.1.174-229.1999.

[336] A. Chatterjee, R. Chakraborty, and T. Basu, "Mechanism of antibacterial activity of copper nanoparticles," *Nanotechnology,* vol. 25, p. 135101, 02/28 2014, doi: 10.1088/0957-4484/25/13/135101.

[337] M. Yamanaka, K. Hara, and J. Kudo, "Bactericidal Actions of a Silver Ion Solution on Escherichia coli, Studied by Energy-Filtering Transmission Electron Microscopy and Proteomic Analysis," *Applied and Environmental Microbiology,* vol. 71, no. 11, pp. 7589-7593, 2005/11/01 2005, doi: 10.1128/AEM.71.11.7589-7593.2005.

[338] G. Tong, M. Yulong, G. Peng, and X. Zirong, "Antibacterial effects of the Cu(II)-exchanged montmorillonite on Escherichia coli K88 and Salmonella choleraesuis," *Veterinary Microbiology,* vol. 105, no. 2, pp. 113-122, 2005/01/31/ 2005, doi: 10.1016/j.vetmic.2004.11.003.

[339] Q. Feng, J. Wu, G.-Q. Chen, F.-Z. Cui, T. Kim, and J. Kim, "A mechanistic study of the antibacterial effect of silver ions on Escherichia coli and Staphylococcus aureus," *Journal of Biomedical Materials Research - J BIOMED MATER RES,* vol. 52, pp. 662-668, 01/01 2000, doi: 10.1002/1097-4636(20001215)52:43.0.CO;2-3.

[340] S. Gunalan, R. Sivaraj, and V. Rajendran, "Green synthesized ZnO nanoparticles against bacterial and fungal pathogens," *Progress in Natural Science: Materials International,* vol. 22, pp. 693–700, 12/01 2012, doi: 10.1016/j.pnsc.2012.11.015.

[341] M. H. Siddique *et al.*, "Effect of Silver Nanoparticles on Biofilm Formation and EPS Production of Multidrug-Resistant Klebsiella pneumoniae," *BioMed Research International,* vol. 2020, 04/20 2020, doi: 10.1155/2020/6398165.

[342] A. Ivask *et al.*, "Toxicity Mechanisms in Escherichia coli Vary for Silver Nanoparticles and Differ from Ionic Silver," *ACS Nano,* vol. 8, no. 1, pp. 374-386, 2014/01/28 2014, doi: 10.1021/nn4044047.

[343] T. A. Qiu *et al.*, "Research highlights: unveiling the mechanisms underlying nanoparticle-induced ROS generation and oxidative stress," *Environmental Science: Nano,* 10.1039/C6EN90021F vol. 3, no. 5, pp. 940-945, 2016, doi: 10.1039/C6EN90021F.

[344] A. Manke, L. Wang, and Y. Rojanasakul, "Mechanisms of Nanoparticle-Induced Oxidative Stress and Toxicity," *BioMed Research International,* vol. 2013, p. 942916, 2013/08/20 2013, doi: 10.1155/2013/942916.

[345] G. Wang *et al.*, "Antibacterial effects of titanium embedded with silver nanoparticles based on electron-transfer-induced reactive oxygen species," *Biomaterials,* vol. 124, pp. 25-34, 2017/04/01/ 2017, doi: 10.1016/j.biomaterials.2017.01.028.

[346] G. Applerot *et al.*, "Understanding the Antibacterial Mechanism of CuO Nanoparticles: Revealing the Route of Induced Oxidative Stress," *Small,* vol. 8, no. 21, pp. 3326-3337, 2012/11/05 2012, doi: 10.1002/smll.201200772.

[347] C. Yang, L. Jiang, H. Zhang, L. A. Shimoda, R. J. DeBerardinis, and G. L. Semenza, "Chapter Twenty-Two - Analysis of Hypoxia-Induced Metabolic Reprogramming," in *Methods in Enzymology*, vol. 542, L. Galluzzi and G. Kroemer Eds.: Academic Press, 2014, pp. 425-455.

[348] H. Kim and X. Xue, "Detection of Total Reactive Oxygen Species in Adherent Cells by 2',7'-Dichlorodihydrofluorescein Diacetate Staining," *Journal of visualized experiments: JoVE,* no. 160, 2020, doi: 10.3791/60682.

[349] R. Gaupp, N. Ledala, and G. A. Somerville, "Staphylococcal response to oxidative stress," (in eng), *Frontiers in cellular and infection microbiology,* vol. 2, pp. 33-33, 2012, doi: 10.3389/fcimb.2012.00033.

[350] S. B. Farr and T. Kogoma, "Oxidative stress responses in Escherichia coli and Salmonella typhimurium," (in eng), *Microbiological reviews,* vol. 55, no. 4, pp. 561-585, 1991, doi: 10.1128/mr.55.4.561-585.1991.

[351] M. Y. Tolstorukov, K. Virnik, V. B. Zhurkin, and S. Adhya, "Organization of DNA in a bacterial nucleoid," (in eng), *BMC microbiology,* vol. 16, pp. 22-22, 2016, doi: 10.1186/s12866-016-0637-3.

[352] K. N. Kreuzer, "DNA damage responses in prokaryotes: regulating gene expression, modulating growth patterns, and manipulating replication forks," (in eng), *Cold Spring Harbor perspectives in biology,* vol. 5, no. 11, pp. a012674-a012674, 2013, doi: 10.1101/cshperspect.a012674.

[353] J. Kapuscinski, "DAPI: a DNA-specific fluorescent probe," (in eng), *Biotech & histochemistry: official publication of the Biological Stain Commission,* vol. 70, no. 5, pp. 220-33, 1995, doi: 10.3109/10520299509108199.

[354] N. Ojkic, E. Lilja, S. Direito, A. Dawson, J. Allen Rosalind, and B. Waclaw, "A Roadblock-and-Kill Mechanism of Action Model for the DNA-Targeting Antibiotic Ciprofloxacin," *Antimicrobial Agents and Chemotherapy,* vol. 64, no. 9, pp. e02487-19, 2020, doi: 10.1128/AAC.02487-19.

[355] M. S. Jadhav, S. Kulkarni, P. Raikar, D. A. Barretto, S. K. Vootla, and U. S. Raikar, "Green biosynthesis of CuO & Ag–CuO nanoparticles from Malus domestica leaf extract and evaluation of antibacterial, antioxidant and DNA cleavage activities," *New Journal of Chemistry,* 10.1039/C7NJ02977B vol. 42, no. 1, pp. 204-213, 2018, doi: 10.1039/C7NJ02977B.

[356] A. Grigor'eva *et al.*, "Fine mechanisms of the interaction of silver nanoparticles with the cells of Salmonella typhimurium and Staphylococcus aureus," *BioMetals,* vol. 26, no. 3, pp. 479-488, 2013/06/01 2013, doi: 10.1007/s10534-013-9633-3.

[357] K. Giannousi, K. Lafazanis, J. Arvanitidis, A. Pantazaki, and C. Dendrinou-Samara, "Hydrothermal synthesis of copper based nanoparticles: Antimicrobial screening and interaction with DNA," *Journal of Inorganic Biochemistry,* vol. 133, pp. 24-32, 2014/04/01/ 2014, doi: https://doi.org/10.1016/j.jinorgbio.2013.12.009.

[358] C. Espírito Santo *et al.*, "Bacterial killing by dry metallic copper surfaces," (in eng), *Applied and environmental microbiology,* vol. 77, no. 3, pp. 794-802, 2011, doi: 10.1128/AEM.01599-10.

[359] O. Choi, K. K. Deng, N.-J. Kim, L. Ross, R. Y. Surampalli, and Z. Hu, "The inhibitory effects of silver nanoparticles, silver ions, and silver chloride colloids on microbial growth," *Water Research,* vol. 42, no. 12, pp. 3066-3074, 2008/06/01/ 2008, doi: 10.1016/j.watres.2008.02.021.

[360] M. Raffi, F. Hussain, T. M. Bhatti, J. I. Akhter, A. Hameed, and M. M. Hasan, "Antibacterial Characterization of Silver Nanoparticles against E. Coli ATCC-15224," *Journal of Materials Science and Technology,* vol. 24, no. 2, pp. 192-196, 2007.

[361] J. R. Morones *et al.*, "The bactericidal effect of silver nanoparticles," *Nanotechnology,* vol. 16, no. 10, pp. 2346-2353, 2005/08/26 2005, doi: 10.1088/0957-4484/16/10/059.

[362] Y. Wang, J. Wan, R. Miron, Y. Zhao, and Y. Zhang, "Antibacterial Property and Mechanisms of Gold-Silver Nanocages," *Nanoscale,* vol. 8, 05/16 2016, doi: 10.1039/C6NR01114D.

[363] S. A. Ahmad *et al.*, "Bactericidal activity of silver nanoparticles: A mechanistic review," *Materials Science for Energy Technologies,* vol. 3, pp. 756-769, 2020/01/01/ 2020, doi: 10.1016/j.mset.2020.09.002.

[364] Y.-H. Hsueh *et al.*, "The Antimicrobial Properties of Silver Nanoparticles in Bacillus subtilis Are Mediated by Released Ag+ Ions," *PLOS ONE,* vol. 10, no. 12, p. e0144306, 2015, doi: 10.1371/journal.pone.0144306.

[365] U. Klueh, V. Wagner, S. Kelly, A. Johnson, and J. D. Bryers, "Efficacy of silver-coated fabric to prevent bacterial colonization and subsequent device-based biofilm formation," *Journal of Biomedical Materials Research,* vol. 53, no. 6, pp. 621-631, 2000/01/01 2000, doi: 10.1002/1097-4636(2000)53:6.

[366] K. Jung Woo, C. Koo Hye, W. Kim Ki, S. Shin, H. Kim So, and H. Park Yong, "Antibacterial Activity and Mechanism of Action of the Silver Ion in Staphylococcus aureus and Escherichia coli," *Applied and Environmental Microbiology,* vol. 74, no. 7, pp. 2171-2178, 2008/04/01 2008, doi: 10.1128/AEM.02001-07.

[367] Q. Feng, J. Wu, G.-Q. Chen, F.-Z. Cui, T. Kim, and J. Kim, "A mechanistic study of the antibacterial effect of silver ions onEscherichia coli andStaphylococcus aureus," *Journal of Biomedical Materials Research - J BIOMED MATER RES,* vol. 52, pp. 662-668, 01/01 2000, doi: 10.1002/1097-4636(20001215)52:43.0.CO;2-3.

[368] R. Garcia-Rubio, H. C. de Oliveira, J. Rivera, and N. Trevijano-Contador, "The Fungal Cell Wall: Candida, Cryptococcus, and Aspergillus Species," (in English), *Frontiers in Microbiology,* Review vol. 10, 2020-January-09 2020, doi: 10.3389/fmicb.2019.02993.

[369] M. Riquelme *et al.*, "Fungal Morphogenesis, from the Polarized Growth of Hyphae to Complex Reproduction and Infection Structures," (in eng), *Microbiology and molecular biology reviews : MMBR,* vol. 82, no. 2, pp. e00068-17, 2018, doi: 10.1128/MMBR.00068-17.

[370] A. Brand and N. A. R. Gow, "Mechanisms of hypha orientation of fungi," (in eng), *Current opinion in microbiology,* vol. 12, no. 4, pp. 350-357, 2009, doi: 10.1016/j.mib.2009.05.007.

[371] H. H. Lara, D. G. Romero-Urbina, C. Pierce, J. L. Lopez-Ribot, M. J. Arellano-Jiménez, and M. Jose-Yacaman, "Effect of silver nanoparticles on Candida albicans biofilms: an ultrastructural study," *Journal of Nanobiotechnology,* vol. 13, no. 1, p. 91, 2015/12/15 2015, doi: 10.1186/s12951-015-0147-8.

[372] W. W. J. van de Sande, M. Tavakol, W. van Vianen, and I. A. J. M. Bakker-Woudenberg, "The effects of antifungal agents to conidial and hyphal forms of Aspergillus fumigatus," *Medical Mycology,* vol. 48, no. 1, pp. 48-55, 2010, doi: 10.3109/13693780802713497.

[373] J. Chen, L. Wu, M. Lu, S. Lu, Z. Li, and W. Ding, "Comparative Study on the Fungicidal Activity of Metallic MgO Nanoparticles and Macroscale MgO Against Soilborne Fungal Phytopathogens," (in English), *Frontiers in Microbiology,* Original Research vol. 11, 2020-March-12 2020, doi: 10.3389/fmicb.2020.00365.

[374] J. Chen *et al.*, "Graphene Oxide-Silver Nanocomposite: Novel Agricultural Antifungal Agent against Fusarium graminearum for Crop Disease Prevention," *ACS Applied Materials & Interfaces,* vol. 8, no. 36, pp. 24057-24070, 2016/09/14 2016, doi: 10.1021/acsami.6b05730.

[375] K.-J. Kim *et al.*, "Antifungal activity and mode of action of silver nano-particles on *Candida albicans*," *BioMetals,* vol. 22, no. 2, pp. 235-242, 2008, doi: 10.1007/s10534-008-9159-2.

[376] V. S. Radhakrishnan, M. K. Reddy Mudiam, M. Kumar, S. P. Dwivedi, S. P. Singh, and T. Prasad, "Silver nanoparticles induced alterations in multiple cellular targets, which are

critical for drug susceptibilities and pathogenicity in fungal pathogen (Candida albicans)," (in eng), *International journal of nanomedicine,* vol. 13, pp. 2647-2663, 2018, doi: 10.2147/IJN.S150648.

[377] J. S. Choi, J. W. Lee, U. C. Shin, M. W. Lee, D. J. Kim, and S. W. Kim, "Inhibitory Activity of Silver Nanoparticles Synthesized Using Lycopersicon Esculentum against Biofilm Formation in Candida Species," *Nanomaterials,* vol. 9, no. 11, 2019, doi: 10.3390/nano9111512.

[378] S. Bouson, A. Krittayavathananon, N. Phattharasupakun, P. Siwayaprahm, and M. Sawangphruk, "Antifungal activity of water-stable copper-containing metal-organic frameworks," *Royal Society Open Science,* vol. 4, p. 170654, 10/01 2017, doi: 10.1098/rsos.170654.

[379] A. d. S. Dantas, A. Day, M. Ikeh, I. Kos, B. Achan, and J. Quinn, "Oxidative stress responses in the human fungal pathogen, Candida albicans," (in eng), *Biomolecules,* vol. 5, no. 1, pp. 142-165, 2015, doi: 10.3390/biom5010142.

[380] D. J. Jamieson, D. W. S. Stephen, and E. C. Terrière, "Analysis of the adaptive oxidative stress response of Candida albicans," *FEMS Microbiology Letters,* vol. 138, no. 1, pp. 83-88, 1996, doi: 10.1111/j.1574-6968.1996.tb08139.x.

[381] R. Vazquez-Muñoz, M. Avalos-Borja, and E. Castro-Longoria, "Ultrastructural Analysis of Candida albicans When Exposed to Silver Nanoparticles," *PLOS ONE,* vol. 9, no. 10, p. e108876, 2014, doi: 10.1371/journal.pone.0108876.

[382] J. R. Price, E. Weindling, J. Berman, A. Buscaino, and A. Di Pietro, "Chromatin Profiling of the Repetitive and Nonrepetitive Genomes of the Human Fungal Pathogen Candida albicans," *mBio,* vol. 10, no. 4, pp. e01376-19, 2019, doi: 10.1128/mBio.01376-19.

[383] M. N. Rai, S. Balusu, N. Gorityala, L. Dandu, and R. Kaur, "Functional Genomic Analysis of Candida glabrata-Macrophage Interaction: Role of Chromatin Remodeling in Virulence," *PLOS Pathogens,* vol. 8, no. 8, p. e1002863, 2012, doi: 10.1371/journal.ppat.1002863.

[384] N. I. Dmitrieva and M. B. Burg, "Analysis of DNA breaks, DNA damage response, and apoptosis produced by high NaCl," (in eng), *American journal of physiology. Renal physiology,* vol. 295, no. 6, pp. F1678-F1688, 2008, doi: 10.1152/ajprenal.90424.2008.

[385] C. A. Sousa, H. M. V. M. Soares, and E. V. Soares, "Nickel Oxide Nanoparticles Trigger Caspase- and Mitochondria-Dependent Apoptosis in the Yeast Saccharomyces cerevisiae," *Chemical Research in Toxicology,* vol. 32, no. 2, pp. 245-254, 2019/02/18 2019, doi: 10.1021/acs.chemrestox.8b00265.

[386] I. Ahamad, F. Bano, R. Anwer, P. Srivastava, R. Kumar, and T. Fatma, "Antibiofilm Activities of Biogenic Silver Nanoparticles Against Candida albicans," (in English), *Frontiers in Microbiology,* Original Research vol. 12, 2022-January-07 2022, doi: 10.3389/fmicb.2021.741493.

[387] H. Wu, C. Moser, H.-Z. Wang, N. Høiby, and Z.-J. Song, "Strategies for combating bacterial biofilm infections," *International Journal of Oral Science,* vol. 7, pp. 1-7, 2015.

[388] P. Singha, J. Locklin, and H. Handa, "A Review of the Recent Advances in Antimicrobial Coatings for Urinary Catheters," *Acta biomaterialia,* vol. 50, pp. 20-40, 2017.

[389] H. Palza, "Antimicrobial Polymers with Metal Nanoparticles," *International Journal of Molecular Sciences,* vol. 16, pp. 2099-2116, 2015.

[390] G. Kampf, "Biocidal Agents Used for Disinfection Can Enhance Antibiotic Resistance in Gram-Negative Species," *Antibiotics (Basel),* vol. 7, no. 4, p. 110, 2018.

[391] S.-U. Victor and V.-B. J. Roberto, "Silver Nanoparticles and PDMS Hybrid Nanostructure for Medical Applications," in *Silver Nanoparticles - Fabrication, Characterization and Applications*, M. Khan Ed. London: Intech, 2018, pp. 147-164.

[392] P. Jing, Z. Yi-cai, Z. Mao-lin, Q. JIN-liang, and W. en-shuan, "Influence of [•]OH Radicals on the Radiation Effect of Polydimethylsiloxane Latex," *Acta Phys. -Chim. Sin.,* vol. 21, no. 08, pp. 873-877, 2005-08-15 2005, doi: 10.3866/pku.whxb20050810.

[393] R. F. Talabani, S. M. Hamad, A. A. Barzinjy, and U. Demir, "Biosynthesis of Silver Nanoparticles and Their Applications in Harvesting Sunlight for Solar Thermal Generation," *Nanomaterials*, vol. 11, no. 9*,* doi: 10.3390/nano11092421.

[394] H. R. Fischer, C. Semprimoschnig, C. Mooney, T. Rohr, E. R. H. van Eck, and M. H. W. Verkuijlen, "Degradation mechanism of silicone glues under UV irradiation and options for designing materials with increased stability," *Polymer Degradation and Stability,* vol. 98, no. 3, pp. 720-726, 2013/03/01/ 2013, doi: 10.1016/j.polymdegradstab.2012.12.022.

[395] B. Schnyder, T. Lippert, R. Kötz, A. Wokaun, V.-M. Graubner, and O. Nuyken, "UV-irradiation induced modification of PDMS films investigated by XPS and spectroscopic ellipsometry," *Surface Science,* vol. 532-535, pp. 1067-1071, 2003/06/10/ 2003, doi: 10.1016/S0039-6028(03)00148-1.

[396] Z. Wang *et al.*, "New Aspects of Degradation in Silicone Rubber under UVA and UVB Irradiation: A Gas Chromatography–Mass Spectrometry Study," *Polymers,* vol. 13, no. 13, 2021, doi: 10.3390/polym13132215.

[397] A. Y. Vasil'kov, R. I. Dovnar, S. M. Smotryn, N. N. Iaskevich, and A. V. Naumkin, "Plasmon Resonance of Silver Nanoparticles as a Method of Increasing Their Antibacterial Action," *Antibiotics (Basel),* vol. 7, no. 3, p. 80, 2018.

[398] F. Galvez, D. Pérez de Lara, J. Spottorno, M. A. García, and J. L. Vicent, "Heating effects of low power surface plasmon resonance sensors," *Sensors and Actuators B: Chemical,* vol. 243, pp. 806-811, 2017/05/01/ 2017, doi: 10.1016/j.snb.2016.12.053.

[399] T. S. Radhakrishnan, "Thermal degradation of poly(dimethylsilylene) and poly(tetramethyldisilylene-co-styrene)," *Journal of Applied Polymer Science,* vol. 99, no. 5, pp. 2679-2686, 2006/03/05 2006, doi: 10.1002/app.22813.

[400] S. Nakamura, N. Ando, M. Sato, and M. Ishihara, "Ultraviolet Irradiation Enhances the Microbicidal Activity of Silver Nanoparticles by Hydroxyl Radicals," *International Journal of Molecular Sciences,* vol. 21, p. 3204, 04/30 2020, doi: 10.3390/ijms21093204.

[401] E. C. Tuazon, S. M. Aschmann, and R. Atkinson, "Atmospheric Degradation of Volatile Methyl-Silicon Compounds," *Environmental Science & Technology,* vol. 34, no. 10, pp. 1970-1976, 2000/05/01 2000, doi: 10.1021/es9910053.

[402] E. Kowalska *et al.*, "Silver-modified titania with enhanced photocatalytic and antimicrobial properties under UV and visible light irradiation," *Catalysis Today,* vol. 252, pp. 136-142, 2015.

[403] R. T. P. da Silva, M. V. Petri, E. Y. Valencia, P. H. C. Camargo, S. I. C. de Torresi, and B. Spira, "Visible light plasmon excitation of silver nanoparticles against antibiotic-resistant Pseudomonas aeruginosa," *Photodiagnosis and Photodynamic Therapy,* vol. 31, p. 101908, 2020.

[404] M. Y. Memar, R. Ghotaslou, M. Samiei, and K. Adibkia, "Antimicrobial use of reactive oxygen therapy: current insights," *Infection and Drug Resistance,* vol. 11, pp. 567-576, 2018.

[405] A. Marguier *et al.*, "Bacterial Colonization of Low-Wettable Surfaces is Driven by Culture Conditions and Topography," *Advanced Materials Interfaces,* vol. 7, no. 20, p. 2000179, 2020/10/01 2020, doi: 10.1002/admi.202000179.

[406] C. R. Crick, S. Ismail, J. Pratten, and I. P. Parkin, "An investigation into bacterial attachment to an elastomeric superhydrophobic surface prepared via aerosol assisted deposition," *Thin Solid Films,* vol. 519, no. 11, pp. 3722-3727, 2011/03/31/ 2011, doi: 10.1016/j.tsf.2011.01.282.

[407] K. Efimenko, W. E. Wallace, and J. Genzer, "Surface Modification of Sylgard-184 Poly(dimethyl siloxane) Networks by Ultraviolet and Ultraviolet/Ozone Treatment," *Journal of Colloid and Interface Science,* vol. 254, no. 2, pp. 306-315, 2002/10/15/ 2002, doi: 10.1006/jcis.2002.8594.

[408] T. Tsuzuki *et al.*, "Hydrophobic Recovery of PDMS Surfaces in Contact with Hydrophilic Entities: Relevance to Biomedical Devices," *Materials,* vol. 15, no. 6, 2022, doi: 10.3390/ma15062313.
[409] Y. Kitajma, "Structural and biochemical characteristics of pathogenic fungus: cell walls, lipids and dimorphism, and action modes of antifungal agents," *Japanese journal of medical mycology,* vol. 41, no. 4, pp. 211-7, 2000, doi: https://doi.org/10.3314/jjmm.41.211.
[410] A. Mai-Prochnow, M. Clauson, J. Hong, and A. B. Murphy, "Gram positive and Gram negative bacteria differ in their sensitivity to cold plasma," *Scientific Reports,* vol. 6, no. 1, p. 38610, 2016/12/09 2016, doi: 10.1038/srep38610.
[411] J. Kang *et al.*, "Suppression of ion migration through cross-linked PDMS doping to enhance the operational stability of perovskite solar cells," *Solar Energy,* vol. 217, pp. 105-112, 2021/03/15/ 2021, doi: 10.1016/j.solener.2021.01.025.
[412] N. Sethy, Z. Arif, P. Mishra, and P. Kumar, "Nanocomposite film with green synthesized TiO2 nanoparticles and hydrophobic PDMS polymer: Synthesis, Characterization & Antibacterial test," *Journal of Polymer Engineering,* vol. 40, 01/14 2020, doi: 10.1515/polyeng-2019-0257.
[413] L. M. Gaetke, H. S. Chow-Johnson, and C. K. Chow, "Copper: toxicological relevance and mechanisms," (in eng), *Archives of toxicology,* vol. 88, no. 11, pp. 1929-1938, 2014, doi: 10.1007/s00204-014-1355-y.
[414] J. J. Kim, K. Konkel, L. McCulley, and I.-L. Diak, "Cases of Argyria Associated With Colloidal Silver Use," *Annals of Pharmacotherapy,* vol. 53, no. 8, pp. 867-870, 2019/08/01 2019, doi: 10.1177/1060028019844258.
[415] Z. Ferdous and A. Nemmar, "Health Impact of Silver Nanoparticles: A Review of the Biodistribution and Toxicity Following Various Routes of Exposure," (in eng), *International journal of molecular sciences,* vol. 21, no. 7, p. 2375, 2020, doi: 10.3390/ijms21072375.
[416] B. M. Andersen, "Prevention of Postoperative Wound Infections," (in eng), *Prevention and Control of Infections in Hospitals: Practice and Theory,* pp. 377-437, 2018, doi: 10.1007/978-3-319-99921-0_33.
[417] J. F. Guest, G. W. Fuller, and P. Vowden, "Cohort study evaluating the burden of wounds to the UK's National Health Service in 2017/2018: update from 2012/2013," *BMJ Open,* vol. 10, no. 12, p. e045253, 2020, doi: 10.1136/bmjopen-2020-045253.
[418] I. Negut, V. Grumezescu, and A. M. Grumezescu, "Treatment Strategies for Infected Wounds," (in eng), *Molecules (Basel, Switzerland),* vol. 23, no. 9, p. 2392, 2018, doi: 10.3390/molecules23092392.
[419] S. Dhivya, V. V. Padma, and E. Santhini, "Wound dressings - a review," (in eng), *BioMedicine,* vol. 5, no. 4, pp. 22-22, 2015, doi: 10.7603/s40681-015-0022-9.
[420] A. M. Scagnelli, "Therapeutic Review: Manuka Honey," *Journal of Exotic Pet Medicine,* vol. 25, no. 2, pp. 168-171, 2016/04/01/ 2016, doi: 10.1053/j.jepm.2016.03.007.
[421] S. Anjum, A. Arora, M. S. Alam, and B. Gupta, "Development of antimicrobial and scar preventive chitosan hydrogel wound dressings," *International Journal of Pharmaceutics,* vol. 508, no. 1, pp. 92-101, 2016/07/11/ 2016, doi: 10.1016/j.ijpharm.2016.05.013.
[422] S. Ye *et al.*, "Flexible Amoxicillin-Grafted Bacterial Cellulose Sponges for Wound Dressing: In Vitro and in Vivo Evaluation," *ACS Applied Materials & Interfaces,* vol. 10, no. 6, pp. 5862-5870, 2018/02/14 2018, doi: 10.1021/acsami.7b16680.
[423] J. Fong and F. Wood, "Nanocrystalline silver dressings in wound management: a review," (in eng), *International journal of nanomedicine,* vol. 1, no. 4, pp. 441-449, 2006, doi: 10.2147/nano.2006.1.4.441.
[424] K. Dunn and V. Edwards-Jones, "The role of Acticoat™ with nanocrystalline silver in the management of burns," *Burns,* vol. 30, pp. S1-S9, 2004/07/01/ 2004, doi: 10.1016/S0305-4179(04)90000-9.

[425] J. J. Castellano *et al.*, "Comparative evaluation of silver-containing antimicrobial dressings and drugs," *International Wound Journal,* vol. 4, no. 2, pp. 114-122, 2007/06/01 2007, doi: 10.1111/j.1742-481X.2007.00316.x.

[426] C. K. Sen *et al.*, "Copper-induced vascular endothelial growth factor expression and wound healing," *American Journal of Physiology-Heart and Circulatory Physiology,* vol. 282, no. 5, pp. H1821-H1827, 2002/05/01 2002, doi: 10.1152/ajpheart.01015.2001.

[427] A. Zarghami, M. Irani, A. Mostafazadeh, M. Golpour, A. Heidarinasab, and I. Haririan, "Fabrication of PEO/chitosan/PCL/olive oil nanofibrous scaffolds for wound dressing applications," *Fibers and Polymers,* vol. 16, no. 6, pp. 1201-1212, 2015/06/01 2015, doi: 10.1007/s12221-015-1201-8.

[428] B. Sanjeevirayar *et al.*, "Preparation and Characterization of Silver Nanoparticle/Aloe Vera Incorporated PCL/PEO matrix for wound dressing application," *Indian Journal of Biochemistry & Biophysics,* vol. 58, pp. 35-44, 02/01 2021.

[429] V. Kupka *et al.*, "Well-Blended PCL/PEO Electrospun Nanofibers with Functional Properties Enhanced by Plasma Processing," *Polymers,* vol. 12, no. 6, 2020, doi: 10.3390/polym12061403.

[430] K.-Y. Law, "Definitions for Hydrophilicity, Hydrophobicity, and Superhydrophobicity: Getting the Basics Right," *The Journal of Physical Chemistry Letters,* vol. 5, no. 4, pp. 686-688, 2014/02/20 2014, doi: 10.1021/jz402762h.

[431] J. Hou *et al.*, "Fabrication of fibrillated and interconnected porous poly(ε-caprolactone) vascular tissue engineering scaffolds by microcellular foaming and polymer leaching," *RSC Advances,* 10.1039/D0RA00956C vol. 10, no. 17, pp. 10055-10066, 2020, doi: 10.1039/D0RA00956C.

[432] M. Deka and A. Kumar, "Ionic transport in P(VdF-HFP)-PEO based novel microporous polymer electrolytes," *Bulletin of Materials Science,* vol. 32, no. 6, pp. 627-632, 2009/12/01 2009, doi: 10.1007/s12034-009-0097-6.

[433] W. Wang and P. Alexandridis, "Composite Polymer Electrolytes: Nanoparticles Affect Structure and Properties," (in eng), *Polymers,* vol. 8, no. 11, p. 387, 2016, doi: 10.3390/polym8110387.

[434] T. Eriksson, J. Mindemark, Y. Ma, and D. Brandell, "Effects of nanoparticle addition to poly(ε-caprolactone) electrolytes: Crystallinity, conductivity and ambient temperature battery cycling," *Electrochimica Acta,* vol. 300, 03/20 2019, doi: 10.1016/j.electacta.2019.01.117.

[435] F. O. Costa, A. A. C. C. Pais, and J. J. S. Sousa, "Analysis of formulation effects in the dissolution of ibuprofen pellets," *International Journal of Pharmaceutics,* vol. 270, no. 1, pp. 9-19, 2004/02/11/ 2004, doi: 10.1016/j.ijpharm.2003.10.002.

[436] A. Huang, Y. Jiang, B. Napiwocki, H. Mi, X. Peng, and L.-S. Turng, "Fabrication of poly(ε-caprolactone) tissue engineering scaffolds with fibrillated and interconnected pores utilizing microcellular injection molding and polymer leaching," *RSC Advances,* 10.1039/C7RA06987A vol. 7, no. 69, pp. 43432-43444, 2017, doi: 10.1039/C7RA06987A.

[437] Z. Xue, D. He, and X. Xie, "Poly(ethylene oxide)-based electrolytes for lithium-ion batteries," *Journal of Materials Chemistry A,* 10.1039/C5TA03471J vol. 3, no. 38, pp. 19218-19253, 2015, doi: 10.1039/C5TA03471J.

[438] D. M. Castilla, Z.-J. Liu, and O. C. Velazquez, "Oxygen: Implications for Wound Healing," (in eng), *Advances in wound care,* vol. 1, no. 6, pp. 225-230, 2012, doi: 10.1089/wound.2011.0319.

[439] A. Sood, M. S. Granick, and N. L. Tomaselli, "Wound Dressings and Comparative Effectiveness Data," (in eng), *Advances in wound care,* vol. 3, no. 8, pp. 511-529, 2014, doi: 10.1089/wound.2012.0401.

[440] T. Aizawa and Y. Wakui, "Correlation between the Porosity and Permeability of a Polymer Filter Fabricated via CO(2)-Assisted Polymer Compression," (in eng), *Membranes,* vol. 10, no. 12, p. 391, 2020, doi: 10.3390/membranes10120391.

[441] G. Borkow, J. Gabbay, and R. C. Zatcoff, "Could chronic wounds not heal due to too low local copper levels?," *Medical Hypotheses,* vol. 70, no. 3, pp. 610-613, 2008/01/01/ 2008, doi: 10.1016/j.mehy.2007.06.006.

[442] P. Dubey, B. Bhushan, A. Sachdev, I. Matai, U. Kumar, and G. Packirisamy, "Silver-nanoparticle-Incorporated composite nanofibers for potential wound-dressing applications," *Journal of Applied Polymer Science,* vol. 132, 06/01 2015, doi: 10.1002/app.42473.

Appendix

Media preparation protocol

Agar/broth powders were measured into weighing boat on analytical scales and poured into Duran bottle. Corresponding volumes of water was added and mixed until fully dissolved. Medium was autoclaved at 121^{o}C for 15mins as instructed on packaging. At cooler temperatures, agar was aseptically poured into petri dishes by hand. For Mueller Hinton agar, a sterile serological pipette was used to measure 20 µl of agar per petri dish. Broth medium was stored at room temperature until required.

Mueller Hinton Agar (MH) (1L of the medium)

Mueller Hinton Broth: 21g

Bacteriological agar: 15g

Nutrient agar (NA) (1L of the medium)

Nutrient agar: 23g

Yeast peptone dextrose agar (YPD) (1L of the medium)

Yeast peptone dextrose agar: 65g

Yeast peptone dextrose broth (YPD broth) (1L of the medium)

Yeast peptone dextrose broth: 50g

Nutrient broth (NB) (1L of the medium)

Nutrient broth: 13g

Mueller Hinton broth (MHB) (1L of the medium)

Mueller Hinton broth: 21g

Antibiotic preparation protocol

Antibiotics were dissolved into the appropriate solvent to make a final concentration of 10 mg/ml. Solutions were then sterilised using milipore 0.22 µm filter and further diluted using sterile distilled water to desired concentration.

Appendix Table 1: Antibiotics and corresponding solvents

Antibiotic	Solvent
Penicillin G	Sterile distilled water
Vancomycin	Sterile distilled water
Streptomycin	Sterile distilled water
Gentamicin	Sterile distilled water
Polymicin B	Sterile distilled water
Trimethoprim	Ethanol
Meropenem	Sterile distilled water
Tigecyclin	Dimethyl sulphide

Resazruin preparation protocol

Desired mass of Resazurin powder was measured into a sterile Eppendorf tube on analytical scale and added to corresponding volume of sterile distilled water to make up 0.02% resazurin solution. In a universal tube wrapped in aluminium foil, the solution was mixed thoroughly using vortex and then used immediately in dim light environment.

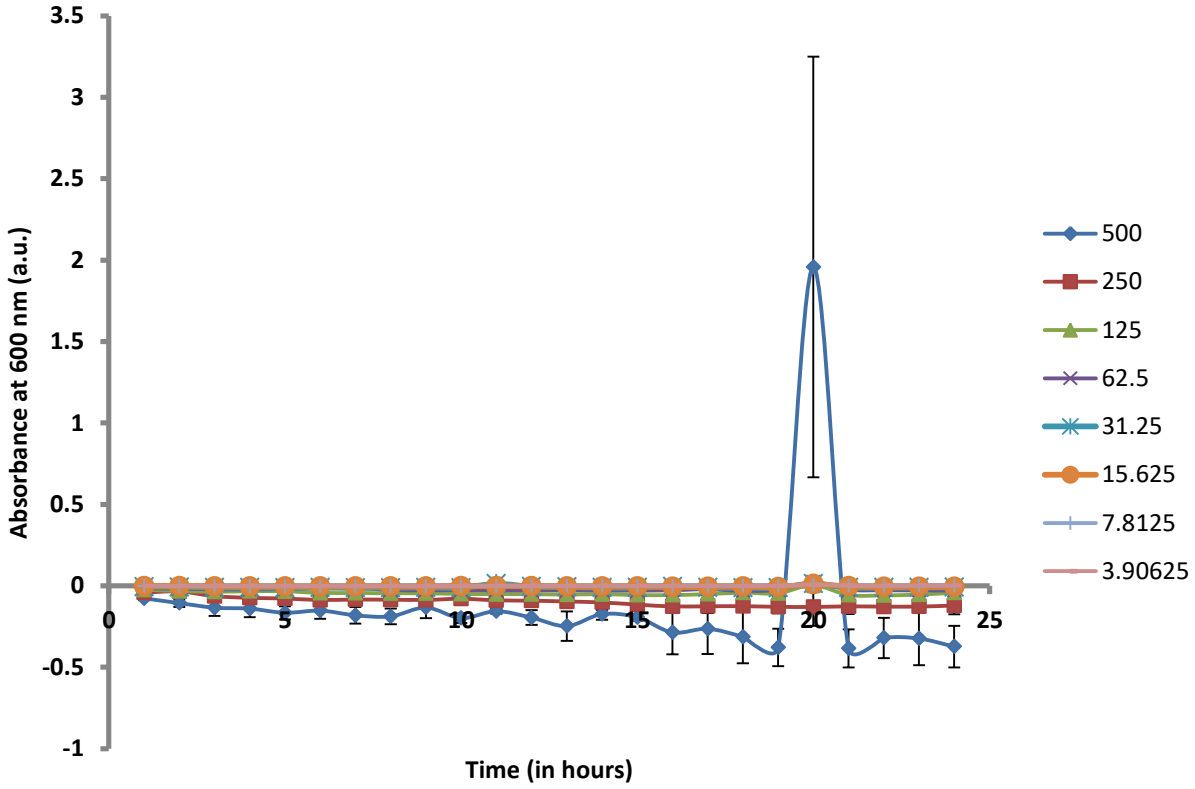

Appendix Figure 1: Absorbance of AgCu nanoparticles at 600 nm from concentrations 500 to 3.9 µg/ml to identify absorbance disturbance of nanoparticles. Error bars denote standard deviations.

Nanoparticle UV-Vis spectrometry results

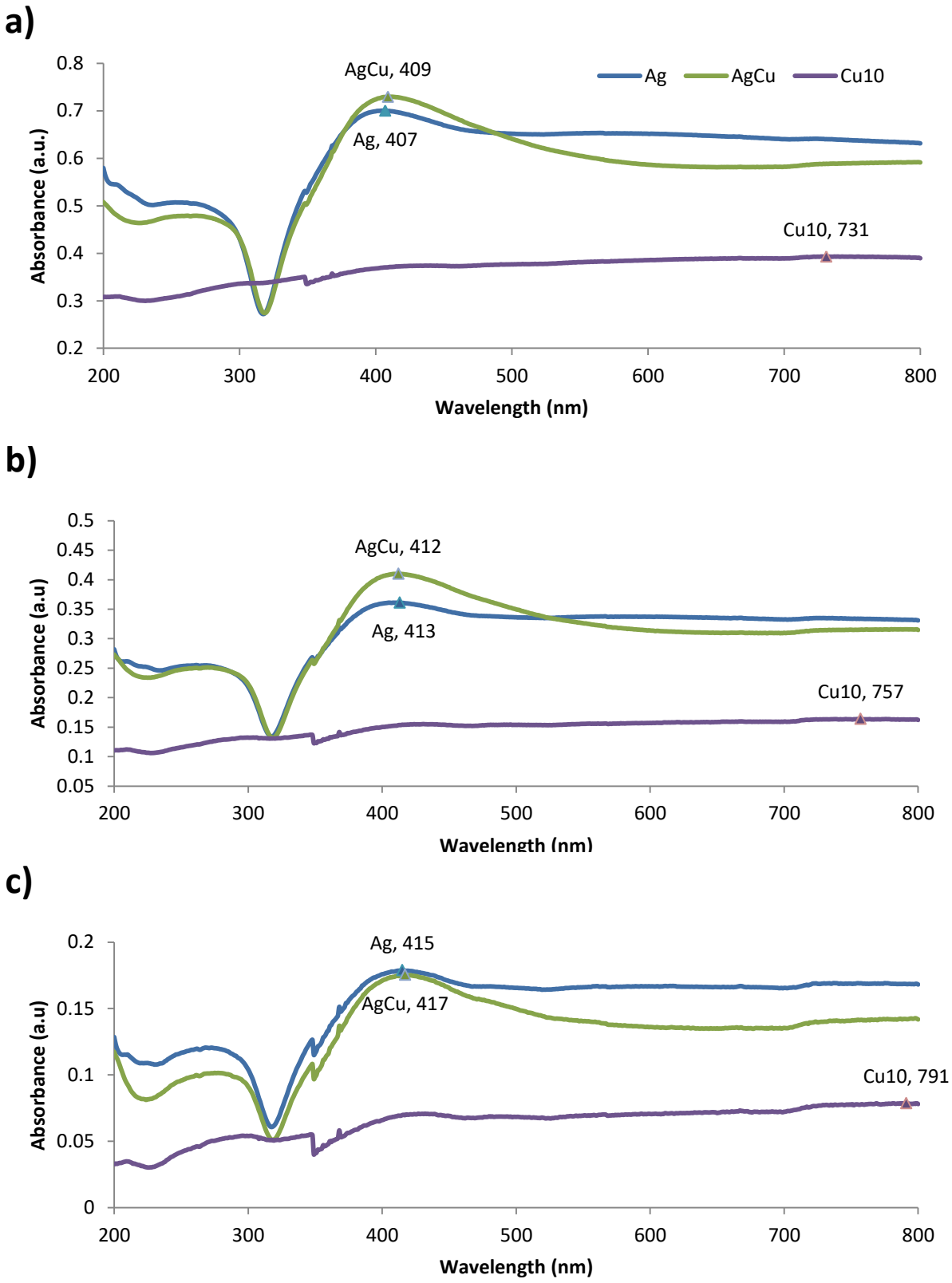

Appendix Figure 2: UV-Vis spectrum of nanoparticles. The UV-Vis spectrum of Ag, AgCu and Cu10 nanoparticle suspensions were measured at concentrations a) 125 µg/ml, b) 62.5 µg/ml and c) 31.25 µg/ml

Kinetic growth of microbes on 1 w/v% AgCu nanoparticle incorporated PDMS film

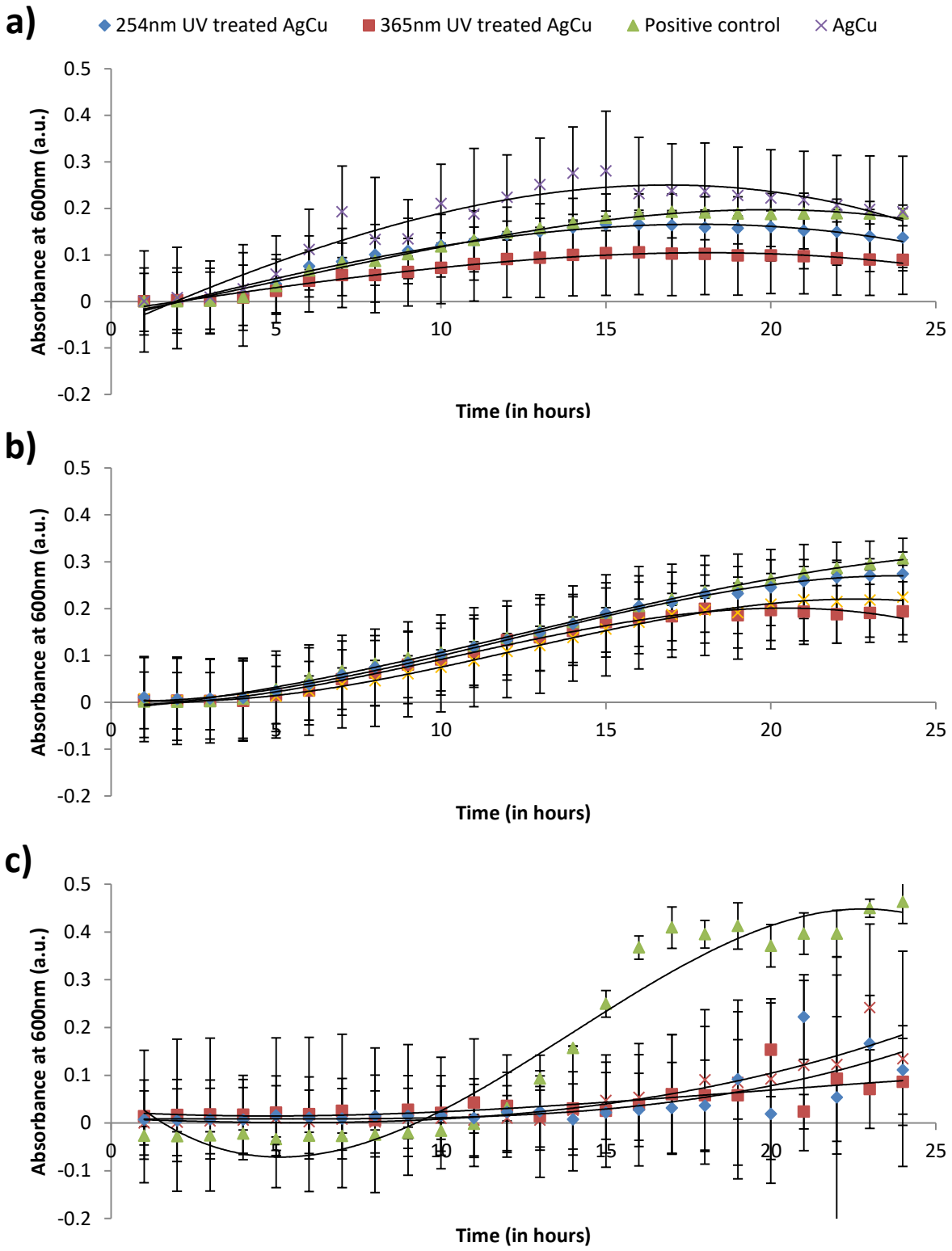

Appendix Figure 2: 24 hour growth rates of microbes on 1 w/v% AgCu nanoparticle incorporated PDMS film. Data points are hourly intervals of absorbance measurements at 600 nm of a) *E. coli,* b) *S. aureus* and c) *C. albicans.* Polynominal regression line, with 3 orders, was used to display the line of best fit and error bars denote standard deviations of results.

PCL/PEO polymer sample examples

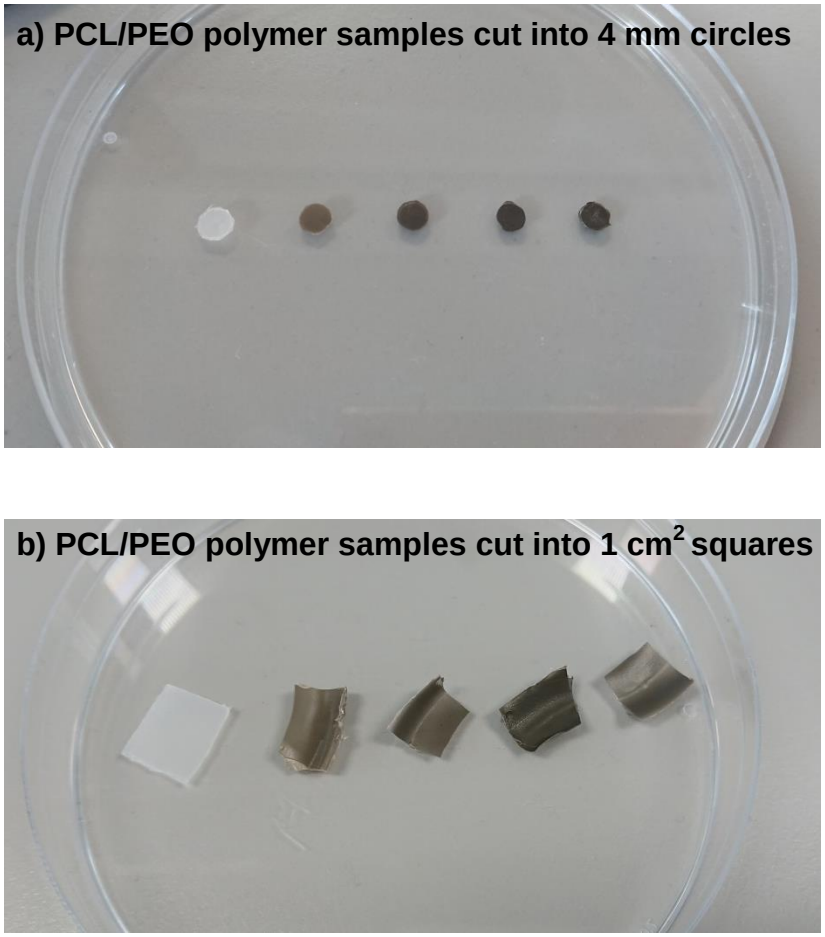

Appendix Figure 4: AgCu nanoparticle incorporated PCL/PEO polymers. The polymers were cut into smaller pieces for experimental use. a) 4 mm circles were made to test for antimicrobial activity through the disk diffusion method. b) 1 cm^2 squares were cut for characterisation testing. The concentration of AgCu nanoparticles (0, 0.1, 1, 5 and 10 w/w%) increase in the samples from left to right.

Publications

[1] Aydogdu, M., Altun, E., **Chung, E.,** Ren, G., Homer-Vanniasinkam, S., Chen, B., Edirisinghe, M. (2021). Surface interactions and viability of coronaviruses. Journal of The Royal Society Interface. 18. 20200798. 10.1098/rsif.2020.0798.

[2] Yang, X. Y., **Chung, E.,** Johnston, I., Ren, G., Cheong, Y. K. (2021). Exploitation of Antimicrobial Nanoparticles and Their Applications in Biomedical Engineering. Applied Sciences. 11. 4520. 10.3390/app11104520.

[3] Altun, E., Aydogdu, M., **Chung, E.,** Ren, G., Homer-Vanniasinkam, S., Edirisinghe, M. (2021). Metal-based nanoparticles for combating antibiotic resistance. Applied Physics Reviews. 8. 041303. 10.1063/5.0060299.

[4] Miranda, A., Akpobolokemi, T., **Chung, E.,** Ren, G., Raimi-Abraham, B.T. (2022). pH Alteration in Plant-Mediated Green Synthesis and Its Resultant Impact on Antimicrobial Properties of Silver Nanoparticles (AgNPs). Antibiotics *11*, 1592. 10.3390/antibiotics11111592

[5] Alotaibi, H., **Chung E.,** Chung S. H., Guogang, R., Singh, V., Huang, J. (2023). Sustainable γ-cyclodextrin frameworks containing ultra-fine silver nanoparticles with enhanced antimicrobial efficacy. Carbohydrate Polymers, 304. 10.1016/j.carbpol.2022.120516

Submitted manuscripts:

Chung, E., Guogang, R., Johnston, I., Matharu, R. K., Ciric, L., Walecka, A., Cheong, Y. K. A comparison of approaches to assess the antimicrobial activity of metallic based nanoparticles